Development of solubility selective mixed-matrix membranes for *n*-butane/methane separation

vorgelegt von
M.Sc.
Deniz Hülagü

von der Fakultät III – Prozesswissenschaften
der Technischen Universität Berlin
zur Erlangung des akademischen Grades

Doktor der Ingenieurwissenschaften
-Dr.-Ing-

genehmigte Dissertation

Promotionsausschuss:

Vorsitzende:	Prof. Dr.-Ing. habil. Jadran Vrabec
Gutachter:	Prof. Dr.-Ing. Matthias Kraume
Gutachter:	Prof. Dr.-Ing. habil. Jens-Uwe Repke
Gutachter:	Dr. Torsten Brinkmann

Tag der wissenschaftlichen Aussprache: 11.10.2019

Berlin 2019

This work is dedicated to my beloved ones: Ada and Berk.

Acknowledgements

This work was carried out during my time as a research assistant at the Chair of Chemical and Process Engineering, Technical University of Berlin within the scope of the research project 'Mixed-Matrix Membranes for Gas Separation'. The research was supported by the German Federal Ministry of Education and Research (BMBF).

First of all, I would like to express my sincere gratitude to my supervisor Prof. Dr.-Ing. Matthias Kraume for his invaluable help, support and guidance. I am very grateful for the trust you had in me since I first came to your department. At the same time, I always had the freedom to develop my own ideas in the field of research. I very much appreciate your constructive ideas, comments and suggestions for the preparation of this dissertation and the numerous opportunities you provided that helped me to complete my dissertation.

My research project was carried out in cooperation with Helmholtz-Zentrum Geesthacht, Blücher GmbH, and Sterling SIHI GmbH. I have been fortunate to work on this research project with smart, creative, and generous individuals. This work would not have been possible without their support. First and foremost, I would like to thank our project coordinator Dr. Torsten Brinkmann. The cooperation with you was outstanding. Your personal commitment made a big difference on this project. You were always a big help with the discussions about mixed-matrix membranes, especially during difficult and dark times. Also very special thanks for agreeing to be a reviewer of my work. Besides, many thanks to Heike Mushardt, Sergey Shishatskiy, Jan Wind, Stefan Kämper, and Henning Schee for our exceptionally good cooperation.

Thanks also to Prof. Dr.-Ing. habil. Jens-Uwe Repke for taking his time and energy to review my dissertation. I am grateful for Prof. Dr.-Ing. habil. Jadran Vrabec who took the responsibility to lead the examination committee.

My colleagues in the department deserve very special thanks for the wonderful working atmosphere. Verena Kramer, thank you first of all for introducing me to the subject of mixed-matrix membranes. It was a pleasure for me to work with you in the same research project. I always enjoyed exchanging our ideas and experience and the time we spent together in the laboratory. I am sure that Prof. Kraume will always remember the noisy days when we shared the same office with you. I am very lucky that you became one of my best friends over the years.

Lutz Böhm, thanks for reading a part of the draft of my work and giving me helpful suggestions. Lena Hohl and Jörn Villwock played a particularly significant role in shaping my defense presentation, thanks for the constructive and honest advices. Besides, thanks Lena for correcting my German abstract and for being a constant member of the volleyball team, the cocktail team, the horror movie team, and the Freysinn team. I would like to thank Sherly Rusly, Frauke Enders, Mathilde Foix Cablé, Chrysoula Bliatsiou, Evgenia Charlafti, Marc Petzold, and Susanne Röhl for your uplifting spirit and the friendly environment in our research group. Daniel Zedel, thanks for our never ending conversations on solution-diffusion model and error analysis. Matheus Pessoa, thanks for always being there when I needed a second hand and muscle power in the laboratory. Stefan Horn, we worked together for a very short time in the department but I must say that I am

very grateful to know you, thanks for being such a good friend and an awesome admin. Furthermore, special thanks to the group who organized “the real defense”.

For their technical support, I would like to thank Ursula Herrndorf, Andrea Hasselmann, Christine Kloth, Rainer Schwarz, and Gabriele Görig-Hedicke.

A big thanks is also to all my students, especially Nastassia König, Uli Dölchow, and Jonas Nowotnick for their hard work they invested into my project.

I would like to thank some of my friends for their careful reading of the draft of my work and for their valuable comments and ideas. Big thanks to Miraç Gül for proofreading without getting tired. You always believed that I will succeed and encouraged me to work harder. Special thanks to Dilek Sağlam also for proofreading. Your suggestions widened my horizon while writing my dissertation.

The support from my family was really important. My mom Beril Teoman has always been a great support. You always encouraged me to get the best education possible and become an independent woman. Without you, this journey would not have begun. Thanks Fırat Akten for being the best younger brother ever. My daughter Ada Hülagü was warmly felt during my pregnancy and she allowed me to hand in my dissertation just before being born. My husband Berk Hülagü has been a great encouragement. You always cheered me up and motivated me. I would like to thank you for your unconditional love and tremendous support. You are the only reason I made it this far.

Abstract

Mixed matrix membranes (MMMs) are developed to enhance separation properties of existing polymeric membranes. MMMs are expected to exhibit high permeability and high selectivity by merging of easy manufacture and advanced feature of organic polymers, and inorganic materials with their unique pore structure having molecular sieving ability, surface chemistry and mechanical strength. However, some researchers reported MMM performances worse than those of polymeric membranes due to the difficulties, which might be encountered in preparation of MMMs. To overcome several challenges that occur during preparation of MMMs, like particle agglomeration or blocking of filler particle pores by polymer chains, is the goal of this work.

This work is divided into two parts. First part focused on various strategies to develop a reliable preparation procedure for reproducible and defect-free laboratory-scale MMMs with high separation performance. Poly(dimethylsiloxane) (PDMS) was chosen as continues polymer phase and activated carbon (AC) was used as porous inorganic dispersed phase. To avoid non-uniformities in the casting suspension of PDMS and AC particles, such as particle agglomerates, intensive experimental investigations were carried out to develop optimal production procedure of homogeneous PDMS/AC suspension. Both the preparation of the casting suspension and the casting tool were varied. To hinder pore blockage of activated carbon by PDMS, investigations were performed on the effect of dispersing the filler in a slightly desorbing solvent before being in contact with PDMS. The MMMs were produced with different particle loadings and cast onto porous support structures with and without a gutter layer. The post-treatment of the MMMs was carried out by various methods. The effect of different preparation procedures on the performance of the produced MMMs was investigated. In a series of experiments, PDMS-based MMMs were prepared with zeolite particles to evaluate the separation performance of the PDMS/zeolite MMMs. The obtained results were compared with the separation performance of the PDMS/AC MMMs. In addition, in another series of experiments, the separation performance of poly(octylmethylsiloxane) (POMS)/AC MMMs, which were produced at the Helmholtz-Zentrum Geesthacht, were evaluated and compared with those of the PDMS/AC MMMs. Cross-sectional and surface morphological structure of the prepared unfilled PDMS membranes and MMMs were characterized by scanning electron microscopy (SEM).

Separation of vaporous higher hydrocarbons and other volatile organics from permanent gas streams is one of the crucial tasks in industrial applications. Methane (CH_4) is the primary product of the natural gas and the *n*-butane (*n*-C_4H_{10}) is one of the valuable hydrocarbon molecules in natural gas. Therefore, the performances of the produced MMMs were evaluated by the pure *n*-C_4H_{10} and pure CH_4 permeabilities, and mixed gas selectivities of binary mixtures of *n*-C_4H_{10}/CH_4 using the newly constructed test rig. Results were compared with those of unfilled PDMS membranes under identical conditions.

In the second part of this work, a series of membrane screening experiments were performed to determine the influence of varying operating conditions such as feed pressure, permeate pressure, temperature or composition on the separation behaviour of the MMMs. The aim of the second

part of the thesis is to find the right combination of operating parameters that would improve the separation efficiency of the membranes.

In addition, statistical analysis and error propagation were performed to provide measured permeability and selectivity data with the highest possible accuracy and reproducibility.

Kurzfassung

Mixed-Matrix-Membranen (MMM) werden entwickelt, um die Trenneigenschaften herkömmlicher Polymermembranen zu verbessern. Die MMM können potentiell eine einfache Herstellung und die Kombination der fortschrittlichen Eigenschaften der organischen Polymere sowie der anorganischen Materialien mit einzigartiger Porenstruktur, Molekularsiebfähigkeit, Oberflächenchemie und mechanischer Festigkeit verbinden, um somit eine hohe Permeabilität und Selektivität zu erhalten. Einige bisherige Studien zu diesem Thema zeigten schlechtere Trennleistungen von MMM im Vergleich zu reinen Polymermembranen, welche in Problemen bei der Herstellung von MMM begründet sein können. Die Untersuchung dieser Herausforderungen bei der Herstellung, wie unter anderem Partikelagglomeration oder Blockierung von Füllstoffpartikelporen durch Polymerketten, sind das übergeordnete Ziel dieser Arbeit.

Diese Arbeit besteht aus zwei Teilen. Der erste Teil konzentrierte sich auf verschiedene Strategien zur Entwicklung einer zuverlässigen Herstellungsprozedur für reproduzierbare und defektfreie MMM im Labormaßstab mit hoher Trennleistung. Polydimethylsiloxan (PDMS) wurde als kontinuierliche Polymerphase ausgewählt und Aktivkohle (AK) als poröse anorganische dispergierte Phase verwendet. Um Ungleichmäßigkeiten in der Beschichtungssuspension wie Agglomerate zu vermeiden, wurden intensive experimentelle Untersuchungen zur optimalen Herstellungsprozedur von homogenen Suspensionen von PDMS und AK Partikeln durchgeführt. Sowohl die Herstellung der Beschichtungssuspension als auch die Beschichtungswerkzeuge wurden dabei variiert. Um Porenverblockung von Aktivkohle durch PDMS zu vermindern, wurden Untersuchungen zum Effekt der Vorsättigung des Füllstoffes mit leicht desorbierendem Lösemittel auf die Verblockung durchgeführt. Die Herstellung der Membranen erfolgte mit verschiedenen Partikelbeladungen. MMM wurden auf die poröse Stützstruktur mit und ohne Gutterlayer (Drainageschicht) aufgetragen. Die Nachbehandlung der Membranen erfolgte mit verschiedenen Methoden. Die Einflüsse der verschiedenen Herstellprozeduren auf die Leistungsfähigkeit der Membranen wurden untersucht. In einer Testreihe wurden PDMS-basierte MMM mit Zeolith Partikel hergestellt um die Trennleistungen der PDMS/Zeolith MMM zu beurteilen und diese mit den Trennleistungen den PDMS/AK MMM zu vergleichen. Bei der zweiten Testreihe wurden zusätzlich die Trennleistungen der Polyoctylmethylsiloxan (POMS)/AK MMM, die beim Helmholtz-Zentrum Geesthacht hergestellt wurden, untersucht und auch diese mit den Trennleistungen den PDMS/AK MMM verglichen. Hergestellte reine PDMS und MMM wurden mittels Rasterelektronenmikroskopie (REM) Aufnahmen der Querschnitte und der Oberflächen hinsichtlich der morphologischen Struktur charakterisiert.

Die Abtrennung dampfförmiger höherer Kohlenwasserstoffe und anderer leicht flüchtiger Organika aus kontinuierlichen Gasströmen ist eine der entscheidenden Aufgaben in industriellen Anwendungen. Erdgas besteht hauptsächlich aus Methan (CH_4) und *n*-Butan (n-C_4H_{10}), was eines der wertvollsten Kohlenwasserstoffmoleküle in Erdgas darstellt. Daher wurden die Leistungsfähigkeiten der produzierten unterschiedlichen MMM über Einzelgas- und Gemischgaspermeationsversuche mit dem Stoffsystem n-C_4H_{10}/CH_4 an einem neu aufgebauten

Gaspermeationsprüfstand beurteilt. Die Ergebnisse wurden mit denen von reinen PDMS Membranen bei identischen Betriebsbedingungen verglichen.

Im zweiten Teil dieser Arbeit wurde eine Reihe von Membran-Screening-Experimenten durchgeführt zur Ermittlung des Einflusses variierender Betriebsbedingungen wie Feeddruck, Permeatdruck, Temperatur oder Zusammensetzung auf das Trennverhalten einer MMM. Das Ziel des zweiten Teils der Arbeit ist die Identifikation einer optimalen Kombination von Betriebsparametern, welche die Trennleistung der Membranen verbessern würde.

Darüber hinaus wurden statistische Analysen und eine Ermittlung der Fehlerfortpflanzung durchgeführt, um Permeabilitäts- und Selektivitätsdaten mit höchstmöglicher Genauigkeit und Reproduzierbarkeit zu liefern.

Contents

List of Figures

List of Tables

Nomenclature

Latin symbols

a	activity	[–]
A	area	[m^2]
$\tilde{A}$	empirical adjustable constant	[–]
b	parameter in Tòth adsorption isotherm	[bar^{-1}]
$\dot{b}$	mobility	[mol s kg^{-1}]
b_0	parameter in Tòth adsorption isotherm	[bar^{-1}]
B	virial coefficient	[–]
$\tilde{B}$	empirical adjustable constant	[–]
c	concentration	[mol m^{-3}]
C	Adsorbed concentration	[mg mg^{-1}]
d	diameter of membrane	[m]
D	diffusion coefficient	[m^2 s^{-1}]
D_0	thermodynamic diffusion coefficient	[m^2 s^{-1}]
D_{pre}	pre-exponential constant	[J mol^{-1}]
E_p	activation energy for permeation	[kJ mol^{-1}]
E_d	activation energy of diffusion	[kJ mol^{-1}]
f	fugacity	[bar]
G	Gibbs free enthalpy	[kJ]
k	Boltzmann's constant	[–]
k_H	Henry's gas constant	[–]
L	permeance	[$m^3_{(STP)}$ m^{-2} h^{-1} bar^{-1}]
L_∞^0	infinite permeance for T	[$m^3_{(STP)}$ m^{-2} h^{-1} bar^{-1}]
m	mass	[g]
m_0	parameter in free-volume model	[bar^{-1}]
m_T	parameter in free-volume model	[K^{-1}]
M	molecular weight	[g mol^{-1}]
n	number of moles	[–]
$\dot{n}''$	molar flux	[mol m^{-2} s]
nc	number of components	[–]
N	Avogadro's number	[6.022 x10^{23} mol^{-1}]
p	pressure	[bar]
P	permeability coefficient	[$m^3_{(STP)}$ m^{-1} h^{-1} bar^{-1}] or [Barrer]
P_{pre}	pre-exponential constant	[–]
q	adsorbed concentration	[mol m^{-3}]
R	ideal gas constant	[8.3144 J mol^{-1} K^{-1}]
S	solubility coefficient	[$cm^3_{(STP)}$ $cm^{-3}_{polymer}$ atm^{-1}]
S_{pre}	pre-exponential constant	[–]
H_{cond}	heat of condensation	[kJ mol^{-1}]

H_{mix}	heat of mixing	[kJ mol^{-1}]
H_s	enthalpy of sorption or heat of sorption	[kJ mol^{-1}]
t	parameter in Tòth adsorption isotherm	[–]
t_0	parameter in Tòth adsorption isotherm	[–]
T	temperature	[K]
T_0	reference temperature	[K]
v	molar volume	[m³ mol^{-1}]
V	polymer specific volume	[cm³ g^{-1}]
V_0	polymer occupied volume	[cm³ g^{-1}]
$\dot{V}$	volumetric flow rate	[m³ h^{-1}]
x	mass fraction	[g g^{-1}]
χ	Flory-Huggins interaction parameter	[–]
y	mole fraction	[mol mol^{-1}]
z	spatial co-ordinate	[m]

Greek symbols

α	selectivity	[–]
α^*	permselectivity	[–]
β	separation factor	[–]
δ	thickness	[m]
ϕ	fugacity coefficient	[–]
ϵ	intermolecular potential energy	[K]
μ	chemical potential	[J mol^{-1}]
σ	diameter of molecule	[Å]
$\emptyset$	volume fraction	[–]
ρ	density	[mol cm^{-3}], [g cm^{-3}]
γ	activity coefficient	[–]
Δ	difference	[–]

Abbreviations

ABS	acrylonitrile–butadiene–styrene
AC	activated carbon
BMBF	Federal Ministry of Education and Research
CT	casting tool
EDX	energy-dispersive x-ray spectroscopy
EOS	equation of state
FFV	fractional free volume
GL	gutter layer
HSD	high speed dispersing
HZG	Helmholtz-Zentrum Geesthacht
IAST	ideal adsorbed solution theory
INC	Institut für nichtklassische Chemie Leipzig
M	method
MG	mixed gas
MMM	mixed-matrix membrane

MMMfGS	mixed-matrix membranes for gas separation
MMMs	mixed-matrix membranes
MS	magnetic stirring
PAN	polyacrylonitrile
PDMS	poly(dimethylsiloxane)
PE	polyester
PES	polyethersulfone
PG	pure gas
PMP	poly(4-methyl-2-pentyne)
POE	propagation of error
POMS	poly(octylmethylsiloxane)
PSA	pressure swing adsorption
PTMSP	poly(trimethylsilyl)propyne
PVC	polyvinyl chloride
PVAc	poly(vinyl acetate)
RSD	relative standard deviation
RSDOM	relative standard deviation of the mean
RT	room temperature
SD	standard deviation
SDOM	standard deviation of the mean
SEM	scanning electron microscopy
TSA	temperature swing adsorption
TUB	Technical University of Berlin
US	ultrasonication
VSA	vacuum swing adsorption
Zeo	zeolite

Subscripts

B	*n*-butane
F	feed side of membrane
m	membrane
M	methane
i	component in gas mixture
j	component in gas mixture
P	permeate side of membrane
STP	standard temperature and pressure

Superscripts

G	gas
M	membrane

1 Introduction

Gas separation mainly aims either the capture of volatile organic compounds to prevent gas emissions or the recovery of valuable components from a main stream. An ideal application would be the one in which both objectives are achieved. Gas separation can be performed by cryogenic distillation or condensation, absorption, adsorption, and membranes [1, 2]. Cryogenic separations can be utilized for instance for air separation or recovery of volatile organic compounds [2]. Cryogenic methods enable separations with high purity and yield for heavy products. The major disadvantage is that the process is not efficient for low concentrated gas streams. Another disadvantage is the need for additional processes in the separation line for removing impurities, which brings high-energy consumption and costs [3]. Adsorbent-based processes, such as pressure swing adsorption (PSA), temperature swing adsorption (TSA), or vacuum swing adsorption (VSA), are commercially used for purification of hydrogen, oxygen production, gas drying or recovery of organic compounds. However, high energy requirement for regeneration of adsorbent and low recovery capacity are disadvantages of adsorption and absorption [2].

Membrane technology to separate gases have gained interest within the past 35 years [4]. Membrane gas separation offers a unique set of advantages, such as no requirement for phase change, operating simplicity, low capital and operating costs, low energy requirement, and high-energy efficiency [5]. Additionally, they are smaller in size, which makes them especially suitable for remote locations with limited space, e.g., offshore facilities. Membrane processes are used to separate non-condensable gases that cannot be easily condensed under the process conditions and remain in the gas phase. Common examples of these separations are nitrogen from air, carbon dioxide from methane, and hydrogen from nitrogen, argon, or methane. Companies such as GMT Membrantechnik GmbH, Mahler AGS GmbH, BORSIG GmbH, Novamem Ltd, and Sterling SIHI GmbH offer gas separation systems with membranes [6-10]. Separating gas mixtures containing condensable gases, such as C_{3+} hydrocarbons from methane or hydrogen, are expected to have a huge market potential. These separations require development of new membranes and processes to compete with current separation technologies [11].

Permeability and selectivity are the most important parameters of a membrane that determine the economics of separation performance. Permeability measures the productivity of a membrane and determines the required membrane area, while selectivity measures effectiveness of a membrane and determines the number of processing steps. The transport properties and selectivity of a single type of material is not enough to perform economical separations. In early 1990s, Robeson plotted permeability versus selectivity of a series of binary gas mixtures and graphically showed that performance of polymeric membranes has an upper limit [12]. In order to enhance separation properties of existing membranes and to exceed the Robeson upper-bound limit, researchers started to developed mixed-matrix membranes (MMMs) [13]. MMMs are composite membranes, in which the easy processability of polymers and superior gas separation performance of porous fillers are combined. MMMs may enhance both permeability and selectivity by merging organic polymer and inorganic particle phases. Inorganic filler materials have unique pore structure.

Molecular sieving ability, surface chemistry and mechanical strength of them provide an attractive improvement of separation properties [14, 15]. Different types of inorganic additives have been used as filler materials such as zeolites, metal-organic frameworks (MOFs), and carbon nanotubes (CNTs). Porous adsorbents have been proposed for industrial gas separation as well as promising filler material for MMMs [16, 17]. Some researches resulted in improved performances of prepared MMMs compared to polymer membranes and gave hope to pass over the Robeson upper bound limit.

However, some other researchers found worse performances due to difficulties which might be encountered in preparation of MMMs [18]. Producing MMMs has difficulties such as poor particle distribution, weak contact of particles in the polymer matrix, or inconvenient filler-polymer combination [18]. Due to the mentioned challenges, MMMs are not yet in the state to be used commercially in industrial applications. On the other hand, MMMs composed of the same polymer and inorganic filler developed by different work groups show quite distinct gas separation properties. Besides the components of MMMs, preparation procedure from priming the filler particles to post-treatment of the membranes has significant influence on membrane performance. Among numerous studies, limited research has been focused specifically on producing MMMs for gas separation.

1.1 Scope of the research

At the Chair of Chemical and Process Engineering, Technical University of Berlin (TUB), MMMs were researched in cooperation with Helmholtz-Zentrum Geesthacht (HZG), Blücher GmbH and Sterling SIHI GmbH, within the scope of the research project 'Mixed-Matrix Membranes for Gas Separation (MMMfGS)'. The scope of the project was to produce and develop silicon based polymeric MMMs in order to develop gas separation technology and to reduce carbon dioxide (CO_2) emissions. The project was funded by the Federal Ministry of Education and Research (BMBF, reference number 033RC1018) within the framework of the research initiative 'Technologies for Sustainability and Climate Protection - Chemical Processes and Material Use of CO_2'.

The aim of this work was to develop a reliable procedure for preparation of reproducible and defect-free next generation MMMs in laboratory-scale for the separation of C_{3+} hydrocarbons from gas mixtures. In this research, the removal of *n*-butane (*n*-C_4H_{10}) from methane (CH_4) was investigated using MMMs made of polydimethylsiloxane (PDMS) as polymer phase and activated carbon as the inorganic particles. PDMS was selected due to the recent interest in using it for separations of hydrocarbons from natural gas. CH_4 was used as the primary product in natural gas and the *n*-C_4H_{10} was used as the representative hydrocarbon molecule in natural gas. Additionally, the performance of the produced MMMs was evaluated under specific operating conditions, such as pressure, temperature and feed composition. The range of the operating conditions was chosen according to the pipeline requirements of the natural gas.

In this work, the investigated pure poly(octylmethylsiloxane) (POMS) membranes and POMS-based MMMs were produced by Mushardt [19] in HZG. Moreover, within the scope of the MMMfGS project, Kramer [20] developed a mechanistic model for mass transfer of the selected gases in MMMs. Therefore, some of the data presented in this work were used for the modeling study of Kramer.

1.2 Outline of the thesis

Section 2 briefly gives the theoretical background and closure terms for gas permeation that are used in this work. Section 2 continues with fundamentals of gas permeation in polymer membranes, where two components of permeability coefficient are described in detail. Additionally, current applications of gas separation membranes in industry and important aspects of hydrocarbon separation with membranes are shortly summarized. The concept of MMM development is introduced and challenges and limitations of MMM preparation are explained in this section. The real gas behavior, which is considered while analyzing the pure and mixed gas permeation, and the calculation method for fugacity coefficients are given.

Section 3 represents the characteristics of materials and the experimental analysis methods used in this thesis. Pure gas adsorption isotherms on pure polymer and activated carbon particles used for material selection are given in this section. Membrane preparation methodology is briefly described. Image analysis techniques used for morphologically characterization of the produced membranes are presented. Gas permeation setup that is designed and built for pure and mixed gas experiments is presented. Additionally, the methods used to determine pure gas permeation behavior and mixed gas permeability and selectivity are shown. The theory and calibration method of gas chromatography are given in this section.

Error analysis is performed in Section 4 to serve two different purposes: to deliver quantitative data as exact as possible and to determine reproducibility of the delivered data. Error analysis starts with basic definitions used in this work and shows applications of the propagation of error method to evaluate the error of delivered gas permeation data in this thesis. Section 4 mainly focuses on detailed evaluation of uncertainty that results from gas chromatographic concentration measurements. The procedure of reporting the obtained experimental data in this work with the calculated error by propagation of error method is also presented.

Section 5, as the first part of the results and discussion, systematically studies fundamental steps of MMM preparation: mixing of PDMS and activated carbon particles and casting this mixture onto a support structure, pre-treatment of activated carbon particles, and drying of membranes as post-treatment step. Different preparation methods of MMMs are discussed to evaluate the influence of preparation methods on the performance of the produced membranes and to develop the most reliable procedure for reproducible and defect-free MMM preparation. Produced membranes are morphological characterized using image analysis methods. The pure and mixed gas *n*-C_4H_{10} and CH_4 permeabilities and *n*-C_4H_{10}/CH_4 mixed gas selectivities of the produced MMMs are reported and results are compared with those of the unfilled PDMS membranes under identical conditions. Additionally, the influence of particle loading degree and usage of support structure with and without gutter layer are studied. Section 5 investigates further impacts of using POMS as a different polymer phase and zeolie-Y particles as a different type of filler.

The content of the Section 6, as the second part of the results and discussion, investigates the influence of process-related parameters on membrane performance, such as feed pressure, permeate pressure, temperature, and feed composition. A series of membrane screening experiments is conducted to find the right combination of operating parameters, which would improve the separation performance of the membranes.

Finally, a summary and conclusions of the present study and further necessary works are presented in Section 7.

2 State of the Art

2.1 Industrial gas separation processes

There are three major industrial applications of gas separation process [2]: Separation by cryogenic processes, separation with adsorbents, separation with solvents.

Separation by cryogenic processes

Cryogenic separation is a well-established process started by Linde AG in 1910 [21]. By cooling the feed stream to temperatures below its critical point, the vapour is removed in liquid form when it condenses on a cooling surface. Cryogenic processes enable separations with high purity and they are usually considered for air separation or recovery of volatile organic compounds. They show sufficient yield for high or medium concentrated products and low flow rates but it is not efficient for diluted gas streams. Low operating temperatures, minimum control possibilities and high temperature differences between feed stream and condenser surface lead to rapid clogging of the heat exchanger due to freezing effects and poor cleaning efficiency. Another disadvantage is high energy consumption due to the necessity of pre-treatment and additional processes for removing impurities. The turndown capability of cryogenic processes, which is the capability of a system at reduced capability, is quite lower compared with other processes [22].

Separation with adsorbents

Adsorption process is based on physical binding of gas molecules to solid adsorbents. Proper selection of the adsorbent, partial pressure of the gas component and operating temperature are critical for performance of the system. In pressure swing adsorption (PSA), the gas mixture flows through a packed bed filled by adsorbent at a high pressure. The adsorbent materials can be zeolite or activated carbon. By reducing the pressure, the adsorbent is regenerated. The adsorbents can be also used in temperature swing adsorption (TSA) and by raising the temperature, the adsorbent is regenerated. Another application is vacuum swing adsorption (VSA). These methods are commercially used for purification of hydrogen, carbon dioxide capture in gas streams, oxygen production, or recovery of organic compounds. However, high energy requirement for regeneration and low capacity and selectivity of common gases such as carbon dioxide are disadvantages of these methods [1, 22].

Separation with solvents

The solvent-based gas separation processes are well established since decades and widely used today. Natural gas treatment, carbon dioxide removal, gas drying with heavy and hydrophilic solvents such as glycols, or removal of sour gases by physical solvents are examples of industrial

applications of gas separations with solvents [2, 23]. Improved solvents could reduce energy requirement but desorption of the solvent is a major cost.

2.2 Gas separation with membranes

In membrane gas separation processes, a membrane separates the gas mixture. A membrane is a physical barrier that allows a certain component in a gas mixture to pass through it. The gas flow in contact with the membrane surface that passes through the membrane is called feed or penetrant (Figure 2.1). The gas flow, which passes through and leaves the membrane is called permeate. The gas flow depleted of feed that leaves the membrane without passing through the membrane to the downstream is called retentate. To achieve a sufficient separation, the membrane should have a high permeability for the permeate gas and a low permeability for the retentate gas. The permeability is the measure of the quantity of a component in the gas mixture permeates through the membrane. The ability of a membrane to perform a certain separation is called selectivity.

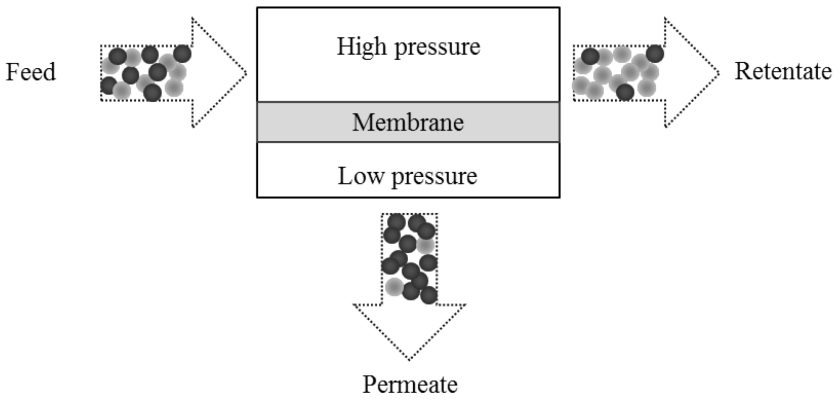

Figure 2.1 Schematic of a one-stage membrane gas separation unit.

Gas separation with membranes has several advantages to compete with current technologies. Installation costs are lower than alternative technologies. Furthermore, no additional facilities for solvent storage or water treatment are required. The main difference between membrane-based gas separation and other gas separation technologies is that membrane-based gas separation does not require a phase change. Single-stage membrane units are extremely simple to operate. The energy cost of multi-stage units is usually comparable to those of traditional technologies. Thus, the capital and operating costs are lower [5]. Additionally, it requires non-harmful materials, which makes it clean and environmental friendly. The space efficiency of membrane units makes them ideal for remote locations and low turndown ratios provide high efficiency. These advantages must be balanced against limitations of product purity and the necessity for compression [1].

Each separation process has its own advantages and disadvantages. It should be noted that selection of the separation process depends on various variables in certain industrial applications. The main target of the application and the requirements for the product, such as purity or

composition, must be taken into account while choosing the most suitable separation process for the particular application.

2.2.1 Current commercial membrane gas separation processes

Galizia et al. [24] recently reviewed the current status and future directions of commercial membrane gas separation application. Currently, nitrogen production, hydrogen separation, natural gas treatment, and vapor recovery are the largest four commercial applications of membrane gas separation. CO_2 removal from natural gas with membranes has relatively small market share and has to be developed. Recovery of light hydrocarbons, separation of C_{3+} hydrocarbons, H_2S, and water separation from air are performed on commercial scale and are considered as developing processes. On the other hand, oxygen enrichment and separations of organic vapor mixtures can be considered as to be developed processes with large potential for membrane application. These membrane-based gas separation applications are briefly discussed below. More information can be found in [3, 5, 25, 26].

Nitrogen separation from air

Nitrogen generation or enrichment evolved into one of the largest applications of membrane gas separation processes. Oxygen in the air permeates faster through the membrane than nitrogen does, thus an oxygen-enriched permeate and nitrogen-enriched retentate is obtained. Impurities such as argon or carbon dioxide remain in the permeate stream as well. This is simply achieved by countercurrent membrane separation plant with one or more membrane stages in series [25]. In most of the nitrogen separation processes, air is compressed and the temperature of the process is controlled in order to enhance membrane performance and product quality [27].

Hydrogen separation

Hydrogen separation and recovery is a highly successful field of membrane gas separations since hydrogen is a small, non-condensable, and highly permeable gas compared to all other gases [25, 26]. High partial pressure of hydrogen in the feed stream is a great advantage for membrane separations. Moreover, simple operation, small footprints, and relatively cheap process components make membrane separation the standard hydrogen separation technology. A typical membrane-based hydrogen separation is hydrogen recovery from ammonia plants with hydrogen-rich permeate stream containing about 90 vol% hydrogen. Hydrogen-selective membranes are usually used in oil refineries. Petrochemical industry applications include removing impurities from gas streams, hydrogen recovery from methanol purge, and carbon monoxide enrichment of hydrogen/carbon monoxide mixtures to adjust specific process requirements [25, 26].

Oxygen enrichment

Nitrogen separation systems produce oxygen-enriched air as a by-product. Oxygen production by membrane systems is still in development and cannot easily compete with adsorption or cryogenic technologies, since most of the industrial applications require purity higher than 90 vol%. Nevertheless, oxygen enrichment with membranes is used in chemical and food industries and for

medical use, where the required oxygen purity is in the range of 25 – 50 vol% and can be reached by one-stage membrane plants [5].

Gas drying

Air-drying or drying gases are performed to fulfill pipeline specifications. Since water molecules are smaller and more condensable than nitrogen or hydrogen, many membrane materials are suitable for sufficient production of dry gas [4]. The relationship between solubility coefficient and condensability of gases will be given in section 2.4.4.

Natural gas treatment

Natural gas is an extremely valuable resource and natural gas treatment has the highest interest among industrial gas treatment applications. Natural gas requires treatment before it can be delivered to the pipelines. The composition of raw natural gas varies depending on the source, but CH_4 is the main component with a content of 75 – 90% [3]. It contains significant amounts of CO_2 (up to 30%), some higher hydrocarbons, and undesired impurities such as nitrogen, hydrogen sulfide (H_2S), water, etc.

To meet the pipeline specifications, CO_2 and H_2S in the natural gas have to be separated. CO_2 causes corrosion and destroys pipelines and equipment. Additionally, it reduces the heating value of natural gas stream. H_2S is toxic at relatively modest levels. Amine absorption technology has been mostly used for CO_2 removal. The first membrane that was used for CO_2 separation from natural gas was anisotropic cellulose acetate in the 1980s [28]. Currently, commercially available membranes used for CO_2 removal are polymer based hollow fibers or spiral-wound formed membranes. Both rubbery and glassy membranes can be used to remove CO_2 and H_2S. Size-selective glassy membranes separate CO_2 better since it is a small molecule and rubbery membranes separate H_2S better, because H_2S is larger and more condensable than CO_2 [4].

The presence of water in natural gas causes corrosion and potentially damage the equipment used as well. In order to avoid hydrate formation, natural gas must be dried before entering the pipeline. Membrane-based processes can be an alternative approach to natural gas dehydration.

Natural gas contains very valuable C_{3+} hydrocarbons such as propane, butane, and others. At high temperatures, natural gas has a single gas phase. When the temperature is lowered, depending on the pressure and concentration, heavy hydrocarbons reach their saturation and condensation occurs. This temperature is called dew point and natural gas enters the liquid/gas two-phase region [28]. To avoid problems caused by condensation in the pipeline, the dew point has to be lowered by removing C_{3+} hydrocarbons. Currently, cooling and condensation or lean oil absorption is used to separate higher hydrocarbons from the natural gas. This process is usually followed by a fractional distillation to recover individual components [26, 28]. The current technology is costly and membranes are great alternatives but they are not used in industrial systems yet. Currently, silicon rubber membranes are used for C_{3+} hydrocarbons removal but the performance of the membrane strongly depends on the pressure and the composition of the feed stream. Development of new membrane materials with higher permeability and selectivity is still in progress. Additionally, removal of heavy hydrocarbons is necessary if the gas is used as fuel for gas engines or turbines. Pre-detonations and coking problems occur when the gas has high levels of hydrocarbons. Engine fuel gas conditioning is the most widely used membrane application for heavy hydrocarbon removal [28].

Vapor/gas separations

The removal of organic gas solvents from gas streams has a great potential in industrial applications. The first installed plants in 1990s were used to recover vapors from gasoline terminal vent gases or chlorofluorocarbon (CFC) vapors from the industrial refrigeration [4]. Recently, recovery of hydrocarbons with membranes from polyethylene and polypropylene plants became the largest application area of vapor/gas separations. The other main industrial applications are processing solvents from petrochemical plants, polyolefin plant resin degassing, polyvinyl chloride manufacturing vent gas, and natural gas processing [22].

Vapor/vapor separations

Separation of vapors in process streams has a great potential to be developed into very large-scale applications, such as ethylene from ethane, propylene from propane, and *n*-butane from isobutane. The fact that they are close-boiling point mixtures makes the separation by distillation very difficult, offering an opportunity for membrane gas separation [4, 11].

2.3 Membrane classification

2.3.1 Membrane structures

Based on the structure, membranes can be porous or dense and symmetric or asymmetric. Basically, a porous membrane has a solid matrix of pores and it serves as a filter. Porous membranes are divided according to their pore diameter as microporous ($d_p < 2$ nm), mesoporous ($2 \text{ nm} < d_p < 50$ nm), and macroporous ($d_p > 50$ nm) [29]. Dense homogeneous membranes have no individual permanent pores, but the separation occurs through fluctuating free volumes by diffusion under the driving force of pressure, concentration, or electrical potential gradient [4]. The separation process is determined by transport rate of the components within the membrane. Usually, dense membranes are utilized for gas separation, reverse osmosis or pervaporation [1].

Figure 2.2 illustrates the morphology of synthetic membranes. Symmetric (isotropic) membranes refer to the membranes with uniform structure. The transport properties of a symmetric membrane are identical over the cross-section of the membrane and the permeation rate is determined by the thickness of the entire membrane [29]. Asymmetric (anisotropic) membranes consist of pore structure gradually changing from large pores to very fine pores, which forms a skin on top of the membrane. This type of structure is called as integrally-skinned. The selective top layer may be nonporous. Alternatively, an asymmetric membrane may have a dense, selective, thin skin layer coated on top of the membrane, then it is called as thin-film composite membrane. The thin skin layer usually has a thickness of few micrometers and stands on a highly porous 100 – 300 µm thick support layer. The top skin layer represents the actual separation layer. The support layer performs no separations but it provides the membrane mechanical and chemical stability. In a thin-film composite membrane, different materials can be used; therefore, the transport properties differ over the cross-section of the membrane. The permeation characteristics of such a membrane are determined by the material properties and the thickness of the selective top skin layer. The porous support layer has negligible effect on the separation characteristics or the mass transfer rate of the membrane [4]. Asymmetric membranes are primarily used in pressure driven membrane processes, such as reverse osmosis and ultrafiltration, due to their high flux and good

mechanical stability [29]. Asymmetric membranes with non-porous skin layer and dense polymer membranes are very suitable for gas separation processes.

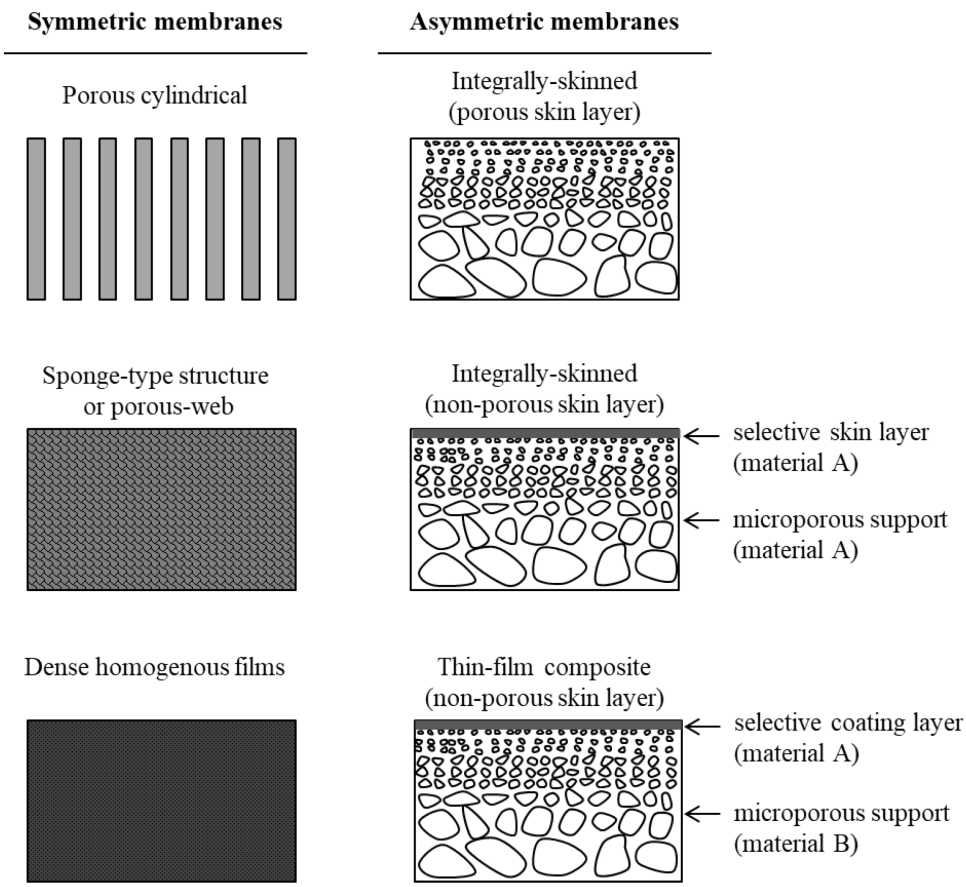

Figure 2.2 Classification of synthetic membrane structures. Adapted from Baker [4].

2.3.2 Membrane materials

Membrane materials are classified into three main groups: Inorganic materials, organic (polymeric) materials, and biological materials [29]. Polymeric membranes are of interest in membrane research and industrial applications [2]. Recently, composite membranes gained enormous attention due to their potential high performance. Biological membranes are excluded here because these membranes are not capable of meeting industrial requirements due to their thermomechanical stability and productivity [4].

Inorganic Membranes

There are five categories of inorganic membranes: Glass membranes, ceramic membranes, metallic membranes, carbon membranes, and zeolite membranes [4]. Although the majority of the commercially used membranes are polymeric membranes today, there is also interest for other membrane types as well. For example, microporous ceramic membranes are used for ultrafiltration and microfiltration [30-32], dense metal membranes are used for hydrogen

separation from gas mixtures [33, 34] and liquid membranes are used for separation of oxygen and nitrogen [35, 36].

Inorganic membranes have advantages and disadvantages. The major advantage is that they show high resistance to harsh environments with their long-term chemical, thermal and mechanical stability [37]. Despite their potential in water purification, they have disadvantages such as high cost and brittleness. Other limitations are low permeability and selectivity for certain applications and low membrane surface per module volume [38]. More research is needed in order to overcome mentioned drawbacks.

Polymer Membranes

Polymer is defined as a substance composed of macromolecules. Macromolecules are considered as structures, which comprise multiple repetitions of units with relatively high molecular mass. A chain is the whole or part of a macromolecule comprising a linear or branched sequence of units between two boundary units. The linear chain to which all other chains are being pendant is called the main chain or the polymeric backbone [39].

Polymers used for gas separation membranes separate gas molecules according to either

- the penetrant size (diffusivity) or
- the penetrant solubility [40].

Polymers that fall into the first category are called glassy polymers. They are more permeable to the smaller molecules in a gas mixture than the larger molecules. Glassy polymers are rigid and tough with a stiff chain and they sieve gas molecules by their molecular size. Rubbery polymers do not sieve gas molecules strictly by size but rather by their solubility. Since larger gas molecules are more soluble than smaller gas molecules, rubbery polymers are more permeable to the larger gas molecules. Such polymers are soft and elastic with a flexible chain and they provide high fluxes of the more permeable molecules.

The certain temperature that changes polymers from glassy to rubbery is called the glass transition temperature (T_g). If the polymer is below its glass transition temperature, polymer behaves as a rigid material by essentially fixed chains and limited segmental motion, and the material is called glassy polymer. When the polymer is above its glass transition temperature, it is in rubbery state. Mechanical properties of a polymer strongly depend on its glass transition temperature [4]

Polymeric membranes are less resistant to high temperature and aggressive chemicals. However, they are the dominating membrane material used for several membrane applications due to their easy preparation, low cost and flexibility. Polymeric membranes have been used for the recovery of hydrocarbons from natural gas [41-45]. Poly(dimethylsiloxane) (PDMS) is one of the commonly used polymeric membranes for the removal of higher hydrocarbons from gas streams [42, 46-49]. PDMS is a highly permeable, hydrocarbon selective rubbery polymer having flexible polymer backbone chains. Its very low glass transition temperature makes it ideal for gas separation applications. The separation of hydrocarbons from gas mixtures is based on solution-diffusion mechanism, where the more permeable component is the larger component in the mixture, which is less mobile but more soluble than methane [40]. In PDMS the permeability of the hydrocarbons increases with increasing of the penetrant size. This makes PDMS a suitable membrane material particularly for n-C_4H_{10}/CH_4 separation. Another higher hydrocarbon selective polymer membrane is poly(octylmethylsiloxane) (POMS), which is a derivative of the

PDMS with one of the methyl groups replaced by a octyl group [42]. Both PDMS and POMS membranes showed good results in permeability and selectivity and have particular advantages due to their low energy and small plant size demand [42, 50-55]. Polysulfone (PSU) [56-58], cellulose acetate (CA) [59, 60], and polyimide (PI) [61, 62] are other most common polymeric materials for gas separation membranes.

However, the challenge of moving the separation efficiency of these membranes from laboratory measurements to an industrial process still remains due to the influence of operating temperature, pressure, and composition on the separation properties. Recently, thin-film composite membranes gained enormous attention for such kind of separations to achieve high permeation rate and separation performance [63].

2.4 Fundamentals of permeation in polymer membranes

2.4.1 The solution-diffusion model

The solution-diffusion model explains and predicts gas permeation through a dense homogeneous polymeric membrane. The model assumes that when a gas is in contact with a membrane the following processes occur [4, 64]:

- Solution: the gas molecule dissolves into the polymer at the feed side
- Diffusion: the gas molecule diffuses inside the membrane by a concentration gradient
- Desorption: the gas molecule desorbs from the permeate side

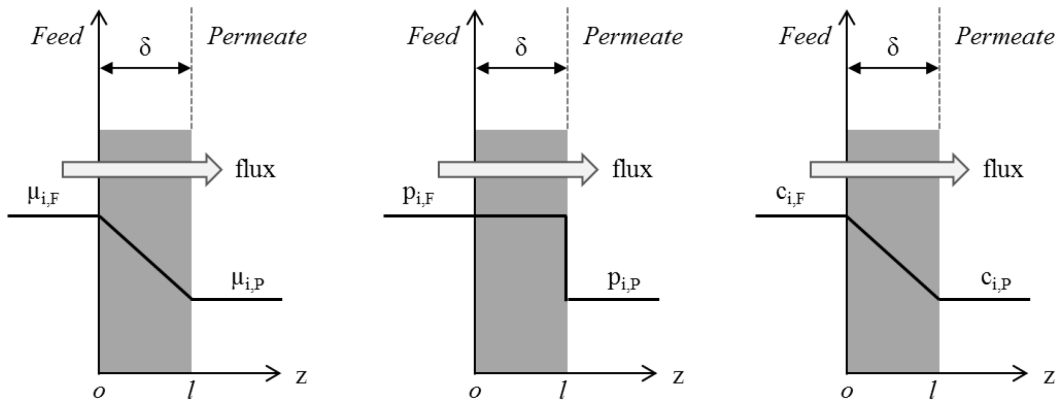

(a) Membrane chemical potential profiles **(b) Membrane pressure profiles** **(c) Membrane concentration profiles**

Figure 2.3 Driving force gradients of a pure gas through a dense polymeric membrane at steady-state according to the solution-diffusion model [4].

The chemical potential difference is the overall driving force for components to move through the membrane, which is related to pressure, temperature, and concentration (or activity). According to the solution-diffusion model, the gas phase on either side of the membrane are in equilibrium with the polymer interface [64]. Thus, the chemical potential over the cross-section of the membrane is

continuous as illustrated in Figure 2.3 (a). This means that the rates of sorption and desorption on the membrane interface are much higher than the rates of diffusion through the membrane. Another assumption of the solution-diffusion model is that no pressure gradient exists in the membrane and the pressure across the membrane is constant at the high-pressure value as illustrated in Figure 2.3 (b). The driving force across the membrane is represented by concentration gradient as illustrated in Figure 2.3 (c). As the feed pressure increases, the concentration in the feed interface of the membrane increases until the saturation vapor pressure of the component. Similarly, as the permeate pressure decreases by creating a vacuum on the permeate side of the membrane, the concentration in the permeate interface of the membrane decreases until it reaches zero [65].

2.4.2 Mass transport in polymer membranes

According to the solution-diffusion model, the flux of a component *i* in a polymer membrane is a product of concentration, mobility and driving force of this component in the polymer phase. Thus, the general form of mass transport in a polymer membrane can be written as follows [66]:

$$\text{flux} = \text{concentration} \cdot \text{mobility} \cdot \text{driving force} \tag{2.1}$$

$$\dot{n}''_{M,i} = -c_{M,i}\, \dot{b}_{M,i}\, \frac{\partial \mu_{M,i}}{\partial z} \tag{2.2}$$

Mobility $\dot{b}$ is the measure of the movability of the component *i* within the polymer phase and depends on the membrane properties. The Nernst-Einstein equation describes the relationship between the mobility $\dot{b}$ and the thermodynamic diffusion coefficient $D_{0M,i}$ as [66]:

$$D_{0M,i} = RT\, \dot{b}_{M,i} \tag{2.3}$$

Substitution of Equation 2.2 and 2.3 yields to:

$$\dot{n}''_{M,i} = -c_{M,i}\, \frac{D_{0M,i}}{RT}\, \frac{\partial \mu_{M,i}}{\partial z} \tag{2.4}$$

where the diffusion of a substance in the polymer matrix is described. In contrast to Fick's law of diffusion, the gradient of the chemical potential and the thermodynamic diffusion coefficient $D_{0M,i}$ is used here, which is less concentration-dependent, even for non-ideal systems. Thus, Equation 2.4 is more appropriate for describing the mass transport in solution-diffusion membranes [66, 67].

The chemical potential gradient represents the driving forces generated by concentration and pressure gradients, and it is written as follows [67]:

$$\mu_i = G_i^{pure}(T, p^0) + RT \ln(a_i) + v_i(p - p_{i,sat}) \tag{2.5}$$

where, G_i is the Gibbs free enthalpy, a_i is the activity and v_i is the partial molar volume.

Activity a_i is defined as the ratio of fugacity to the saturation fugacity of the component *i* at a given temperature, where the saturation fugacity is the fugacity at the saturation pressure. Activity is a function of activity coefficient γ_i and mole fraction of the penetrant y_i, and calculated as [67]:

$$a_i = \frac{f_i}{f_{i,sat}} = \gamma_i y_i \tag{2.6}$$

Then, Equation 2.5 can be written as:

$$\mu_i = G_i^{pure}(T, p^0) + RT \ln\left(\frac{f_i}{f_{i,sat}}\right) + v_i(p - p_{i,sat}) \tag{2.7}$$

Substitution of Equation 2.5 into Equation 2.4 yields [66, 67]:

$$\dot{n}''_{M,i} = -c_{M,i} D_{0M,i}\left(\frac{\partial}{\partial z}\ln a_{M,i} + \frac{v_i}{RT}\frac{\partial p}{\partial z}\right) \tag{2.8}$$

The term $\partial p/\partial z$ is zero for gas separation since no pressure gradient exists in the membrane, then Equation 2.8 simplifies to [67]:

$$\dot{n}''_{M,i} = -c_{M,i} D_{0M,i}\left(\frac{\partial}{\partial z}\ln a_{M,i}\right) \tag{2.9}$$

In Equation 2.9, sorption isotherms are required to determine the concentration of the component i in the membrane. The sorption coefficient S_i gives the ratio of the dissolved penetrant concentration on the feed side of the membrane to the penetrant partial pressure on the feed side in the gas phase. Henry's law is often applied with the following relationship [64, 67]:

$$c_{M,i} = S_i f_i \tag{2.10}$$

Combining Equations 2.9 and 2.10 [67]:

$$\dot{n}''_i = S_{M,i} D_{0M,i} \frac{1}{\delta}\left(f_{MR,i} - f_{MP,i}\right) \tag{2.11}$$

where, δ is the thickness of the active separation layer of the membrane.

Equation 2.11 is the general mass transfer equation in a dense polymeric gas permeation membrane and used to evaluate and predict permeation properties of the membrane.

2.4.3 Permeability coefficient

Permeability coefficient P is a product of two different terms: a thermodynamic parameter the sorption coefficient S and a kinetic parameter the diffusion coefficient D:

$$P_i = S_i D_i \tag{2.12}$$

Equation 2.11 can be used to rewrite Equation 2.12 as:

$$P_i = \frac{\dot{n}''_i \delta}{\left(p_{i,F} - p_{i,P}\right)} \tag{2.13}$$

Molar flux of the component *i* can be converted to volumetric flow rate of the component *i* at the permeate side by dividing it by membrane area. Then the permeability can be expressed as:

$$P_i = \frac{\dot{V}_{i,P}\delta}{A_m\left(p_{i,F} - p_{i,P}\right)} \tag{2.14}$$

where, $\dot{V}_{i,P}$ is the volumetric flow rate of component *i* on the permeate side, A_m is the membrane surface area, $p_{i,F}$ and $p_{i,P}$ are the partial pressure of component *i* on the feed and permeate side of the membrane, respectively.

Alternatively, feed and permeate pressures can be replaced with fugacities as:

$$P_i = \frac{\dot{V}_{i,P}\delta}{A_m\left(f_{i,F} - f_{i,P}\right)} \tag{2.15}$$

Permeability can be evaluated from permeation experiment of either pure gas or mixed gas. Pure gas permeability of a component is calculated as given in Equation 2.15. Permeability of one component in a gas mixture can be calculated as follows:

$$P_i = \frac{\dot{V}_P y_{i,P}\delta}{A_m\left(f_{i,F} - f_{i,P}\right)} \tag{2.16}$$

Some researches express permeability in Barrer, named after R. M. Barrer who conducted pioneering gas permeation tests. Barrer is defined as follows:

$$1\ \text{Barrer} = 1 \times 10^{-10}\ \frac{\text{cm}^3_{(STP)}\ \text{cm}}{\text{cm}^2\ \text{sec}\ \text{cm}_{Hg}} \tag{2.17}$$

In membrane technology papers, authors report the parameters to characterize performance of a membrane in different ways. In 2003, in his letter to the editor, Wijmans [68] suggested to report performance data of a membrane by taking the driving forces for permeation into account. Normalized permeate fluxes with respect to driving force provides clear and useful data that is comparable to the performance data of different membranes under identical conditions or one particular membrane under different operating conditions. This procedure allows data from widely different sources to be easily compared [69]. Permeability describes the transport flux per unit transmembrane driving force per unit membrane thickness. Permeability of a gas in a membrane is considered as flux normalized by pressure and thickness.

Permeance

Permeance describes the transport flux per unit transmembrane driving force. It is calculated as permeability divided by thickness of the membrane:

$$L_i = \frac{\dot{V}_{i,P}}{A_m\left(p_{i,F} - p_{i,P}\right)} = \frac{P_i}{\delta} \tag{2.18}$$

Similar to permeability, permeance can be evaluated from permeation experiments of a pure or mixed gas.

Some researches express permeance in gas permeation unit (GPU) and it is calculated as follows:

$$1\ \text{GPU} = 1 \times 10^{-6}\ \frac{\text{cm}^3_{(\text{STP})}}{\text{cm}^2\ \text{sec}\ \text{cm}_{\text{Hg}}} \tag{2.19}$$

Permeance is a characteristic parameter of a particular membrane and it depends on the thickness of the membrane. Permeance is higher for thin membranes than the thick ones. Therefore, it is useful to define a characteristic that is particular for material.

Selectivity

Selectivity describes the ability of a membrane to perform a certain separation. For a binary gas mixture, selectivity is defined as the ratio of the permeability coefficient or permeance of a component *i* to that of component *j*. It is determined with mixed gas experiments. Selectivity is the measure of the quality of the membrane and calculated as follows:

$$\alpha_{ij} = \frac{L_i}{L_j} = \frac{P_i}{P_j} = \frac{y_{i,P}}{\left(p_{i,F} - p_{i,P}\right)} \frac{\left(p_{j,F} - p_{j,P}\right)}{y_{j,P}} \tag{2.20}$$

Selectivity is also expressed as:

$$\alpha_{ij} = \frac{P_i}{P_j} = \left[\frac{S_i}{S_j}\right]\left[\frac{D_i}{D_j}\right] \tag{2.21}$$

where S_i/S_j is the ratio of solubility coefficients of components *i* and *j* in the gas mixture and referred as solubility selectivity, and D_i/D_j is the ratio of diffusion coefficients and referred as the diffusivity selectivity (or mobility selectivity).

In membrane gas separation literature, membrane performance is described with several terms. In order to avoid confusion or misconception using faulty terminology, it is important to define permselectivity and separation factor to distinguish them precisely.

Permselectivity

If the selectivity is calculated as a ratio of the permeability coefficient or permeance of a component *i* to that of component *j* determined with pure gas experiments, it is called permselectivity. Permselectivity does not define a separation factor, because in most cases permeability is affected due to the presence of other components in mixed gas and it is not equal to selectivity. Permselectivity is defined as follows [70]:

$$\alpha^*_{ij} = \frac{L_{i,PG}}{L_{j,PG}} = \frac{P_{i,PG}}{P_{j,PG}} \tag{2.22}$$

Separation factor

Separation factor is a ratio of the concentrations of the components *i* and *j* in the permeate side of the membrane relative to the concentrations of these components in the feed side. Separation factor is defined as follows [71]:

$$\beta_{ij} = \frac{\left(y_{i,P}/y_{j,P}\right)}{\left(y_{i,F}/y_{j,F}\right)} \cong \alpha_{ij} \tag{2.23}$$

2.4.4 Solubility coefficient

The first factor determining the permeability in a polymer is solubility coefficient. The solution of a gas molecule in a polymer includes two thermodynamic steps [40]: (1) condensation of the penetrant gas molecule to a liquid-like density governed by penetrant condensability, (2) mixing the penetrant and the polymer segments depending on the polymer-penetrant interactions.

Solubility coefficient depends on the operating conditions such as temperature, pressure, and composition of the gas mixture. In addition to operating conditions, gas solubility also depends on factors such as condensability of the penetrant gas, polymer morphology, and interactions between the penetrant gas and the polymer. The solubility coefficient increases as the condensability of the penetrant gas increases [72]. A measure for condensability is the boiling point of the penetrant gas. Since larger molecules are more condensable than smaller ones, solubility thus increases with molecular size [4, 72].

2.4.5 Diffusion coefficient

The diffusion coefficient is the second factor that determines permeability in a polymer. The diffusion of gas molecules is controlled by the motion of the polymer chains. Besides the operating conditions (temperature, pressure, composition of the gas mixture), the diffusion coefficient mainly varies depending on the polymer studied due to the polymer's free volume and the size of the gas molecule. This variation in polymer is mostly described by the Free-Volume Model [2], which suggests that a gas molecule can move in the polymer from the area of high concentration to the area of low concentration when a local cavity exceeds a critical free volume value. The effect of free volume on diffusion is stronger than the effect of free volume on solubility. Moreover, the polymer segmental mobility and the efficiency of chain packing determine the amount of free volume, which in turn strongly influences the diffusion of the gas molecule through the polymer [40]. Diffusion strongly depends on the amount and the distribution of the fractional free volume (FFV) present in the polymer. FFV is referred as the fraction of total polymer specific volume, which is not occupied by polymer molecules and available for the penetrant molecules to transport [2, 40, 72] and is expressed as:

$$\mathrm{FFV} = \frac{V - V_0}{V_0} \tag{2.24}$$

where, V is the polymer specific volume and V_0 is the occupied volume of the polymer. For rubbery and glassy polymers, FFV is generally about 10-15% and 15-20%, respectively [4].

The relationship between the diffusion coefficient and the FFV of a polymer is typically given by the empirical equation as shown below [73]:

$$D = RT\widetilde{A}\exp\left(-\frac{\widetilde{B}}{FFV}\right) \tag{2.25}$$

where $\widetilde{A}$ is an empirical adjustable constant which depends weakly on temperature and $\widetilde{B}$ is another empirical adjustable constant, which is a characteristic parameter of the polymer-penetrant system related to minimum free volume size.

Since diffusion is a thermally activated process, the FFV increases with increasing temperature. Consequently, the diffusion coefficient increases as temperature increases [2]. The larger molecules need bigger free volume elements to diffuse. Thus, for both rubbery and glassy polymers, the diffusion coefficient decreases with increasing molecular size. In rubbery polymers, the diffusion coefficient weakly depends on molecular size because the relatively large polymer segmental motions, due to the higher chain flexibility, are not refined enough to let only small molecules to diffuse. In glassy polymers, on the other hand, the diffusion coefficient strongly depends on molecular size because polymer segmental motions are refined enough to discriminate against the larger gas molecules [4, 40, 72]. Diffusion and solubility coefficients of various gases in silicone rubber are presented in Figure 2.4 as a function of critical volume V_c, which is a convenient average measure of penetrant size [74]. In general, the larger the penetrant gas molecule, the larger the activation energy of diffusion. Usually, diffusion coefficients increase with increasing penetrant concentration, but examples of contrary cases were also reported in both rubbery and glassy polymers [40].

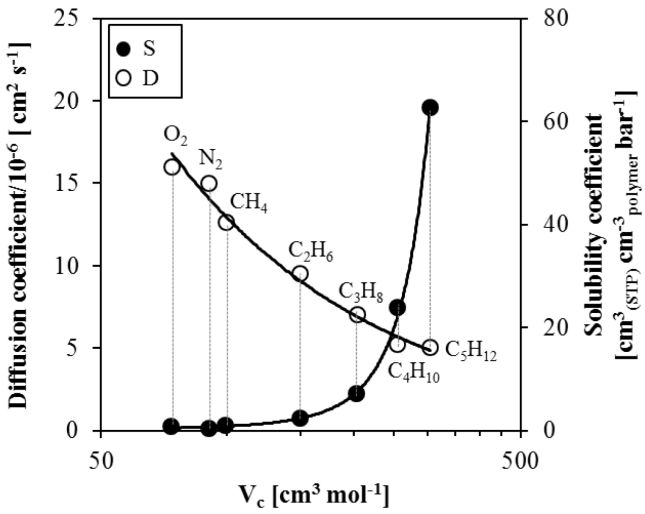

Figure 2.4 Diffusion and solubility coefficients of several components in silicon rubber at 30 ºC. Reproduced from [63].

Free-volume model

The concentration, temperature and pressure dependency of pure gas permeance in a polymer material is described by the free-volume model developer by Fang et al. [73]:

$$L_i = L_{i,\infty}^{0} \exp\left[-\frac{E_{i,act}}{R\,T} + m_{i,0}\, f_{i,m} \exp(m_{i,T}\, T)\right] \tag{2.26}$$

where $L_{i,\infty}^{0}$ is the infinite dilution permeance, which is the permeance in the limit of zero fugacity, for a given temperature, $E_{i,act}$ is the activation energy, $m_{i,0}$ and $m_{i,T}$ are parameters in the free-volume model, and $f_{i,m}$ is the mean fugacity.

However, Equation 2.26 describes only the interactions of a pure gas with the polymer matrix and does not describe the influence of the presence of other components in the gas mixture on the mass transfer [63]. An extension of this model was suggested to sufficiently predict multicomponent permeation behavior as follows [63, 67, 75]:

$$L_i = L_{i,\infty}^{0} \exp\left[-\frac{E_{i,act}}{R\,T} + \sum_{j=1}^{nc}\left(\frac{\sigma_i}{\sigma_j}\right)^2 m_{j,0}\, f_{j,m} \exp(m_{j,T}\, T)\right] \tag{2.27}$$

where σ *is* the diameter of molecule.

Free-volume model is generally used to correlate experimental permeation data [63]. The empirical relation given below is used to correlate permeation behavior of a pure gas in a polymer using least-square fit of the experimental data [76, 77]:

$$P_i = P_i^{0} \exp(m_i\, f_{i,m}) \tag{2.28}$$

with

$$f_{i,m} = \frac{(f_{i,F} - f_{i,P})}{2} \tag{2.29}$$

where P_i^0 and m_i are constant at a certain temperature.

Temperature dependency of permeability, solubility and diffusion coefficient

In most cases, the effect of temperature on gas permeability, solubility and diffusion is described by Arrhenius equation with a reasonable approximation [51, 78, 79]:

$$P_i = P_0 \exp\left(-\frac{E_p}{RT}\right) \tag{2.30}$$

$$S_i = S_0 \exp\left(-\frac{\Delta H_S}{RT}\right) \tag{2.31}$$

$$D_i = D_0 \exp\left(-\frac{E_d}{RT}\right) \tag{2.32}$$

Since permeability is calculated by multiplying solubility and diffusivity, the following expression is obtained:

$$E_p = E_d + \Delta H_S \tag{2.33}$$

where, P_0, S_0, and D_0 are the pre-exponential constants and E_p, ΔH_s, and E_d are the experimentally determined activation energy for permeation, enthalpy of sorption, and activation energy of diffusion.

2.4.6 Other transport effects

In order to estimate the membrane separation performance, mass transport in the membrane needs to be taken into account. However, additional mass transfer resistances, such as concentration polarization on the feed and permeate side of the membrane, mass transfer resistance of the support layer, and pressure lose, can diminish the potential of a membrane and should be considered in process design as well [80].

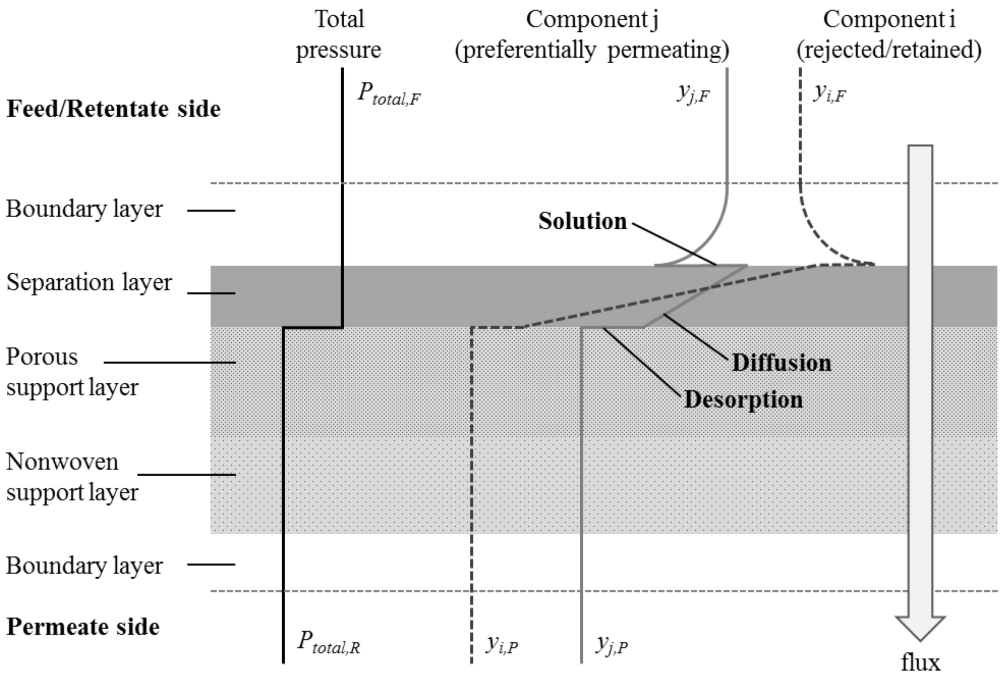

Figure 2.5 Total pressure and concentration profiles of a binary gas mixture through a polymeric composite membrane. Reproduced from [63].

Mass transport of components in a binary gas mixture through a thin-film polymeric composite membrane by solution-diffusion mechanism considering concentration polarization was illustrated by Ohlrogge et al. [63]. For a better understanding, a reproduced graph showing the total pressure and and concentration profiles (identical to partial pressure profiles) of the components through the membrane is given in Figure 2.5. During permeation two boundary layers are formed being on the feed and permeate side of the membrane. Depending on the velocity of the feed flow, the feed boundary layer is enriched by the slower permeating component (in other words; rejected or retained component) to a certain extent. This is accompanied by the corresponding decrease of the preferentially faster permeating component and creates an additional resistance for that component. As a result, both permeability and selectivity reduce. Formation of concentration gradients on both sides of the membrane due to the

different permeation rates of the components is called concentration polarization. The effect of concentration polarization is reduced with increasing feed gas velocity and it is increased with increasing membrane thickness. The concentration polarization on the permeate side is negligible.

2.5 Mixed-matrix membranes

Ideally, membranes should exhibit high selectivity and high permeability. A high permeability decreases the amount of membrane area needed and the capital costs of the membrane unit. A high selectivity results in a higher purity of the product. In 1991, Robeson [12] did an intensive literature survey and collected a large number of available permeation data of different gas pairs in polymeric membranes. He plotted selectivity versus permeability of many polymeric membranes for several binary gas mixtures and found that there was an upper limit to the performance of polymer membranes later referred to as Robeson's upper bound. This trade-off is one of the biggest problems faced by pure polymeric membranes, which mostly limits their economical applications in industries. A new approach was needed to enhance separation properties of the membranes and to produce cost-effective and defect-free membranes above the upper bound. Over the years, research in polymer materials led to a slight upward shift of the upper bound as indicated by Robeson in 2008 [81]. Furthermore, several investigations have been performed on how the upper bound is connected to the membrane properties [82]. In Figure 2.6, Robeson upper bound for CO_2/CH_4 gas pair in 1991 and 2008 are compared. Many polymers have been researched over the years leading to a slight increase in data points. Only a few new polymers are able to surpass the upper bound. Thermally rearranged polymers (TR polymers) comprising structural improvement are also presented in this graph by the author showing exceptional CO_2/CH_4 separation capabilities.

The latest membrane morphology, taking a different approach, is mixed-matrix membranes (MMM). In an MMM inorganic particles are dispersed in the polymer layer of the membrane [13, 15, 18, 48, 49, 83-87]. The strategy for the development of mixed-matrix membranes is to combine the advanced features of polymeric membranes and inorganic materials into one composite membrane. The solid inorganic particles, which can be porous or non-porous, are called the dispersed phase and the polymer matrix where they are incorporated in is called the continuous phase. A typical composite dense MMM includes dispersed phase embedded in an appropriate polymer matrix, which is coated on a porous support structure. Figure 2.7 illustrates such an MMM cast on a highly permeable support structure that consists of an upper porous polyester (PE) layer and a carded web bottom layer of polyacrylonitrile (PAN). The continuous phase is typically a polymer and selected due to its low cost and easy processability. Some of the most common polymeric materials are PDMS, POMS, PSU and polyimides. The dispersed phase inorganic materials include zeolite, activated carbon, microporous molecular sieves, graphite, carbon nano-tubes, or metal organic frameworks (MOF). These inorganic materials can provide an attractive improvement of separation properties with their unique pore structure having molecular sieving ability, surface chemistry and mechanical strength [14, 15]. When these highly selective porous fillers are added to the polymer, MMMs have the potential to achieve not only higher permeability of the desired component, but also higher overall selectivity, compared to the pure polymeric membranes. Some of the recent researches with the MMM approach exceeded upper bound behavior [49, 88, 89]. However, some other researchers found worse performances due to different difficulties which might be encountered in preparation of MMMs [18].

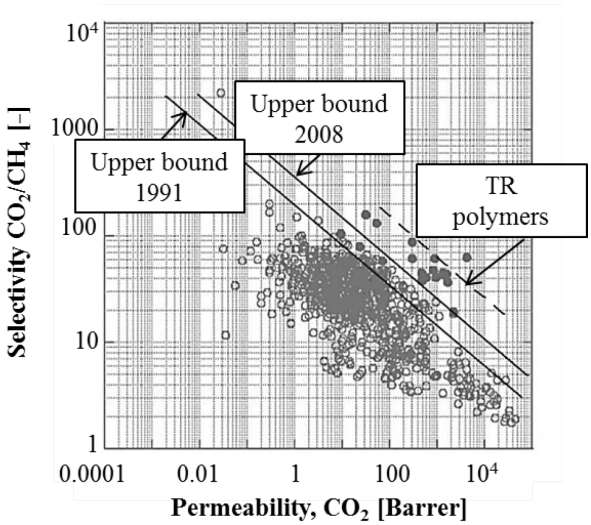

Figure 2.6 Robeson upper bound for CO_2/CH_4 separations [81].

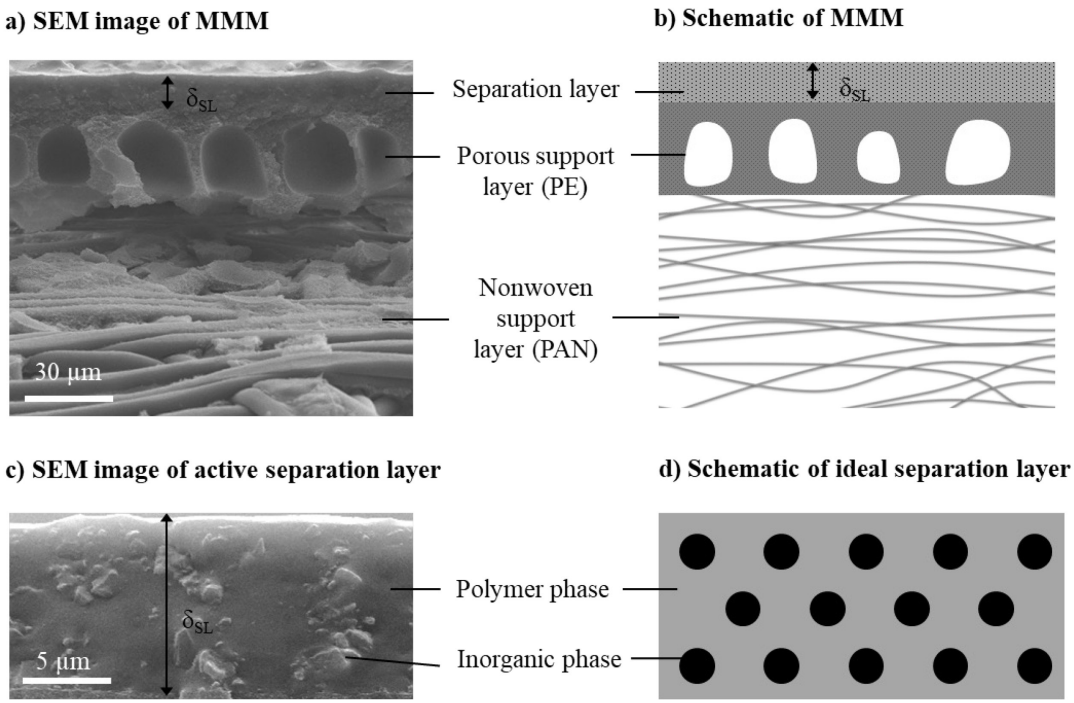

Figure 2.7 SEM image of MMM consisting of PDMS and activated carbon: (a) three-layer membrane composed of active separation layer (with thickness δ_{SL}), porous and nonwoven support layer (with 500x magnification), (c) active separation layer (with 1000x magnification). Schematic of: (b) a three-layer MMM, (d) an ideal separation layer.

2.5.1 Challenges and limitations in preparation of MMM

The main aim to produce MMMs is to overcome selectivity and permeability limitations by merging organic polymer and inorganic particle phases. However, production of MMMs has difficulties, such as poor particle distribution, weak contact of particles in the polymer matrix, or

inconvenient filler-polymer combination [18, 90-92]. A successful production can be achieved by solving both material selection and defect formation limitations. Despite a lot of research over the last 20 years, there are still many problems that are yet to be solved.

Among numerous studies, limited research has been specifically focused on MMM production for gas separation. The main scope of this work is to develop a reliable procedure for preparation of reproducible and defect-free laboratory-scale MMMs. Thus, the importance of the challenges that might come across in the membrane preparation procedure is below outlined.

Material selection

Material selection is the key parameter of forming successful MMMs. With the assumption of absence of defects, the minimum separation performance of the membrane can be predicted, because it depends on the selected polymer [92]. It is expected that the addition of a properly selected inorganic filler may increase separation performance [91]. An ideal separation layer of an MMM is achieved by matching appropriate polymer and the filler particles.

The separation performance of the selected polymer must be sufficient for the industrial applications and it must have mechanical stability during processing at various operation temperatures and pressures. Similarly, the complementary phase, which is the inorganic dispersed phase, plays an essential role to determine final separation properties of the MMM. If the selected polymer prefers solubility-selectivity, the overall separation performance can be enhanced when the dispersed phase possesses solubility-selectivity as well [93].

Interfacial morphology

In addition to the material selection, three interactions determine the formation of a successful MMM having defect-free morphology: polymer-solvent, polymer-particle, and solvent-particle [91]. The overall gas transport properties of the membrane strongly depend on that interaction between the selected polymer and the filler. A mismatch between polymer phase and dispersed phase can cause low performance. The following important morphological factors must be considered in preparation of advanced MMMs:

Blockage of the pores of the particles by polymer chains

One of the major difficulties discovered in early attempts of successful MMM formation occurs at the polymer-particle interaction, which is blockage of the surface region and/or external pores (macro pores) of inorganic filler particles [13, 53, 94, 95]. It describes the penetration of polymer chains into the particle pores when they are mixed. Depending on the pore size of inorganic fillers, the polymer chain can fill the pores in various degrees [37] and partial blockage may narrow a part of the pores [96]. In some cases, the partial blockage may improve the separation performance of a membrane if the reduced pore size is suitably small for the molecular sieving mechanism to occur [93]. On the other hand, the filler particles could be completely excluded from the transport process as a result of filling by the polymer chains, which do not allow gases to pass through the pores. Thus, effectiveness of the fillers reduces and no improvement in separation performance of the membrane could be obtained. In most cases, such a pore blockage occurs. Bhatia et al. [97] investigated the effect of irreversible trapped iodine molecules on adsorption isotherms of activated carbon and proved that the pore blockage alters the pore

structure and influences the dynamics of adsorption. Since blockage of the pores by polymer chains may completely eliminate the function of the inorganic filler, investigations are necessary to suppress this effect. There is strategies to hypothetically optimize polymer-particle interfaces for various material combinations [91, 95, 98].

Low adhesion between the polymer and the particle

Low adhesion is a factor that depends on the chemical nature of both materials. Due to several reasons, for instance the stress encountered from solvent removal during the membrane preparation, detachment of polymer chains from the filler surface leads to the formation of interface voids, resulting in unselective by-pass in the selective layer of the membrane. This morphology is called “sieve in a cage” [13, 18, 86, 90].

Polymer chain rigidification

The gas transport around the particles may be altered due to the inhibition of polymer chain mobility in a local region. This effect is called polymer chain rigidification. This phenomenon can be hindered by increasing the mobility of polymer chains [13, 93]. A proper selection of the polymer phase maintains flexibility during membrane preparation and determines the interfacial morphology of the MMMs. Rubbery polymers have advantages due to their flexibility during membrane preparation and low glass transition temperatures.

Dispersion of particles

The main aim of using MMMs instead of pure polymeric membranes is to facilitate the superior gas transport properties of inorganic particles. Therefore, an ideal MMM requires sufficient amount of inorganic particles in polymer matrix as well as good dispersion of those particles in the polymer matrix. Homogenous dispersion of particles in the polymer matrix is essential to achieve enhanced selectivity.

At relatively low loadings, particles can be considered as better distributed. At higher loadings, particles tend to come together and form agglomerates [91]. Those agglomerates may connect each other and create continues pathways. When the loading of particles is higher than a critical volume that allows creating channels of particles in the polymer layer is called percolation threshold [93]. These extra channels act as voids that gas molecules transport through, thus, selectivity of the membrane reduces.

Plasticization

Plasticization is a pressure-dependent phenomenon that refers to the increase of penetrant diffusivity resulting from increased FFV in the polymer matrix due to the presence of penetrant molecules. Especially, higher hydrocarbons such as *n*-C_4H_{10} plasticizes the polymer matrix with its high concentration in polymer. In many works, it is reported that the plasticization can dramatically affect the separation performance of a polymer membrane to undesirable values. However, Lin *et al*. [99] demonstrated in their study that plasticization can further improve polymer membrane separation performance, in contrast to the general view.

Thickness

Apart from the ability to control the rates of permeation of different gases (selectivity), a membrane also should have a high rate of permeation (permeability). Since the rate of permeation is inversely proportional to the membrane thickness, a membrane has to be very thin in order to be economically competitive. The size of the particles relative to the final thickness of the membrane has to be considered.

2.5.2 Prediction of MMM performance

Great effort has been made in the past to develop models to predict permeation properties of MMMs as functions of the permeabilities of the continuous and dispersed phases. Dong et al. [93] revised the existing models and they pointed out that most of the available models deal with MMMs with ideal morphology assuming no defects in the membrane structure. The existing models for permeation through MMMs are basically adapted from thermal and electrical conductivity models to permeation in composite membranes since the gas transport through a MMM is analogous to the dielectric properties of composite materials [100, 101].

In 1873, Maxwell [102] developed a model to simulate the electrical conductivity of composite materials, which has been the mostly applied model to predict effective permeability of a MMM. The Maxwell equation calculates the overall permeability of a MMM P_{eff}, as a function of the volume fraction of the dispersed phase $\emptyset_d$, permeability of the dispersed inorganic particle phase, P_d, and the permeability of the continuous polymer phase P_c, as given by the following explicit function:

$$P_{eff} = P_c \frac{2(1-\emptyset_d)+(1+2\,\emptyset_d)(P_d/P_c)}{(2+\emptyset_d)+(1-\emptyset_d)(P_d/P_c)} \tag{2.34}$$

The Maxwell equation is used for well-distributed, homogeneous and non-interacting solid spherical particles as dispersed phase and it describes the permeability well when the dispersed phase fraction $\emptyset_d$ is less than about 0.2. Input parameters of the equation permeability of the continuous phase P_c, and the dispersed phase fraction $\emptyset_d$ can be determined. However, permeability of the dispersed phase P_d cannot be measured since the activated carbon particles used in this work are in powder form. Therefore, the Maxwell equation cannot be used in this work.

Bruggeman model [103], Lewis–Nielsen model [104], and Pal model [105] are the well-known improvements of the Maxwell model recently discussed by Dong et al. [93]. Bruggeman model can be used for slightly higher particle loadings than the Maxwell model but it is inadequate to estimate the permeability when the particle loading approaches the maximum level. The other limitations of this model are that the effect of particle morphology is ignored and the implicit function of the model requires a numerical resolution. Lewis–Nielsen model and Pal model are capable to predict permeability at maximum particle loadings. Additionally, in these models the influences of the particle size distribution, particle shape, and aggregation of particles are considered. The Lewis–Nielsen model is easy to solve since it is an explicit function, whereas the Pal model is an implicit function. These existing models for permeation still have certain limitations and disadvantages because they do not take into account deterministic parameters for a sorption selective MMM like sorption characteristics, mass transfer coefficient and operation conditions.

2.5.3 Literature review on MMM

In the past 30 years, a vast number of polymers has been evaluated as potential membrane materials. The aim was to understand the structure-property relationship of these materials to produce tailor-made polymeric membranes for specific fields of application. Although this approach produced useful empirical correlations, relatively few attempts succeeded to increase gas separation performance of these polymeric membranes [24]. Therefore, membrane researchers attempted to develop MMMs to obtain high selectivity by combining the processability of polymers and the separation properties of inorganic materials.

Several inorganic materials such as zeolites, carbon molecular sieves (CMS), metallic organic frameworks (MOF), and lamellar materials are used in MMMs [54, 93]. Among them, zeolites are good candidates for MMMs with their defined pore structure. Kulprathipanja et al. [106] studied zeolites for the first time as inorganic particles in the concept of MMMs. Afterwards, various researchers studied MMMs in which several types of zeolites were incorporated as adsorptive fillers into polymeric continues phase [49, 84, 89, 91, 98, 107-114]. Zeolites have been evaluated in combination with both rubbery polymers and glassy polymers for gas separation. In terms of separation performance of MMMs containing zeolite, some types of zeolites showed promising results. For instance, Süer et al. [107] reported 2 times higher CO_2 permeability and CO_2/N_2 selectivity with 50 wt% zeolite-4A filled polyethersulfone (PES) membranes. However, in the study of Duval et al. [114], zeolite-5A filled PDMS membranes led to decreased CO_2 permeability and unchanged CO_2/CH_4 selectivity. Despite some promising results reported, polymer/zeolite MMMs have not been commercially used due to their practical challenges like poor interfacial compatibility, no uniform dispersion at high loadings, polymer rigidification or pore blockage [24].

Only few studies used activated carbon (AC) as dispersed adsorbents in MMMs. Kusworo et al. [115] investigated PES/AC flat-sheet MMMs for O_2/N_2 gas separation. They reported increased O_2 pure gas permeability up to 5 wt% AC loading. Marchese et al. [116] characterized MMMs composed of acrylonitrile–butadiene–styrene (ABS) copolymer filled with two different activated carbons for CO_2/CH_4 separations. An increased permselectivity was observed with increasing carbon content in the polymer matrix. Anson et al. [117] determined CO_2 and CH_4 pure gas permeabilities in MMMs, which were prepared with ABS copolymer and two different activated carbons. For both ACs, they reported that pure gas permeabilities and CO_2/CH_4 permselectivities increase with increasing AC content in the ABS matrix. Although the MMMs showed increased performances, they did not exceed the Robeson upper bound. They also studied the effects of feed pressure and temperature on CO_2 and CH_4 pure gas permeabilities using the same material combinations. For both gases, permeabilities increased with increasing temperature from 20 to 50 °C. However, increasing the feed pressure showed no significant effect on permeabilities in the investigated range. H_2, N_2, O_2, CO_2 and CH_4 pure gas permeabilities were evaluated in MMMs composed of polyvinyl chloride (PVC) as continuous phase and a commercial activated carbon as dispersed phase by Garcia et al. [85]. They investigated the effect of particle content up to 60 wt% using both cross-linked and un-cross-linked MMMs and reported promising increments of pure gas permeabilities at relatively high particle loading. These researches showed that embedding of activated carbon particles into some polymer matrices increased the pure gas permeability and permselectivity of the selected gas pairs. This implies that activated carbon shows high potential as a new generation of inorganic filler for forming high performance MMMs. However, these studies did not evaluate the mixed gas selectivities of the MMMs, which determine the actual separation performances for industrial membrane applications.

Mushardt et al. [42] investigated separation performance of MMMs composed of POMS and AC with two different mean particle sizes (d_{50} = 3.5 and 1.5 µm) for binary gas mixtures of 5 vol% *n*-C_4H_{10} in CH_4 at different feed pressures. For both ACs, mixed gas selectivity increased with increasing the feed pressure at a constant temperature of 30 °C. They also investigated the influence of particle content up to 40 wt% and results showed that the optimum particle content was 20 wt%. In addition, Mushardt et al. [54] evaluated the separation performance of the same MMMs of POMS and AC (with d_{50} = 3.5 µm) for the binary gas mixtures *n*-C_4H_{10}/CH_4 under varying operating conditions (feed and permeate pressure, temperature, feed gas composition). Selectivity of the MMMs were increased with increasing feed pressure, increasing permeate pressure, and increasing the concentration of *n*-C_4H_{10} in the feed mixture. These two studies of Mushardt et al., within the scope of the MMMfGS project, present the investigations on effect of particle size and particle loading on membrane performance as well as the influence of operating parameters. Experimental results showed a decrease in pure gas permeance but an improvement of mixed gas selectivity with optimum activated carbon content of 20 wt%.

Within the scope of the MMMfGS project, Kramer [20] also developed a mechanistic model for the permeation process in silicon polymers and AC. For the purpose of model adjustment and validation, she carried out experimental investigations of pure and mixed gas permeation of *n*-C_4H_{10} and CH_4 in pure polymers of PDMS and POMS, PDMS/AC MMMs and POMS/AC MMMs in addition to measurements of solubility and adsorption equilibria. Experimentally determined *n*-C_4H_{10} and CH_4 permeabilities in MMMs were always lower than those in pure polymer membranes, but MMMs showed 15% higher selectivities than pure polymer membranes. Kramer's innovative approach for modeling is based on one-dimensional discretisation of the separation layer and can also be applied for other systems. In her work, mass transfer mechanisms within the MMMs were identified, membrane materials were evaluated and the influences of certain parameters on membrane performance were forecasted. It was possible to achieve a very good agreement with experimental results of pure polymer membranes of PDMS and POMS, and POMS/AC MMMs. However, an adaptation of model to PDMS/AC MMMs was not feasible due to the assumed change in structure of PDMS in MMM formation.

Polymeric membranes were evaluated for the separation of hydrocarbons from natural gas. However, in gas separation literature, only few researches focused on the preferential separation of condensable hydrocarbons such as *n*-C_4H_{10} from permanent CH_4 gas streams with MMMs. For instance, Schultz and Peinemann [45] tested *n*-C_4H_{10}/CH_4 selectivity in more than 40 polymers. Yave et al. [43] investigated *n*-C_4H_{10}/CH_4 separations with poly(4-methyl-2-pentyne) (PMP)/TiO_2 hybrid nano-composite membranes and observed an improvement of *n*-C_4H_{10} pure gas permeability and *n*-C_4H_{10}/CH_4 mixed gas selectivity. Khanbabaei et al. [118] studied pure and mixed gas *n*-C_4H_{10} and CH_4 gas permeation in PDMS nano-composite membranes with different amounts of fumed silica. They reported 38% and 30% enhancement of *n*-C_4H_{10} pure gas permeability and mixed gas selectivity for binary mixtures of 3 vol% *n*-C_4H_{10} in CH_4 with 11 wt% filler loading in comparison to the membranes prepared from unfilled PDMS.

Regarding membrane preparation procedures, Aroon et al. [15] reviewed the preparation techniques of MMMs and proposed methods to overcome interface defects. Chung et al. [13], Dong et al. [93], and Mahajan et al. [90] discussed the challenges and limitations of forming defect-free successful MMMs with high separation performances. These reviews proposed strategies to tackle challenges and to match the necessary transport characteristics of materials to form high performance MMMs for gas separation. Mahajan and Koros [91] defined a protocol to prime the particle surface with several solvents. SEM images clearly indicated improvement on

the interface of the primed particles; however, their MMMs composed of polymer and zeolite exhibited reduced permeability and selectivity. Duval et al. [98] reported similar observations in their study with surface modified zeolite filled glassy polymer membranes. Li et al. [95] proposed a coupling agent, (3-aminopropyl)-diethoxymethyl silane (APDMES), to create a nano-scale distance between polymer chains and particle surface in polyethersulfone/zeolite MMMs to reduce the partial pore blockage and achieved higher gas permeability and selectivity with modified polymer-particle interface.

Key requirements of membrane preparation that would be necessary to achieve full potential of MMM concept can be summarized as: proper material selection for suitable combination of polymer and filler particles, sufficient amount of filler particle loading into the polymer matrix, priming the filler particles, good preparation of polymer/filler particle suspension to avoid particle agglomeration, and optimization of interface morphology to avoid nonselective voids, pore blockage and chain rigidification. However, these strategies are not evaluated for MMMs made of PDMS and activated carbon.

2.6 Non-ideal gas behavior

The hydrocarbon separation processes are generally operated at different pressures. Increasing the feed pressure creates the driving force for the permeation to occur. Normally, the driving force increases proportionally with increasing pressure. In case of high-pressure applications, especially when the pressure is higher than 10 bar, the driving force for permeation is not anymore proportional due to the real gas behavior [119]. For such cases, partial pressure difference between the feed and the permeate side of the membrane has to be replaced by partial fugacity difference for the calculation of permeability of a component [42, 63, 119].

For a better understanding, an example from this work was presented here. Using mixed gas experimental results of a binary mixture of 4 vol% *n*-C_4H_{10} in CH_4 through unfilled PDMS membrane, the ideal gas and the real gas behavior were compared. Experiments were conducted at 10, 20, and 30 bar feed pressures at 20 °C. The permeate pressure was atmospheric (p_P = ca. 1 bar). Figure 2.8 shows the driving force for permeation of *n*-C_4H_{10} and CH_4 as a function of feed pressure, which was calculated based on the difference of partial pressures and fugacities at feed and permeate side for each pressure step. The driving forces of both permeating components reduced due to the real gas behavior. The influence of the real gas behavior was more pronounced for the faster permeating component *n*-C_4H_{10} and stronger for the permeation at higher feed pressures. This indicates that the influence of real gas behavior is not negligible when the hydrocarbon separations are performed at feed pressures higher than 10 bar. For both gases, the slope of the ideal driving force remained constant due to the proportionality. On the other hand, the slope of the real driving force reduced as the pressure increased, particularly for *n*-C_4H_{10}. It is inferred that the driving force cannot be further increased by increasing feed pressure.

Figure 2.9 compares ideal selectivity and real selectivity, in other words, the effective selectivity. The ideal selectivity is determined by the difference of feed and permeate pressures and the permeate mole fractions of the components. The real selectivity is determined with consideration of real gas behavior dependent on difference of feed and permeate fugacities and the permeate mole fractions of the components. Apparently, the real selectivity increases with increasing feed pressure, while ideal selectivity slightly decreases. The reason for that is the fugacity coefficients

used to calculate partial fugacities in order to determine selectivity are smaller than 1, which results higher calculated permeability. These results are in agreement with Alpers et al. [119] and apparently, the permeability of a component should be calculated based on fugacity instead of pressure due to the strong non-ideality of *n*-C_4H_{10}.

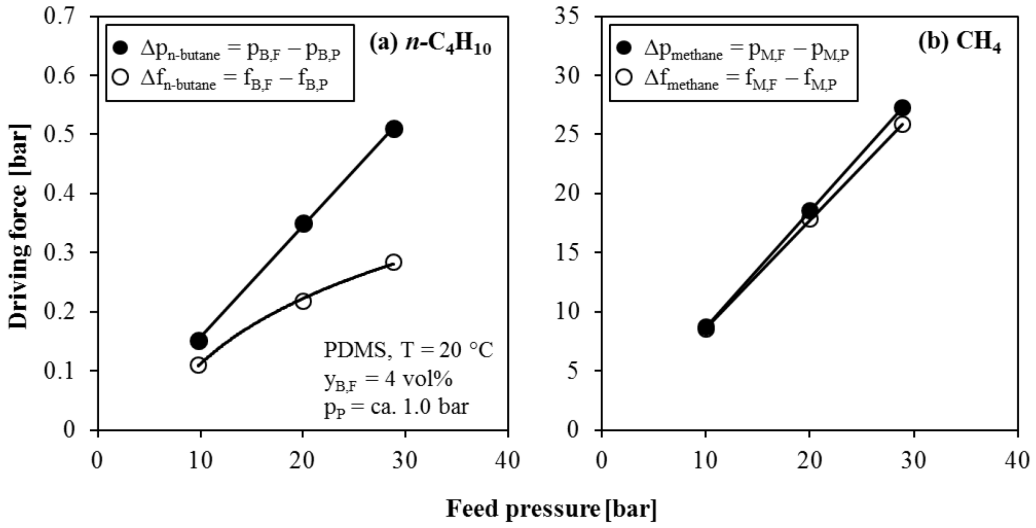

Figure 2.8 Calculated ideal and real driving force of (a) *n*-C_4H_{10} and (b) CH_4 in binary mixture of 4 vol% *n*-C_4H_{10} in CH_4 in a PDMS membrane at different feed pressures at 20°C.

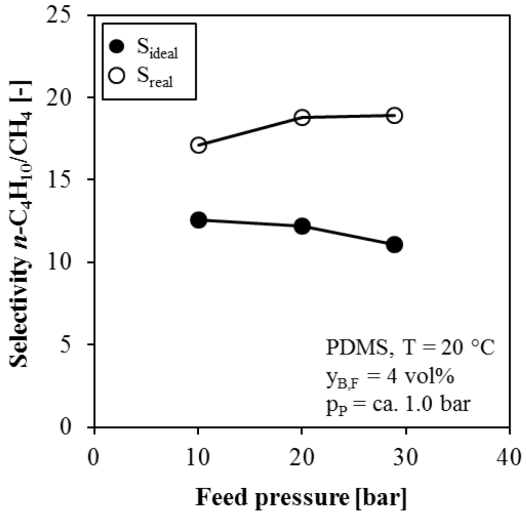

Figure 2.9 Calculated ideal and real selectivity of *n*-C_4H_{10}/CH_4 of a binary mixture of 4 vol% *n*-C_4H_{10} in CH_4 in a PDMS membrane at different feed pressures at 20°C.

2.6.1 Calculation of fugacity and fugacity coefficient

The fugacity coefficient is a function of temperature, pressure, and composition. An equation of state is a mathematical relation between volume, pressure, temperature and composition. Thus, fugacity can be calculated by means of an equation of state (EOS), for instance the Soave–

Redlich–Kwong EOS or the Peng–Robinson EOS. The difficulty is establishing a reliable equation of state for gas mixtures. In literature, many EOS exist. Unfortunately, most of them are either totally or partially empirical where the constants of the EOS have just approximate physical significance. The virial equation of state provides physical significant parameters [120]. In this work, the fugacity calculations follow Lüdecke and Lüdecke [121] and virial coefficients are calculated according to Kaul and Prausnitz [122].

For a pure component, the fugacity of the component is obtained from multiplying the pressure p by fugacity coefficient ϕ:

$$f = p\,\phi \tag{2.35}$$

Fugacity coefficient can be expressed in terms of independent variables of p and T as follows:

$$\ln \phi = \frac{1}{RT}\int_0^p \left[v_m - \frac{RT}{p}\right] dp \tag{2.36}$$

where v_m is the molar volume of the component. By using the virial equation according to the second coefficient, the fugacity coefficient becomes:

$$\phi = \exp\left(B\frac{p}{RT}\right) \tag{2.37}$$

In a mixture, the fugacity of a component i is obtained via multiplying the partial pressure of the component p_i by fugacity coefficient of the component ϕ_i:

$$f_i = p_i\,\phi_i = y_i\,p\,\phi_i \tag{2.38}$$

The fugacity coefficient of a component in a mixture is defined similar to pure gas as follows:

$$\ln \phi_i = \frac{1}{RT}\int_0^p \left[v_{i,m} - \frac{RT}{p}\right] dp \tag{2.39}$$

where $v_{i,m}$ is the partial molar volume of the component.

By performing the indicated differentiations and integrations, the fugacity coefficient yields:

$$\phi_i = \exp\left[\left(2\sum_{j=1}^{m} y_j B_{ij} - B_{mix}\right)\frac{p}{RT}\right] \tag{2.40}$$

where B_{ij} is the second virial coefficient that takes the interactions between two molecules into account.

The great advantage of the virial equation of state is its theoretical relation between the virial coefficients and the intermolecular forces. Thus, the parameters have physical significance, unlike the parameters of other fully empirically derived equations of state. Furthermore, the virial equation can be directly extended to mixtures. For a binary mixture of two components of *i* and *j,* there are three types of molecular interactions, *i-i*, *j-j*, and *i-j*. Including all possible molecular interactions, the virial coefficient of a binary mixture is given by:

$$B_{mix} = \sum_{i=1}^{m} \sum_{j=1}^{m} y_i y_j B_{ij} \tag{2.41}$$

In a binary gas mixture, fugacity coefficients of the components are calculated as follows:

$$\phi_i = \exp\left[\left(2\left(y_i B_{ii} + y_j B_{ij}\right) - B_{mix}\right)\frac{p}{RT}\right] \tag{2.42}$$

$$\phi_j = \exp\left[\left(2\left(y_i B_{ij} + y_j B_{jj}\right) - B_{mix}\right)\frac{p}{RT}\right] \tag{2.43}$$

with

$$B_{mix} = y_i^2 B_{ii} + 2\, y_i y_j B_{ij} + y_j^2 B_{jj} \tag{2.44}$$

where B_{ii} is the second virial coefficient of two molecules of pure component i, B_{jj} is the second virial coefficient of two molecules of pure component j, and B_{ij} is the second virial coefficient of molecular interactions of one molecule of component i and one molecule of component j, which is also called cross coefficient.

2.6.2 Calculation of second virial coefficients

Kaul and Prausnitz [122] present a simple method for estimating second virial coefficients of gas mixtures containing both small and large nonpolar molecules. The following expression is used in this work to calculate second virial coefficients of gas mixtures containing *n*-butane and methane:

$$\frac{B_{ij}}{b_{0ij}} = 1 - \left[g_{ij}^3 - 1\right]\left[\exp\left(\frac{\epsilon_{ij}}{kT}\right) - 1\right] \tag{2.45}$$

where,

$$b_{0ij} = \frac{2\pi N_A}{3}\sigma_{ij}^3 \tag{2.46}$$

$$g_{ij} = \frac{\sigma_{ij}+2}{\sigma_{ij}} \tag{2.47}$$

where N_A is the Avogadro's number, k is the Boltzmann's constant, ϵ is the intermolecular potential energy (or well depth), and σ is the diameter of molecule.

The cross coefficients of the diameter of the molecule σ_{ij} and the intermolecular potential energy ϵ_{ij} are calculated by the arithmetic mean and geometric mean, respectively, as follows:

$$\sigma_{ij} = \frac{\sigma_i + \sigma_j}{2} \tag{2.48}$$

$$\epsilon_{ij} = \sqrt{\epsilon_i \epsilon_j} \tag{2.49}$$

Parameters used to calculate second virial coefficients according to Kaul and Prausnitz [122] are listed in Table 2.1

Table 2.1 Parameters used to calculate second virial coefficients.

Component	σ_{ij} [Å]	ϵ_{ij}/kT [K]	Temperature range [K]
CH_4	3.35	141.25	110-600
n-C_4H_{10}	5.14	425.38	250-560
n-C_4H_{10}/CH_4	4.24	245	298-510

3 Experimental

3.1 Materials

3.1.1 Polymer phase

PDMS was selected as the continuous polymer phase of the MMMs to be prepared. PDMS was primarily used as a solution in solar energy installations and as a dielectric coolant [123]. In the course of time, many industrial applications started to use PDMS due to its various advantages. For instance, it has been commonly used for production of fiber-optic cables [124] and by paper-coating industry [125]. Today, PDMS is one of the most frequently used rubbery polymers in membrane preparation, which enables solubility-selective separations. Mechanical properties of PDMS offer several advantages in membrane preparation. Low glass transition temperature (T_g = – 123 °C) and flexibility at room temperature make its polymer chains easy to surround the inorganic filler particles during membrane preparation [15, 89]. So far, many studies have been carried out regarding its transport properties for pure and binary gas mixtures [51, 52, 118].

POMS is another state of the art polymer, which is a derivative of PDMS with one of the methyl groups substituted by an octyl group (Figure 3.1). POMS exhibits high selectivity for higher hydrocarbon separations [42, 45, 54]. In this work, the main focus is to develop MMMs consisting of PDMS and activated carbon. Additionally, pure and mixed gas performances of composite membranes of POMS and activated carbon, which were produced at Helmholtz-Zentrum Geesthacht, were also determined and the influence of using a different polymer on membrane performance was investigated.

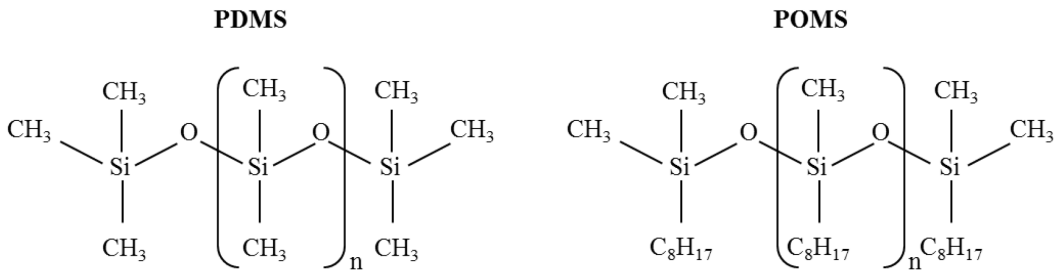

Figure 3.1 Chemical structure of PDMS and POMS.

Pure gas adsorption on PDMS

Sorption isotherms of pure *n*-C_4H_{10} in PDMS were experimentally determined by Kramer [20] at different temperatures (10, 25, 40 °C) at the Chair of Chemical and Process Engineering, Technische Universität Berlin. Besides, sorption isotherms of pure CH_4 in PDMS were experimentally determined at Institut für nichtklassische Chemie e.V. (INC) at Universität Leipzig at the same temperatures (10, 25, 40 °C). For pure gas sorption measurements, thick film

membrane samples produced with 9 wt% PDMS were used. Pure gas solubility coefficients were calculated using experimentally determined data by Kramer and INC and compared with the available data in literature.

Figure 3.2 (a) presents *n*-C_4H_{10} pure gas sorption isotherms in PDMS determined by Kramer. The maximum fugacity was 1.0 bar for *n*-C_4H_{10}. The isotherms are given as the mass of gas adsorbed per unit mass of PDMS as a function of fugacity. The isotherms are nonlinear and convex to the fugacity axis due to the great condensability of *n*-C_4H_{10}. Consequently, the solubility of *n*-C_4H_{10} into PDMS increases as *n*-C_4H_{10} fugacity increases, which is typical for sorption of highly soluble gases in rubbery polymers [52, 78, 126]. In Figure 3.2 (b), pure gas sorption isotherms of *n*-C_4H_{10} in PDMS are presented as a function of activity ($a = f/f_{sat}$). When sorption data is plotted as the function of activity, all data collapses on a single line. This means that the sorbed *n*-C_4H_{10} concentration in the PDMS is same at the same activity and it is independent of temperature or fugacity. The isotherm determined at 25 °C by Kramer was compared with previously reported isotherm by Raharjo et al. [52]. The data are in an excellent agreement with those reported.

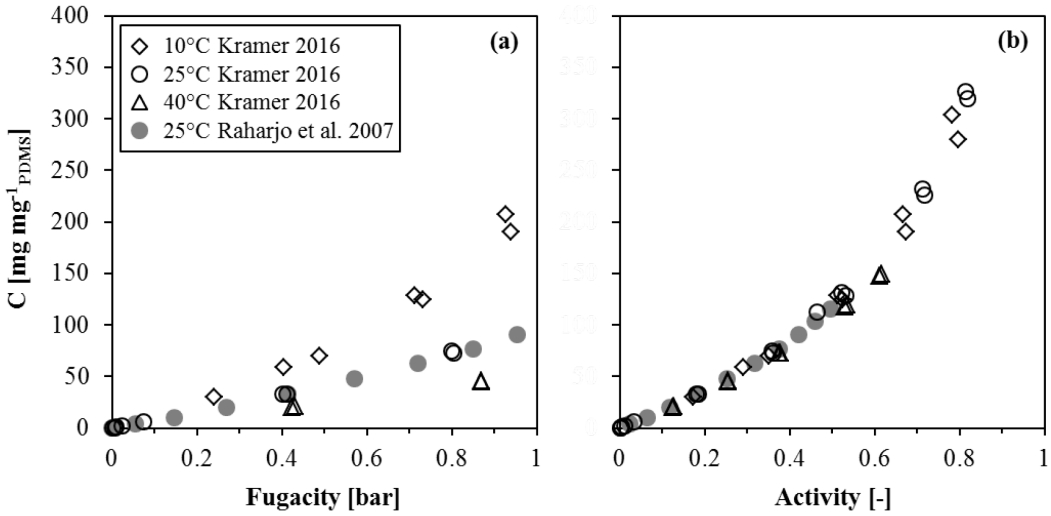

Figure 3.2 Pure gas *n*-C_4H_{10} sorption isotherms in PDMS at different temperatures (a) as a function of fugacity, (b) as a function of activity ($a = f/f_{sat}$).

A convex sorption isotherm to the x axis (pressure or fugacity) is a characteristic of vapor dissolution in polymers above their glass transition temperature (rubbery polymers) and the concentration of the penetrant gas in the polymer is often described by Flory-Huggins model [52, 63, 74, 127] as given:

$$\ln(a) = \ln \emptyset + (1 - \emptyset) + X(1 - \emptyset)^2 \tag{3.1}$$

with

$$\emptyset = \frac{cv}{22.414 + cv} \tag{3.2}$$

where; *a* is the vapor activity, ∅ is the volume fraction of the penetrant gas in polymer, *c* is the concentration of the penetrant gas, *v* is the partial molar volume of the penetrant, and χ is the Flory-Huggins interaction parameter.

For highly soluble gases like *n*-C_4H_{10}, the solubility coefficient is reported as the infinite dilution solubility, which is the solubility in the limit of zero fugacity:

$$S^{\infty} = \lim_{f \to 0} \frac{c}{f} \tag{3.3}$$

Figure 3.3 presents CH_4 pure gas sorption isotherms in PDMS determined by INC Leipzig at 10, 25, and 40 °C as a function of fugacity. The maximum fugacity was 38 bar for CH_4. The isotherms are linear, which is consistent with the previously reported CH_4 pure gas sorption isotherms in PDMS [126, 128]. Consequently, the solubility of CH_4 in PDMS is independent of fugacity and constant at a given temperature. The isotherm determined at 25 °C was compared with previously reported isotherms by Raharjo et al. [52] and the data are in an excellent agreement with those reported.

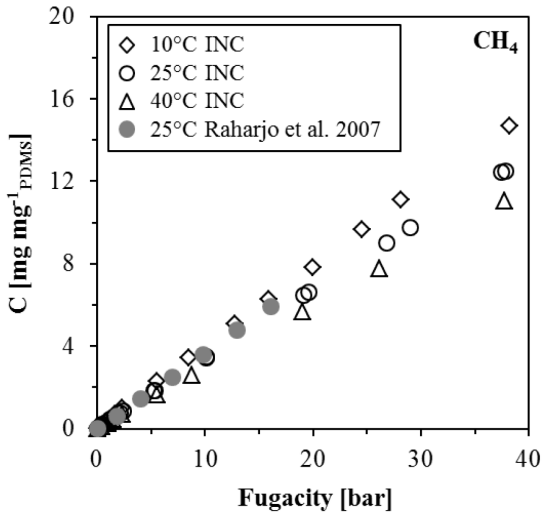

Figure 3.3 Pure gas CH_4 sorption isotherms in PDMS at different temperatures as a function of fugacity.

Sorption isotherms of light gases, such as CH_4, in rubbery polymers are essentially linear and characterized by Henry's law as follows [126]:

$$c = k_H f \tag{3.4}$$

where k_H is the Henry's gas constant.

The equilibrium solubility coefficient of CH_4 is reported as the ratio of the concentration of the dissolved gas in the polymer to the fugacity:

$$S = \frac{c}{f} = k_H \tag{3.5}$$

As indicated before, the temperature dependence of solubility is described as given by Equation 2.38:

$$S_i = S_0 \exp\left(-\frac{\Delta H_S}{RT}\right) \tag{2.38}$$

The ΔH_S values for n-C_4H_{10} and CH_4 were reported by Raharjo et al.[52] as -23 ± 0.5 and -5.8 ± 0.3 kJ mol^{-1}, respectively. The negative ΔH_S values indicate exothermic sorption process.

Table 3.1 shows n-C_4H_{10} pure gas solubility coefficients calculated based on infinite dilution value that was estimated from a second order polynomial fit of solubility versus fugacity. Pure gas CH_4 solubility coefficients are presented as the mean value. The selectivity solubility was calculated as the ratio of n-C_4H_{10} infinite dilution solubility coefficient to the CH_4 mean solubility coefficient.

Table 3.1 Pure gas n-C_4H_{10} and CH_4 solubility coefficients and n-C_4H_{10}/CH_4 solubility selectivity in PDMS, including comparison with previously reported data.

Literature	T [°C]	$S^{\infty}_{n\text{-}C_4H_{10}}$ [cm^3 $_{(STP)}$ cm^{-3} $_{polymer}$ atm^{-1}]	$S^{\infty}_{CH_4}$	$S^{\infty}_{n\text{-}C_4H_{10}}/S^{\infty}_{CH_4}$ [-]
Raharjo et al 2007 [52]	0	61 ± 2	0.63 ± 0.02	97 ± 4
This work	10	44.1	0.55	80.2
This work	25	31.2	0.46	67.8
Raharjo et al. 2007 [52]	25	26 ± 1	0.50 ± 0.02	52 ± 3
Raharjo et al. 2007 [52]	35	18.6 ± 0.6	0.47 ± 0.02	40 ± 2
Merkel et al. 2000 [74]	35	–	0.42 ± 0.01	–
This work	40	16.8	0.42	40.0
Raharjo et al. 2007 [52]	50	12.5 ± 0.4	0.42 ± 0.02	30 ± 2

3.1.2 Activated carbon

Activated carbon particles were used as inorganic dispersed phase. Activated carbon, in gas separation process, is the solid where adsorption takes place. It is produced specifically to achieve a very large internal surface, which makes activated carbon ideal for the adsorption. Pore structure and the pore size distribution of the activated carbon particles may vary depending on the production procedure. Previous experimental research showed that a large amount of micropores and a high specific surface area are advantageous to enhance transport capacity of the AC [42]. The characteristics of the precursor polymer affect the shape and the particle size distribution of the produced activated carbon. Polymeric precursors with low impurities are suitable for production of activated carbon and provide highly reproducible properties, a perfect round shape and a very clean product with pure surface [129]. Stable performance, lowest aging effects and excellent resistance against acidic and basic loads are ensured. Furthermore, the

adsorption characteristics of the activated carbon are highly dependent on the elemental composition and the surface chemistry.

Activated carbon particles can be produced in two variations: granular activated carbon and powder activated carbon. Granular activated carbon has larger particle size compared to the powder activated carbon. For this work, polymer-based spherical activated carbons in both variations were supplied from Blücher GmbH. Granular activated carbon with a mean particle size of 431 µm was used for pore blockage investigation. In the preliminary stage of activated carbon production, the spherical particles with a diameter of 100 µm were ground. This pre-ground product was subjected to grinding to produce a finer product with a narrow particle size distribution. The resulting product of spherical powder activated carbon particles with a mean diameter of 3.5 µm was used as inorganic filler during membrane preparation. Fine grinding particles and pre-ground spherical carbon particles show the same pore structures [20, 42].

Table 3.2 Characteristic properties of AC 100050 provided by Blücher GmbH.

Parameter	Value	Unit
Product name	100050	[-]
Mean particle size	3.5	[µm]
Mean pore size	18.68	[Å]
BET surface area	1335	$[m^2g^{-1}]$
External pore volume	0.1029	$[cm^3g^{-1}]$
Micro pore volume (pores < 2 nm)	0.5328	$[cm^3g^{-1}]$
Total pore volume	0.6357	$[cm^3g^{-1}]$
Bulk density	588	$[gL^{-1}]$

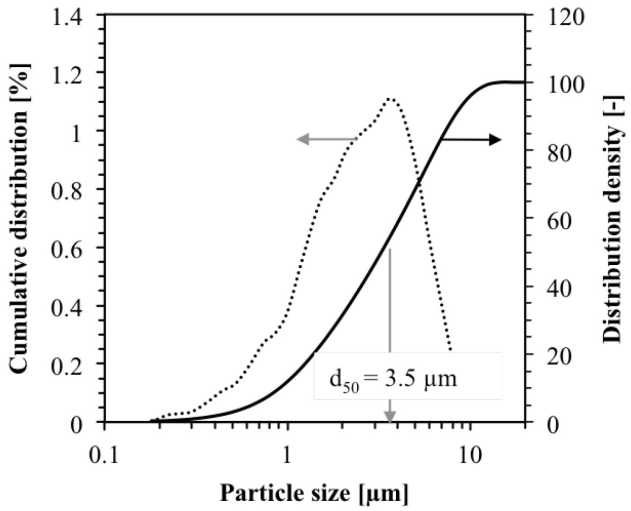

Figure 3.4 Particle size distribution of AC 100050 provided by Blücher GmbH.

Blücher GmbH produced two types of fine grinding activated carbon (AC 100050 and AC 100877) with different pore structures. Kramer [20] provided detailed information about pore structure, particle size distribution, and sorption properties of these activated carbon particles.

Kramer reported that AC 100050 had more pore volume than AC 100877. Additionally, both types of activated carbon particles show similar CH_4 sorption capacity. However, AC 100050 shows higher *n*-C_4H_{10} sorption capacity, which makes AC 100050 more solubility-selective. A combination of activated carbon AC 100050 and PDMS seems promising to develop MMMs with high performance. Thus, AC 100050 was selected as inorganic filler to from MMMs in this work. Informative physical properties of the selected activated carbon are summarized in Table 3.2. Particle size distribution of the activated carbon particles used in this work measured in accordance with DIN ISO 13320-1:1999-11 is given in Figure 3.4.

Gas adsorption properties

Sorption properties of the activated carbon particles are important as well as the pore structure when selecting activated carbon particles for specific purposes. In this investigation, sorption properties are crucial in order to predict the separation performance of the produced MMMs. Therefore, sorption isotherms of pure *n*-C_4H_{10} and CH_4 on activated carbon were experimentally determined with a magnetic suspension balance at INC Leipzig over the temperature and pressure range studied in this work.

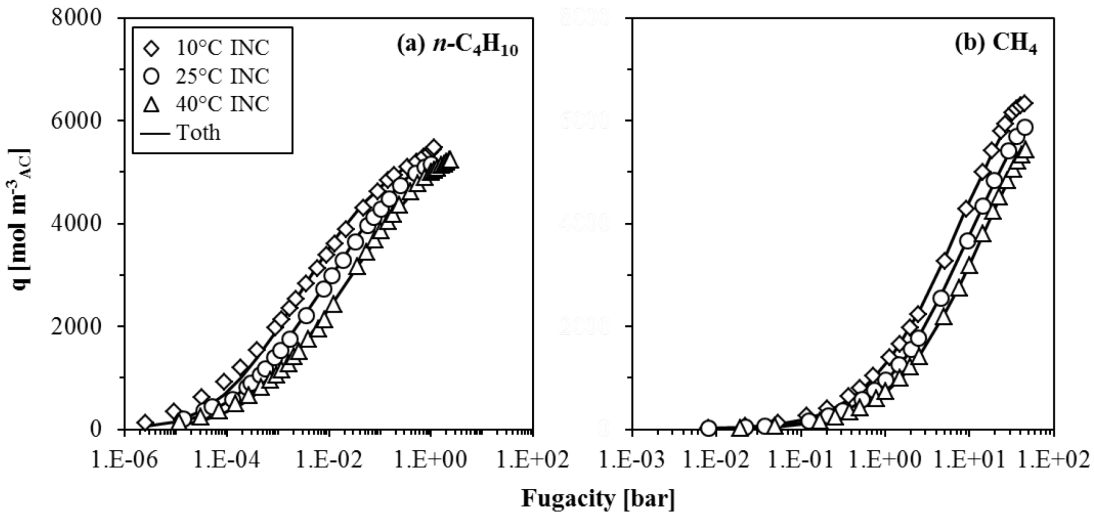

Figure 3.5 Pure gas sorption isotherms of (a) *n*-C_4H_{10}, (b) CH_4 on AC 100050 at different temperatures as a function of fugacity.

Figure 3.5 presents pure gas sorption isotherms of *n*-C_4H_{10} and CH_4 on activated carbon determined by INC Leipzig. The isotherms are given as the mass of gas adsorbed per unit volume of activated carbon as a function of fugacity. The maximum fugacities were 2.2 and 46.5 bar for *n*-C_4H_{10} and CH_4, respectively. The Tóth isotherm is commonly used to describe equilibrium hydrocarbon sorption on activated carbon, which is valid at low and high pressure ranges and it has the following form [42, 130-132]:

$$c = c_{max} \frac{bp}{[1 + (bp)^t]^{1/t}} \tag{3.6}$$

where c is the adsorbed concentration, c_{max} is the maximum adsorbed concentration, and b and t are temperature dependent parameters for specific adsorbate-adsorbent pairs with:

$$b = b_0 \exp\left[\frac{Q}{RT}\left(\frac{T}{T_0} - 1\right)\right] \tag{3.7}$$

$$t = t_0 + a\left(1 - \frac{T}{T_0}\right) \tag{3.8}$$

Table 3.3 presents the fitted temperature dependent Tóth parameters of *n*-C_4H_{10} and CH_4 pure gas equilibria.

Table 3.3 Tóth parameters of *n*-C_4H_{10} and CH_4 pure gas equilibria.

Adsorbate	T [°C]	C_{max} [mol m^{-3}]	b [bar^{-1}]	t [-]
n-C_4H_{10}	10	5924.3	5924.3	0.3761
	25	6589.7	5489.7	0.3140
	40	6718.1	2875.7	0.2981
CH_4	10	8265.5	0.2364	0.7011
	25	8059.5	0.1613	0.7094
	40	8222.8	0.1181	0.6785

Mushardt et al. [42] compared pure gas *n*-C_4H_{10} and CH_4 sorption on activated carbon and binary adsorption equilibrium of two different mixtures of *n*-C_4H_{10}/CH_4 (5 and 10 vol% *n*-C_4H_{10} in CH_4) predicted by the ideal adsorbed solution theory (IAST) using pure gas data at 25 °C. It was seen that the binary equilibria was between those pure gas data but closer to pure *n*-C_4H_{10}. This means that activated carbon shows high sorption selectivity for *n*-C_4H_{10}, which makes it an appropriate inorganic filler for the investigations in this work.

3.1.3 Zeolite

Alternatively, zeolite nanoparticles were selected as another type of inorganic filler dispersed in PDMS matrix in order to investigate the impact of using a different filler on membrane performance. Zeolites are porous crystalline alumino-silicates composed of Al_2O_3 and SiO_2. The pore size of zeolites extraordinarily effects the adsorption processes. Ions with diameters larger than the zeolite's pore size cannot pass though the entrance of the channel to absorb, which is why zeolites are also known as molecular sieves and are particularly useful in separating organic molecules. Zeolites have been used in many different fields due to their unique properties as adsorbents and they are pioneer inorganic particles used in concept of mixed-matrix membranes [84, 93].

The zeolite unit is electrically neutral if the framework atom is silicon while an aluminum atom results in a negative charge site [114]. An extra non-framework cation like hydrogen is needed to compensate the negative charge of the framework generated by replacement of a silicon atom by an aluminum atom [133]. SiO_2/Al_2O_3 ratio determines the number of cations and thus hydrophilicity of the zeolite framework. The presence of cations makes zeolites polar adsorbents

and hydrocarbons are more strongly adsorbed on polar adsorbents [114]. Concentration of cations strongly influences the gas selectivity [134, 135] and zeolites with high SiO_2/Al_2O_3 ratios have more thermal stability [134].

Zeolite Y produced by Zeolyst International was selected to use in this work due to its pore structure and high SiO_2/Al_2O_3 mole ratio. Zeolite Y exhibits the FAU (faujasite) structure. It has a 3-dimensional pore structure while pores are perpendicular to each other in the x, y, and z planes. It is beyond the scope of this work to give extended information on zeolite considered, however, some basic material specifications of the chosen zeolite particles are summarized in Table 3.4.

Table 3.4 Characteristic properties of zeolite Y particles [136].

Parameter	Value	Unit
Product name	Zeolite Y (CVB780)	[-]
Unit cell size	24.24	[Å]
Pore size	3 to 10	[Å]
Surface area	780	$[m^2g^{-1}]$
SiO_2/Al_2O_3 mole ratio	80	[-]
Nominal cation from	Hydrogen	[-]
Na_2O weight percentage	0.03	[%]
Micro pore volume (pores < 2 nm) [137]	0.32	$[cm^3g^{-1}]$

3.1.4 Support structure

An economically competitive membrane should have a very thin active separation layer. As the thickness of the active separation layer is reduced, so is the required membrane area and equipment cost. However, very thin active separation layers are fragile and need a mechanical support. Therefore, composite membranes are designed to have a very thin active separation layer on top that provides high selectivity and permeability, and a highly porous support structure that adequately supports the active separation layer during the formation and operation by exhibiting chemical, thermal and mechanical stability (Figure 3.6). The active separation layer can be either directly cast on the support structure or an intermediate gutter layer can be cast before the separation layer. The gutter layer is usually very thin, highly permeable but very low selective. Gutter layer provides a smooth surface and protects the membrane active separation layer [11].

In this work, the support structures (with and without a gutter layer) used for MMM preparation were produced and provided by Helmholtz-Zentrum Geesthacht. The Helmholtz-Zentrum Geesthacht developed a machine that allows casting of microporous support structure onto fleece material on rolls up to 70 cm width. These support structures were produced by a precipitation process from polymer solutions into water. They are highly porous and show an evenly smooth surface. The support structure was highly permeable and consists of an upper porous polyester (PE) layer and a carded web bottom layer of polyacrylonitrile (PAN). The porous support structure was made with dimethylformamide (DMF) and gamma-butyrolactone (GBL) as solvents. At the end of the production line of the support structure, it was dried in an oven after solvent exchange and almost no solvent was left. The second type of support structure with gutter layer was produced by casting relatively low concentrated PDMS solution (0.5 wt%) on top of it

with an ultrathin thickness (150-200 nm). The support structure with gutter layer was dried as well after casting, since PDMS solution involves solvents. More information is given by Mushardt [19].

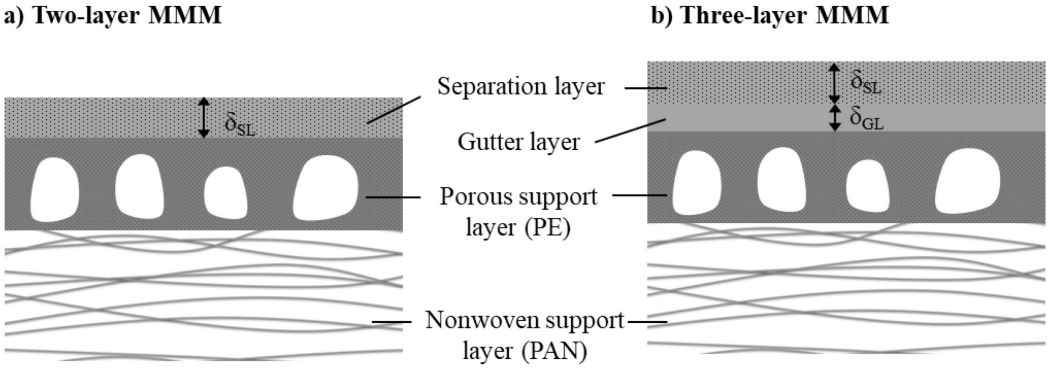

Figure 3.6 Schematic of composite MMM: (a) two-layer membrane composed of active separation layer (with thickness δ_{SL}), porous and nonwoven support layer, (b) three-layer membrane with gutter layer (with thickness δ_{GL}) between active separation layer and support.

3.1.5 Gases

The pure gases of *n*-C_4H_{10} and CH_4 were purchased from Air Liquide with high purity as presented in Table 3.5. The shape, effective size and length of the molecules considered in this work are demonstrated in Figure 3.7 according to the work of Mao and Sinnott [138].

The binary gas mixtures of *n*-C_4H_{10}/CH_4 with different concentrations used for the mixed gas experiments were prepared at the designed gas permeation experimental setup in the laboratory of the Chair of Chemical and Process Engineering, Technische Universität Berlin. Preparation procedure of the binary gas mixtures will be explained in section 3.4.3.

The gas mixture standards used for the calibration of the gas chromatography were purchased from Air Liquide and Linde. The gas mixture standards were used to achieve a calibration curve for *n*-C_4H_{10} concentration (between 1.024 and 74.50 vol% *n*-C_4H_{10}). The information about the gas mixture standards will be given in section 3.5.2.

Table 3.5 Gases used for pure and mixed gas experiments [139, 140].

Component	Producer	Cylinder type [L]	Filling pressure [bar]	Purity [vol%]
n-C_4H_{10}	Air Liquide	50	2.1	≥ 99.5 (N25) (Rest: H_2O, O_2, CO_2, H_2, N_2, iso-butane, and others)
CH_4	Air Liquide	50	200	≥ 99.5 (N25) (Rest: air, H_2O, CO_2, others)

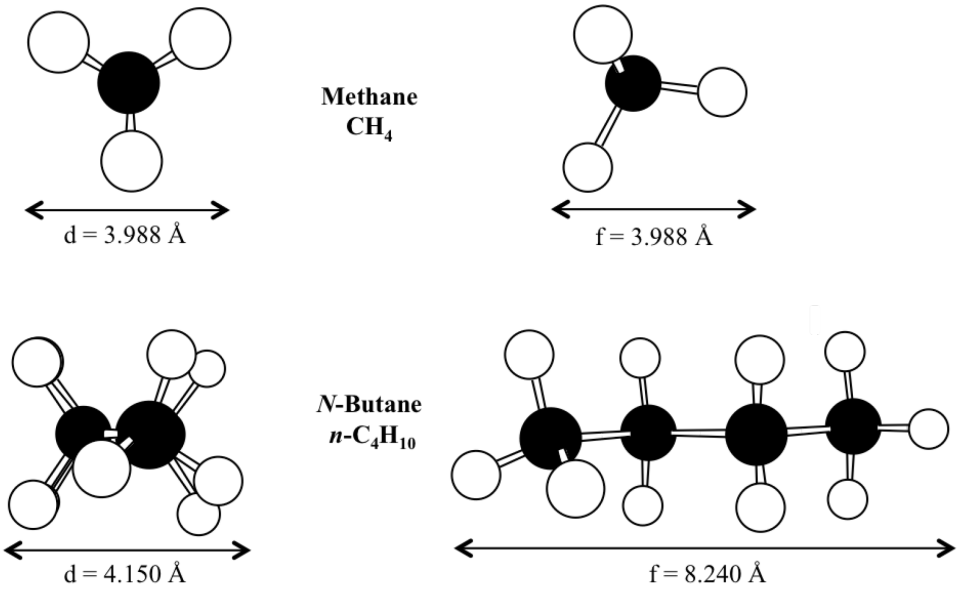

Figure 3.7 Molecular structures of *n*-C_4H_{10} and CH_4 (*d* is the molecular diameter and *f* is the molecular length). Reproduced from [138].

3.2 Membrane preparation

A typical MMM contains dispersed inorganic particles in a bulk polymer phase. Principally, the improvement in the separation properties of a MMM is attributed to positive effects of inorganic particles merged into the polymer phase. Selecting an inorganic dispersed phase with sufficient separation properties in terms of permeability and selectivity is of great significance. Another crucial point is, how to prepare morphologically defect-free and high-selective membranes by following several preparation steps.

In literature, preparation methods of the MMMs are very similar. Researchers described a general procedure for the preparation of laboratory scale MMMs in four fundamental steps as follows [5, 13, 141]:

1. preparation of a homogenous polymer and inorganic particle suspension,
2. casting the suspension onto a smooth support structure,
3. evaporation of the solvents, and
4. annealing the membranes at high temperatures to remove residual solvent.

Although this general procedure exists, there are no detailed procedures for the particular steps. The first step, in which the polymer-particle suspension is prepared, is the most curial step. Different methods are available and Aroon et al. [15] presented three different procedures:

1. The particles are first dispersed into the solvent and after stirring the polymer is added.
2. The polymer is first dissolved into the solvent and after stirring the inorganic particles are added.
3. The particles are dispersed into the solvent and the polymer is dissolved in a solvent separately. Following this, the particle suspension is added to the polymeric solution.

Despite a lot of research, influence of applying different methods during membrane preparation on the morphology and gas permeation properties of the produced membranes has not been evaluated yet. One of the goals of this work was to develop a reliable procedure for the preparation of reproducible and defect-free laboratory-scale MMMs and to overcome the particle agglomeration and pore blockage encountered during membrane preparation. Therefore, particular emphasis was put on each membrane preparation step.

The strategies to develop a reliable procedure for preparation of defect-free, high permeable and selective mixed-matrix membranes are presented in *Results and Discussion Part I*. In the following, the ultimate steps of membrane preparation obtained on the basis of these results are given.

For a better understanding, some terms used in this work during membrane preparation are briefly described and illustrated in Figure 3.8. *Batch* was used to describe the casting solution of either PDMS or a mixture of PDMS and activated carbon prepared at once. Depending on the amount of one batch of casting solution, one or more support structures were cast, each of them was called as *sheet*. After post-treatment of the membrane sheet in the oven, round membrane *stamps* were cut using a stamp cutter tool. Diameter of the stamp was appropriate for the membrane test cell at the gas permeation setup. In order to check reproducibility, membranes were produced in different batches, and morphology and the permeation behavior of several stamps of the prepared membranes were evaluated.

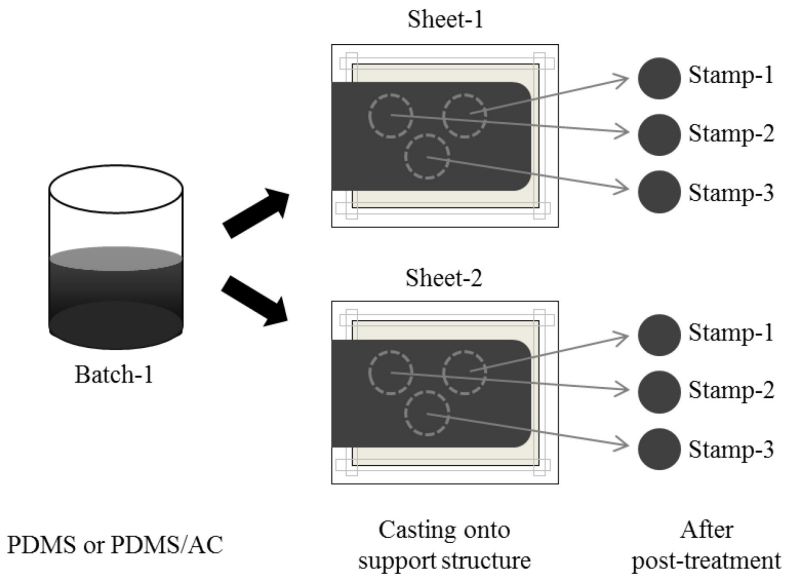

Figure 3.8 Description of the terms used during membrane preparation.

3.2.1 Preparation of PDMS membranes

Preparation of PDMS solution

PDMS solution was prepared using a pre-polymer *DEHESIVE® 944* purchased from Wacker Chemie AG, which was a solvent-based, cross-linkable, vinyl-containing silicone polymer (Si-V) consisting of 30 wt% active PDMS in toluene. The unfilled PDMS membranes and MMMs were

prepared using PDMS solutions at different concentrations. In this work, unfilled PDMS membranes were prepared with 9 wt% PDMS solution. For MMMs, 9 and 12 wt% PDMS solutions were necessary.

The poly(dimethylsiloxane) pre-polymer solution was diluted with isooctane (AppliChem, purity > 99.9 %) and stirred with a magnetic stirrer and a dumbbell-shaped magnetic stirring bar at 400 min^{-1} for 30 min at room temperature. To establish cross-linking, the proprietary additives were purchased from a company that cannot be disclosed due to confidentiality reasons and the formulation supported by the producer was followed. The first additive was used as cross-linker, which was a solvent-free hydrogen containing silicon polymer with high percentage of Si-H groups and 100 wt% active content. It was diluted with isooctane to a weight fraction of 5 wt%. In order to initialize an accurate cross-linking system, diluted cross-linker was added to the pre-polymer solution This mixture was stirred with a magnetic stirrer at 400 min^{-1} for 15 min. Second additive was used as catalyst, which was a highly active platinum (Pt) complex and had a 100 wt% active content. Similar to cross-linker, catalyst was also diluted with isooctane to a weight fraction of 5 wt% and added to the mixture. Then, the mixture was further stirred at 400 min^{-1} for another 15 min to get a homogeneous mixture and to avoid local over-concentrations. The cross-linking is a hydrosilylation reaction, in which Si-H groups of cross-linker react with two vinyl (-CH=CH_2) end groups of pre-polymer (Si-V) in the presence of Pt catalyst [142, 143]. Re-illustrated schematic of cross-linking mechanism of the PDMS according to Esteves et. al. [142] is depicted in Figure 3.9.

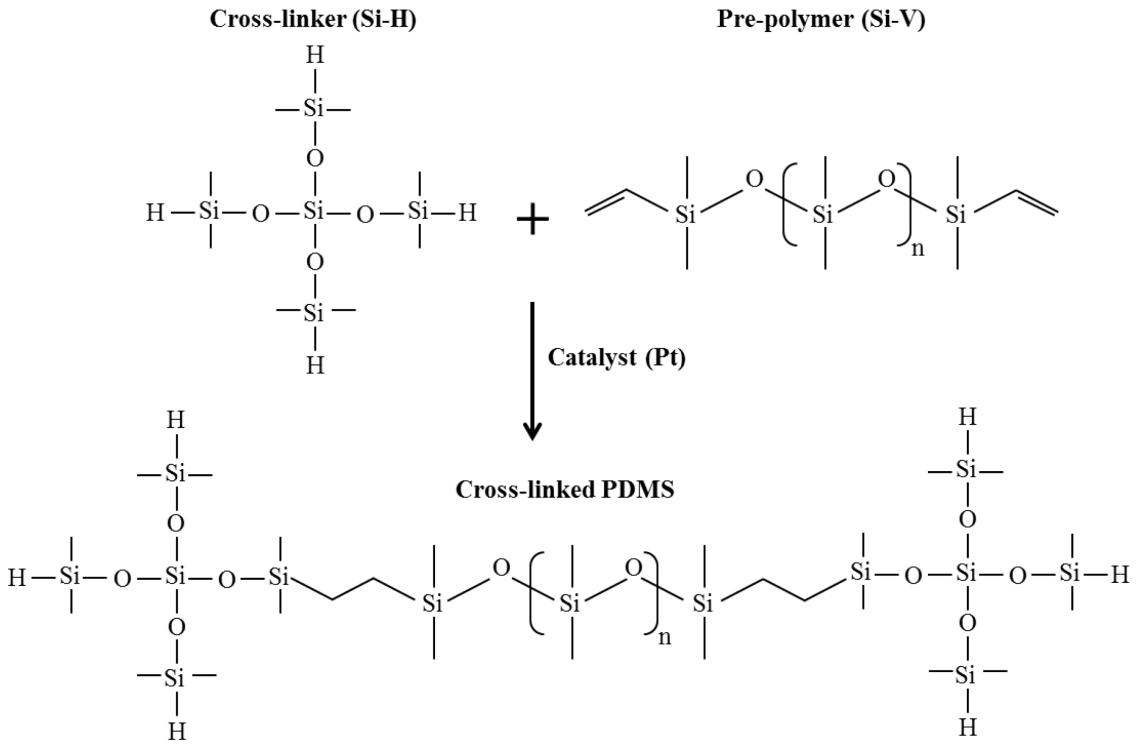

Figure 3.9 Schematic of PDMS cross-linking mechanism [142].

Depending on the application, different cross-linker/pre-polymer ratios can be studied. In this work, corresponding to the stoichiometry of the reaction between cross-linker and pre-polymer,

all PDMS solutions were prepared at the same cross-linker/pre-polymer ratio ($R_{H/V} = 0.02062$) and catalyst/pre-polymer ratio ($R_{Pt/V} = 0.02234$), which were recommended by the supplier. According to the constant $R_{H/V}$ and $R_{Pt/V}$ ratios, the required amounts of additives for 9 and 12 wt% PDMS solutions were calculated as follows.

The required amount of pre-polymer was calculated as:

$$m_{\text{pre-polymer}} = \frac{m_{\text{total}} x_{\text{PDMS,final}}}{x_{\text{pre-polymer}}} \tag{3.9}$$

where, m_{total} is the total amount of final PDMS solution required for membrane preparation, $x_{PDMS,final}$ is the desired weight fraction of PDMS in the final solution, and $x_{pre\text{-}polymer}$ is the weight fraction of PDMS in the pre-polymer *DEHESIVE® 944* used.

The required amount of cross-linker was calculated as:

$$m_{\text{cross-linker}} = \frac{m_{\text{pre-polymer}}\ x_{\text{pre-polymer}}\, R_{H/V}}{x_{\text{cross-linker}}} \tag{3.10}$$

where, $R_{H/V}$ is the applied cross-linker/pre-polymer ratio, and $x_{cross\text{-}linker}$ is the weight fraction of the cross-linker used.

The required amount of catalyst was calculated as:

$$m_{\text{catalyst}} = \frac{m_{\text{pre-polymer}}\, x_{\text{pre-polymer}} R_{Pt/V}}{x_{\text{catalyst}}} \tag{3.11}$$

where, $R_{Pt/V}$ is the applied catalyst/pre-polymer ratio, and $x_{catalyst}$ is the weight fraction of the catalyst used.

Lastly, the required amount of isooctane was calculated as:

$$m_{\text{isooctane}} = m_{\text{total}} - (m_{\text{pre-polymer}} + m_{\text{cross-linker}} + m_{\text{catalyst}}) \tag{3.12}$$

where, $m_{isooctane}$ is the amount of isooctane to be used.

In Table 3.6, the amounts of additives used for the preparation of PDMS solution in this work regarding to specific cross-linker/pre-polymer and catalyst/pre-polymer ratios were presented.

Preparation of support structure

The support structure was prepared before the separation layer was cast onto it. Therefore, the support structure was cut into small pieces large enough for the casting applicator. Subsequently, bottom side of the cut support structure was wetted with distilled water and affixed onto the custom-engineered glass plate to prepare an even surface for casting. The wet support structure was taped from the sides in order to keep the structure stretched and as flat as possible and to avoid thickness fluctuations after casting. The support structure was dried under different conditions in laboratory to remove residual water in a sufficient way. Investigations showed that drying in the fume hood for at least 60 min at room temperature has to be applied before use. The fume hood accelerates drying process of the support structure and enables to keep the support structure free of dust particles to avoid surface irregularities.

Table 3.6 Required amounts of additives used for the preparation of PDMS solution at two different concentrations.

Desired ratio	Unit	9 wt% PDMS	12 wt% PDMS
$R_{H/V}$	[g/g]	0.02062	0.02062
$R_{Pt/V}$	[g/g]	0.02234	0.02234
Desired PDMS solution			
$x_{PDMS,final}$	[-]	0.09	0.12
m_{total}	[g]	50.00	50.00
Additives used			
$x_{pre\text{-}polymer}$	[-]	0.30	0.30
$x_{cross\text{-}linker}$	[-]	0.05	0.05
$x_{catalyst}$	[-]	0.05	0.05
Required amounts			
$m_{pre\text{-}polymer}$	[g]	15.00	20.00
$m_{isooctane}$	[g]	31.13	24.85
$m_{cross\text{-}linker}$	[g]	1.86	2.47
$m_{catalyst}$	[g]	2.01	2.68
m_{total}	[g]	50.00	50.00

Casting of the membrane

Two different film-casting applicators were used to cast the separation layer onto the prepared support structure. One of those was a 4-sided film applicator frame made of stainless steel, which had four standard gap heights as 50, 100, 150 and 200 µm. Second film applicator (Film Applicator UA 3000) had an adjustable gap height from 0 to 3000 µm with finest adjustable value of 5 µm. Both applicators were made of stainless steel and obtained from MTV Messtechnik. Pictures of the used film applicators and product information are given in Table 3.7.

Table 3.7 Two different coating applicators used for membrane preparation.

Applicator model	Film Applicator UA 3000	4-sided film applicator frame
	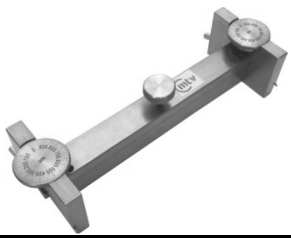	
Material	stainless steel	stainless steel
Width	220 mm	90 mm
Setting range	0 – 3000 µm	50, 100, 150, 200 µm
Fine adjustment	5 µm	standard splitting heights

Post-treatment of the membrane

Casting the PDMS solution was performed at room temperature and ambient pressure. Therefore, the produced membrane needed to be treated further. The initial step of post-treatment was considered as solvent evaporation in the fume hood. It was followed by drying in a vacuum oven under controlled conditions, at high temperature and low pressure, to remove any remaining solvents from the separation layer. Before putting the membrane in the oven, the membrane sheet was first removed from the glass plate, and then fixed to a metal plate of the oven. Afterwards, membrane stamps to be measured were cut. Post-treatment conditions of membranes will be discussed in section 5.3. The steps to prepare a pure PDMS membrane are exhibited in Figure 3.10.

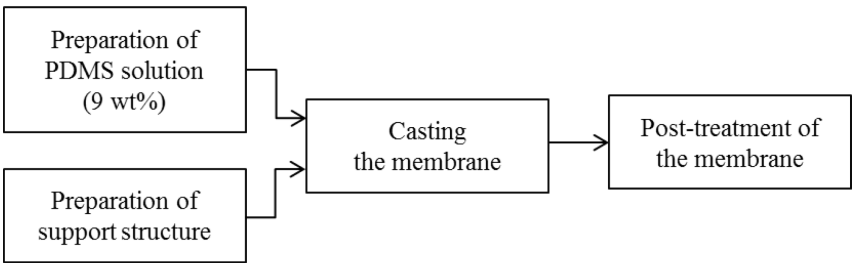

Figure 3.10 Preparation steps of PDMS membrane.

3.2.2 Preparation of mixed-matrix membranes

In this work, an MMM containing activated carbon particles, which are dispersed in a solvent prior to mixing them with PDMS, is briefly called a saturated MMM. In a similar way, an MMM containing activated carbon particles, which are not dispersed in a solvent, is called an unsaturated MMM. Preparation steps of both types of MMMs are described below.

Pre-treatment of activated carbon

Initial step to prepare an MMM is pre-treatment of the activated carbon particles. In this work, the activated carbon particles with mean particle diameter of d_{50} = 3.5 µm were used. Prior to using, the activated carbon particles were dried at 150 °C in a vacuum oven at 110 mbar for at least 18 h to remove any adsorbed components. The activated carbon lost approximately 4% of its mass during the drying. The same pre-treatment was applied to prepare MMMs with zeolite nanoparticles. The mass losing during the drying of zeolite particles was approximately 12%. The change in the mass before and after drying is important to calculate accurately the necessary amount of the filler particles in order to achieve desired dispersed mass fraction of the filler particles in the polymer phase.

The desired dispersed mass fraction x_i was calculated as follows:

$$x_i = \frac{m_{filler}}{m_{filler} + m_{PDMS}} \tag{3.13}$$

where m_{filler} is the mass of inorganic filler particles (activated carbon or zeolite) in the polymer matrix and m_{PDMS} is the mass of the PDMS with a 100 wt% active content in the solution.

Preparation of PDMS/activated carbon suspension

Mixed-matrix membranes may have interfacial defects, such as poor interfacial adhesion, sieve-in-a-cage morphology, matrix rigidification or pore blockage. Among those morphological problems, the most important one might be pore blockage. It refers to the penetration of polymer chains into the particle pores, which results in a decrease of the performance of the membrane. This makes the step of mixing inorganic particles with prepared polymer solution the most crucial step to prepare mixed-matrix membranes.

A sufficient amount of inorganic particles in polymer matrix is critical to form successful MMMs. Increasing the amount of inorganic particles usually results in agglomeration of particles, which causes voids thus reducing the selectivity. In the *Results and Discussion Part I*, strategies developed to avoid irregularities, such as agglomerates or poor particle dispersion, during the preparation of polymer/activated carbon suspension will be discussed. Many preparation methods with different aspects varying preparation parameters were tested and the best obtained procedure for the preparation of homogenous polymer/activated carbon suspension is described here.

Preparation of unsaturated mixed-matrix membranes

Preparation of MMMs was partially similar to preparation of unfilled PDMS membranes. In order to prevent any agglomeration the particles were sieved and then half of the necessary amount of the prepared PDMS (9 wt%) was added to the particles. The dispersion was mixed for 15 or 30 min with a magnetic stirrer at 400 min^{-1} using a cross-shaped magnetic bar. Afterwards, the rest of the PDMS (9 wt%) solution was added and the dispersion was mixed for 15 or 30 min. In this step, a combination of magnetic stirring from the bottom at 400 min^{-1} with a cross-shaped magnetic bar and high speed dispersion at 10000 min^{-1} from the top was used to mix the suspension. Later, the membrane was cast and treated as described for unfilled PDMS membranes. The steps to prepare an unsaturated MMM are exhibited in Figure 3.11.

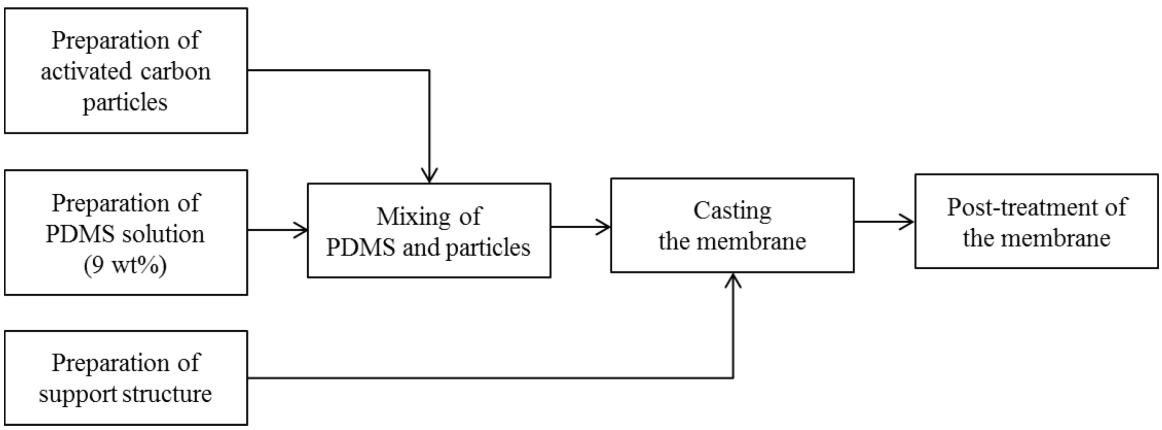

Figure 3.11 Preparation steps of an unsaturated MMM.

Preparation of saturated mixed-matrix membranes

The difference between the preparation of saturated MMMs and unsaturated MMMs was the additional step of dispersing the activated carbon particles in a solvent. Initially, five different solvents were tested (isooctane, toluene, ethanol, n-heptane, and cyclohexane) and three of them

(isooctane, toluene and ethanol) showed more promising results than the other two. Preliminary investigations to find the suitable solvents for the saturation process will be discussed in *Results and Discussion Part I*. In the following, the preparation steps of a MMM for the case of isooctane or toluene saturation and for the case of ethanol saturation are briefly explained. The steps to prepare a saturated MMM are exhibited in Figure 3.12.

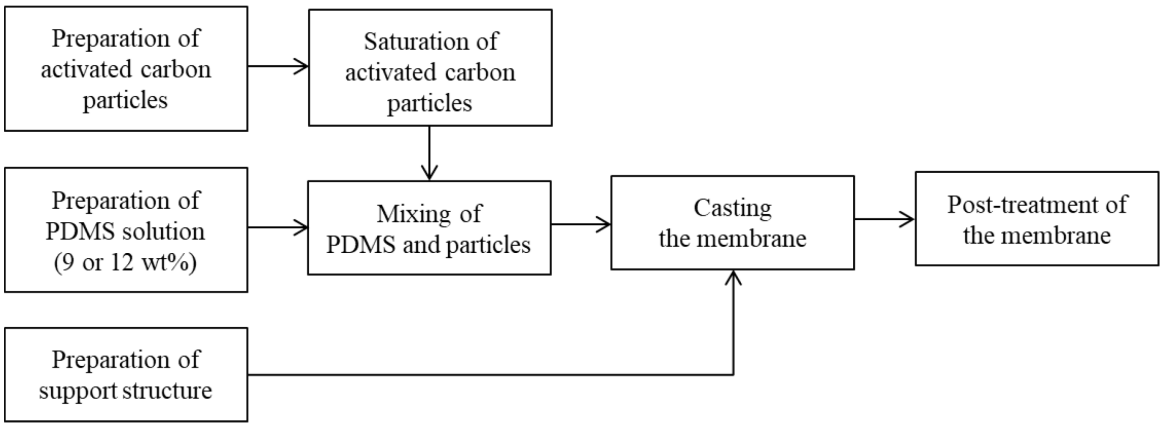

Figure 3.12 Preparation steps of saturated MMM.

Isooctane or toluene

When isooctane or toluene was used for the saturation of activated carbon particles, higher concentrated PDMS solution was required. In this case, 12 wt% PDMS solution was used to achieve final 9 wt% PDMS concentration in the end. The solvent, equivalent to the mass of one-third of the 12 wt% PDMS solution, was added to the dried activated carbon particles and ultrasonication was applied for 5 min in order to saturate the particles with the solvent. Then, one-third of the 12 wt% PDMS solution was added to the saturated particles and stirred magnetically for 15 or 30 min using a cross-shaped magnetic bar. Afterwards, the remaining 12 wt% PDMS solution was added to the dispersion and mixed for 15 or 30 min with a combination of high speed disperser from the top at 10000 min^{-1} and a magnetic stirrer from the bottom using the cross-shaped magnetic bar at 400 min^{-1}. The casting and post-treatment of the membranes were equal to the procedure explained before for unfilled PDMS membranes.

Ethanol

In contrast to the saturation of active carbon particles with isooctane or toluene, the influence of ethanol mass to the final concentration of PDMS solution was negligible. Thus, a 9 wt% PDMS solution was used. The dried activated carbon particles were saturated with ethanol using double the amount of particles and subsequently 5 min ultrasonication was applied. Firstly, half of the 9 wt% PDMS solution was added to the saturated particles and mixed for 15 or 30 min with a magnetic stirrer using the cross-shaped magnetic bar. Secondly, the rest of the 9 wt% PDMS solution was added and the dispersion was mixed for 15 or 30 min with a combination of high speed disperser from the top at 10000 min^{-1} and a magnetic stirrer from the bottom using the cross-shaped magnetic bar at 400 min^{-1}. The casting and post-treatment of the membranes were equal to the procedure explained before for unfilled PDMS membranes.

3.3 Morphological characterization of membranes

Morphological characterization of the prepared membranes was performed using two methods. The first method was based on optical techniques, which were taking pictures of the membranes either by a digital camera (macro photography) or with a Scanning Electron Microscopy (SEM) (micro photography) (Figure 3.13). The second method was evaluating the permeation behavior and separation performance of the produced membranes with the constructed gas permeation experimental setup. The gas permeation experimental setup and the procedure of the pure and the mixed gas measurements are described in the next section.

3.3.1 Macro photography with digital camera

The membrane was stretched in front of a light box and pictures of the membrane were taken with a digital camera (Canon EOS 400D). The light box was illuminated by a fluorescent light bulb, which provides better visualization. The light box allowed taking pictures with high contrast that allowed agglomerates to be seen more clearly. This method was applicable only for mixed-matrix membranes composed of PDMS and activated carbon. Since the carbon particles gave black color to the suspension, the formed agglomerates of the filler particles on the surface of the membrane were seen as black dots. Those dots were counted from the taken pictures using software ImageJ. The number of the agglomerates allowed judging whether or not the casting suspension of polymer and particles was homogenized well. The number of counted agglomerates from the surface of the membrane was divided by the investigated membrane surface area. This allowed comparing different membranes. Fewer number of agglomerates per membrane surface area means better distribution of particles in the in the polymer.

To pixelate the image, the mosaic filter of software Photoshop CS5 was used. A numerical value between 0 and 100 was given to each pixel by the software, which evaluated the color intensity of the membrane surface where 0 was indicating white color and 100 was indicating black color. The color intensity corresponds to a proportion of filler particles, thus, enabling the comparison of proportions of the filler particles on the surface of the membrane produced. The more particles were present in the polymer matrix, the greater the average of the color intensity. The standard deviation of the color intensity values of a whole membrane was considered as a parameter to compare as well as a measure of particle distribution homogeneity. Thus, the smaller the standard deviation, the more uniform particles were distributed in the separation layer of the membrane.

3.3.2 Scanning electron microscopy

Cross-section and surface morphology of the prepared membranes were examined using Scanning Electron Microscopy (SEM) images. The thickness of the separation layer of the membrane was necessary for permeability calculation and it was measured from the SEM images as well. All the SEM measurements were performed at Zentraleinrichtung Elektronenmikroskopie (ZELMI) at the TU Berlin using a Hitachi S-2700 Scanning Electron Microscope. Magnifications up to 5000x were applied to make images for different purposes.

An important issue before taking SEM images was sample preparation. The preparation method should not affect membrane morphology or thickness. Therefore, samples were prepared by

freeze fracturing after several minutes of immersion in liquid nitrogen. Afterwards, a piece of the membrane was mounted on a specimen stub. Specimens tend to charge when scanned by the electron beam, especially in secondary electron imaging mode. This causes scanning faults and other image artifacts. In order to avoid these effects, samples were investigated after sputter coating by gold.

Energy-Dispersive X-ray Spectroscopy (EDX) was used to investigate pore blockage. EDX is an analytical technique, which works as an integrated feature of a SEM. EDX is used for elemental analysis of a sample where elements are characterized based on measurements of the number and energy of the X-rays emitted from the sample when they are exposed to a high-energy beam of electrons. The output of an EDX analysis is an EDX spectrum that is a plot of how frequently an X-ray is received for each energy level. An EDX spectrum normally displays peaks corresponding to the energy levels for X-rays received. Each of these peaks is unique to an atom, and therefore corresponds to a single element. Due to the unique atomic structure of the elements, they show individual peaks in the EDX spectrum. The higher a peak in a spectrum, the more concentrated the element in the specimen. To avoid charging effects, EDX samples were investigated after sputter coating either by gold or by carbon.

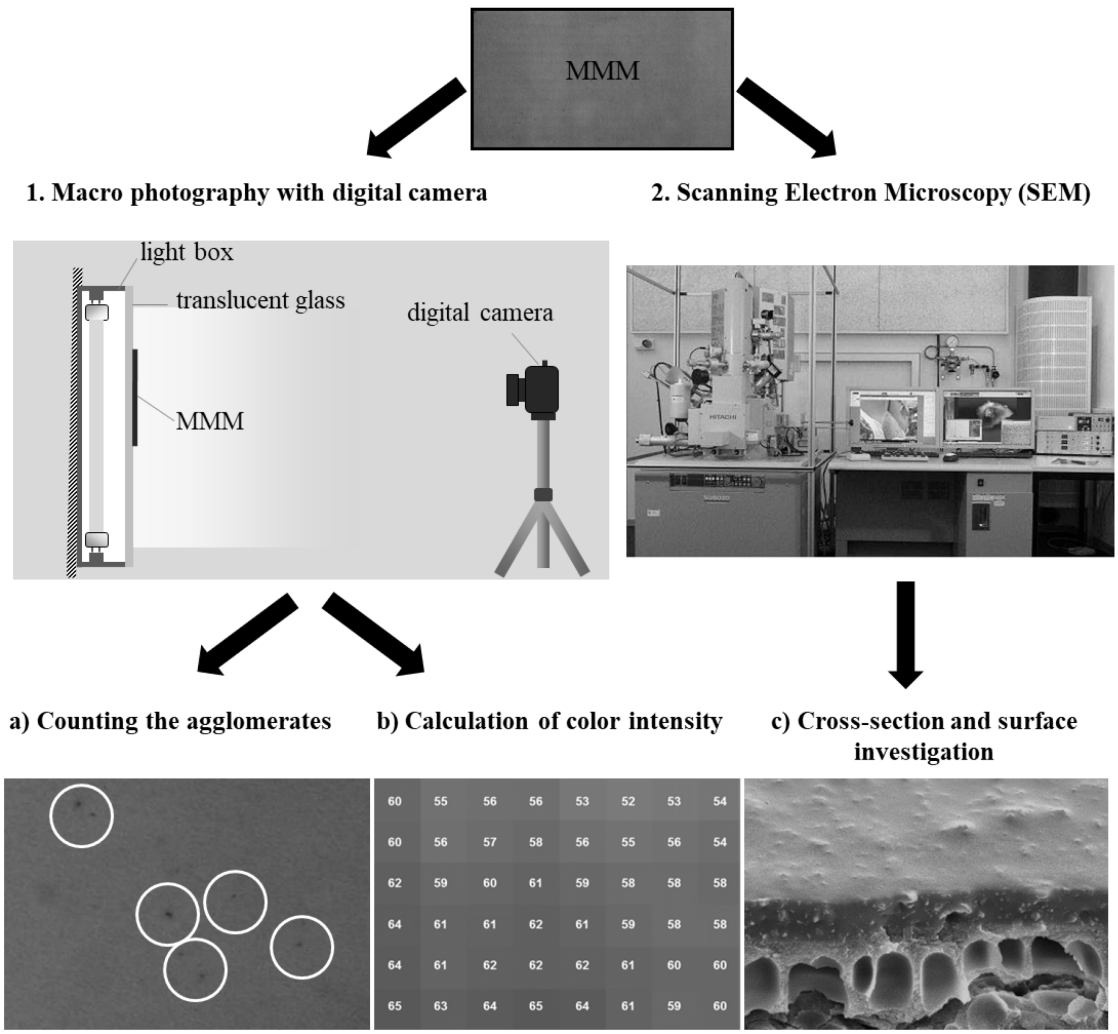

Figure 3.13 Schematic representation of the image analysis methods.

3.4 Gas permeation experiments

3.4.1 Experimental setup

To determine permeation behavior of pure *n*-C_4H_{10} and CH_4 and binary mixtures of them through the produced membranes, a gas permeation plant was designed. A detailed process and instrumentation diagram of the gas permeation experimental setup is given in Figure 3.14 and operating ranges are listed in Table 3.8.

Table 3.8 Operating range of the gas permeation experimental setup.

Parameter	Unit	Min	Max
Feed temperature	[°C]	10	40
Permeate temperature	[°C]	10	40
Feed pressure	[bara]	0.75	30
Permeate pressure	[bara]	0.2	1
Feed *n*-C_4H_{10} concentration	[vol%]	2	20

Additionally, the gas permeation experimental setup was designed having features of negligible pressure drop caused by the pipes and the connections, minimum leakage of gases from the connections, no physical damage of the membrane caused by several reasons, no back flows were provided with check valves, and pressure relief positions to meet safety requirements.

Product selection was reviewed to ensure adequate material functionality and trouble-free performance. The proper installation and maintenance of the system was provided by the workshop of the Chair of Chemical and Process Engineering, Technische Universität Berlin. The parts and accessories of the system were stainless steel, except for hosing of quick connections to sample cylinders. A list of the important components used for the construction of the experimental setup and their supplier are listed below:

- Temperature sensors: Unitherm Messtechnik GmbH, Germany
- Pressure sensors: BD Sensors, Germany
- Pressure regulators: Swagelok Company, Germany
- Pressure reducers for pure gas cylinders: Air Liquid, Germany
- Mass flow meters and mass flow controller: Brooks Instrument GmbH, Germany
- Valves (ball valves, check valves, needle valves, relief valves and magnetic valve): Swagelok Company, Germany
- Vacuum pump (VP): Siemens, Germany
- Permeate vacuum pump (PVP): VWR International GmbH, Germany
- Sample cylinders: Swagelok Company, Germany
- Fittings, hoses and flexible tubing, quick connections and filters: Swagelok Company, Germany

The gas permeation experimental setup consisted of three parts: the gas supply, the circulation part, and the vacuum part. In the gas supply part, a gas cylinder cabinet (GCC), a mixture vessel (MV), and two pressure regulators (PR1 and PR2) were installed. Gas cylinders containing pure

gas components (n-C_4H_{10}, CH_4, N_2) were stored in the gas cylinder cabinet. Each pure gas cylinder had a separate piping having a ball valve and a check valve (non-return valve) installed on the pipeline following the pressure reducers. The pure gas from the gas cylinder could go either into the mixture vessel or to the feed side of the membrane test cell in the circulation part by leading the pure gas in either directions using the appertaining ball valve manually. The mixing vessel was used to prepare gas mixtures of n-C_4H_{10} and CH_4 at different concentrations in case of mixed gas experiments. Another ball valve and a magnetic regulation valve were installed on the inlet piping of the mixture vessel to control the amount of the gas filled in the mixing vessel. Since the inner side of the mixing vessel was made of hot zinc dipped steal, a filter was placed on the outlet piping to avoid particle contamination in the feed gas. A pressure sensor on the outlet piping measured the pressure in the mixing vessel. On the inlet of the circulation part, two pressure regulators with different operational ranges were installed to perform the experiments more accurate at the desired feed pressures. The working range of the pressure regulator 1 (PR1) was from 0 to 15 bar and the working range of the pressure regulator 2 (PR2) was from 0 to 40 bar.

The circulation part consisted of a membrane test cell (MC), a gas circulator (GC), a heat exchanger (HE), and two hold-up vessels (HV1 and HV2). The membrane test cell was suitable for prepared round flat-sheet membranes with a 74 mm diameter. The quick connections on the feed, permeate, and retentate side of the membrane test cell enabled to change the membrane test cell easily when it was necessary. The gas circulator (GC) generates a sufficient flow with high velocity to avoid concentration polarization. The feed gas in the piping was heated or cooled to the desired process temperature with the heat exchanger before entering the membrane test cell. Thus, the heat introduced by the gas circulator was removed as well. Additionally, the membrane test cell was located in a water bath (WB) to keep the upstream and downstream temperature constant during the experiments. Hold-up vessels were required to increase feed gas volume. The smaller hold-up vessel (HV1) was purchased from Swagelok Company. HV1 was a double-ended cylinder with a volume of 2.25 liter and permanently used. The larger hold-up vessel (HV2) was a custom made vessel manufactured by Silica Verfahrenstechnik GmbH. HV2 had a volume of 13.8 liter and was optionally used if more gas hold-up was required. The permeate flow was connected to the outlet. In some pure gas experiments vacuum was applied on the permeate side of the membrane test cell. The retentate flow was recycled using the gas circulator in case of mixed gas experiments and some amount of it was purged into the outlet after adjusting flow rate and pressure of the retentate flow.

On the feed side of the membrane test cell, a pressure sensor (PR-2), a temperature sensor (TR-1) and a flowmeter (FR-1) were installed. On the retentate side a temperature sensor (TR-2) and a pressure sensor (PR-3) were installed. On the permeate side a pressure sensor (PR-4), a temperature sensor (TR-3) and two flowmeters (FR-3 and FR-4) were installed. The working range of the pressure sensor on the feed side (PR-2) was 0 – 40 bar, whereas the working range of the pressure sensor on the retentate side (PR-3) was 0 – 10 bar. The pressures on feed and retentate side were assumed to be equal. For measurements at a feed pressure below 9 bar, the pressure sensor from the retentate side was used, which had a higher accuracy at lower pressures. For measurements with a pressure above 9 bar, the pressure sensor on the feed side was used. The two flowmeters on the permeate side had different working ranges as well. FR-3 had a working range of 0 – 1 $L_{(STP)}min^{-1}$ and FR-4 had a working range of 0 – 5 $L_{(STP)}min^{-1}$. Thus, FR-3 was used for permeate flow rates below 0.95 $L_{(STP)}$ min^{-1}, and FR-4 was used for permeate flow rates above 0.95 $L_{(STP)}$ min^{-1}.

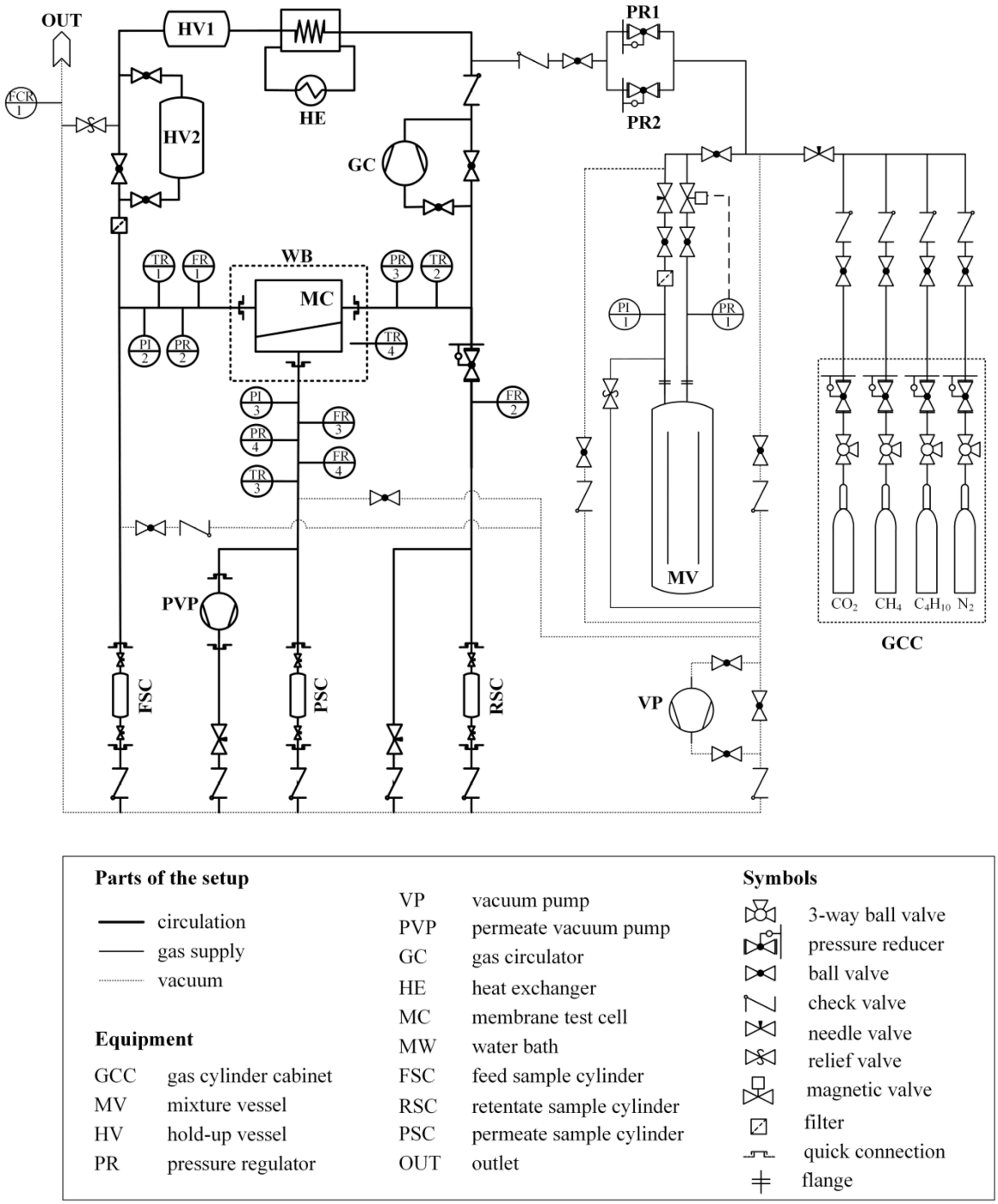

Figure 3.14 The gas permeation experimental setup.

The last part of the experimental setup was the vacuum part where a vacuum pump (VP) was placed. The gas supply part and the circulation part of the setup were connected to the outlet to release the high pressure from the system after conducting experiments. A mass flow meter/controller (FCR-1) was installed on the outlet piping to control the amount of released gas from the experimental system to the outlet canal according to the laboratory security instructions. After both parts were depressurized, they were led to the vacuum part separately that allows to evacuate the system completely.

Gas samples on the feed and permeate side of the membrane test cell were stored in sample cylinders during the experiments. Then, the sample cylinders were easily disconnected from the experimental setup by quick connections and the gas composition on both sides was analyzed by a gas chromatograph.

Check valves were installed at several positions of the experimental setup to prevent back flows, which could interrupt experimental procedures if they occur. Additionally, several pressure relief valves were located, which could open gradually as the pressure increases in the system in order to meet safety requirements.

Data collection of the operating parameters such as pressure, temperature and flow on both sides of the membrane was supported by The Laboratory Virtual Instrument Engineering Workbench (LabVIEW) software, National Instruments, Germany. The outlet flow with the implemented mass flow controller (FCR-1) on the outlet piping was also controlled by the LabVIEW software.

Membrane test cell

Membrane test cell was provided by Helmholtz-Zentrum Geesthacht and it was suitable for round flat-sheet membranes with a diameter of 74 mm. The test cell was waterproof and located in a water bath during the experiments to regulate the temperature of the permeation experiments. Figure 3.15 shows a schematic representation of the membrane test cell.

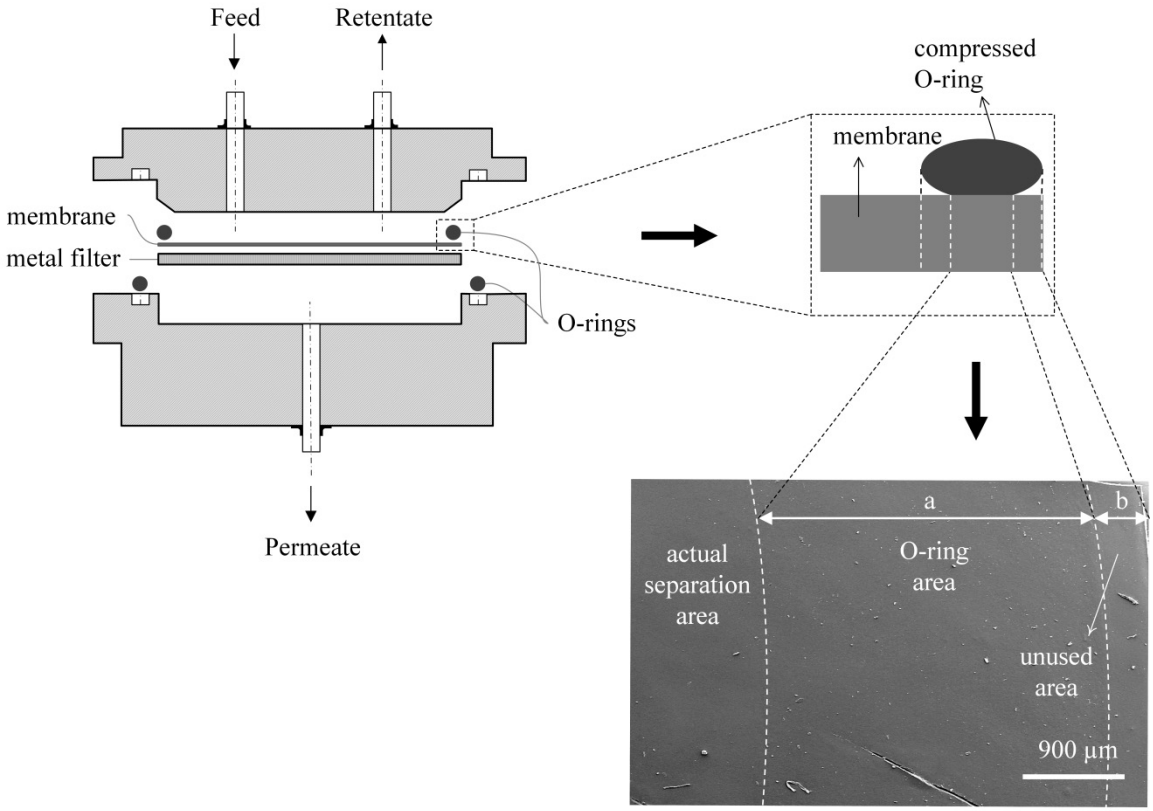

Figure 3.15 Schematic representation of the membrane test cell (left) and the reduced membrane diameter (upper right), and SEM image of a tested membrane used for calculating the actual membrane separation area (bottom right).

The membrane test cell was connected to the gas separation experimental setup with stainless steel flexible tubing and quick connections that allowed easy change and move for the test cell when it was required. The feed gas entered from the top of the cell, flowed over the membrane, and left the cell via permeate gas outlet. The membrane was placed on a porous metal sintered filter disc so that the membrane was mechanically supported from the bottom during the experiment. In case of a pure gas experiment, the membrane test cell allowed performing a dead-end permeation. Two O-rings sealed the membrane test cell where one of them was positioned between the upper and bottom parts of the cell, and the second one was positioned on the membrane.

The O-ring placed on the membrane compressed the surface of the membrane from the edge and reduced the actual surface area of the membrane used for the separation. For the accurate calculations of permeability, the actual diameter of the membrane was needed. Therefore, the actual diameter of a membrane was measured from a SEM image after being tested and the active separation area was calculated as:

$$d_m = d - 2(a+b) \tag{3.14}$$

$$A_m = \frac{\pi}{4}(d_m)^2 \tag{3.15}$$

where d_m is the actual separation diameter of the membrane, d is the total diameter of the membrane, and A_m is the actual separation area of the membrane. The effective membrane area was then 34.21 cm^2.

Mixing vessel

The preparation of binary gas mixtures was realized in a feed vessel that was a custom made apparatus manufactured by Silica Verfahrenstechnik GmbH. The principle that was used to design the vessel was based on an optimal geometry of a jet loop reactor [144]. The shape of the vessel was cylindrical and the vessel contained a volume of 38.6 liter. Both top and the bottom ends of the vessel were closed with bumped boiler ends. The vessel had an outer shell and a draft tube which were made of hot zinc dipped steel. The draft tube was fixed to the outer shell with four holders from top and bottom. Design parameters and actual dimensions of the vessel are given in Table 3.9 and technical drawing is depicted in Figure 3.16.

Table 3.9 Design parameters and actual dimensions of the mixing vessel.

Dimension	D	d	H	L	a	b	c
Optimum design	-	0.59 D	5.00 D	4.40 D	0.35 D	0.06 D	0.25 D
Actual value [mm]	219	114	1100	960	80	13	60

The vessel allowed preparing gas mixtures up to 70 bar and the maximum allowed preparation temperature was 30 °C. On top of the vessel two nozzles were placed as gas inlet and outlet. The gas inlet nozzle was centrically positioned. The maximum experimental time depends on the volume of the vessel and the initial pressure of the experiment is performed, because the vessel was only filled batchwise.

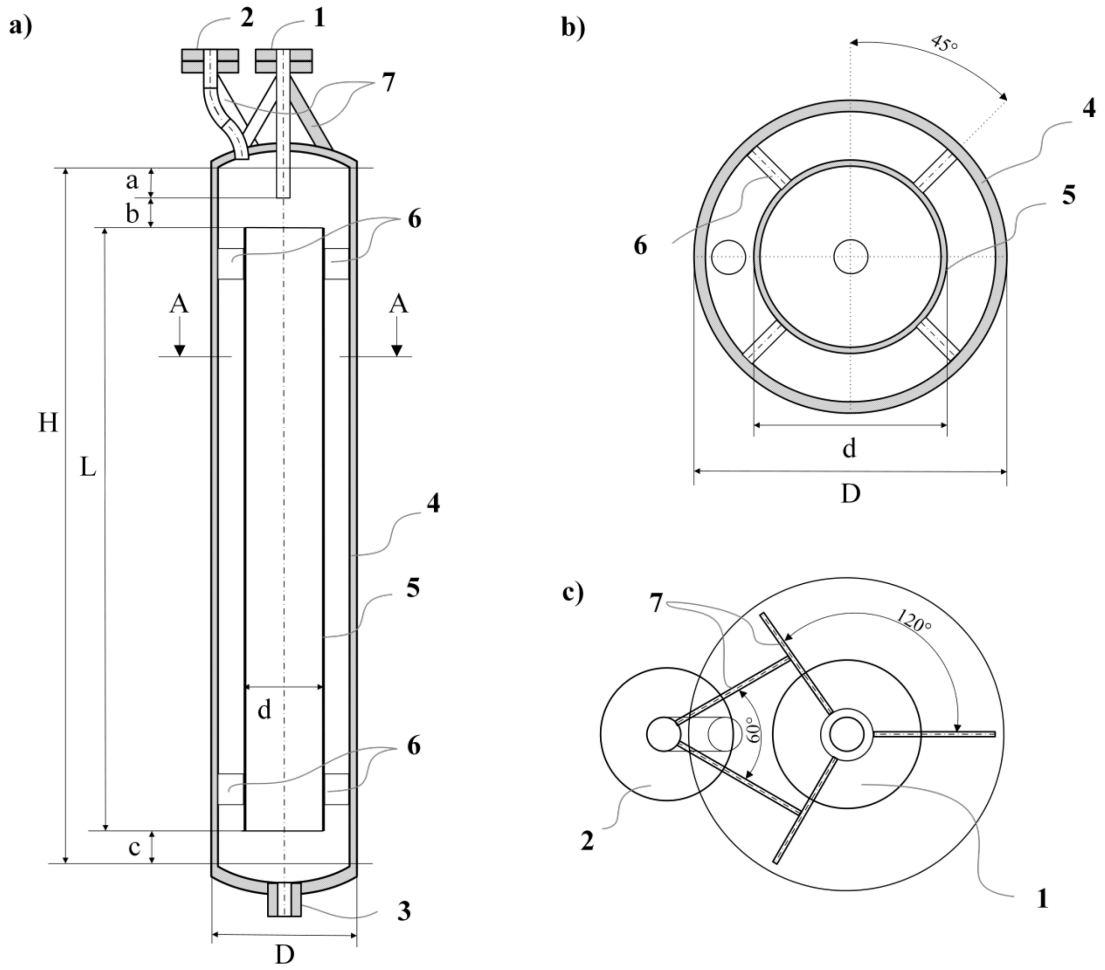

Figure 3.16 Geometry of mixing vessel: a) frontal cross-section, b) A-A cross-section, c) top view. Description of the positions: (1) gas inlet nozzle, (2) gas outlet nozzle, (3) closed nozzle (outlet for hot zinc dipping), (4) outer shell, (5) draft tube, (6) holder for draft tube, (7) holder for nozzle.

Gas circulator

A continues flow at high velocity on the feed side of the membrane was necessary to prevent concentration polarization. For this purpose, a DLE-2 model air driven high-pressure booster suitable for the experimental gases (*n*-C_4H_{10} and CH_4) with an air driven pressure of 6 bar was purchased from Maximator GmbH. The retentate gas flow was mostly recycled to the feed using the gas compressor and some amount of it was purged into the outlet. The feed velocity inside the membrane test well varied between 5.5 and 8 ms^{-1} in mixed gas experiments.

Sample cylinders

Six miniature gas sample cylinders with double-ended stainless steel construction were purchased from Swagelok Company (Figure 3.17). Each cylinder had an inner volume of 50 ± 2.5 cm^3 and worked up to 100 bar between –50 and 50 °C. Six cylinders allowed three consecutively samplings during a mixed gas experiment. At each sampling, a gas sample was filled from the feed side of the membrane into one cylinder and a gas sample was filled from the permeate side

of the membrane into the second cylinder. Thus, the gas composition of the feed and permeate side of the membrane was measured for each sampling and it was repeated three times.

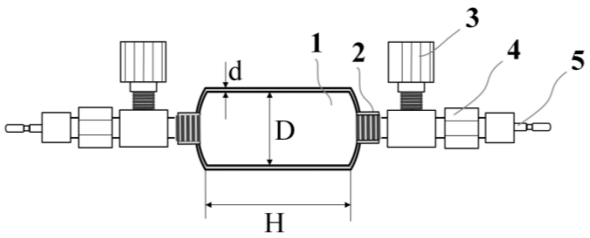

Figure 3.17 Geometry of a sample cylinder (D = 30 mm, H = 6 mm, d = 3 mm). Description of the positions: (1) stainless steel gas cylinder, (2) welded outage tube, (3) needle valve, (4) outage tube adapter, (5) male quick connection.

3.4.2 Pure gas measurements

Before performing the experiment, the startup procedure was applied to check whether the setup was filled with the inert gas and at atmospheric pressure. The purpose of inerting with nitrogen (N_2) was to avoid unwanted chemical reactions within the system such as formation of any explosive mixture and to set it to a standard state. This means that no gas was left in the system from earlier experiments that could contaminate the results of the next experiments. If the pressure was released the membrane to be measured was placed into the membrane test cell. The respective pure gas cylinder was opened and the gas was directed to the upstream side of the membrane. The water bath that tempers the membrane test cell was set to the desired operation temperature and the temperature indicator in the form of a digital thermometer was placed into the water bath. Thus, the temperature of the measurement was kept constant during the experiment. Before the actual measurement step started, the system was evacuated three times and between each evacuation it was purged with the test pure gas. Figure 3.18 exhibits the flow chart of a pure gas experiment.

For the *n*-C_4H_{10} and CH_4 pure gas permeation experiments the constant pressure method was employed. For the ease of understanding and application, it is assumed that the first test gas to measure is *n*-butane, followed by a gas change to methane. For *n*-C_4H_{10}, the feed pressure was varied from 0.75 to 2 bar depending on the saturated vapor pressure of the *n*-C_4H_{10} at the measurement temperature. The temperature of the measurement ranged from 10 to 40 °C. The saturated vapor pressure of *n*-C_4H_{10} varies from 1.48 to 3.78 bar in this temperature range. Nevertheless, permeabilities of *n*-C_4H_{10} were determined at feed pressures lower than 2.10 bar since the *n*-C_4H_{10} pure gas cylinder was stored at room temperature and the saturation vapor pressure of *n*-C_4H_{10} was approximately 2 bar at room temperature. However, the pressure of the feed side was actually controlled by the pressure regulator not by the pressure in the gas cylinder. The pressure was kept constant at the highest possible feed pressure, approximately 2 bar, for 10 min. Then, the pressure at feed side of the membrane was reduced gradually using pressure regulator and kept constant at each pressure step for 10 min. By this way, the pressure was reduced gradually up to a feed pressure of 1.2 bar by taking as many as possible constant pressure steps. The permeate pressure in the measurement was at ambient pressure. Additionally, a vacuum was created at the permeate side by connecting a vacuum pump. Depending on the

conditions, the vacuum pump induced a pressure on the permeate side between 200 and 500 mbar. The feed pressure was again regulated approximately to 2 bar and after being kept constant for 10 min, it was gradually decreased by taking several pressure steps. This is illustrated in the Figure 3.19 (a).

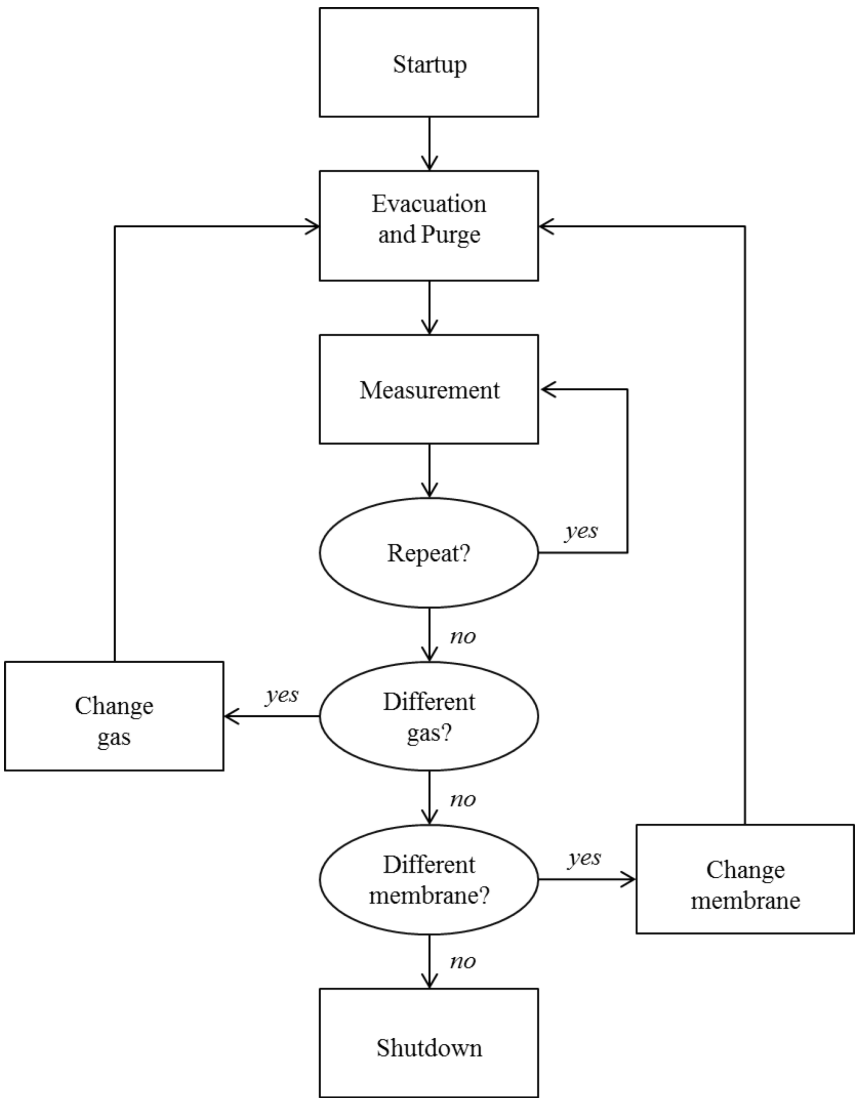

Figure 3.18 Flow chart for pure gas experimental procedure.

The pure gas measurement could start either at atmospheric permeate pressure or with a vacuum at the permeate side. In Figure 3.19 (b), an example of pure CH_4 measurement starting with vacuum on the permeate side is given. The system was filled with CH_4 up to a feed pressure of 5 bar and then the vacuum pump was connected to the permeate side. In contrast to the *n*-C_4H_{10} measurement, the feed pressure was gradually increased due to the ease of application. For CH_4 pure gas permeation experiments, the feed pressure ranged from 5 bar to 30 bar.

Slow permeation rate of CH_4 compared to *n*-C_4H_{10} allowed performing experiments at relatively high pressures. Saturation vapor pressure of CH_4 was not a limiting factor to perform experiments at such feed pressures. The feed pressure was stepwise increased and it was kept constant for 10 min for each step. Subsequently, permeation measurement was continued at several feed

pressure steps between 5 and 30 bar with atmospheric pressure on the permeate side when the vacuum pump was disconnected. Similar to *n*-C_4H_{10}, more pressure steps could be applied creating vacuum at the permeate side of the membrane. The temperature of the measurement varied between 10 to 40 °C. After the experiments were conducted, the pressure was released, the whole system was evacuated and purged with N_2 for the shutdown.

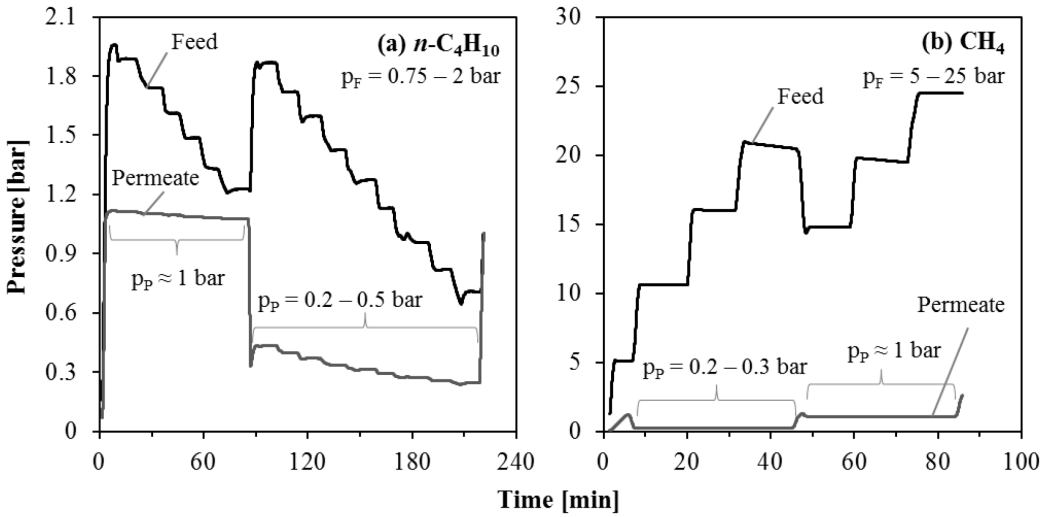

Figure 3.19 Exemplary pressure curves for pure gas experiments of (a) *n*-C_4H_{10}, (b) CH_4.

3.4.3 Mixed gas measurements

Figure 3.20 exhibits flow chart for a mixed gas experimental procedure. The startup for a mixed gas experiments was similar to a pure gas experiment. A short list of necessary startup steps is given below:

- check whether the system is purged with N_2,
- check whether the system is at atmospheric pressure, otherwise release the pressure,
- insert the membrane to be investigated,
- open the required pure gas cylinder, and
- prepare the water bath of the membrane test cell.

Before starting the mixed gas measurement, a mixture of *n*-C_4H_{10} and CH_4 had to be prepared in the mixing vessel. For the mixture preparation, the remaining pressure was released from the mixing vessel, and the mixing vessel and the gas supply part of the setup were evacuated. Then, the mixing vessel was filled with the first component *n*-C_4H_{10} up to its saturated vapor pressure. Afterwards, the part of the system leading up to the mixing vessel was again evacuated to remove any residual *n*-C_4H_{10} that could potentially influence the composition of the mixture. Hereafter, the desired amount of the second component CH_4 was added to the vessel. The necessary amount of CH_4 was calculated using Dalton's Law of partial pressures:

$$p_{n\text{-}C_4H_{10}} = y_{n\text{-}C_4H_{10}}\, p_{total} \tag{3.16}$$

Since the mixture was binary, the total pressure equals the sum of the partial pressures of *n*-C_4H_{10} and CH_4:

$$p_{total} = p_{n\text{-}C_4H_{10}} + p_{CH_4} \tag{3.17}$$

Figure 3.21 compares calculated *n*-C_4H_{10} concentration and measured *n*-C_4H_{10} concentration during mixture preparation. Apparently, the gas mixtures were prepared with a tolerance of ±8 vol% *n*-C_4H_{10}.

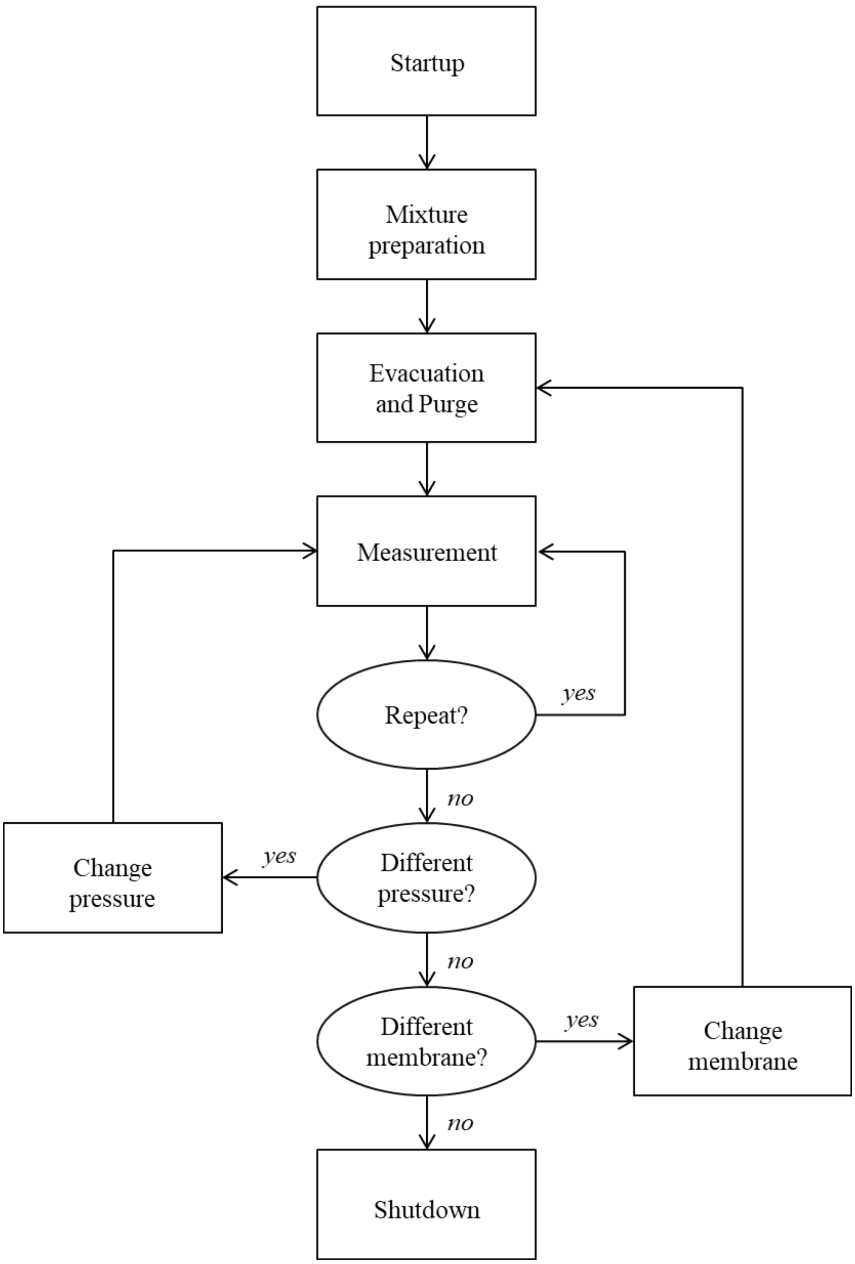

Figure 3.20 Flow chart for mixed gas experimental procedure.

After the preparation of the mixture, the system was evacuated to remove the residuals and purged with the prepared gas mixture. The evacuation and the purge were repeated two times. The

feed gas was directed to the membrane test cell through the feed piping and the thermostat connected to the heat exchanger was turned on to temper the feed gas. A sufficient retentate flow was maintained to prevent concentration polarization and a part of it was recycled to the feed side using the gas compressor. The sample cylinders for permeate and retentate were inserted. When the temperature of the feed gas was at the desired experimental temperature and the temperature was constant, the sample cylinders were opened so that the gas flowed through the sampling cylinders. The feed pressure was regulated to the desired pressure. The permeate flow was maintained at atmospheric pressure.

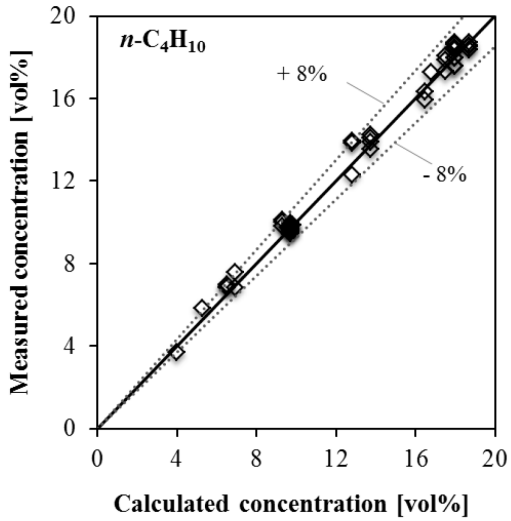

Figure 3.21 Accuracy of n-C_4H_{10}/CH_4 binary mixture preparation depending on the n-C_4H_{10} concentration in the mixture.

Figure 3.22 shows an example of a mixed gas experiment conducted with binary mixtures of 4 vol% n-C_4H_{10} in CH_4 at 20 °C at feed pressures of 30, 20, and 10 bar. Prior to collecting the gas samples from feed and permeate side of the membrane, the system was required to be at steady-state condition. In order to understand whether the system was at steady-state, several gas samples were taken and the composition of them were analyzed to observe the fluctuations in gas composition in the feed gas. An example is given in Figure 3.23**.** The change of gas composition in the feed gas was insignificant after 30 min. Therefore, it was necessary to wait for at least 30 min to reach steady-state before taking gas samples for each pressure step. Permeate and feed sample cylinders were filled up to 1.6 bar in order to have enough pressure in the cylinder to perform enough gas chromatography measurements. After 5 min the next sample cylinders were filled and new sample cylinders were inserted, so that, in the end of one pressure step, three permeate samples and three retentate samples were taken. After the measurements of the first pressure step and the corresponding sample taking, it was possible to change the feed pressure or the membrane or to end the mixed gas experiment.

To continue the measurement at a lower pressure, the circulator was turned off, the feed temperature was adjusted again, and some gas was released from the system until the feed pressure was the desired feed pressure. After the circulator was turned back on, it was necessary to wait until the temperature of the system remained constant. The following steps (setting retentate purge stream, regulating the feed pressure, reaching the steady-state condition, and

sample taking) were identical to the procedure described above. To change the membrane, the circulator was turned off. The pressure in the system was released and the system was evacuated. Then, it was purged with N_2 and the membrane was changed after the excess N_2 pressure was released. The measurement with the new membrane started with the evacuation and purge. After the mixed gas experiment was conducted, the gas circulator and the tempering of the feed gas was simply turned off, the high pressure was released, the whole system was evacuated and purged with N_2 for the shutdown.

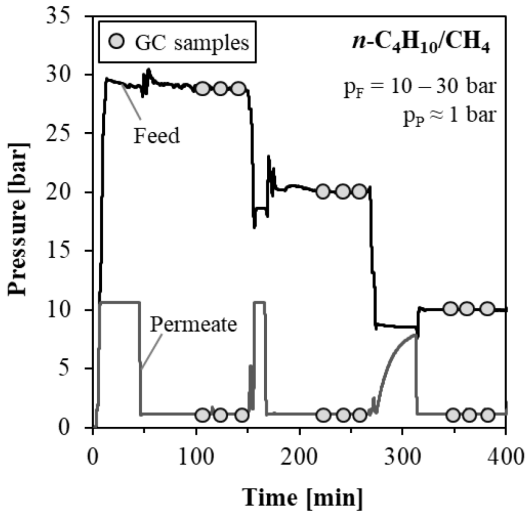

Figure 3.22 Exemplary pressure curve for mixed gas experiments of *n*-C_4H_{10}/CH_4.

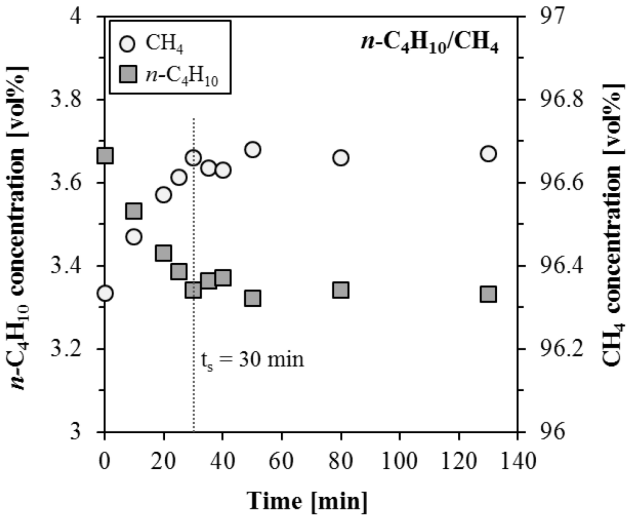

Figure 3.23 Minimum time necessary for steady-state condition (t_s) in a mixed gas experiment.

3.5 Gas chromatography

The calculated values of mixed gas selectivity involve experimental error. In this work, the error analysis, which will be discussed in Section 4, revealed that the uncertainty of gas composition

was the main contributing factor to the total error in selectivity. Therefore, technical and operational optimizations were performed to improve measurement accuracy of the gas chromatography and to reduce the experimental error. Moreover, calibration procedure of the gas chromatography was intensively studied, as it was crucial to perform accurate measurements and to produce reliable results.

3.5.1 Fundamentals of gas chromatography

Gas chromatography is a widely used method for identifying and measuring thermally stable volatile organic compounds. There is a variety of applications of gas chromatography in every laboratory and industrial processes to perform process and product control. Gas chromatography presents a physical method of separation where the components of a sample distribute themselves between two phases: the stationary phase and the mobile phase. A gas chromatography system consists of an injector where the sample is injected in an inlet port, a column where the separation takes place and the stationary phase accommodates, a supply of compressed gas called the carrier gas, which represents the mobile phase, and a detector, which detects the components and gives out the response.

Column

Separation of the components takes place in the column. Depending on the properties of the sample, the column can be a packed column or a capillary column. Most gas chromatographic separations are carried out on packed columns. A packed column is a metal or glass tube filled with the packing. The packing consists of an inert support whose surface is uniformly coated with the stationary phase. The support is most often diatomite, which is a sedimentary rock composed of skeletal remains of single-celled aquatic plants called diatoms. The properties and use of the inert support determine column efficiency and absorptivity. As the gas flow passes through the column, the components of the sample move at velocities that are influenced by the degree of interaction of each component with the stationary phase in the column. Consequently, the different components separate. Since the process is temperature dependent, the column is usually contained in a thermostatically controlled oven.

A gas chromatography system must show high selectivity for the components of interest. This selectivity is maintained by selection of a sufficient stationary phase. The physical dimensions of the selected column determine the fundamental separation characteristics of a column. When the column is selected and installed, it is not practical and economic to adjust the length of the column or replace it with another one. Thus, once the column is selected and installed, the operation variables can be optimized.

In this work, a gas chromatography system from SRI Instruments, model 8610C, was used. A column was selected particularly suitable for efficient separations of *n*-C_4H_{10} and CH_4 by elution development separation technique. It was a 2 m packed column made of stainless steel with an outer diameter of 3.18 mm and an inner diameter of 2 mm. The packing consisted of a stationary phase and support with a ratio of 20%. The support was Chromosorb P-NAW, a certain type diatomite that was not treated (NAW = nonacid washed). The stationary phase was OV-1, which was 100% PDMS, meaning that it was completely saturated with methyl-groups.

Detector

Detection of each individual component is achieved by a detector, which is a device that signals the presence of a component eluted from the column. In this work, a thermal conductivity detector (TCD) was used. It was a chamber in which an electrically heated element reflects changes in thermal conductivity within the chamber atmosphere. The detector signals were recorded and evaluated with the software Peak Simple provided by SRI Instruments.

Peak and retention time

The detector gives out a chromatogram when a compound emerges from the column that is a plot of the detector response (peak) versus time. The area enclosed between the peak and peak base (baseline) is named peak area. The position of the peak maximum on the x-axis qualitatively identifies the component and the area under the peak quantitatively represents the amount of each component. The retention time of the components in a sample is different due to chemical composition. Figure 3.24 gives an example of a chromatogram for a binary gas mixture of *n*-C_4H_{10} and CH_4.

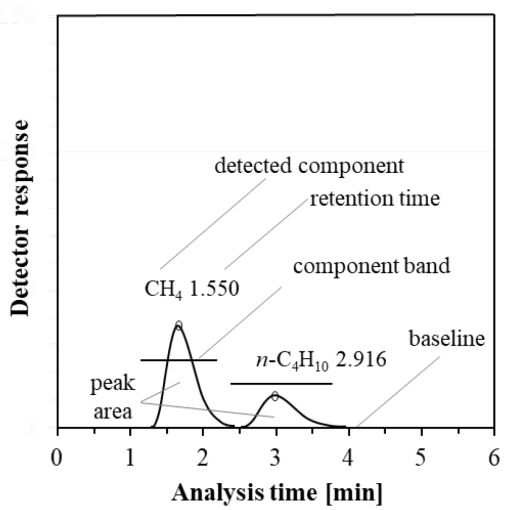

Figure 3.24 Exemplary chromatogram from the measurement of a gas mixture sample containing 16 vol% *n*-C_4H_{10} in CH_4.

Carrier gas

The carrier gas has an important role in transporting the sample through the column and into the detector. The carrier gas must be inert or at least must not react with the stationary phase in the column. Helium, nitrogen, argon and hydrogen are commonly used as carrier gases. The selection of the carrier gas depends on the type of detector, column, application, and safety requirements. On the other hand, separation efficiency and speed are other important requirements. For instance, hydrogen has the lowest viscosity of all gases; thereby, it provides the highest mobile phase velocity and the shortest analysis time. However, the use of hydrogen must be considered carefully in terms of laboratory safety requirements. Helium, on the other hand, gives the best overall performance and peak resolutions for many applications. Therefore, helium was selected

as the carrier gas in this work in order to improve peak resolution and shorten the analysis time compared to other carries gases. The system was operated at approximately 5 bar helium pressure.

Sample loop

A gas chromatography is equipped with a sample loop to control the volume of the injected sample gases. In this work, two sample loops with different volumes (1 mL and 100 mL) were tested. Resulted peaks of *n*-C_4H_{10} and CH_4 using the sample loop with a volume of 1 mL were clear and not overlapped for all concentrations. Therefore, 1 mL sample loop was connected to the sampling valve and used for all measurements. The gas sample was injected into the gas chromatograph using the quick-connection of the gas sampling cylinder.

Temperature programming

Temperature programming is a procedure where the temperature of the column is changed systematically during the whole separation process or a part of the separation process. The relationship of column temperature and retention time is not linear. Small changes in the temperature program of the column may have pronounced effects on the individual peaks in the resulting chromatogram. With an appropriate temperature program of the column, more favorable retention time for individual components can be achieved.

In this work, the TCD was set to operating temperature of 255 °C prior to use. During the measurements, the detector temperature was kept constant at 255 °C as well and the carrier gas pressure was kept constant at 10 psi (≈ 0.69 barg). Several temperature programs were tested in order to get clear and unmerged *n*-C_4H_{10} and CH_4 peaks, and a temperature program was decided to be used in which the temperature of the column during the separation remains unchanged. Initial column temperature was set at 100 °C and it was kept constant for 6 min. Although the temperature profile of the column was programmed for a 6 min measurement, the measurement could be interrupted when the peak areas of the expected components were completed. With this system, the retention time of the *n*-C_4H_{10} and CH_4 was around 1.6 and 2.9 min, respectively. Therefore, the measurements were interrupted after 4 min, and a new measurement was started.

3.5.2 Calibration of the gas chromatography

Before gas samples of an experiment were analyzed with gas chromatography, an initial calibration had to be performed using standard mixtures of known composition containing various amounts of the components of interest. A calibration represents the relationship between the detector response and the concentration of the known sample introduced into the instrument and its graphical representation is called the calibration curve.

In this work, customer tailored standard gas mixtures of *n*-C_4H_{10} and CH_4 with various compositions produced by Air Liquide GmbH and Linde AG were used to achieve a calibration curve for *n*-C_4H_{10}. An advantage of using customer tailored gas standards was that the error in concentration during preparing and diluting the gas samples was avoided. The gas standards used in this work and their respective concentrations are given in Table 3.10.

Table 3.10 Gas standards used for n-C_4H_{10} calibration.

Standard number [-]	Concentration, n-C_4H_{10} [vol%]	Accuracy [vol%]	Cylinder type [L]	Producer [-]
1	1.024	± 0.020	10	Air Liquide
2	1.99	± 0.040	10	Air Liquide
3	4.958	± 0.099	10	Air Liquide
4	9.64	± 0.19	10	Air Liquide
5	16.44	± 0.33	10	Air Liquide
6	35.0	± 1	10	Linde
7	49.90	± 1	10	Linde
8	74.50	± 1	10	Linde
9	99.50	± 0.5	50	Air Liquide

Steps for calibration

The procedure to calibrate the gas chromatography as follows:

1. The sample cylinder was connected to the standard gas bottle and flushed for approximately 5 seconds at 2 bar. Subsequently, the outlet and inlet of the sample cylinder were closed and the sample cylinder was disconnected.
2. The filled sample cylinder was connected to the gas chromatography system. The gas was inserted into the system by opening the inlet of the sample cylinder. Immediately afterwards, the measurement was started using the software.
3. The measurement was repeated several times until the amount of the gas in the sample cylinder was not enough for the next measurement. Usually, 5 to 7 measurements were performed with a filled sample cylinder.
4. The remaining pressure in the sample cylinder was released.
5. The sample cylinder was filled with standard gas twice to perform more measurements for the same concentration. At least 15 measurements were performed for each calibration gas standard.
6. Same procedure was repeated using another gas standard with different concentration.

Steps for measurements of actual experimental samples

The procedure to measure the samples taken during the mixed gas measurements was as follows:

1. One of the calibration gas standards was measured (minimum 10 times) to check whether the calibration was still valid. These measurements were performed as precautionary measurements and used for statistical process control.
2. Subsequently, the compositions of the sample cylinders filled during the mixed gas experiment were measured. The maximum number of measurements that could be performed using one sample cylinder depended on the amount of the gas inserted into the sample cylinder during the experiment.
3. Lastly, the sample taken from the feed gas mixture was measured to test the mixture preparation accuracy.

Best-fit calibration curve

Several publications outline requirements for a good gas chromatographic calibration method [145-147]. Examples of suggested requirements are given below:

- *Calibration linearity* The calibration curve for chromatographic methods is expected to be linear. Given the limitations or specific method demands, it is allowed to use both linear and nonlinear models for the calibration data. The linear range is a characteristic of the detector and the detected non-linearity in the calibration curve can be avoided by partition into the linear range.
- *Correlation coefficient* A correlation coefficient $R^2 \geq 0.999$ is mostly considered acceptable.
- *Y-Intercept* In a linear function of $y = mx + n$, m is the slope and n is the y-intercept, which demonstrates how far is the fitted line away from the origin. The y-intercept is expected to be zero or quite close to zero. Some approaches force the regression line to pass through the origin assuming x and y is proportional.
- *Precision and Accuracy* The precision is expressed as standard deviation (SD) of multiple measurements and a relative standard deviation (RSD) of ±1 is reasonable. Accuracy defines how close the experimental data is to the "true" value and it is expected to be within 3–5% of the target concentration. These two concepts will be discussed in Section 4 *Error Analysis*.

The goal was to select the most appropriate calibration function using the measurements of gas standards to determine *n*-C_4H_{10} concentration in a sample of a mixed gas experiment as well as the requirements listed above were met. It was aimed to calculate *n*-C_4H_{10} concentration in a sample with the fitted calibration curve and the rest of the sample was assumed to contain only methane. Calibration data of *n*-C_4H_{10} and error in measurements in terms of SD and RSD are given in Table 3.11.

The method of least squares is the standard approach for data fitting. The best fit in the least squares minimizes the sum of the squares of residuals (vertical distances between the measured value and the fitted value provided by the model). The literature highly recommends the calibration model to be linear. Figure 3.25 (a) shows the calibration fit for *n*-C_4H_{10} concentrations between 1.024 and 99.50 vol% using linear regression method. The function of the fitted line (fit-1) is given in Table 3.12. The calibration data did not follow a linear trend for the entire calibration range adequately. Although the correlation coefficient of fit-1 was equal to 0.99920, which signified an adequate regression, the residuals for the *n*-C_4H_{10} concentrations particularly lower than 10 vol% were too large. Other least-squares models (exponential, polynomial, etc.) were also applied for the whole concentration range as well, which are not listed here. However, none of them were capable of fitting the entire calibration range sufficiently.

To solve that problem, it was proposed to apply the linear interpolation method using discrete set of successive linear segments with different slopes to construct a whole calibration fit within the concentration range of interest. Figure 3.25 (b) represents a two segmental interpolation (fit-2) involving two linear functions f1 and f2 for different intervals. The first function f1 was valid from 1 to 10 vol% and the second function f2 was valid from 10 to 99.50 vol%. The equations of the functions are given in Table 3.12. By applying two segmental interpolation, a better fitting for the *n*-C_4H_{10} concentrations lower than 10 vol% was achieved where the y-intercept was pretty close to zero (–0.04275) and the correlation coefficient was higher than that of fit-1 (0.99999). The second function f2 for the *n*-C_4H_{10} concentration between 10 and 99.50 vol% had a higher

correlation coefficient (0.99956) as well, although the *y*-intercept was considerable far from the origin due to the different slopes of the functions. Nevertheless, this could be ignored, because the linear interpolation method was used to simply model the relationship between the measured peak area and the known concentration of *n*-C_4H_{10}. The major drawback of fit-2 was the difference of the concentrations calculated by function f1 and f2 when *n*-C_4H_{10} concentration was close to 10 vol%.

Table 3.11 Summary of calibration data of *n*-C_4H_{10} and error in measurements.

Standard number [-]	Concentration, *n*-C_4H_{10} [vol%]	Peak area, *n*-C_4H_{10} [-]	Error	
			SD [-]	RSD [%]
1	1.024	293.05	0.918	0.313
2	1.99	570.56	0.779	0.137
3	4.958	1377.46	2.538	0.184
4	9.64	2678.77	5.374	0.201
5	16.44	4625.93	5.874	0.127
6	35.0	9266.24	14.036	0.152
7	49.90	12740.47	19.996	0.157
8	74.50	18613.09	31.177	0.168
9	99.50	24374.96	85.618	0.351

A further step was excluding the measurement data of the 1st and the 9th calibration gas standard in order to avoid the possible additional error in data fitting. Eventually, in this work, the interesting concentration range of *n*-C_4H_{10} was between 1.99 and 74.50 vol%. This range involved all measurements from the lowest feed concentration to the highest permeate concentration. Figure 3.25 (c) represents a three segmental interpolation (fit-3) involving three linear functions: f1 from 1.99 to 9.64 vol%, f2 from 9.64 to and 35 vol%, and f3 from 35 to 74.50 vol% *n*-C_4H_{10} concentration. The equations of the functions are given in Table 3.12. It was seen that by applying three segmental interpolations the distance between the fitted functions at the intervals were not as significant as those of the two segmental interpolation.

Lastly, a five segmental interpolation (fit-4) between 1.99 and 74.50 vol% *n*-C_4H_{10} calibration measurement data was tested involving five linear functions: f1 from 1.99 to 9.64 vol%, f2 to f5 an interpolation between every two data points for *n*-C_4H_{10} concentrations above 9.64 vol% as shown in Figure 3.25 (d). This is the most accurate linear segmental interpolation method providing the highest reproducibility with the highest correlation coefficients for each segment (Table 3.12).

In order to evaluate the influence of the different calibration fits on resulting selectivity in a mixed gas experiment, mixed gas selectivity of a PDMS membrane was calculated applying four different calibration fits to actual experimental data. The experiments were performed with binary mixtures of *n*-C_4H_{10} and CH_4 where *n*-C_4H_{10} concentration varied between 4 and 18 vol%. The

experiments were performed at several feed pressures between 5.5 and 30 bar at 20 °C. Figure 3.26 presents *n*-C_4H_{10} /CH_4 mixed gas selectivity calculated with four different calibration fits as a function of mean *n*-C_4H_{10} fugacity. Apparently, the selectivity of PDMS calculated by fit-1 was extremely high and unrealistic, especially for the mean fugacity of *n*-C_4H_{10} lower than 0.30 bar. The feed *n*-C_4H_{10} concentrations in those experiments were between 3 and 6 vol%, where the regression did not follow a linear trend for the entire calibration range and the residuals for the *n*-C_4H_{10} concentration were too large. Additionally, the selectivity values were scattered when the feed *n*-C_4H_{10} concentration was higher than 10 vol% (mean *n*-butane fugacity > 0.37 bar). This means that the results were not reproducible. When fit-2 was applied as a calibration curve to the data, the mixed gas selectivity did not show unexpected values, but the selectivity values were still scattered, which led to high error and uncertainty. Therefore, both fit-1 and fit-2 were eliminated.

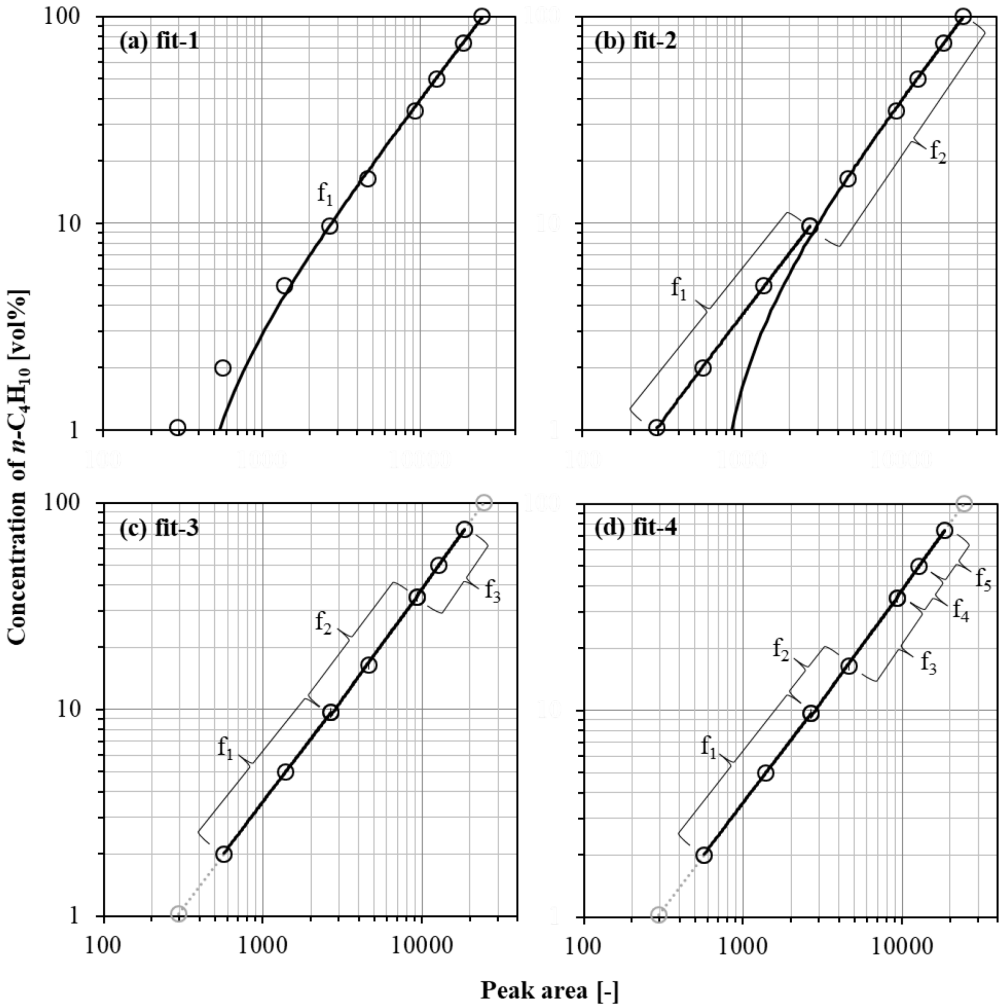

Figure 3.25 Linear calibration fits with different intervals.

The mixed gas selectivities calculated with fit-3 and fit-4 were very close to each other and both calibration fits showed high reproducibility. However, the slopes of each function of fit-3 were considerably different from each other. Due to that, there was still differences between the concentrations calculated by function f1 and f2 when *n*-C_4H_{10} concentration was close to

9.64 vol% and between the concentrations calculated by function f2 and f3 when *n*-C_4H_{10} concentration was close to 35 vol%. As a result, calculated selectivity values scattered. Higher accuracy was required for selectivity calculations. Thus, it was necessary to use the most accurate calibration fit that would add minimum error to the resulting selectivity. Therefore, it was decided to use fit-4, which was the most adequate regression model, which described the relationship between the concentration and the response by five linear segmental interpolations providing high quality results with the highest reproducibility and minimum error.

Table 3.12 Functions of the linear fitted lines using measurements of gas standards.

	Function: y = mx + n				
Calibration fit	no	Intervals	m	n	R^2
[-]	[-]	[vol% – vol%]	[-]	[-]	[-]
1	f1	1.024 – 99.50	0.00408	- 1.20111	0.99920
2	f1	1.024 – 9.64	0.00362	- 0.04275	0.99999
	f2	9.64 – 99.50	0.00416	- 2.58318	0.99956
3	f1	1.99 – 9.64	0.00362	- 0.04779	0.99998
	f2	9.64 – 35.0	0.00388	- 1.05890	0.99911
	f3	35.0 – 74.50	0.00423	- 4.11343	0.99995
4	f1	1.99 – 9.64	0.00362	-0.04818	0.99999
	f2	9.64 – 16.44	0.00349	0.28387	1
	f3	16.44 – 35.0	0.00400	-2.06601	1
	f4	35.0 – 49.90	0.00426	-4.49009	1
	f5	49.90 – 74.50	0.00422	-3.96536	1

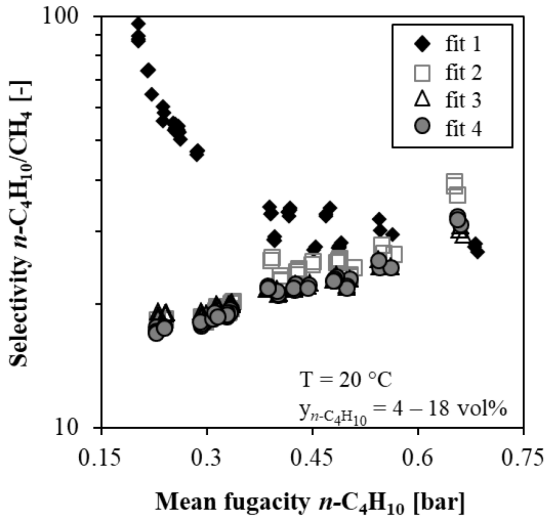

Figure 3.26 Influence of linear calibration fits with different intervals on selectivity.

Statistical process control

As mentioned before, one of the calibration gas standard samples was measured many times before the measurements of actual experimental samples. With those measurements, the performance of gas chromatography was monitored at appropriate intervals to detect any indication of performance degradation before the degradation was sufficient to affect quality of measurements. Recording and plotting these precautionary measurements on a control chart was a process control method to see the change in the response of known concentrations used for calibration previously.

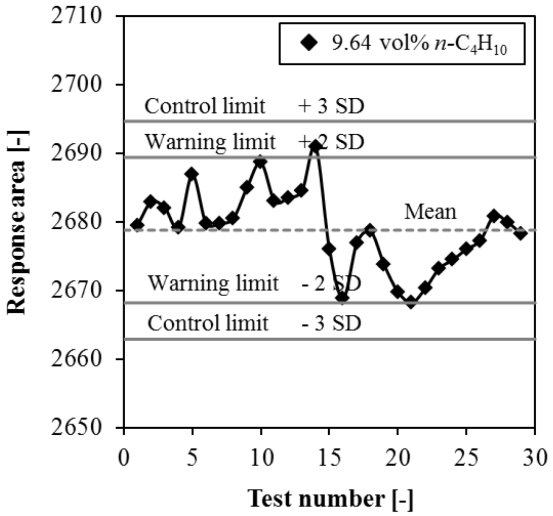

Figure 3.27 Exemplary statistical process control chart for a calibration gas standard with 9.64 vol% *n*-C_4H_{10} in CH_4.

An exemplary statistical process control chart is given in Figure 3.27. Statistical analysis was performed by calculating the mean and standard deviation of the measurements when a sufficient number of precautionary measurements (about 20) was obtained. The values of detector response were plotted on the vertical axis and the test number was plotted on the horizontal axis chronologically. This was repeated for each calibration gas standard. The lines showing plus and minus two times the standard deviation indicated *warning limits*, likewise, the lines showing plus and minus three times the standard deviation indicated *control limits*. When measurements were performed, results were plotted immediately to the control chart corresponding concentration. If a value exceeded the warning limits, the calibration was repeated. On the other hand, if a value exceeded control limits, which never happened, it might have indicated a potential problem. In this work, this approach allowed the operators to control the risk of using the analytical method in routine and to have full information about its performance.

4 Error Analysis

Inevitable errors exist in every scientific measurement. When a quantity is measured for the second time, it is usually a different value than the first one. The absolute true value of a physical quantity cannot be determined; however, errors can be reduced by improved measurement techniques and carefully repeated experiments, and the true value can be more closely approximated with great confidence. Error analysis is the study of uncertainties in physical measurements.

In gas permeation calculations, in this work, extremely small variations in measurements of individual physical quantities produced huge differences in overall outcomes. Therefore, great emphasis was particularly put on error analysis to provide highly accurate, reliable experimental data with well-estimated error. Accordingly, the total error in calculated pure and mixed gas permeability and selectivity was estimated by propagation of error method to establish the validity of the results and to confirm their reliability. Furthermore, the impact of uncertainties in individual quantities on the calculated permeability and selectivity was analyzed, which was crucial to find out the main contributing factor.

In the beginning of this chapter, the important terms related to error analysis are introduced. Afterwards, the evaluation of individual uncertainties in pure and mixed gas permeability and selectivity measurements by propagation of error method will be presented. The instrumental uncertainties inherent in the gas permeation setup will also be discussed.

4.1 Basic definitions

Three important concepts will be briefly described here before leading in propagation of error method: (i) uncertainty and error, (ii) accuracy and precision, and (iii) random and systematic error. The explanations given in this section are based on Bevington and Robinson [148] and Taylor [149].

Uncertainty and error

Uncertainty defines the fluctuations in measurements and *error* defines the difference between an observed (or calculated) value and the true value. The main goal of error analysis is to estimate the true value as good as possible and the uncertainties inherited in it. A result that has the smallest error can be considered the most reliable. The correct way of stating a result of a measurement is to make the best estimate of the measured quantity and the confidence range in which the quantity lies:

$$\text{measured value of } x = x_{best} \pm \Delta x \tag{4.1}$$

where x_{best} is the best estimate for the true value and Δx is the best estimate of the error.

The best estimate for the true value is usually the arithmetic average of several measurements of a quantity. The quality of a measurement is indicated not only by the error Δx, but also by the ratio of Δx to x_{best}, which leads to relative error or fractional error:

$$\text{relative error} = \frac{\Delta x}{|x_{best}|} \tag{4.2}$$

Relative error of 10% is usually obtained from rough measurements. 1% or 2% relative error is the indicator of reasonably careful measurements. Relative error less than 1% is considered as quite good but also hard to achieve.

Accuracy and precision

Accuracy measures the closeness of a result to the true value. The accuracy needed in an experiment depends on particularly the sensitivity of the calculated value to the measured value meaning how much a small error in the measurement will affect the final calculation.

Precision, on the other hand, measures how close two or more results are determined under identical conditions (same method, same operator, same laboratory conditions, etc.) independently of the true value. Precision is also a measure of *reproducibility* or *repeatability*. When determining the uncertainty in an experimental result, it refers to the precision. Figure 4.1 illustrates the concept of accuracy and precision very well by comparison of the grouping of arrows in a target.

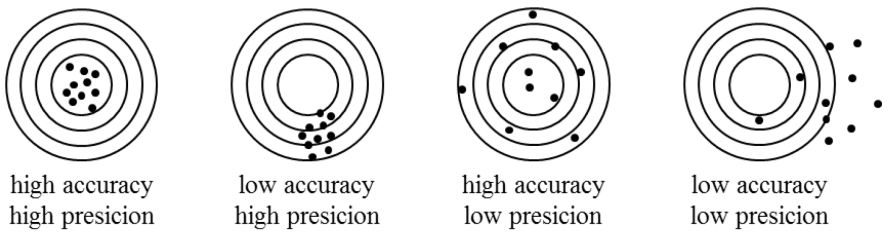

Figure 4.1 Schematic of accuracy and precision.

Random and systematic error

Random errors are fluctuations in reading of instruments, which either come from the imperfections in the equipment or arise due to the observer. It can be a combination of both as well. They provide different results when the experiment is repeated which affects the precision of the measurement. Random errors can be reduced by using better equipment or by repeating the experiment.

Systematic errors are errors that affect the accuracy of a measurement, which lead to a discrepancy from the true value of a quantity. A faulty calibration and incorrect readings of an equipment are common examples of systematic errors. Simply repeating the experiments cannot reveal systematic errors, even though results show high precision. They can only be reduced by carefully examining the experimental procedure and techniques used. It is possible to get a reliable estimate of random errors; however, systematic errors are usually hard to evaluate or even to detect.

4.2 Propagation of error

Dependent variables cannot be determined in a single direct measurement. First, one or more different quantities are measured directly, and then the variable of interest is calculated as a function of these measured quantities.

The uncertainties in these quantities have to be estimated first. Then, it can be determined how these uncertainties propagate through the calculation of the dependent variable of interest [149]. The method used to estimate the overall error of a calculated variable is called the *Propagation of Error* (POE). The strategy of the POE is the estimation of the individual contribution of each uncertainty to the final calculated result. Great advantage of the method is that the error can be quantified and it is possible to distinguish which uncertainties are more significant or negligible.

Assuming a dependent variable q is calculated from the measured quantities of $x_i, \ldots, x_n$: $q = f(x_i, \ldots, x_n)$, the total error in the calculated variable q can be estimated by the general POE equation as given below [148]:

$$\Delta q = \sqrt{\sum_{i=1}^{n} \left(\frac{\partial f}{\partial x_i} \Delta x_i \right)^2} \tag{4.3}$$

The term $(\partial f/\partial x_i)$ in the equation is the derivative of the function with respect to parameter x, Δx_i is the uncertainty of measurements of parameter x, and Δq is the total error.

4.2.1 Application of POE for pure gas permeation measurements

In a pure gas permeation experiment, permeability P is the calculated variable of interest. Permeability is a function of the following measured independent quantities: thickness of the active separation layer of the membrane δ, volumetric flow rate on the permeate side $\dot{V}_P$, diameter of the membrane d_m, pressure on the feed side p_F, pressure on the permeate side p_P, and temperature T. To determine the total propagated error in calculated permeability the partial derivatives of permeability with respect to each measured quantities were calculated as given below.

Permeability P is calculated as:

$$P = \frac{\dot{V}_P \delta}{A_m (f_F - f_P)}. \tag{2.15}$$

Derivation of P with respect to thickness δ:

$$\frac{\partial P}{\partial \delta} = \frac{\dot{V}_P}{A_m (f_F - f_P)} \tag{4.4}$$

with respect to permeate flow rate $\dot{V}_P$:

$$\frac{\partial P}{\partial \dot{V}_P} = \frac{\delta}{A_m (f_F - f_P)} \tag{4.5}$$

with respect to diameter of the membrane d_m:

$$\frac{\partial P}{\partial d_m} = \frac{\dot{V}_P \delta}{\frac{1}{8}\pi d_m^3 (f_F - f_P)} \tag{4.6}$$

with respect to feed pressure p_F:

$$\frac{\partial P}{\partial p_F} = \frac{\dot{V}_P \delta \exp\left(\frac{B p_F}{RT}\right)\left(B_F p_F + RT\right)}{A_m RT (f_P - f_F)^2} \tag{4.7}$$

with respect to permeate pressure p_P:

$$\frac{\partial P}{\partial p_P} = \frac{\dot{V}_P \delta \exp\left(\frac{B_P p_P}{RT}\right)\left(B_P p_P + RT\right)}{A_m RT (f_F - f_P)^2} \tag{4.8}$$

with respect to temperature T:

$$\frac{\partial P}{\partial T} = \frac{\dot{V}_P \delta B\left(p_F f_F - p_P f_P\right)}{A_m RT^2 (f_F - f_P)^2} \tag{4.9}$$

The total error for permeability is calculated as follows:

$$\Delta P = \sqrt{\begin{array}{c}\left(\Delta\delta \frac{\partial P}{\partial \delta}\right)^2 + \left(\Delta \dot{V}_{i,P} \frac{\partial P}{\partial \dot{V}_P}\right)^2 + \left(\Delta d_m \frac{\partial P}{\partial d_m}\right)^2 + \\ \left(\Delta p_F \frac{\partial P}{\partial p_F}\right)^2 + \left(\Delta p_P \frac{\partial P}{\partial p_P}\right)^2 + \left(\Delta T \frac{\partial P}{\partial T}\right)^2\end{array}} \tag{4.10}$$

4.2.2 Application of POE for mixed gas permeation measurements

The calculated variables of interest in a mixed gas permeation experiment are permeability P_i, and selectivity α_{ij}. The uncertainties in permeability of each component in the mixture and overall selectivity were calculated separately by POE method.

Permeability

In addition to the independent quantities of a pure gas permeation experiment, permeability of a component i in a gas mixture is dependent on the mole fractions of that component on the feed side, $y_{i,F}$, and permeate side $y_{i,P}$ of the membrane during the mixed gas experiment.

To determine the total propagated error in calculated mixed gas permeability of the component i, the partial derivatives of permeability with respect to each measured quantities were calculated as given below.

Permeability of the component *i* P_i is calculated as:

$$P_i = \frac{\dot{V}_P y_{i,P} \delta}{A_m \left(f_{i,F} - f_{i,P}\right)}. \tag{2.16}$$

Derivation of P_i with respect to thickness δ:

$$\frac{\partial P_i}{\partial \delta} = \frac{\dot{V}_P y_{i,P}}{A_m \left(f_{i,F} - f_{i,P}\right)} \tag{4.11}$$

with respect to permeate flow rate $\dot{V}_{i,P}$:

$$\frac{\partial P_i}{\partial \dot{V}_{i,P}} = \frac{y_{i,P} \delta}{A_m \left(f_{i,F} - f_{i,P}\right)} \tag{4.12}$$

with respect to diameter of the membrane d_m:

$$\frac{\partial P_i}{\partial d_m} = \frac{\dot{V}_P y_{i,P} \delta}{\frac{1}{8} \pi d_m^3 \left(f_{i,F} - f_{i,P}\right)} \tag{4.13}$$

with respect to feed pressure p_F:

$$\frac{\partial P_i}{\partial p_F} = \frac{\dot{V}_P y_{i,P} \delta f_{i,F} \left(\frac{B_{i,F} p_F}{RT} + 1\right)}{A_m p_F \left(f_{i,P} - f_{i,F}\right)^2} \tag{4.14}$$

with respect to permeate pressure p_P:

$$\frac{\partial P_i}{\partial p_P} = \frac{\dot{V}_P y_{i,P} \delta f_{i,P} \left(\frac{B_{i,P} p_P}{RT} + 1\right)}{A_m p_P \left(f_{i,P} - f_{i,F}\right)^2} \tag{4.15}$$

with respect to temperature T:

$$\frac{\partial P_i}{\partial T} = \frac{\dot{V}_P y_{i,P} \delta \left(B_{i,F} p_F f_{i,F} - B_{i,P} p_P f_{i,P}\right)}{A_m R T^2 \left(f_{i,F} - f_{i,P}\right)^2} \tag{4.16}$$

with respect to mole fraction of component *i* on feed side $y_{i,F}$:

$$\frac{\partial P_i}{\partial y_{i,F}} = \frac{\dot{V}_P y_{i,P} \delta f_{i,F}}{A_m y_{i,F} \left(f_{i,P} - f_{i,F}\right)^2} \tag{4.17}$$

with respect to mole fraction of component *i* on permeate side $y_{i,P}$:

$$\frac{\partial P_i}{\partial y_{i,P}} = \frac{\dot{V}_P \delta f_{i,F}}{A_m \left(f_{i,P} - f_{i,F}\right)^2} \tag{4.18}$$

The total uncertainty for permeability of component *i* is calculated as follows:

$$\Delta P_i = \sqrt{\begin{array}{c} \left(\Delta\delta \frac{\partial P}{\partial \delta}\right)^2 + \left(\Delta \dot{V}_{i,P} \frac{\partial P}{\partial \dot{V}_{i,P}}\right)^2 + \left(\Delta d_m \frac{\partial P}{\partial d_m}\right)^2 + \\ \left(\Delta p_F \frac{\partial P}{\partial p_F}\right)^2 + \left(\Delta p_P \frac{\partial P}{\partial p_P}\right)^2 + \left(\Delta T \frac{\partial P}{\partial T}\right)^2 + \\ \left(\Delta y_{i,F} \frac{\partial P}{\partial y_{i,F}}\right)^2 + \left(\Delta y_{i,P} \frac{\partial P}{\partial y_{i,P}}\right)^2 \end{array}} \tag{4.19}$$

Selectivity

The other dependent variable of interest in a mixed gas permeation experiment is selectivity. Selectivity is a function of the following measured independent quantities: pressure on the feed and permeate side p_F and p_P, mole fractions of the component *i* on the feed and permeate side $y_{i,F}$ and $y_{i,P}$, and temperature *T*.

To determine the total propagated error in calculated selectivity, the partial derivatives of selectivity with respect to each measured quantity were calculated. Analytical forms of the partial derivatives of selectivity were quite complicated due to the complex calculations of second virial coefficients in fugacity coefficient calculations. Therefore, a simplification was applied to the error estimation that the uncertainties in the second virial coefficients with respect to independent quantities, which were necessary to calculate second virial coefficients themselves (mole fractions of the component *i* on the feed and permeate side $y_{i,F}$ and $y_{i,P}$, and temperature *T*), were assumed to be negligible. Sensitivity analysis of the second virial coefficients will be discussed later in this section.

Selectivity α_{ij} is calculated as:

$$\alpha_{ij} = \frac{y_{i,P}}{y_{j,P}} \frac{\left(f_{j,F} - f_{j,P}\right)}{\left(f_{i,F} - f_{i,P}\right)} \tag{2.20}$$

When the fugacity calculations were introduced, selectivity was equal to:

$$\alpha_{ij} = \frac{y_{i,P}}{y_{j,P}} \frac{\left[p_F y_{j,F} \exp\left(\frac{B_{j,F}\, p_F}{RT}\right) - p_P y_{j,P} \exp\left(\frac{B_{j,P}\, p_P}{RT}\right)\right]}{\left[p_F y_{i,F} \exp\left(\frac{B_{i,F}\, p_F}{RT}\right) - p_P y_{i,P} \exp\left(\frac{B_{i,P}\, p_P}{RT}\right)\right]} \tag{4.20}$$

Derivation of α_{ij} with respect to feed pressure p_F:

$$\frac{\partial \alpha_{ij}}{\partial p_F} = \frac{y_{i,P}}{y_{j,P}} \frac{\left[\begin{array}{c}\left(B_{j,F} - B_{i,F}\right) f_{i,F}\, f_{j,F} - \left(\frac{RT}{p_F} + B_{j,F}\right) f_{i,P}\, f_{j,F} + \\ \left(\frac{RT}{p_F} + B_{i,F}\right) f_{i,F}\, f_{j,P}\end{array}\right]}{RT\left(f_{i,P} - f_{i,F}\right)^2} \tag{4.21}$$

with respect to permeate pressure p_P:

$$\frac{\partial \alpha_{ij}}{\partial p_P} = -\frac{y_{i,P}}{y_{j,P}} \frac{\left[\begin{array}{c}\left(B_{i,P} - B_{j,P}\right) f_{i,P} f_{j,P} - \left(\frac{RT}{p_P} + B_{i,P}\right) f_{i,P} f_{j,F} + \\ \left(\frac{RT}{p_P} + B_{j,P}\right) f_{i,F} f_{j,P}\end{array}\right]}{RT\left(f_{i,F} - f_{i,P}\right)^2} \tag{4.22}$$

with respect to temperature T:

$$\frac{\partial \alpha_{ij}}{\partial T} = -\frac{y_{i,P}}{y_{j,P}} \frac{1}{T^2\left(f_{i,F} - f_{i,P}\right)^2} \frac{1}{R} \left[\begin{array}{c} f_{j,F}\left(\begin{array}{c} f_{i,F} p_F \left(B_{j,F} - B_{i,F}\right) - \\ f_{i,P}\left(B_{j,F} p_F - B_{i,P} p_P\right)\end{array}\right) + \\ \exp\left(\frac{B_{j,P} p_P}{RT} + 1\right) \\ \left(\begin{array}{c} f_{i,F}\left(B_{i,F} p_F - B_{j,P} p_P\right) - \\ f_{i,P} p_P \left(B_{i,P} - B_{j,P}\right)\end{array}\right)\end{array}\right] \tag{4.23}$$

with respect to mole fraction of component i on feed side $y_{i,F}$:

$$\frac{\partial \alpha_{ij}}{\partial y_{i,F}} = -\frac{y_{i,P}}{y_{j,P}} p_F \frac{\left[\begin{array}{c} p_F \exp\left(\frac{B_{j,F} p_F}{RT}\right) \exp\left(\frac{B_{i,F} p_F}{RT}\right) - \\ \exp\left(\frac{B_{j,F} p_F}{RT}\right) f_{i,P} - \exp\left(\frac{B_{i,F} p_F}{RT}\right) f_{j,P}\end{array}\right]}{\left(f_{i,F} - f_{i,P}\right)^2} \tag{4.24}$$

with respect to mole fraction of component i on permeate side $y_{i,P}$:

$$\frac{\partial \alpha_{ij}}{\partial y_{i,P}} = \frac{1}{\left(y_{i,P} - 1\right)^2} \frac{\left[\begin{array}{c} f_{j,F}\left(f_{i,F} - f_{i,P} y_{i,P}\right) - \\ p_P \exp\left(\frac{B_{j,P} p_P}{RT}\right) f_{i,F}\left(y_{i,P} - 1\right)^2\end{array}\right]}{\left(f_{i,F} - f_{i,P}\right)^2} \tag{4.25}$$

The total uncertainty for permeability of a component i is calculated as follows:

$$\Delta \alpha_{ij} = \sqrt{\begin{array}{c}\left(\Delta p_F \frac{\partial \alpha_{ij}}{\partial p_F}\right)^2 + \left(\Delta p_P \frac{\partial \alpha_{ij}}{\partial p_P}\right)^2 + \left(\Delta T \frac{\partial \alpha_{ij}}{\partial T}\right)^2 + \\ \left(\Delta y_{i,F} \frac{\partial \alpha_{ij}}{\partial y_{i,F}}\right)^2 + \left(\Delta y_{i,P} \frac{\partial \alpha_{ij}}{\partial y_{i,P}}\right)^2\end{array}} \tag{4.26}$$

4.2.3 Uncertainty of instruments

In order to calculate contributions of each independent quantity to the result, the accuracy of each measurement instruments must be known. When a quantity is measured using a physical instrument, the uncertainty in the measurement is due to the instrument. This might result either from imperfection of the equipment, which leads to low reproducibility, or from the observer imprecision. It might be combination of both as well and such uncertainties are called *instrumental uncertainty*. The uncertainty from the equipment itself can be estimated by some external methods. In case of digital instruments, the manufacturer usually specifies a tolerance of the instrument, which means the accuracy of the instrument. The uncertainties obtained from the external method and the tolerance given by the manufacturer of the equipment should ultimately agree.

In this work, each manufacturer, except for gas chromatography, provided the accuracy of the instrument. The list of the instruments used for pure and mixed gas permeation experiments and their accuracy are given in Table 4.1. The uncertainty resulting from concentration measurements by gas chromatography will be discussed later.

Thickness of the active separation layer and the actual diameter of the membrane were measured from the cross-sectional and surface SEM images of the membranes. For separation layer measurements, five SEM cross-sectional images were taken from different positions of the membrane sample. From each SEM image, separation layer thickness was measured at five different positions using ImageJ software. Finally, arithmetic average of these 25 thickness measurements was calculated and the uncertainty of these measurements was reported as relative standard deviation (RSD). Average actual diameter of the membrane and the uncertainty of it were calculated in the same way as the active separation layer. The only difference was that the measurements were performed using SEM surface images.

Table 4.1 Accuracy of the instruments used for pure and mixed gas permeation experiments.

Independent quantity	Measurement range	Measurement accuracy
Permeate flow rate $\dot{V}_P$	0 to 1 $L_{CH_4(STP)}min^{-1}$	±1.0 % of measurement reading in N_2-eq.
	0 to 5 $L_{CH_4(STP)}min^{-1}$	±1.0 % of measurement reading in N_2-eq.
Feed pressure p_F	0 to 10 bar	±10 mbar
	0 to 40 bar	±40 mbar
Permeate pressure p_P	0 to 10 bar	±10 mbar
Temperature T	0 to 80 °C	±0.1 K
Actual diameter of membrane d_m		±0.5 % of measurement reading
Active separation layer thickness δ		±3.5 % of measurement reading

4.2.4 Uncertainty of gas chromatography

The estimation of the uncertainty in gas chromatography measurements was essential for the interpretation of the results correctly. The main aim of the statistical analysis given here is to achieve a good estimation of measurement uncertainty. It was particularly difficult to do that for gas chromatography because too much data should have been obtained, which means huge experimental time and money. In this work, a new strategy to estimate measurement uncertainty of gas chromatography is recommended which will be discussed in the following section.

Statistical approach for the estimation of the uncertainty

The first measurement is not expected to estimate the true value of a quantity of *x*. By repeating the measurement, a discrepancy between the two results of the measurements is expected due to the random error and neither measurement is expected to be exactly the true value of *x*. When the measurement is repeated several times, the results are expected to distribute around the true value assuming the systematic errors are to be negligible small. The exact distribution would be described with infinite measurements. Even though infinite measurements are impossible to make, the existence of such distribution can be hypothesized and it is called the parent distribution. Furthermore, it can be hypothesized that the measurements made represent a sample from the parent population, resulting in a distribution called the sample distribution [148]. Thus, as the number of measurements approaches infinity, the sample distribution approaches the parent distribution. The area under the parent distribution in the interval a $\leq x \leq$ b essentially corresponds to the probability that a single measurement of *x* will be between a and b such as illustrated in Figure 4.2 (a).

For a set of *N* measurements for quantity *x*, the mean of *x* is represented by $\bar{x}$ and calculated by the following formula:

$$\bar{x} = \frac{1}{N}\sum_{i=1}^{N} x_i \tag{4.27}$$

As previously stated, the sample distribution approaches the parent distribution as *N* approaches infinity. Thus, the mean of the parent distribution is represented by μ and is defined as:

$$\mu = \lim_{N\to\infty}\left(\frac{1}{N}\sum_{i=1}^{N} x_i\right) \tag{4.28}$$

The standard deviation of the parent distribution represented by the symbol σ_x is a parameter that measures how widely spread the measured values on either side of the mean, and is given by the formula:

$$\sigma_x = \sqrt{\frac{1}{N}\sum_{i=1}^{N}(x_i - \mu)^2} \tag{4.29}$$

The standard deviation of the sample distribution represented by s_x is defined as:

$$s_x = \sqrt{\frac{1}{N-1}\sum_{i=1}^{N}(x_i - \bar{x})^2} \tag{4.30}$$

where the factor *N-1*, rather than *N*, in the denominator accounts for the fact that the parameter $\bar{x}$ has been determined from the measurement itself. The standard deviation of the parent distribution σ_x is simply the square root of the variance of the parent distribution σ_x^2. Similarly, the standard deviation of the sample distribution s_x, is the square root of the variance of the sample distribution s_x^2.

When measurements are subjected to small random errors and negligible systematic errors, the parent distribution will be symmetric bell-shaped curve, which is called normal distribution or Gauss function. The Gauss function is centered on the true value of *x* and has a width parameter σ, which indicates the width of the shape as illustrated in Figure 4.2 (b). The width is linked to the precision of the measurements. The larger the width, the more widely spread the data and the lower the precision.

The parent distribution of measurements of a quantity *x* displays the probability of obtaining any given value of *x* in a random measurement performed under the same conditions. In case of the normal distribution, the probability that a measurement will fall within one σ_x of the true value *x* is 68%. In other words, 68% of the results will fall within a distance σ_x on either side of the true value of *x*. For $2\sigma_x$ the probability is 95% and for $3\sigma_x$ it is 99.7%. These intervals are called *confidence intervals* stating the probability of a measurement will fall within the range of one, two, or three σ_x as shown in Figure 4.2 (c).

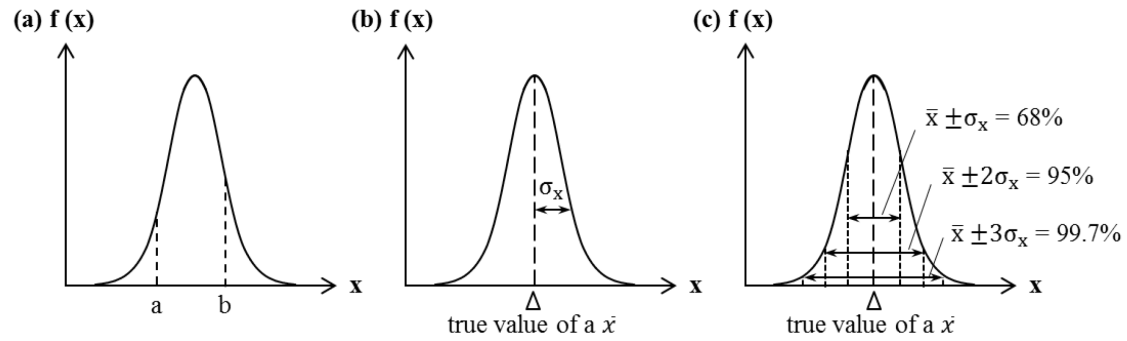

Figure 4.2 Schematic of normal distribution.

Unfortunately, the parent distribution is unknown so that the true value of *x* and the width parameter σ have to be estimated from the finite number of measured values. To find the best estimate of *x* and σ, *principle of maximum likelihood* [150] method is applied. This method shows that the best estimate for the true value of *x* is the mean of the *N* measurements $\bar{x}$. If *N* measurements are repeated many times, the resulting value of the mean will be normally distributed as well. They will center on the true value of *x* and a width $s_{\bar{x}}$ which is called the standard deviation of the mean. It characterizes the uncertainty within the estimate of the true value $\bar{x}$ and it is calculated as follows [149]:

$$s_{\bar{x}} = \frac{s_x}{\sqrt{N}} \tag{4.31}$$

As more data is collected, the standard deviation s_x will be more precise but it is not predictable whether the standard deviation of a larger sample will be bigger or smaller. The standard deviation of the mean $s_{\bar{x}}$, on the other hand, slowly decreases as N increases, because the mean of a large sample is likely to be closer to the true value of the mean than the mean of a small sample. For that reason, evaluation of the uncertainties in measurements is reasonable. The concept of confidence intervals applies here as well.

Estimation of uncertainty of gas chromatography

The uncertainties in gas chromatography measurements were evaluated using the statistical approach described above.

The best estimate for the true value of a gas chromatography measurement x was calculated as the mean of N measurements as follows:

$$x_{best} = \bar{x} \tag{4.32}$$

The uncertainty in the measurements was best estimated by the standard deviation of the mean as follows:

$$\Delta x = s_{\bar{x}} \tag{4.33}$$

During this work, different operators repeated the calibration of gas chromatography several times. Furthermore, prior to the measurements of actual gas mixture samples, one of the calibration gas standards was measured at least 10 times in order to check whether the calibration was still valid according to the calibration control procedure. For that, each time a different calibration gas standard was used depending on the *n*-C_4H_{10} concentration of interest for the mixed gas experiment. When all of the data obtained in this work were considered, the number of measurements for each calibration gas standard was quite high, on the average more than 100 repeats. However, in order to calculate the standard deviation of the mean the number of measurements was assumed to be N=25. Using standard deviations presented in Table 3.11, the standard deviation of the mean (SDOM) and the relative standard deviation of the mean (RSDOM) with two different confidence intervals were calculated and results are presented in Table 4.2.

In Figure 4.3 (a) and (b), the calculated RSD and RSDOM for *n*-C_4H_{10} measurements are plotted, respectively, over *n*-C_4H_{10} concentration in calibration gas standards. Since no mixed gas experiments were performed with *n*-C_4H_{10} concentration lower than 1.99 vol% in the feed and higher than 74.50 vol% in the permeate during this work, the data for the first and the last calibration gas standards were considered not being in the area of interest. When these data were excluded, the RSDOM values in the area of interest were below 0.08% and 0.04% with confidence interval of 95% and 68%, respectively. The best estimated uncertainty of gas chromatography measurements for *n*-C_4H_{10} concentration in both feed and permeate gas samples was assumed to be 0.08% with confidence interval of 95%. This value was used for POE calculations in order to estimate total error in selectivity.

Table 4.2 Uncertainties of gas chromatography measurements for n-C_4H_{10} (N=25).

Conc. n-C_4H_{10} [vol%]	Peak area [-]	SD [-]	RSD 68% conf. [%]	RSD 95% conf. [%]	SDOM [-]	RSDOM 68% conf. [%]	RSDOM 95% conf. [%]
1.024	293.05	0.918	0.313	0.625	0.184	0.063	0.125
1.99	570.56	0.779	0.137	0.275	0.156	0.027	0.055
4.958	1377.46	2.538	0.184	0.368	0.508	0.037	0.074
9.64	2678.77	5.374	0.201	0.395	1.075	0.040	0.080
16.44	4625.93	5.874	0.127	0.254	1.175	0.025	0.051
35.0	9266.24	14.036	0.152	0.303	2.807	0.030	0.061
49.90	12740.47	19.996	0.157	0.314	3.999	0.031	0.063
74.50	18613.09	31.177	0.168	0.335	6.235	0.034	0.067
99.50	24374.96	85.618	0.351	0.701	17.124	0.070	0.140

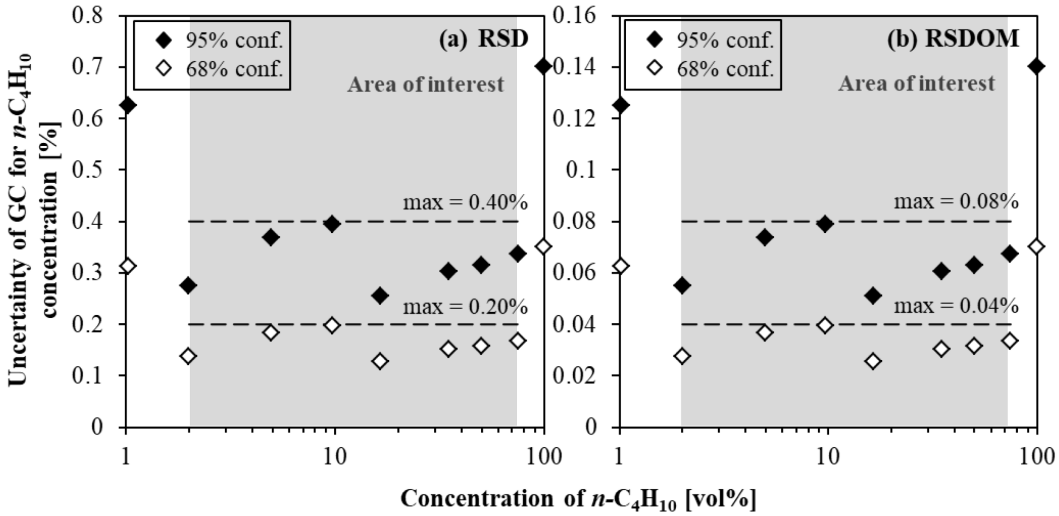

Figure 4.3 Uncertainty of gas chromatography measurements for n-C_4H_{10} concentration with 68% and 95% confidence intervals as: (a) RSD and (b) RSDOM.

Sensitivity analysis of gas chromatography measurements

A sensitivity analysis was performed to examine the influence of the uncertainty in measured n-C_4H_{10} concentration on the calculated error in mixed gas selectivity. For this investigation, mixed gas selectivity results of binary gas mixtures of n-C_4H_{10}/CH_4 in unfilled PDMS membranes at several operating conditions were used. The resulting error in mixed gas selectivity was recalculated by repeating the propagation of error method ats slightly altered RSDOM values while keeping all other instrumental uncertainties constant as given in Table 4.1.

The calculated error in mixed gas selectivity by POE is illustrated in Figure 4.4 (a) as a function of uncertainty in *n*-C_4H_{10} concentration given as RSDOM. In these calculations, mixed gas selectivity results of binary gas mixtures of 4 vol% *n*-C_4H_{10} in CH_4 in unfilled PDMS membranes at 20 °C at three different feed pressures of 10, 20, and 30 bar were used. The relationship between calculated error in selectivity and the uncertainty in *n*-C_4H_{10} concentration was almost linear. Even though considerably low RSDOM was studied for those calculations, the resulted error in selectivity was still large. For the mixed gas experiments conducted at 10 bar feed pressure, if *n*-C_4H_{10} concentration in feed and permeate gas sample was measured with an uncertainty of 0.08%, the calculated selectivity was 17.1 ± 1.15, which equals to ± 6.7% error in selectivity. The average selectivity of an individual experiment can have an error up to ± 9% when the RSDOM of the *n*-C_4H_{10} concentration measurements was 0.1%. With the same uncertainty, the selectivity was 18.61 ± 1.08 at 20 bar feed pressure, which equals to ± 5.8% error. When the feed pressure of the experiment increased from 10 bar to 20 bar, the error in selectivity slightly reduced, but remained high. Additionally, no significant difference in error was seen between the experiments performed at 20 and 30 bar feed pressures over the range of investigated uncertainty in *n*-C_4H_{10} concentration.

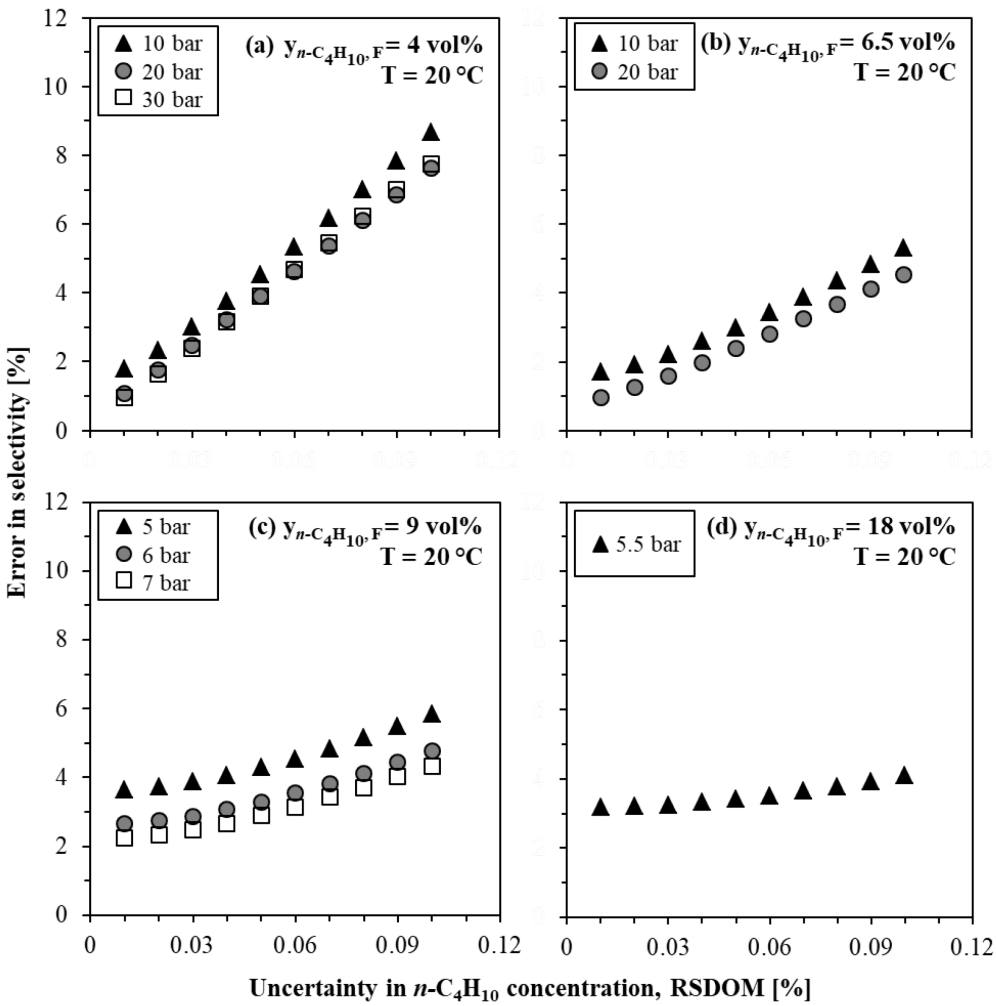

Figure 4.4 Influence of uncertainty in *n*-C_4H_{10} concentration on resulting error in mixed gas *n*-C_4H_{10}/CH_4 selectivity for different feed compositions (T = 20 °C).

As another parameter, the influence of n-C_4H_{10} concentration in feed gas composition was tested. Figure 4.4 (b) shows that increasing of feed n-C_4H_{10} concentration up to 6.5 vol% led to less error in selectivity than those in the experiments with 4 vol% n-C_4H_{10} concentration. For example, when the uncertainty in n-C_4H_{10} concentration is 0.08%, the selectivity at 10 bar feed pressure was 20.98 ± 0.90 with ± 4.3% error and 22.29 ± 0.82 at 20 bar with ± 3.7% error. However, in the experiments with 9 vol% n-C_4H_{10} concentration in the feed, error in selectivity increased due to the low feed pressures applied, as seen in Figure 4.4 (c). The mixed gas selectivity with 9 vol% n-C_4H_{10} concentration in the feed at 5 bar feed pressure was 21.93 ± 1.13, which equals to ± 5.1% error. On the other hand, when the experiment was repeated with the same feed n-C_4H_{10} concentration but at 7 bar feed pressure, the selectivity was 22.92 ± 0.85, which equals to ± 3.7% error. Figure 4.4 (d) shows that when the experiment was performed at 5.5 bar feed pressure with considerably high n-C_4H_{10} concentration in the feed, such as 18 vol%, selectivity was 33.24 ± 1.26, which equals to ± 3.8% error. This indicates that the contribution of the feed pressure to the total error in selectivity is another important parameter, which will be further discussed later.

Lastly, the influence of temperature was studied. Mixed gas experiments were performed at different temperatures when the feed pressure was constant at 10 bar and the n-C_4H_{10} concentration in the feed mixture was constant at 6.5 vol%. Figure 4.5 illustrates the predicted error in selectivity at different values of uncertainty in n-C_4H_{10} concentration. Lowering temperature from 40 to 10 °C led to increased error in selectivity from 2.6 to 4.1% for the uncertainty in n-C_4H_{10} concentration was 0.08%. Results indicated that the error in selectivity increases at lower temperatures.

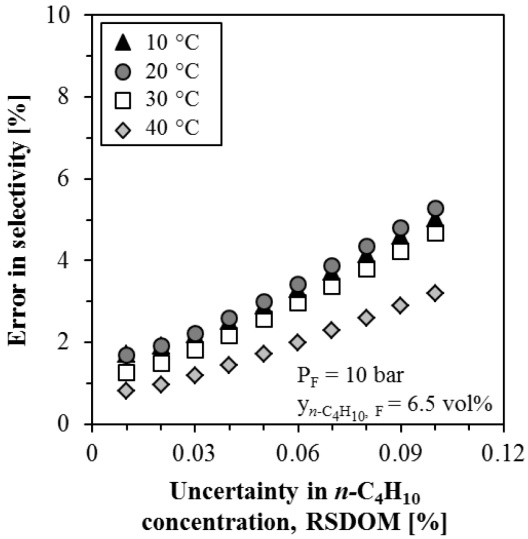

Figure 4.5 Influence of uncertainty in n-C_4H_{10} concentration on error in mixed gas selectivity determined at different temperatures with binary mixtures of 6.5 vol% n-C_4H_{10} in CH_4 at 10 bar feed pressure.

Apparently, the crucial error source was the measurements of n-C_4H_{10} concentration. The estimated uncertainty of feed and permeate n-C_4H_{10} concentrations as 0.08% as RSDOM with 95% confidence was a considerable small number, but its impact on the total error was remarkable. The mixed gas selectivity was considerably sensitive to the precision of the gas

chromatography measurements. The deviation in the measurements of gas composition and correspondingly estimated fugacity originated significant fluctuations in calculated selectivity in an individual mixed gas experiment.

Evaluation of RSDOM approach

It was important to check whether the POE method with RSDOM approach provides a good estimation for the uncertainty in *n*-C_4H_{10} concentration measurements Thus, a test was performed to compare the determined error in selectivity by POE using respectively RSD and RSDOM approach to estimate the uncertainty in *n*-C_4H_{10} concentration measurements.

For comparison, the results of a mixed gas experiment of unfilled PDMS membrane with binary gas mixture of 4 vol% *n*-C_4H_{10} in CH_4 at 20 °C at 10 bar feed pressure were used due to the highest determined error in selectivity by POE method using RSDOM approach. During the mixed gas experiment, the gas cylinders on feed and permeate side of the membrane were filled with the gas sample simultaneously for 3 times at different time intervals. The compositions of both feed and permeate gas samples were measured 4 times with gas chromatography. As a result, 12 selectivity values were determined from one mixed gas experiment at constant operating conditions. The arithmetic mean of the 12 selectivity values was 16.81, which was assumed to be the best estimated selectivity.

The next step was to estimate the error in mean selectivity by POE method. Previously in Figure 4.3, the RSD and the RSDOM values for *n*-C_4H_{10} measurements with 68% and 95% confidence intervals were plotted over *n*-C_4H_{10} concentration in calibration gas standards. The RSDOM values were simply 5 times smaller than RSD values since they were divided by the square root of number of experiments (N=25). Firstly, POE was applied to the calculated selectivity by using 0.20% and 0.40% RSD as the uncertainty in *n*-C_4H_{10} concentration. The resulted total errors in selectivity for both confidence intervals are presented in Figure 4.6 (a). The selectivity value was 16.81 ± 3.02, which equals to ± 18.0% error with 68% confidence. This is shown as the error bars of the mean between the upper and lower limits of the light grey area in the Figure 4.6 (a). All of the 12 individual selectivity values were located almost in the middle of the 68% confidence interval area. Apparently, RSD approach with 68% confidence led to an overestimation of the total error in selectivity. Increasing the confidence interval to 95% using 0.40% RSD produced ± 35.8% total error in selectivity (16.81 ± 6.02). The 95% confidence interval area is shown between the upper and lower limits of the dark grey area in Figure 4.6 (a). This value was extremely high and underestimated the accuracy of the work.

Figure 4.6 (b) presents resulted total error in selectivity using the suggested approach RSDOM. When the error was calculated by POE with 0.04% uncertainty in *n*-C_4H_{10} concentration as RSDOM, the error was ± 3.9% with 68% confidence (16.81 ± 0.66). Most of the individual selectivity values were within the area showing 68% confidence. Only two values were on the critical boundary between 68% and 95% confidence, and one value were in 95% confidence area. On the other hand, using 95% confidence interval with RSDOM=0.08% involved all of the 12 individual selectivity values with ± 7.3% error (16.81 ± 1.23).

The RSDOM approach for estimation of the uncertainty in *n*-C_4H_{10} concentration was found to be the most reasonable one, which provided the best estimation for the total error in selectivity and represented the accuracy of the work well enough. Considering various experimental conditions and numerous experiments conducted in this work, it was decided to use 0.08% RSDOM as the

uncertainty of the gas chromatography measurements for POE method calculations, which provides 95% confidence for all data presented in this work.

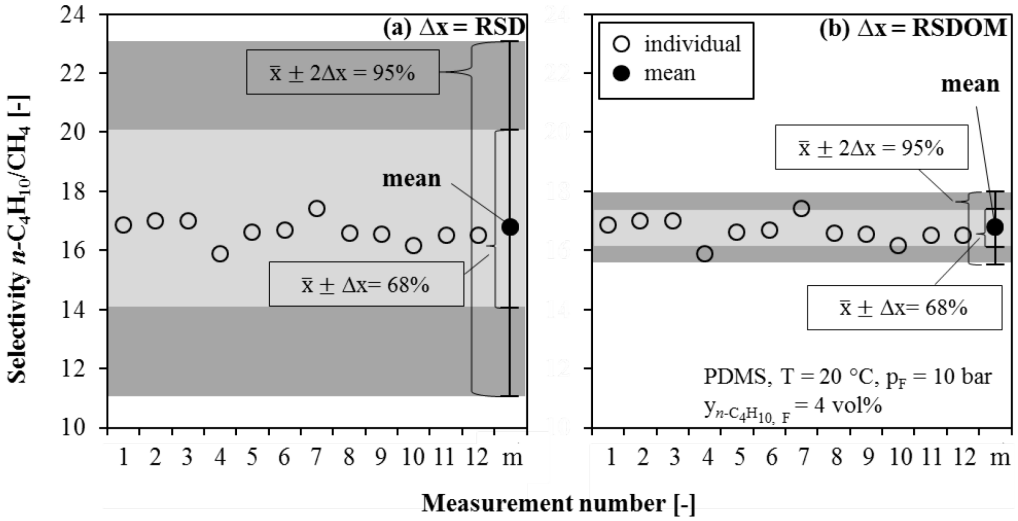

Figure 4.6 Error in selectivity determined by POE using (a) RSD and (b) RSDOM as the uncertainty in n-C_4H_{10} concentration with 68% and 95% confidence intervals (m = mean).

Evaluation of uncertainty in second virial coefficients

During the derivations in the POE method for mixed gas selectivity, the virial coefficients in Equation 4.20 ($B_{i,F}$, $B_{i,P}$, $B_{j,F}$, and $B_{j,P}$) were assumed to be constant. Because, the contributions of the uncertainties in the second virial coefficients, which are the derivations with respect to n-C_4H_{10} mole fractions on the feed and permeate side $y_{n\text{-}C4H10,\ F}$ and $y_{n\text{-}C4H10,\ P}$ and temperature T, were assumed to be negligible. The virial coefficients B_{ii}, B_{jj}, and B_{ij} are only functions of temperature. However, the virial coefficient B_{mix} is dependent on the mole fraction of n-C_4H_{10}. So, the error contributed by $y_{n\text{-}C4H10}$ through the virial coefficient of the mixture should be evaluated. Therefore, a sensitivity analysis was performed to determine how different values of these quantities affect particularly the second viral coefficients.

For this analysis, results of a mixed gas experiment of unfilled PDMS membrane with binary mixture of 4 vol% n-C_4H_{10} in CH_4 performed at 10 bar feed pressure and 20 °C were used. The second virial coefficients were recalculated, as previously presented in Section 2.6.2, using the varied values of $y_{n\text{-}C4H10,\ F}$, $y_{n\text{-}C4H10,\ P}$, and T (up to ± 10%) separately. The other experimental parameters, such as feed and permeate pressure, were kept constant.

Figure 4.7 (a) shows the calculated second virial coefficients when n-C_4H_{10} mole fraction on the feed side was either increased or decreased gradually up to 10%. Apparently, no difference was seen in the calculated values of second virial coefficients in the investigated range of variation in n-C_4H_{10} mole fraction. Figure 4.7 (b) shows the calculated second virial coefficients when n-C_4H_{10} mole fraction on the permeate side was altered. A slight difference was only seen in $B_{n\text{-}C4H10,\ P}$ when the n-C_4H_{10} mole fraction on the permeate side either increased or decreased more than 2%. Changing the temperature up to ± 10% led no difference in $B_{CH4,\ F}$ and $B_{CH4,\ P}$ as seen in Figure 4.7 (c). Very low differences were seen in $B_{n\text{-}C4H10,\ F}$ and $B_{n\text{-}C4H10,\ P}$ when the temperature changed more than ± 2%, however the magnitude of these differences were insignificant. It was

seen that the contributions of neglected quantities to the overall error in mixed gas selectivity were unimportant. These results confirm that the assumption stated before to simplify POE derivations for the mixed gas selectivity was reasonable.

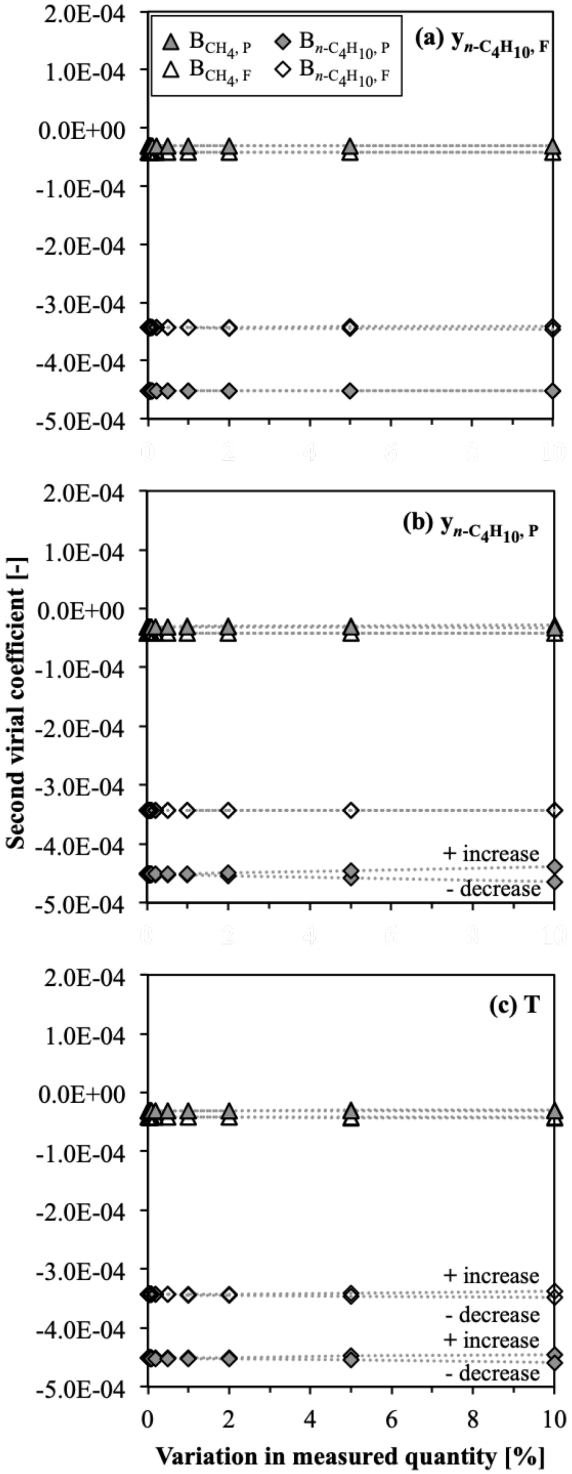

Figure 4.7 Influence of uncertainty of (a) feed *n*-C_4H_{10} concentration, (b) permeate *n*-C_4H_{10} concentration, and (c) temperature on the second virial coefficients.

4.2.5 Distribution of error

POE has a great advantage that it can easily be analyzed how much an error in a single quantity q_i contributes to the overall error in the calculated variable Δq. The fractions of the error show which error sources are predominant or negligible.

By rearranging Equation 4.3, the error contribution of a single measured quantity is simply calculated as:

$$q_i\,[\%] = \frac{\left(\frac{\partial f}{\partial x_i}\Delta x_i\right)^2}{(\Delta q)^2}\,100 \tag{4.34}$$

Figure 4.8 (a) and (b) present contributions of error sources in pure gas experiments. Results were collected from measurements of both PDMS and MMM samples performed at 20 °C. The feed pressure was varied from 0.75 to 2 bar for *n*-C_4H_{10}, and from 10 to 20 bar for CH_4 pure gas permeability measurements. The permeat pressure was varied from 0.2 to 0.5 bar for *n*-C_4H_{10}, and from 0.2 to 0.3 bar for CH_4. Figure 4.8 (a) shows that permeate flow rate $\dot{V}_P$ and membrane thickness δ were the most dominant quantities for the error with up to 50% and 48% contribution, respectively. Moreover, in an individual *n*-C_4H_{10} pure gas measurement, the contribution of permeate flow rate increases linearly with increasing feed pressure and the contribution of membrane thickness decreases linearly with increasing pressure. Both feed pressure p_F and permeate pressure p_P had contributions up to 17%. Temperature T and actual membrane diameter d_m had negligible contributions. Figure 4.8 (b) shows that the distribution of errors in pure CH_4 permeability measurements remained relatively constant. Membrane thickness δ contributed the largest error with averagely 80%. Other two quantities which had contributions were the permeate flow rate $\dot{V}_P$ with 9% and the active membrane diameter d_m with 14%. As expected, in a pure gas experiment no errors occur due to the feed or permeate compositions.

Figure 4.8 (c) and (d) compare contribution of error sources in mixed gas experiments. Mixed gas results were collected from measurements of both PDMS and MMM samples performed with several *n*-C_4H_{10} concentrations in feed ($y_{n\text{-}C4H10,F}$ = 4 – 18 vol%) at feed pressures between 5 and 30 bar at a constant temperature of 20 °C. Mixed gas experiments were carried out at atmospheric permeate pressure (p_P = ca. 1 bar). Figure 4.8 (c) shows that all independent quantities, except of temperature T and permeate *n*-C_4H_{10} concentration $y_{B,P}$, contribute to the overall error. Apparently, contributions of errors in mixed gas *n*-C_4H_{10} permeability strongly depend on operating conditions. Depending on the feed *n*-C_4H_{10} concentration and the feed pressure of the experiment, the contributions of independent quantities remarkably change. For instance, the contribution of permeate flow rate $\dot{V}_P$ was between 26% and 45% and the contribution of membrane thickness δ was between 20% and 36% for experiments performed under different operating conditions. Actual membrane diameter d_m slightly contributed up to 7%. Similar to pure gas, the distribution of error sources in CH_4 mixed gas permeability measurements was the same for all operating conditions as shown in Figure 4.8 (d). Same independent quantities produced errors in mixed gas permeability but in different percentages than pure gas permeability. In mixed gas experiments, permeate flow rate $\dot{V}_P$ and membrane thickness δ produced averagely 50% and 40% of the overall error, respectively. Additionally, actual membrane diameter d_m had a low contribution of 7% and feed pressure had slight contribution up to 2% in experiments with the highest *n*-C_4H_{10} concentrations in feed.

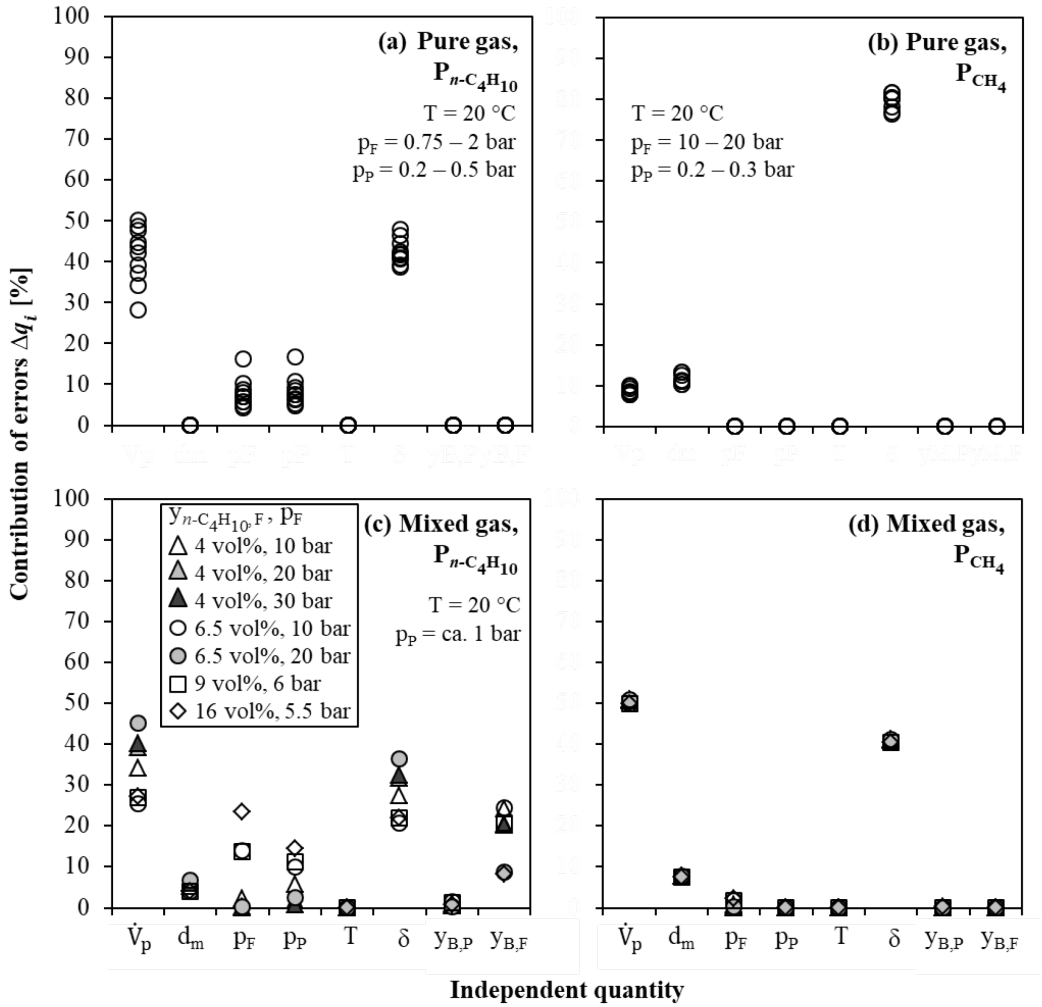

Figure 4.8 Contribution of errors in pure gas permeability of (a) *n*-C_4H_{10}, (b) CH_4, and in mixed gas permeability of (c) *n*-C_4H_{10}, (d) CH_4.

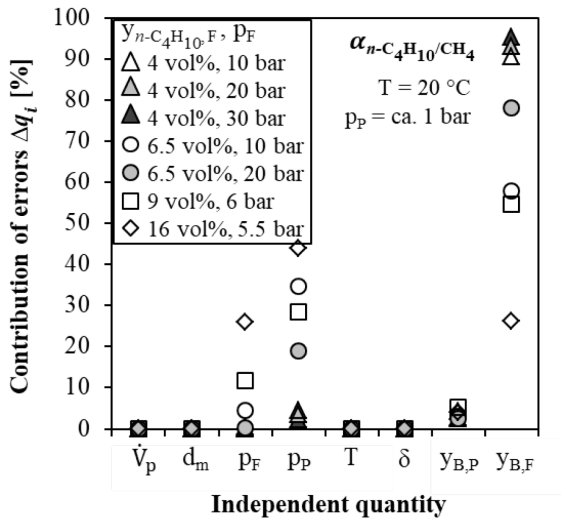

Figure 4.9 Contribution of errors in mixed gas selectivity.

The distribution of error in mixed gas selectivity is presented in Figure 4.9. The error in the mole fraction of n-C_4H_{10} on the feed side $y_{B,F}$ contributed the greatest to the overall error in selectivity. The contribution of n-C_4H_{10} concentration in feed increases up to 95% in the mixed gas experiment with the lowest n-C_4H_{10} concentration in the feed (4 vol%) performed at the lowest feed pressure (10 bar). The contribution decreases with increasing the mole fraction of n-C_4H_{10} on the feed side. Apparently, feed n-C_4H_{10} concentration is the most crucial error source in a mixed gas experiment. Besides, the feed pressure p_F and permeate pressure p_P contributed 26% and 44%, respectively. Distributions of both errors increase with increasing the mole fraction of n-C_4H_{10} on the feed side.

4.3 Reporting the results of experimental measurements

In order to check the reproducibility of the experimental results, the permeability of each gas through the membrane and the selectivity of the membrane were measured at least three times. The measurements were carried out either using the same membrane stamp or using different membrane stamps under identical operating conditions. The result of a set of experimental measurement was reported in two parts. First, the best estimate of a set of measurements was reported as the average of the measurements. The error in the best estimate was reported as the largest error that involves the error of each individual experiment calculated by POE method.

Examples of pure gas permeability

Figure 4.10 (a) represents 6 individual experiments of pure gas n-C_4H_{10} permeation in unfilled PDMS at 20 °C. Error in each individual experiment was calculated by propagation of error method. Table 4.3 lists n-C_4H_{10} permeability coefficients and slopes of the exponential fits. To simplify the presentation of the data, a best estimate of the set of measurements was necessary. Therefore, the average permeability coefficient was calculated as the aritmetic average of the individual permeability coefficients and the average slope was calculated as the aritmetic average of the individual slopes. Using the calculated average permeability coefficient and the average slope, one average permeation trend for the repetitions was presented as given in the Figure 4.10 (b). The experimental points on the average permeability trend are the calculated permeabilities at several mean n-C_4H_{10} fugacity values. These mean n-C_4H_{10} fugacity values were the values which were taken from one of the indivudual experiments. The error bars presented in Figure 4.10 (b) involve all the errors of individual experiments calculated by POE method. Thus, all 6 individual measurements and their errors are represented by the reported average permeation trend for PDMS measured at 20 °C.

Another example is given in Figure 4.10 (c) for pure gas CH_4 permeability of 3 individual experiments in unfilled PDMS at 20 °C. In Table 4.3, CH_4 permeability coefficient of each individual experiments is listed. The average CH_4 permeability was reported as given in Figure 4.10 (d), where the average CH_4 permeability coefficient equals to the aritmetic mean of the individual permeability coefficients and the error bars involve all the errors of individual experiments calculated by POE method. Unless specifically stated otherwise, this method was applied to all pure gas n-C_4H_{10} and CH_4 permeability data reported in this work.

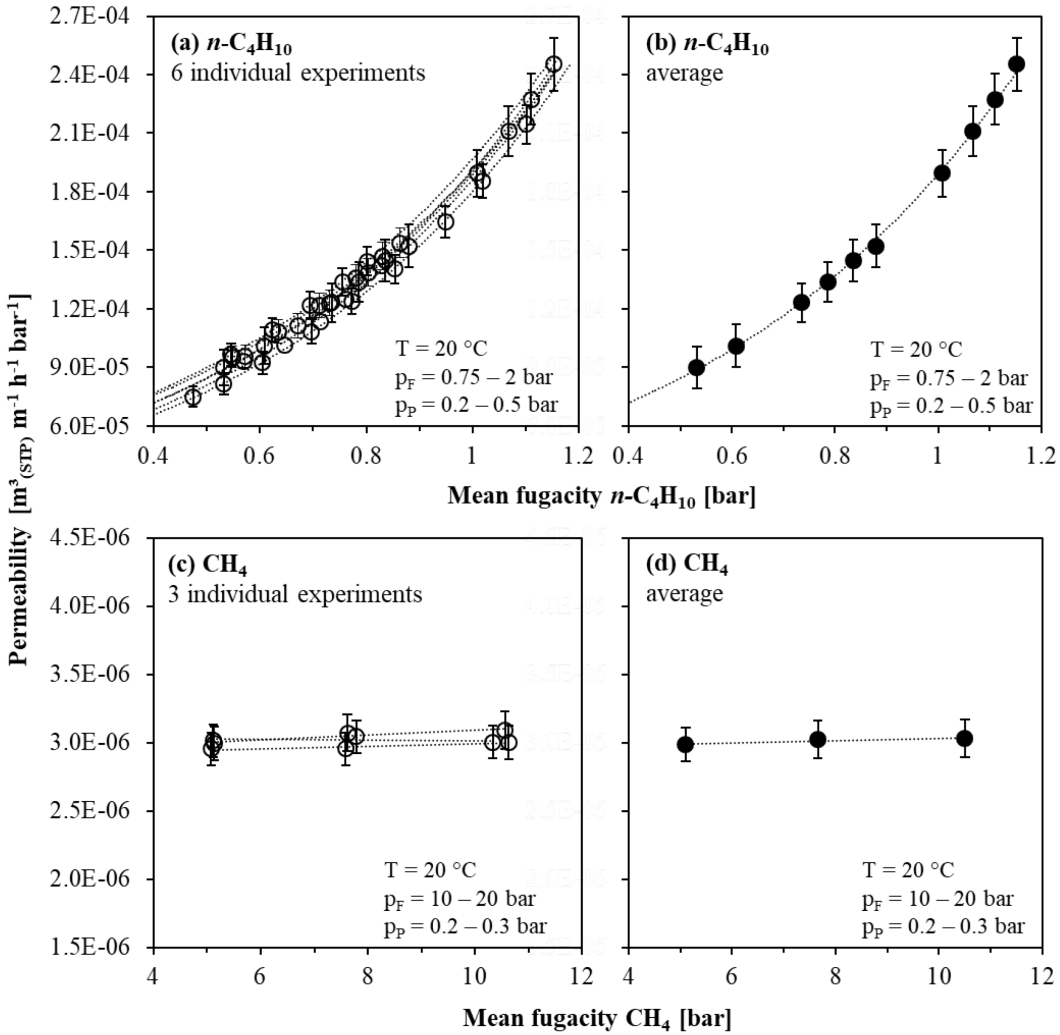

Figure 4.10 Reporting pure gas permeability.

Table 4.3 Individual and average pure gas n-C_4H_{10} and CH_4 permeability coefficients of unfilled PDMS at 20 °C.

Measurement	$P^0_{n\text{-}C_4H_{10}}$ [$m^3_{(STP)}$ m^{-1} h^{-1} bar^{-1}]	$m_{n\text{-}C_4H_{10}}$ [-]	$P=P^0_{CH_4}$ [$m^3_{(STP)}$ m^{-1} h^{-1} bar^{-1}]
1	3.77E-05 ± 3.08E-06	1.613	3.05E-06 ± 1.31E-07
2	4.05E-05 ± 1.93E-06	1.558	2.97E-06 ± 1.20E-07
3	3.66E-05 ± 1.95E-06	1.631	3.02E-06 ± 1.20E-07
4	4.05E-05 ± 1.86E-06	1.540	
5	3.50E-05 ± 1.81E-06	1.658	
6	3.31E-05 ± 1.81E-06	1.681	
average	3.72E-05 ± 3.81E-06	1.613	3.01E-06 ± 1.37E-07

Examples of mixed gas permeability and selectivity

Exemplary, results of 4 individual mixed gas experiments were used here, which were carried out with binary mixtures of 4 vol% of *n*-C_4H_{10} in CH_4 in MMMs of PDMS filled with 20 wt% zeolite Y particles. Measurements were performed at 10, 20 and 30 bar feed pressure at 20 °C. Figure 4.11 (a) shows *n*-C_4H_{10} permeability data of 4 mixed gas experiments as function of mean *n*-C_4H_{10} fugacity. Permeability values were scattered but formed groups for 3 different feed pressures. To simplify, the measured permeability values at each feed pressure step were reported as arithmetic average as shown in Figure 4.11 (b). The error bars in y-direction involve all the errors of individual experiments calculated by POE method and the error bars in x-direction show the range of mean *n*-C_4H_{10} fugacity, in which experiments were performed. Likewise, Figure 4.11(c) shows CH_4 permeability data of 4 mixed gas experiments as function of mean CH_4 fugacity and (d) shows arithmetic average values at different feed pressures with both x- and y-direction error bars. Finally, Figure 4.12 (a) shows calculated selectivity values of 4 individual experiments as function of mean *n*-C_4H_{10} fugacity and (b) shows arithmetic average selectivity values at different feed pressures with both x- and y-direction error bars. Unless specifically stated otherwise, this method was applied to all mixed gas *n*-C_4H_{10} and CH_4 permeability and *n*-C_4H_{10}/CH_4 selectivity data reported in this work.

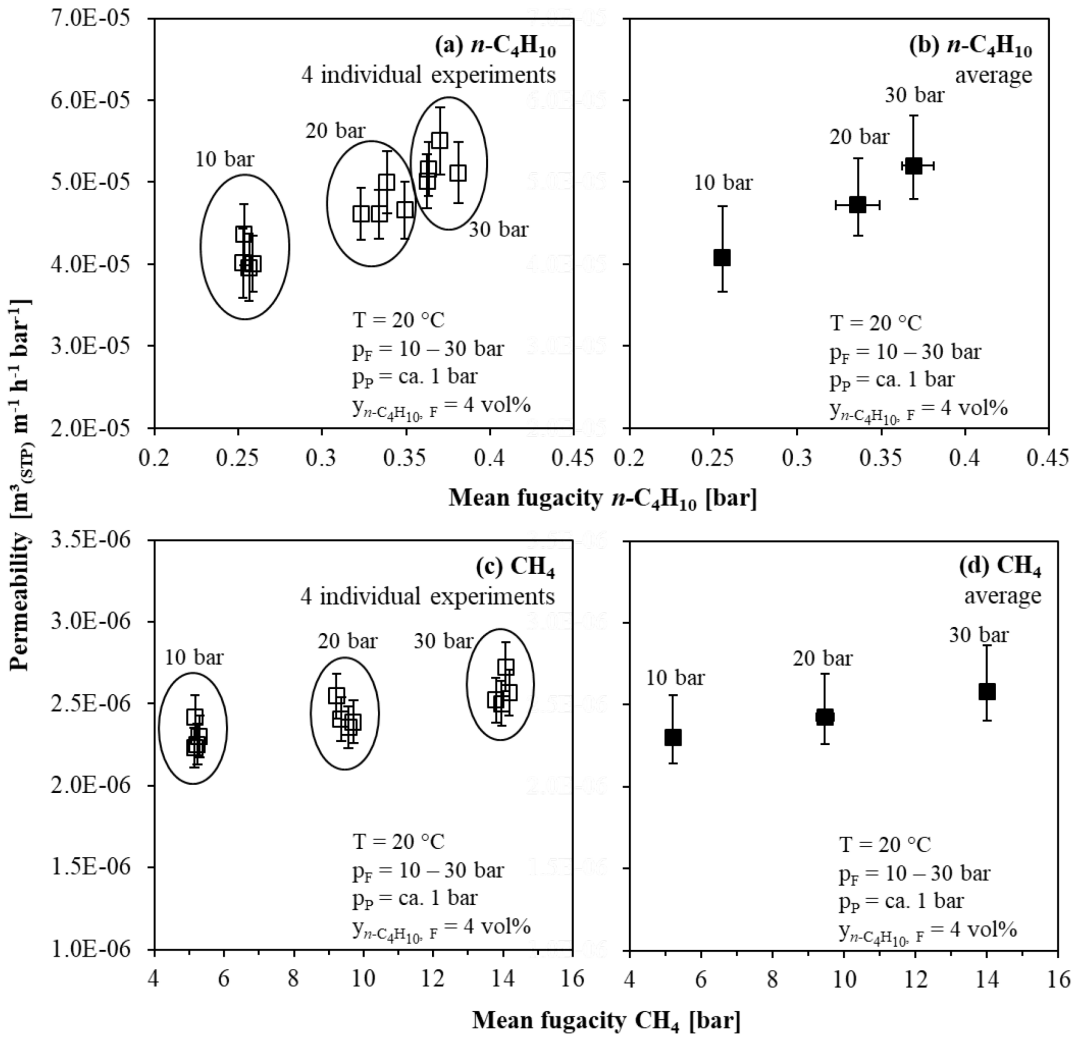

Figure 4.11 Reporting mixed gas permeability.

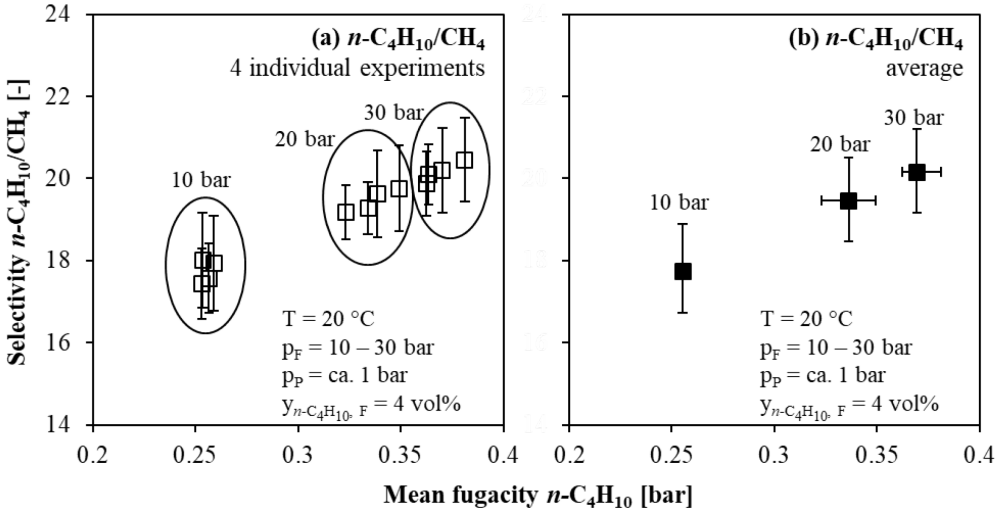

Figure 4.12 Reporting mixed gas selectivity.

5 Results and Discussion Part I: Mixed-Matrix Membrane Preparation and Characterization

The general procedures followed by most research groups to form MMMs were described before in Section 3.2. Since these procedures were highly dependent on the selected polymer, solvents and filler particles, no standard procedure has been identified for any types of composite membranes. Currently, the major concerns in research on MMM preparation are selection of suitable combination of polymers and filler particles, physical properties of the filler particles (e.g., particle size and agglomeration), and investigation of polymer/particle interface morphology.

Many variables during preparation may seriously affect membrane performance. In this section, fundamental steps of MMM preparation, which can be listed as:

- pre-treatment of activated carbon particles,
- mixing of PDMS and activated carbon particles,
- casting this mixture onto a support structure,
- drying of membranes as the post-treatment step,

were systematically investigated to find out how to enhance the performance of the membranes. Different preparation methods of MMMs were discussed to evaluate the impact of the preparation strategy on the performance of the produced membranes and to develop a reliable procedure for reproducible and defect-free MMM preparation. The influence of particle loading degree and usage of support structure with and without a gutter layer were also investigated. The produced membranes were morphologically characterized using methods as described in Section 3.3. The pure and mixed gas permeabilities and mixed gas selectivities of the prepared MMMs were evaluated using *n*-C_4H_{10} and CH_4. Results were compared with those of unfilled PDMS membranes under identical conditions. Additionally, impacts of using POMS as a different polymer phase and zeolite Y as a different type of filler were investigated in this section.

5.1 Preparation of PDMS/activated carbon suspension

The active separation layer of an MMM is formed by casting a homogeneous suspension of polymer and filler particles onto a support structure. Since the performance of a membrane strongly depends on the active separation layer [151], it is essential to prepare an appropriate PDMS/activated carbon casting solution to obtain good quality composite membranes. This layer must be thin and defect-free to provide acceptable flux or permeability. A good dispersion of activated carbon particles in PDMS is crucial, but extremely difficult to obtain, especially when relatively small particles are involved [113].

5.1.1 Comparison of PDMS/AC suspension preparation methodologies

The initial step of membrane preparation is to prepare the membrane materials. Required PDMS solutions with different concentrations were prepared as explained in section 3.2.1. The viscosity of the PDMS solution should be sufficiently high to perform a defect-free casting [46]. A highly viscous PDMS solution reduces the sedimentation of particles, but forms thicker membranes with lower permeability [152]. Moreover, at high concentrations, PDMS can easily penetrate into the activated carbon pores and cause pore blockage. To have a relatively low PDMS concentration with adequate viscosity can hinder pore blockage and provide thin and defect-free casting. In literature, the concentration of PDMS solution used for membrane preparation is generally between 9 and 20 wt% [18, 152-155]. Ahmad and Hägg [152] tested several concentrations of polymer to prepare polyvinyl acetate/zeolite 4A suspensions and they concluded that 10 wt% polymer was the optimum amount to prepare MMMs. In this work, the final PDMS concentration in the casting suspension in all preparation methods was kept at a fixed amount of 9 wt%. As filler, activated carbon with a mean particle diameter of d_{50} = 3.5 µm, which was pre-treated in a vacuum oven at 110 ºC and 110 mbar for 18 h, was used as explained in section 3.2.2. The amount of activated carbon charged to the PDMS solution was kept at 20 wt%.

The methods to prepare a polymer/particle suspension that exist in literature were considered as preferential basis in this work and they were further modified to provide an opportunity to enhance separation performance of the prepared MMMs. As illustrated in Figure 5.1, PDMS/activated carbon suspensions were prepared following two different methods (method-1 and method-2). Several MMMs (Table 5.1) were produced through casting these suspensions.

Method-1

Method-1 was identical to the pure polymer membrane preparation and used for MMM production as well. This was the simplest procedure for preparation of polymer/particle suspensions where polymer solution and the particles were directly stirred. This method was commonly reported in literature to disperse nanoparticles in a polymer matrix [153, 155-158]. The method was adapted to disperse activated carbon particles in PDMS. The corresponding amount of dried activated carbon was weighed into a glass jar and 9 wt% PDMS solution was gently added to the activated carbon under magnetic stirring at 400 min^{-1}. The mixing was done at room temperature either for 15 or 30 min. 5 min ultrasonication step was applied to some casting suspensions (casting suspensions 1-4 as shown in Table 5.1) to investigate whether it helps to prevent particle agglomeration. To observe the impact of the casting technique, two casting tools were manually applied to cast the films. Half of each prepared suspension was cast with the film applicator UA 3000 onto a support structure and the rest was cast with a 4-sided film applicator (4-S FA) onto a different support structure. Herewith, 8 different membrane samples were prepared.

Method-2

Method-2 was used to improve dispersion step of the activated carbon particles in PDMS where particles were pre-dispersed in a solvent before the polymer was added. This enables using higher share rates during dispersion step and preventing particle agglomeration. Several research groups used this procedure to produce MMMs with different polymer/particle/solvent combinations [109, 115, 159, 160]. The method was adapted for preparation of PDMS/activated carbon suspension.

Isooctane was used as solvent because it is the solvent used for PDMS solution preparation. The corresponding amount of dried activated carbon was weighed into a glass jar and mixed with predetermined amount of isooctane under magnetic stirring at 400 min^{-1} either for 15 or 30 min. Then, a concentrated PDMS solution (18 wt%) was added to the activated carbon/solvent dispersion and mixed further with magnetic stirrer at 400 min^{-1} either for 15 or 30 min. The final PDMS concentration in casting solution was equal to 9 wt% after mixing with activated carbon/solvent dispersion. The procedure was finalized with or without applying an ultrasonication step for 5 min. As in method-1, 4 different casting suspensions were prepared (casting suspensions 5-8 in Table 5.1) and cast with both casting tools separately. Herewith, 8 different membrane samples were prepared.

In the end, 16 different MMMs were prepared with method-1 and method-2. All membranes were cast at 200 µm initial thickness and they underwent the same post-treatment that is drying at room temperature for one day in a fume hood and further annealing at 110 °C and 110 mbar for at least 18 h in a vacuum oven.

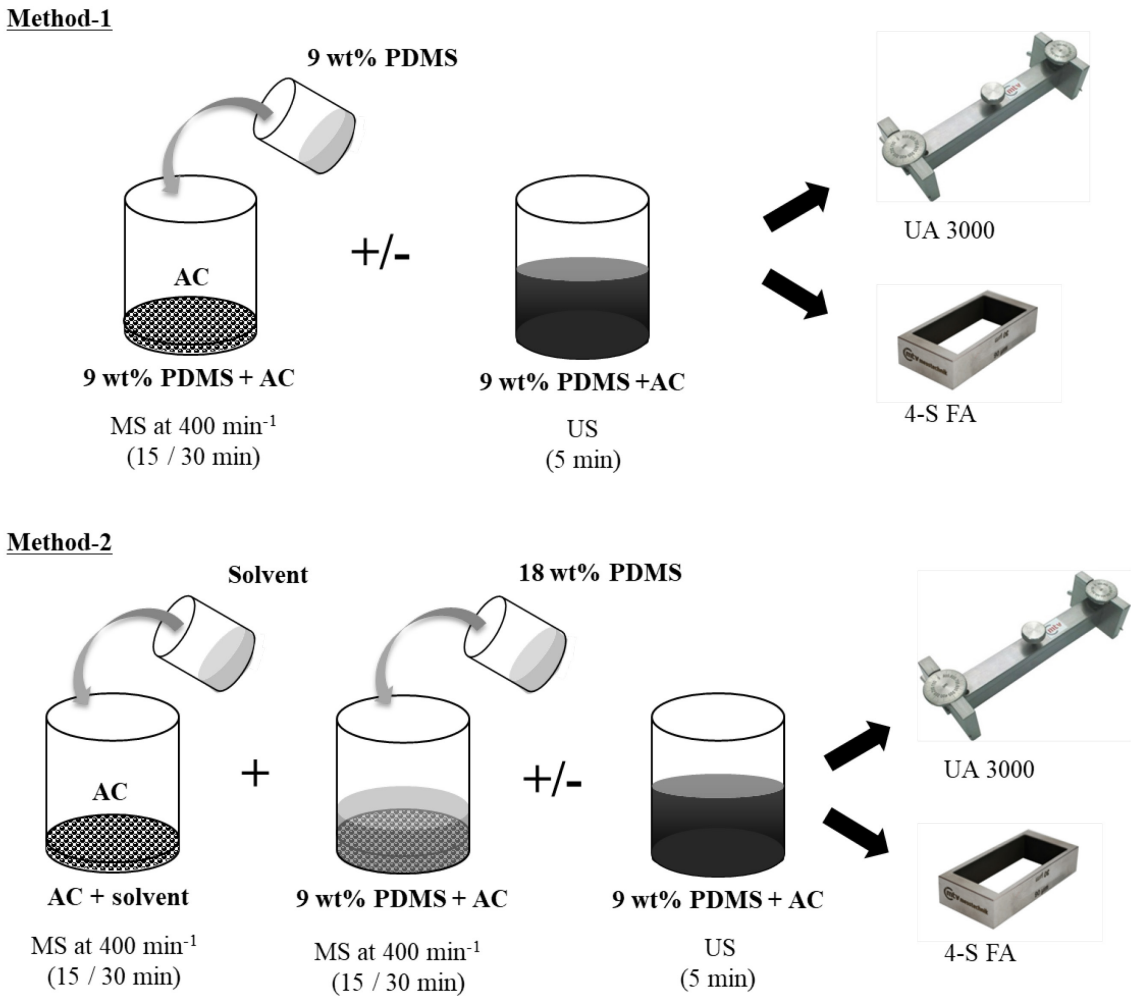

Figure 5.1 Schematic illustration showing method-1 and method-2 for preparation of PDMS/AC suspension (*AC*: activated carbon, *MS*: magnetic stirring, *US*: ultrasonication, *UA 3000*: film applicator UA 3000, *4-S FA*: 4-sided film applicator).

Table 5.1 List of the membranes prepared with method-1 and method-2 (*AC*: activated carbon, *MS*: magnetic stirring, *US*: ultrasonication).

Method	PDMS/AC suspension	MS at 400^{-1} min		MS at 400^{-1} min		US	Casting tool
		with	for	with	for		
M-1	1	9 wt% PDMS	30 min	-	-	no	both
	2	9 wt% PDMS	15 min	-	-	no	both
	3	9 wt% PDMS	30 min	-	-	yes	both
	4	9 wt% PDMS	15 min	-	-	yes	both
M-2	5	isooctane	30 min	18 wt% PDMS	30 min	no	both
	6	isooctane	15 min	18 wt% PDMS	15 min	no	both
	7	isooctane	30 min	18 wt% PDMS	30 min	yes	both
	8	isooctane	15 min	18 wt% PDMS	15 min	yes	both

Morphological characterization techniques explained in Section 3.3 were used to examine the produced membranes and compare method-1 and method-2. The pictures of the produced 16 membrane samples were obtained by the digital camera and Figure 5.2 (a) shows average color intensity of them. It was observed that all membranes cast by film applicator UA 3000 had almost two times higher average color intensity than the membranes cast by 4-sided film applicator, regardless of the preparation method, mixing time, and ultrasonication step. This difference can only be explained by the different amount of activated carbon particles in the active separation layer, although each casting suspension contained 20 wt% filler particles in PDMS solution and each membrane was cast at the same initial thickness. In each method, a new suspension was prepared, which was enough for two casting processes; one by film applicator UA 3000 and the other by 4-sided film applicator. The suspension was cast onto the support structures immediately after the preparation to avoid settling of the particles. Since the suspension was directly poured into the frame of the 4-sided film applicator, one operator realized the casting. Therefore, the particles can settle down until the casting was started manually, which may influence the particle proportion in the suspension and result in a particle mass fraction less than 20 wt%. This effect was insignificant when the film applicator UA 3000 was used, because the casting was carried out with the support of a second operator, where one operator poured the suspension continuously in front of the film applicator while the second operator cast the suspension at the same time. This way of casting hinders settlement of the particles, especially at the beginning of the casting, and allows a better distribution of the particles over the support structure.

Figure 5.2 (b) shows the standard deviation of the color intensity of the membranes. For all preparation methods, the standard deviation was greater for the membranes cast by 4-sided film applicator than those of cast by film applicator UA 3000. This confirms that the particles were not uniformly distributed on the support structure cast by a 4-sided film applicator. Additionally, among the membranes prepared by film applicator UA 3000, no significant difference of standard deviation was observed between method-1 and method-2. This means that a better uniformity was achieved by casting with film applicator UA 3000. When the mixing time was decreased from 30 to 15 min, standard deviation either stayed constant or slightly increased. The application of ultrasonication for 5 min as a final step in both preparation methods slightly increased the standard deviation of the color intensity; however, the increment was not significant. When the

membranes cast by 4-sided film applicator are considered, results were not consistent. For instance, in case of method-1, decreasing the mixing time from 30 to 15 min resulted in a lower standard deviation, when no ultrasonication was applied. Whereas method-2 showed contrary results for the same condition: decreasing the mixing time resulted in higher standard deviation without ultrasonication step. When an ultrasonication step was applied, decreasing the mixing time has not varied the standard deviation for method-1, but a decrease of standard deviation was observed for method-2. Since the 4-sided film applicator is a very light instrument, the casting speed and pressure on the frame have a significant influence on membrane morphology. Therefore, it was not possible to prepare membranes with reproducible characteristics with this instrument.

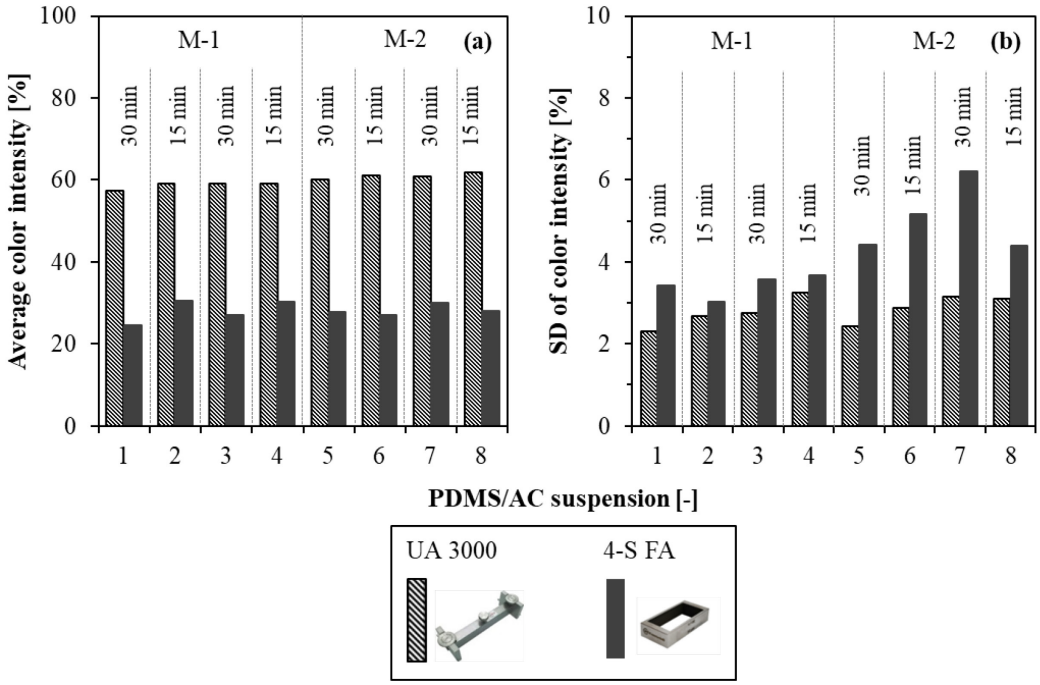

Figure 5.2 Comparison of (a) average color intensity and (b) SD of color intensity of the MMMs prepared with method-1 and method-2 (*AC*: activated carbon, *M*: method, *UA 3000*: film applicator UA 3000, *4-S FA*: 4-sided film applicator).

To observe the impact of casting tools on membrane morphology in detail, two MMMs were prepared using the same method (method-2) and the same PDMS/AC suspension (number 7), but cast by two different tools. Instead of comparing the average color intensity of total membrane surface area, the membrane surface was divided into 6 columns in the casting direction up to 12 cm and the average color intensity of each column was compared. Figure 5.3 (a) and (b) show digital camera pictures of MMMs cast by film applicator UA 3000 and 4-sided film applicator, respectively. Pixelated images of same samples are shown in Figure 5.3 (c) and (d). Although both membranes were prepared under identical conditions (including casting thickness and post-treatment) the impact of the casting tool on the color intensity was significant. The average color intensity of the MMM cast by the 4-sided film applicator was lower than the MMM cast by film applicator UA 3000 over the investigated casting distance. Moreover, the average color intensity of the MMM cast by 4-sided film applicator reduced continuously with increasing the casting distance, while the average color intensity of the MMM cast by film applicator UA 3000

stayed almost constant. This proves that the 4-sided film applicator does not provide a homogenous distribution of particles in the PDMS layer and that mass fraction of filler particles in the active separation layer must have varied over the casting distance.

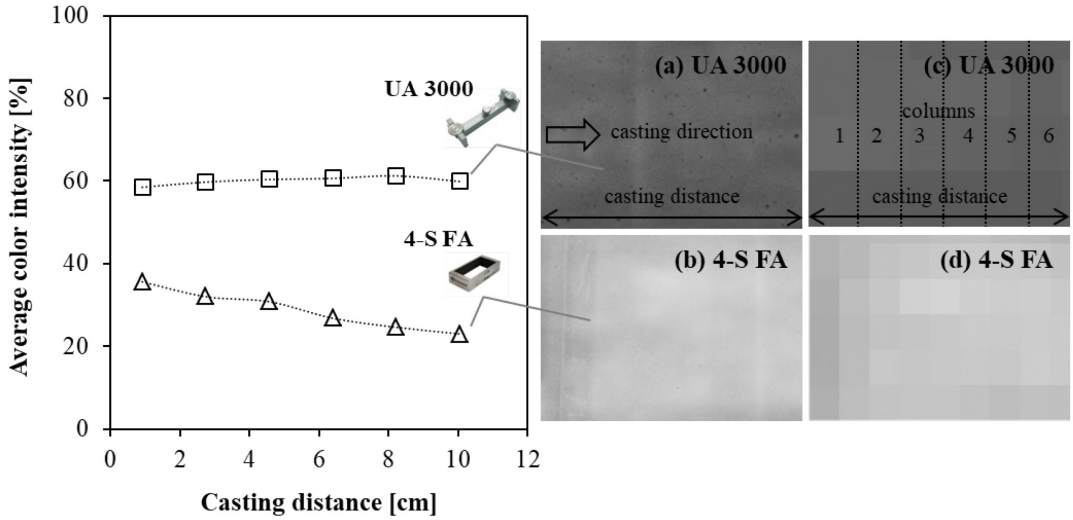

Figure 5.3 Average color intensity of the MMM (prepared with suspension 7) as a function of the casting distance (left). Digital camera images of the MMM (right) (a) cast by UA 3000, (b) cast by 4-S FA, (c) pixelated image of the picture a, and (d) pixelated image of the picture b.

The cross-section and surface SEM images of these MMMs were also investigated (Figure 5.4). The average separation layer thicknesses were measured as 7.06 ± 1.47 µm and 4.22 ± 1.86 µm for the MMMs cast by film applicator UA 3000 and 4-sided film applicator, respectively. Although both MMMs were cast at the same initial thickness of 200 µm, the MMM cast by the 4-sided film applicator was much thinner and almost equal to the mean particle diameter of the activated carbon (d_{50} = 3.5 µm). In this case, the PDMS matrix cannot cover the particles sufficiently, which may cause undesired defects in the separation layer. Cross-section images revealed that it was not possible to have a smooth membrane surface and an uniform film thickness by 4-sided film applicator.

Another important parameter is the number of agglomerates that form during the dispersing step. Figure 5.5 shows that considerably more agglomerates formed with method-2 compared to method-1. For both methods, ultrasonication step partially broke up the formed agglomerates and the number of agglomerates significantly increased when the mixing time was increased from 15 to 30 min. On the other hand, the number of agglomerates of the membranes cast by 4-sided film applicator was noteworthy fewer than those cast by film applicator UA 3000. However, this was not a result of a better dispersing process, but most probably a result of particle settling during the casting step by 4-sided film applicator, as discussed before. Based on these observations, film applicator UA 3000 was selected to cast the MMMs in this work to produce reproducible and reliable permeation data.

To automate the casting process, a motorized membrane preparation setup was developed, where the film applicator UA 3000 was mounted to a motor arm and cast the film automatically on a glass plate with a support structure (Figure 5.6). The slope of the glass plate was checked with a round spirit level or bubble level to achieve a uniform active separation layer thickness. If

necessary, a few very tiny metal plates were used to fix the slope of the glass plate. The casting solution (either pure PDMS or PDMS/AC suspension) was poured out manually from the glass jar directly on the support structure. The solution was then cast at a constant speed of 250 rpm (~ 1.2 cm/s). With the improved casting system, membranes were cast rapidly, which partially prevents possible particle sedimentation.

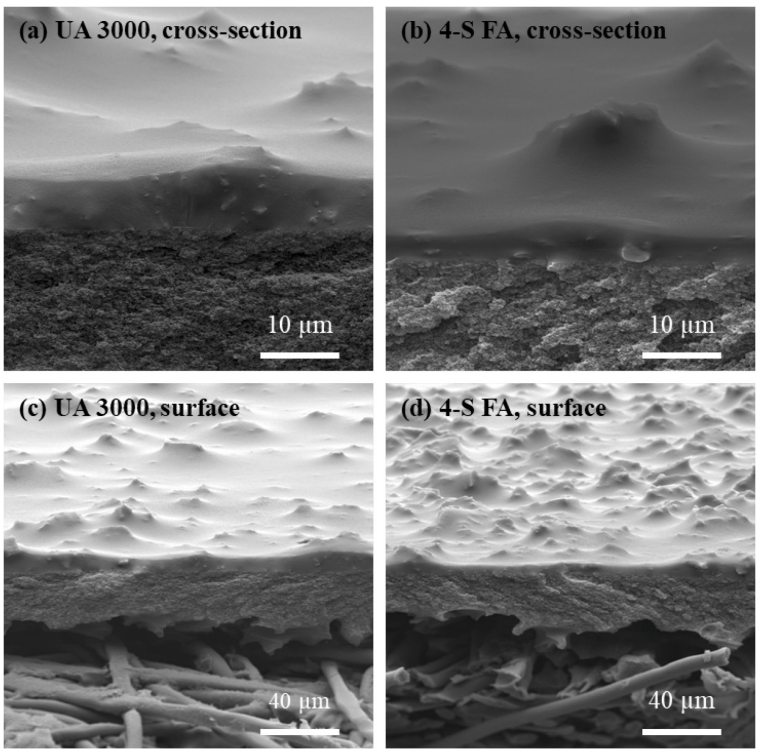

Figure 5.4 Cross-sectional and surface SEM images of the MMMs (prepared with suspension 7) cast by film applicator UA 3000 (UA 3000) and 4-sided film applicator (4-S FA).

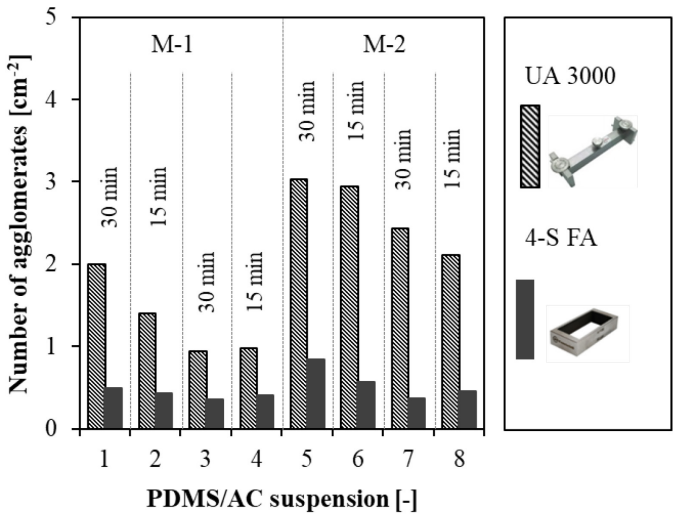

Figure 5.5 Comparison of number of agglomerates of the MMMs prepared with method-1 and method-2 (*AC*: activated carbon, *M*: method, *UA 3000*: film applicator UA 3000, *4-S FA*: 4-sided film applicator).

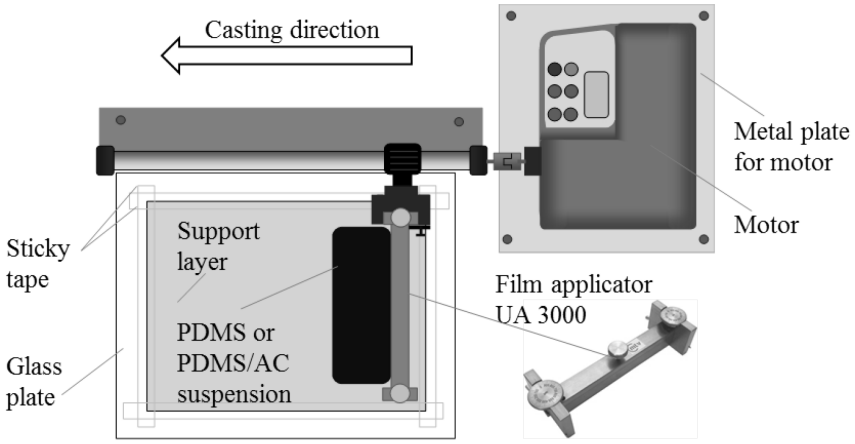

Figure 5.6 Schematic drawing of automated membrane casting setup.

5.1.2 Further investigations to improve PDMS/AC suspension preparation

Method-1, consisting of a 15 min magnetic stirring and 5 min ultrasonication step, is a promising procedure to disperse activated carbon particles in PDMS. However, in this strategy saturation of the activated carbon pores is absent. To disperse activated carbon particles in isooctane, as done in method-2, can be useful to prevent penetration of the PDMS chains into the pores of the particles. On the other hand, the drawback of method-2 is that the activated carbon/isooctane dispersion is mixed with a highly viscous PDMS solution (18 wt%) which requires a cross-shaped magnetic bar. This results in formation of many agglomerates. Since both methods were not suitable for saturation process, new methods (method-3 and method-4) were developed as illustrated in Figure 5.7 and evaluated. In these new methods activated carbon particles with mean particle diameter of d_{50} = 3.5 µm were used, which were identical particles as used for method-1 and method-2. Particles underwent the same pre-treatment and the produced membranes, as listed in Table 5.2, underwent the same post-treatment as described before.

The final concentration of PDMS solution was 9 wt% and the amount of activated carbon charged to the PDMS solution was 20 wt%. With the improved membrane casting set-up, the prepared suspensions were cast at 300 µm initial thickness, which was thicker than method-1 and method-2 (200 µm). By increasing the initial casting thickness, it was aimed to form a slightly thicker active separation layer, where the PDMS can properly cover the particles and the configuration of the activated carbon particles can form adequate layers in PDMS matrix. It was observed previously that 18 wt% PDMS solution was too viscous to disperse activated carbon/isooctane suspension in it. Therefore, a less viscous PDMS solution (12 wt%) was used for method-3 and method-4. Since a less viscous PDMS solution was used, it was anticipated that shorter mixing times might already be sufficient to obtain a dispersed state of activated carbon particles. It was also observed that fewer agglomerates were formed at shorter mixing times. Therefore, 5 min mixing was also investigated in method-3 and method-4.

Method-3

The activated carbon was weighed into a glass jar. The required amount of isooctane, to obtain a final PDMS concentration of 9 wt% in the casting suspension, was added to the activated carbon particles and ultrasonication was applied for 5 min as the initial step of preparation instead of

magnetic stirring. This step was considered as saturation of the filler particles with the solvent prior to mixing with polymer to avoid blockage of the filler pores with polymer chains. Then saturated particles were directly mixed with the 12 wt% PDMS solution by magnetic stirrer at 400 min^{-1}. The mixing was performed at room temperature either for 5, 15 or 30 min.

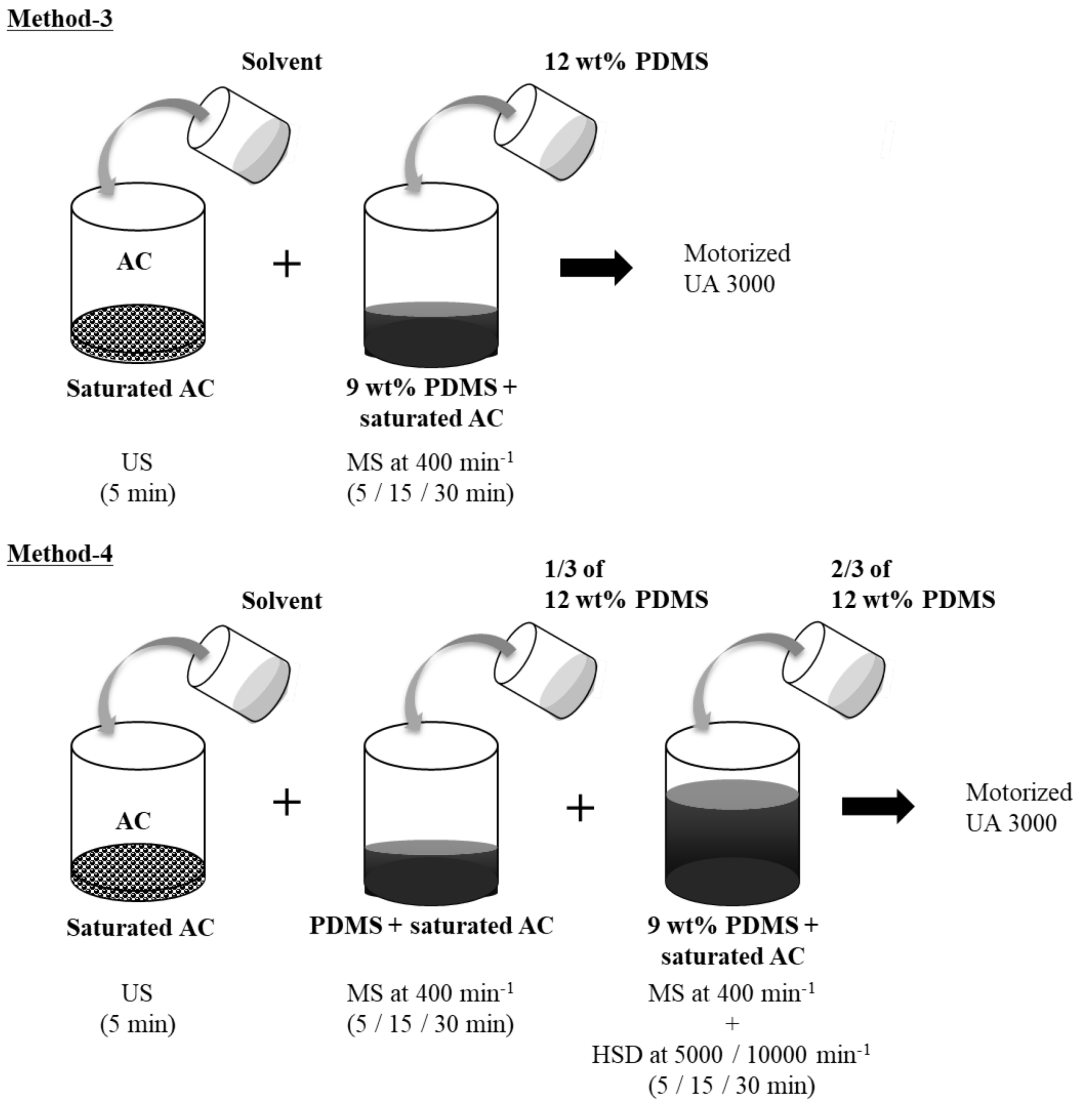

Figure 5.7 Schematic illustration showing method-3 and method-4 for preparation of PDMS/AC suspension (*AC*: activated carbon, *US*: ultrasonication, *MS*: magnetic stirring, *HSD*: high-speed dispersing, *UA 3000*: film applicator UA 3000).

Method-4

Differently from method-3, PDMS (12 wt%) solution was stepwise mixed with activated carbon/isooctane suspension. Firstly, one-third of the 12 wt% PDMS solution was added to the saturated particles and mixed by magnetic stirrer at 400 min^{-1}. Then, the remaining 12 wt% PDMS solution (two-thirds) was added to this mixture. To provide a better distribution of the particles, a combination of a high speed disperser and magnetic stirrer was used in this step. The high-speed disperser works up to 30000 min^{-1}. However, such high speed or longer mixing times

than 30 min were avoided not to cause any change in PDMS structure due to the heating. Therefore, the high speed disperser at the top was operating either at 5000 or 10000 min^{-1} and magnetic stirrer at the bottom at 400 min^{-1}. In these two steps, time for mixing was varied between 5, 15 or 30 min.

Table 5.2 List of the membranes prepared with method-3 and method-4 (*AC*: activated carbon, *M*: method, *US*: ultrasonication, *MS*: magnetic stirring, *HSD*: high-speed dispersing).

Method	PDMS/AC suspension	US	MS at 400^{-1} min		MS at 400^{-1} min + HSD at 5000/10000 min^{-1}		
			PDMS (12 wt%)	for	PDMS (12 wt%)	HSD	for
M-3	1	5 min	whole	5 min	-	-	
	2	5 min	whole	15 min	-	-	
	3	5 min	whole	30 min	-	-	
M-4	4	5 min	1/3	5 min	whole	5000 min^{-1}	5 min
	5	5 min	1/3	15 min	whole	5000 min^{-1}	15 min
	6	5 min	1/3	30 min	whole	5000 min^{-1}	30 min
	7	5 min	1/3	5 min	whole	10000 min^{-1}	5 min
	8	5 min	1/3	15 min	whole	10000 min^{-1}	15 min
	9	5 min	1/3	30 min	whole	10000 min^{-1}	30 min

MMMs produced with method-3 and method-4 were evaluated by observing average color intensity and standard deviation of the color intensity as shown in Figure 5.8 (a) and (b), respectively. These two values of the MMMs prepared with method-3 stayed almost constant when the mixing time was increased, showing no effect of mixing time on particle dispersion. Moreover, these values were almost the same as those observed for the MMMs prepared with method-1 and method-2 cast by the film applicator UA 3000. This means that method-3 did not improve the dispersing of particles. On the other hand, 5 min ultrasonication as the initial step had no undesired effect.

Applying additional high-speed dispersing, as done in method-4, resulted in higher average color intensity when compared with method-3. This means that the settlement of particles during preparation was hindered, more particles were dispersed, and probably fewer agglomerates were formed. Therefore, the particle loading in the separation layer was kept unchanged and MMMs were successfully prepared with 20 wt% particle loading. This made them appear darker. As a result, the agglomerates were not visible and countable anymore on the surface of the membranes. Standard deviation of the color intensity values of the MMMs prepared with method-4 were the lowest values of the investigated methods. This indicated that the particles were homogenously distributed in PDMS when method-4 was used.

Increasing the mixing time and the speed of disperser decreased the standard deviation, while average color intensity almost stayed the same. To find out the sufficient mixing time and speed with HSD, the morphologies of the MMMs produced with method-4 were investigated from the surface and cross-section with SEM. Figure 5.9 shows surface morphologies of the MMMs

prepared with method-4 at varying mixing time and the speed. The SEM image of the MMM prepared by mixing at 5000 min^{-1} for 5 min revealed that randomly distributed particles were present in PDMS matrix. This caused high roughness on the surface. Due to the particle agglomeration, a curve shaped cross-section was also formed. At the same speed, more uniform separation layer was formed as the mixing time was increased. Apparently, filler particles were better dispersed in PDMS, when the HSD speed increased up to 10000 min^{-1} and it was mixed for 5 min. A more homogenous distribution and smoother membrane surface was observed when the time of mixing was increased to 15 min. No morphological difference was visible in MMMs and no curve-shaped cross-section formation was observed for 15 and 30 min mixing time at 10000 min^{-1}. The bottom surface of the separation layer was continuous and defect-free. Figure 5.10 shows the cross-section morphologies of these MMMs at higher magnification. In all cases, good contact between activated carbon particles and PDMS was observed. Cross-sections showed no formation of sieve-in-a-cage morphologies or interfacial gaps.

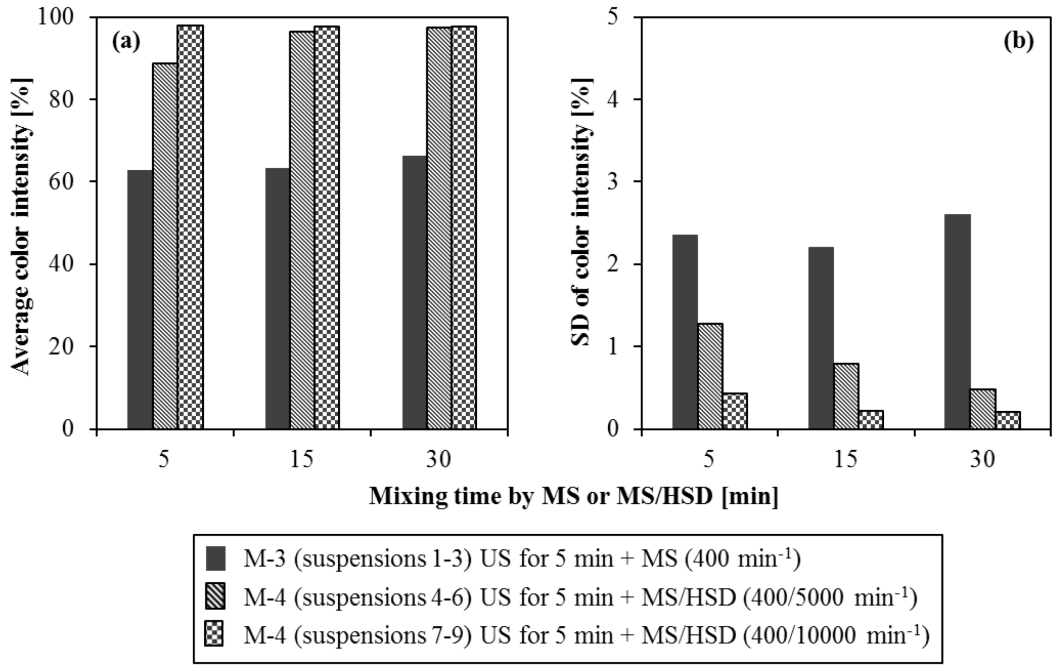

Figure 5.8 Comparison of (a) average color intensity and (b) SD of color intensity of the MMMs prepared with method-3 and method-4 (*M*: method, *US*: ultrasonication, *MS*: magnetic stirring, *HSD*: high-speed dispersing).

To sum up, the obtained data from morphological characterization techniques showed that among the investigated methods to prepare PDMS/activated carbon suspension, method-4 was the most efficient one. It provided uniformly distributed particles within the PDMS layer with fewer agglomerates, when compared to those formed using other studied methods. The surfaces of the MMMs prepared with this method were smooth, which shows that the casting solution was evenly spread out on the support structure. Additionally, 300 µm was a suitable initial thickness for casting, since it gave enough particle coverage with PDMS.

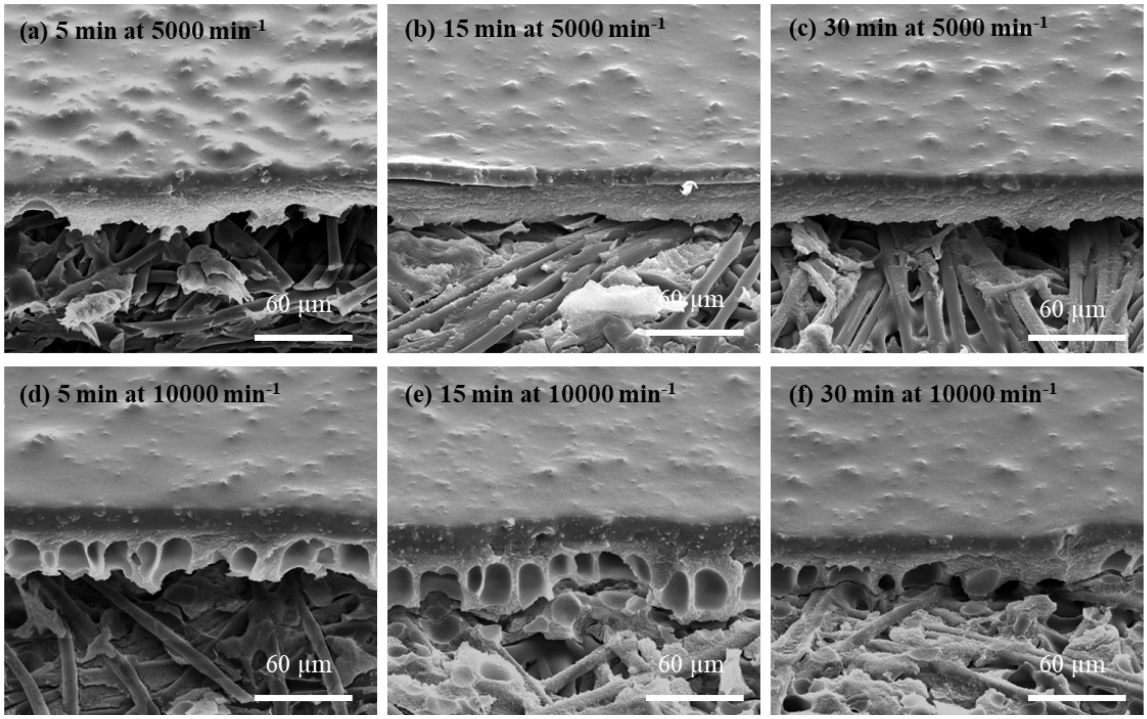

Figure 5.9 Surface SEM images of the MMMs prepared with method-4.

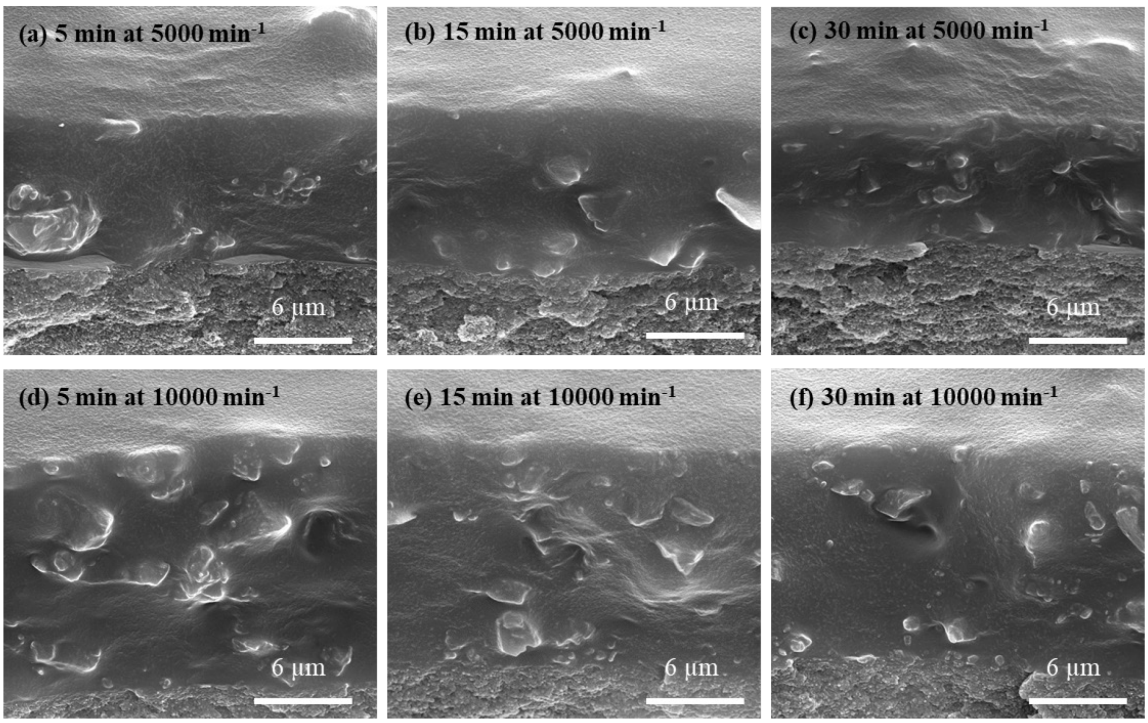

Figure 5.10 Cross-sectional SEM images of the MMMs prepared with method-4.

5.1.3 Gas permeation performance of the membranes

To determine the most efficient mixing time of HSD in method-4, pure gas permeabilities and mixed gas selectivities of MMMs were evaluated. Permeation behaviors of these membranes were compared with those prepared with method-3. The permeation behavior of *n*-C_4H_{10} and CH_4 in MMMs were determined and compared with each other and PDMS membranes containing no filler material (unfilled PDMS).

For this investigation, the activated carbon particles were saturated with ethanol instead of isooctane. The influence of saturation with different solvents will be discussed in Section 5.2. Since PDMS and ethanol are immiscible, activated carbon particles were suspended in a minimum amount of ethanol, giving a particle to ethanol mass ratio 1:2. In this case, the influence of ethanol mass on the final PDMS concentration was negligible. Therefore, 9 wt% PDMS solution was used, instead of 12 wt%. Due to the negligible amount of ethanol used for saturation, more PDMS solution was required to perform magnetic stirring. Half of the 9 wt% PDMS solution was added to the saturated particles and mixed with magnetic stirrer for 15 min. Then, the rest was performed similar to as explained above in method-4. To avoid inevitable concentration differences in PDMS solutions during each preparation, unfilled PDMS membranes and all MMMs were produced using the same 9 wt% PDMS solution, which was produced in one batch.

Gas permeation measurements were performed at 20 °C using the gas permeation setup. Figure 5.11 (a) and (b) present pure gas permeabilities of *n*-C_4H_{10} and CH_4 in unfilled PDMS membranes and MMMs. Results are given as a function of mean fugacity, which is the average of feed and permeate fugacities. Mean fugacity was used as reference for the corresponding concentration of the gas component within the membrane. Each pure gas measurement was repeated 3 times and experimental results were reported as explained in Section 4.3. The errors were calculated using the propagation of error method as discussed in Section 4.2.

The feed pressure was varied from 0.75 to 2 bar for *n*-C_4H_{10}, and from 10 to 25 bar for CH_4 pure gas permeability measurements. Due to the saturation pressure of *n*-C_4H_{10} at 20 °C, feed pressures higher than 2 bar were not applied. The gas permeation experimental setup allowed permeation experiments to be performed under vacuum on the permeat side. In this way, permeat pressure was varied from 0.2 to 0.5 bar for *n*-C_4H_{10}, and from 0.2 to 0.3 bar for CH_4.

For *n*-C_4H_{10}, the relationship between fugacity and pure gas permeability is exponential. This trend is shown with dotted lines in Figure 5.11 (a) and is represented by the following equation:

$$P_i = P_i^0 \exp(m_i f_{i,m}) \tag{5.1}$$

with

$$f_{i,m} = \frac{(f_{i,F} + f_{i,P})}{2} \tag{5.2}$$

where P_i^0 is the infinite dilution permeability when $f_m = 0$, m is the adjustable parameter, which is constant for a given temperature. The experimental data for pure *n*-C_4H_{10} were fitted to this equation and the resulting infinite permeability coefficients are given in Table 5.3.

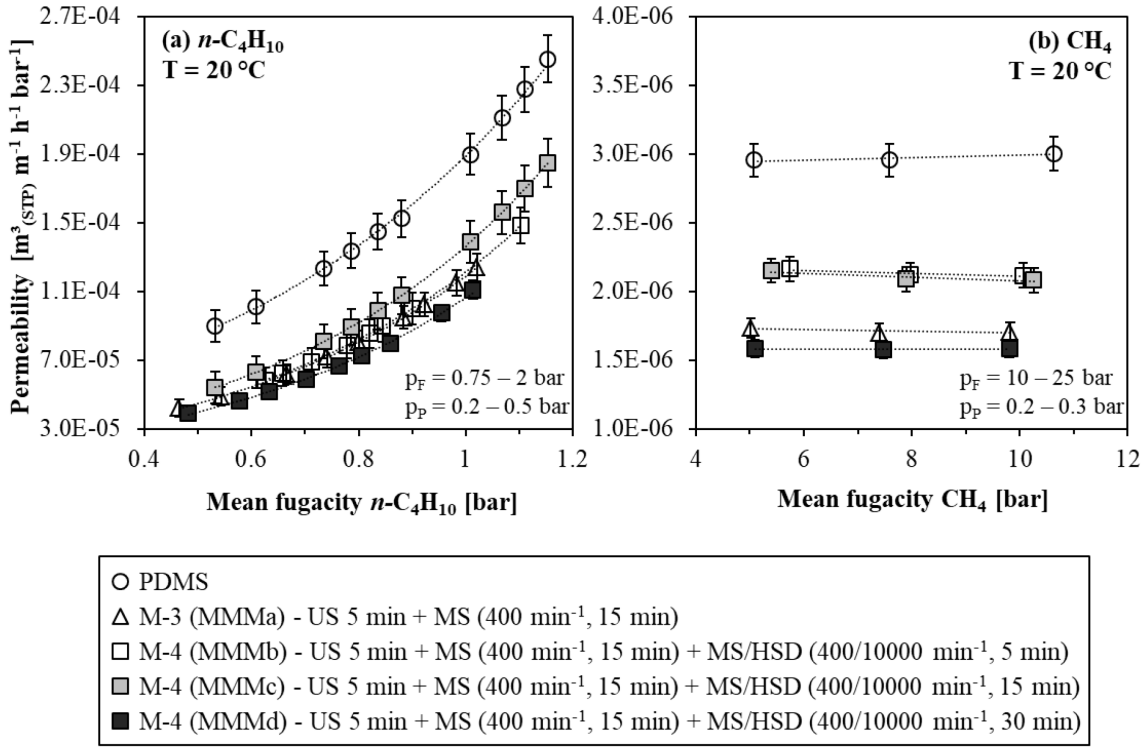

Figure 5.11 Pure gas permeability of (a) *n*-C_4H_{10} and (b) CH_4 in unfilled PDMS and ethanol-saturated MMMs prepared with method-3 and method-4 (T = 20 °C) (*M*: method, *US*: ultrasonication, *MS*: magnetic stirring, *HSD*: high-speed dispersing). Dotted lines represent exponential and linear trend curves and the error bars were determined using the propagation of error method.

Table 5.3 Pure gas *n*-C_4H_{10} and CH_4 permeability coefficients and *n*-C_4H_{10}/CH_4 permselectivity in unfilled PDMS and ethanol-saturated MMMs with 20 wt% AC loading (T = 20 °C).

Method	Membrane	$P^0_{n\text{-}C_4H_{10}}$ [$m^3_{(STP)}$ m^{-1} h^{-1} bar^{-1}]	$m_{n\text{-}C_4H_{10}}$ [-]	$P=P^0_{CH_4}$ [$m^3_{(STP)}$ m^{-1} h^{-1} bar^{-1}]	$\alpha^*_{n\text{-}C_4H_{10}/CH_4}$ [-]
-	PDMS	3.72E-05 ± 3.81E-06	1.613	3.01E-06 ± 1.26E-07	12.4 ± 1.3
M-3	MMMa	1.69E-05 ± 1.11E-06	1.950	1.71E-06 ± 7.02E-08	9.9 ± 0.6
M-4	MMMb	1.72E-05 ± 1.19E-06	1.953	2.13E-06 ± 8.76E-08	8.1 ± 0.6
	MMMc	1.88E-05 ± 1.05E-06	1.980	2.10E-06 ± 8.75E-08	9.0 ± 0.5
	MMMd	1.48E-05 ± 3.01E-07	1.972	1.58E-06 ± 6.43E-08	12.4 ± 1.6

Before discussing the influence of mixing methods, it is of interest to consider the roles of activated carbon particles and PDMS in the solution, diffusion, and adsorption processes. Solubility of *n*-C_4H_{10} in PDMS increases with increasing fugacity. Consequently, permeability of *n*-C_4H_{10} increases. It is apparent that *n*-C_4H_{10} shows a solution-controlled permeation behaviour in PDMS. This exponential increase with increasing mean fugacity occurs partially due to a plasticization effect. Plasticization is a pressure-dependent phenomenon that refers to an increase

of penetrant diffusivity resulting from increased fractional free volume (FFV) in the polymer due to presence of dissolved penetrant molecules. As expected, *n*-C_4H_{10} plasticizes PDMS with its high concentration in the polymer. Same trend was observed for *n*-C_4H_{10} permeability in all MMMs. In case of MMM, the increase of *n*-C_4H_{10} permeation with increasing fugacity can be explained with combined effect of solution of *n*-C_4H_{10} in PDMS and adsorption on activated carbon. At a constant temperature, adsorption of *n*-C_4H_{10} strongly depends on fugacity (or pressure). Moreover, the adsorption of *n*-C_4H_{10} on the activated carbon particles is indicated by the higher slopes of the exponential trends for permeation in MMMs than that of in PDMS (as given in Table 5.3.). Unlike *n*-C_4H_{10}, no feed pressure dependency was observed for CH_4 in PDMS and MMMs. This behaviour is typical for permeation of non-condensable gases in polymers and this type of permeation is diffusion-controlled.

To evaluate the effect of mixing procedure on pure gas permeation, MMMs prepared by method-3 and method-4 were compared. For *n*-C_4H_{10} permeability, no difference was observed when method-3 (MMMa) or method-4 for 5 min mixing (MMMb) were applied. Mixing for 15 min with method-4 improved the permeability of *n*-C_4H_{10} (MMMc). Increasing the mixing time to 30 min, on the other hand, reduced the permeability (MMMd). A similar trend was observed for CH_4 permeation. Mixing procedure used in method-4 resulted in higher permeabilities for 5 and 15 min mixing than that of used in method-3. CH_4 permeability reduced when the suspension was mixed for 30 min with method-4.

However, determined permeabilities of both gases in all MMMs were lower than that observed in unfilled PDMS membranes. To figure out why, the solubility, diffusivity, and adsorption behaviour of the gases must be considered. First of all, activated carbon particles dispersed in the PDMS matrix may behave as impermeable barriers. If the gas molecules cannot follow a straight diffusion pathway in PDMS matrix due to the presence of the particles, they may find a longer way around the filler particles to diffuse. As a result, the rate of permeation or permeability reduces. This effect is called tortuosity and it has been often discussed in literature [54, 79, 161]. The shape and the size of the filler then should have an influence on the pathway of the penetrant gas. On the other hand, activated carbon particles may impact mobility of PDMS by changing its structure. The gas transport around the particles may be altered due to the inhibition of PDMS chain mobility in a local region. This effect is called polymer chain rigidification [94, 95, 162]. The loading of the activated carbon particles into the PDMS matrix appears to have a strong effect on pure gas permeabilities.

The slopes of the permeation trend of *n*-C_4H_{10} in unfilled PDMS and MMMs were different from each other, which makes it interesting to investigate the magnitude of the filler effect over the studied mean fugacity range. This effect was calculated as the reduction in permeability of an MMM compared to the permeabilty in unfilled PDMS at several mean fugacities by using the equation below:

$$\text{Reduction [\%]} = \frac{(P_{PDMS} - P_{MMM})}{P_{PDMS}} \text{ x } 100 \qquad (5.3)$$

Figure 5.12 (a) illustrates the reduction in *n*-C_4H_{10} permeability as a function of mean fugacity in MMMs prepared either with method-3 or method-4 and compares those with unfilled PDMS. In all MMMs, the degree of reduction in *n*-C_4H_{10} permeability was not constant over mean fugacity (or feed pressure), but proportional to the mean fugacity. For example, the reduction in *n*-C_4H_{10} permeability in MMMa compared to PDMS was decreased from 46 to 33% when mean fugacity of *n*-C_4H_{10} was increased from 0.5 to 1.15 bar, which was almost the same in MMMb. The

permeation reductions in MMMs were much beyond the 20 wt% activated carbon loading. It is very difficult to estimate how much of the reduction is due to the replacement of PDMS by obstructive activated carbon particles or due to the tortuosity of the diffusion path. Nevertheless, the higher the feed pressure, the lower the reduction. This means that more *n*-C_4H_{10} dissolves in the PDMS and more adsorption of *n*-C_4H_{10} occurs through the activated carbon particles. MMMc showed the best results among the MMMs with 39 and 23% reduction at 0.5 to 1.15 bar mean fugacity of *n*-C_4H_{10}, respectively. This indicates that mixing the casting suspension by method-4 for 15 min hinders the agglomerate formation and helps to obtaion well-dispersed particles in PDMS. The reduction observed for MMMd (52 to 40%) was considerably greater than those observed for the other MMMs. The degree of reduction in CH_4 permeability was constant over the mean fugacity. Differently from *n*-C_4H_{10}, MMMb and MMMc showed the lowest reduction in CH_4 permeability (29 and 30%, respectively), compared to MMMa and MMMd (43 and 47%, respectively).

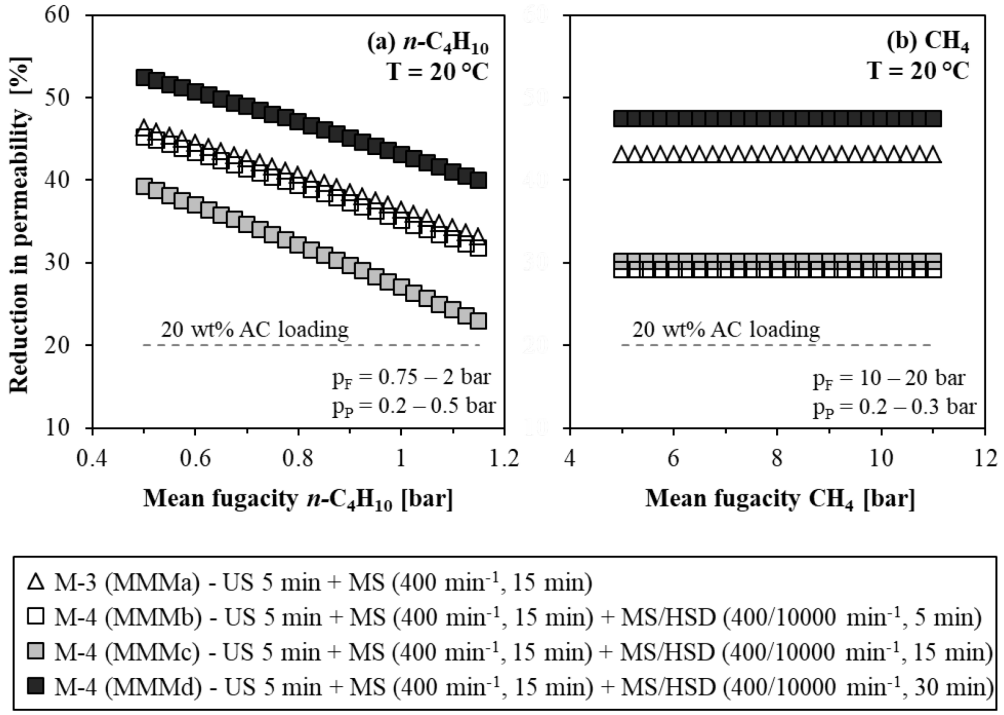

Figure 5.12 Reduction in pure gas permeability of (a) *n*-C_4H_{10} and (b) CH_4 in ethanol-saturated MMMs prepared with method-3 and method-4 compared to unfilled PDMS (T = 20 °C) (*M*: method, *US*: ultrasonication, *MS*: magnetic stirring, *HSD*: high-speed dispersing).

One way to estimate the selectivity of the membranes is to calculate permselectivity, which is the ratio of the infinite permeability coefficient of *n*-C_4H_{10} to the CH_4 mean permeation coefficient determined with pure gas experiments as presented in Table 5.3. Determined permselectivities of the MMMs were lower than that of unfilled PDMS, except for MMMd. Although this approach is frequently encountered in the literature, it is not satisfactory to determine real separation performance of a membrane, since the permeation behavior of the gases in a mixture is completely ignored. For example, the adsorption of the gas molecules on the surface of the activated carbon particles might vary in a binary mixture. Furthermore, in case of a pure methane

permeation, the effect of plasticization caused by butane is not taken into account. Therefore, the actual separation performance of the membranes is determined by mixed gas experiments.

Since the pure gas experiments revealed that MMMs produced with method-4 showed the highest permeabilities, the actual separation performances of the MMMs produced only with this method were investigated by mixed gas experiments. These results were compared with the mixed gas selectivities of unfilled PDMS membranes. Experiments were performed with binary mixtures of 4 vol% of *n*-C_4H_{10} in CH_4 at 20 °C. The mixed gas experiments with unfilled PDMS were conducted at 10, 20 and 30 bar and with MMMs at 15 and 30 bar feed pressure. The experiment at each feed pressure step was repeated 3 times and the results were reported as previously explained in Section 4.3. The errors were calculated using the propagation of error method as discussed in Section 4.2.

Figure 5.13 presents mixed gas selectivity of *n*-C_4H_{10}/CH_4 in PDMS and MMMs as a function of mean *n*-C_4H_{10} fugacity. For both types of membranes, incresing mean *n*-C_4H_{10} fugacity (or feed pressure) resulted in slightly increased selectivity. This influence of feed pressure on membrane performance will be discussed in detail in Section 6.1. The average selectivity of PDMS showed an increase from 17.1 to 18.9, when the feed pressure increased from 10 to 30 bar. MMMb and MMMc showed the same average mixed gas selectivity of 20.7 at 15 bar, while the average mixed gas selectivity of MMMs was 20.5. The same trend was observed for the measurements conducted at 30 bar. Average selectivity of both MMMb and MMMc were 21.8 at 30 bar. However, MMMd showed a slightly decreased selectivity, which was 21.5, than other MMM samples. It has to be considered that differences in the determined average selectivities of MMM samples were too small and the average selectivity values of them were within the experimental error. Anyway, the mixed gas selectivity trends of the MMM samples were similar to the trends observed for their pure gas permeability. In both experiments, MMMc, where the casting suspension was mixed for 15 min with HSD, showed the highest performance. It can, therefore, be concluded that satisfactory membrane structures with method-4 can be obtained when these conditions are used.

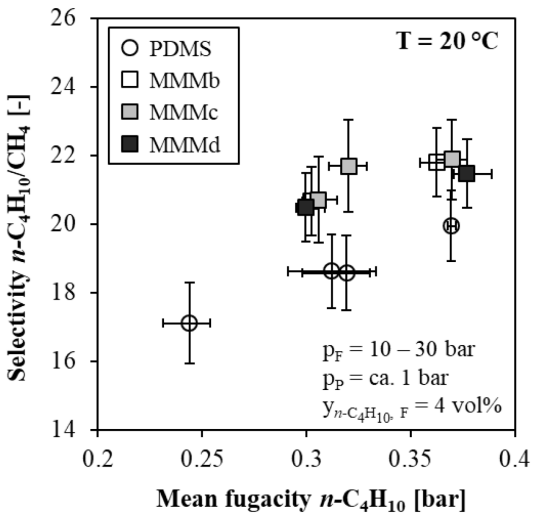

Figure 5.13 Mixed gas selectivity of binary mixture of 4 vol% *n*-C_4H_{10} in CH_4 in unfilled PDMS and ethanol-saturated MMMs prepared with method-4 (T = 20 °C). Error bars are determined using the propagation of error method.

Although the improvement in selectivity with MMMs was very low, addition of 20 wt% activated carbon particles into the PDMS matrix slightly enhanced the selectivity of MMMs in comparison to unfilled PDMS membranes over the investigated range of parameters. This improvement in selectivity can be partially explained by the reduced swelling of the PDMS layer in the presence of activated carbon particles. Morever, a selective surface flow may exist through the pores of activated carbon particles having a preferential surface diffusion of *n*-C_4H_{10} over CH_4. In this way, CH_4 diffusion might be blocked by formation of a condensed layer [54]. Mixed gas selectivity results of MMMs indicates that the selected activated carbon particles clearly have a higher adsorption selectivity for *n*-C_4H_{10} than for CH_4.

For a successful MMM formation, filler particles should be well distributed in the polymer matrix that a sufficient portion of the penetrant gas can cross the particles. If this is achieved, filler particles can enhance the permeability and selectivity of the polymer phase [116]. MMMs that were prepared in this work showed higher selectivities than those of unfilled PDMS membranes. This indicates that the interaction between activated carbon particles and PDMS was good and the produced composite membranes were defect-free. These results also suggest that the preparation procedure for MMMs strongly effects the permeability of the gases. The order of the preparation steps and the variation in the mixing time of casting suspension mainly effects the polymer/filler particle interactions and the morphology of the membranes. In addition, incorporation of activated carbon particles into PDMS offers an opportunity to improve separation performances of the polymeric membranes.

5.2 Pre-treatment of filler particles

A strategy for the pre-treatment of the activated carbon particles was developed to avoid potential blockage of the pores by the polymer chains. This strategy was a simple priming step of the activated carbon particles with a solvent prior to mixing with PDMS. This initial step of membrane preparation is called *solvent saturation* in this work. In this section, first solvent saturation technique was explained in detail and then the influence of this pre-treatment strategy on the morphology and the gas permeation behavior of the prepared MMMs was discussed.

Solvent saturation technique

Solvent saturation of activated carbon particles might facilitate further dispersing step in PDMS solution. As explained in Section 5.1, dispersing the activated carbon particles first in a solvent with a 5 min ultrasonication step prior to mixing with PDMS solution was useful to avoid agglomerate formation. Another expected benefit of such pre-treatment is that the solvent fills the pores of the activated carbon particles, not allowing PDMS chains to penetrate into the pores upon mixing the particles with PDMS. During the post-treatment of the membrane (annealing), the solvent in the pores is desired to be desorbed and the pores are expected to be free for the necessary mass transport. The ideal solvent saturation protocol for activated carbon particles is illustrated in Figure 5.14.

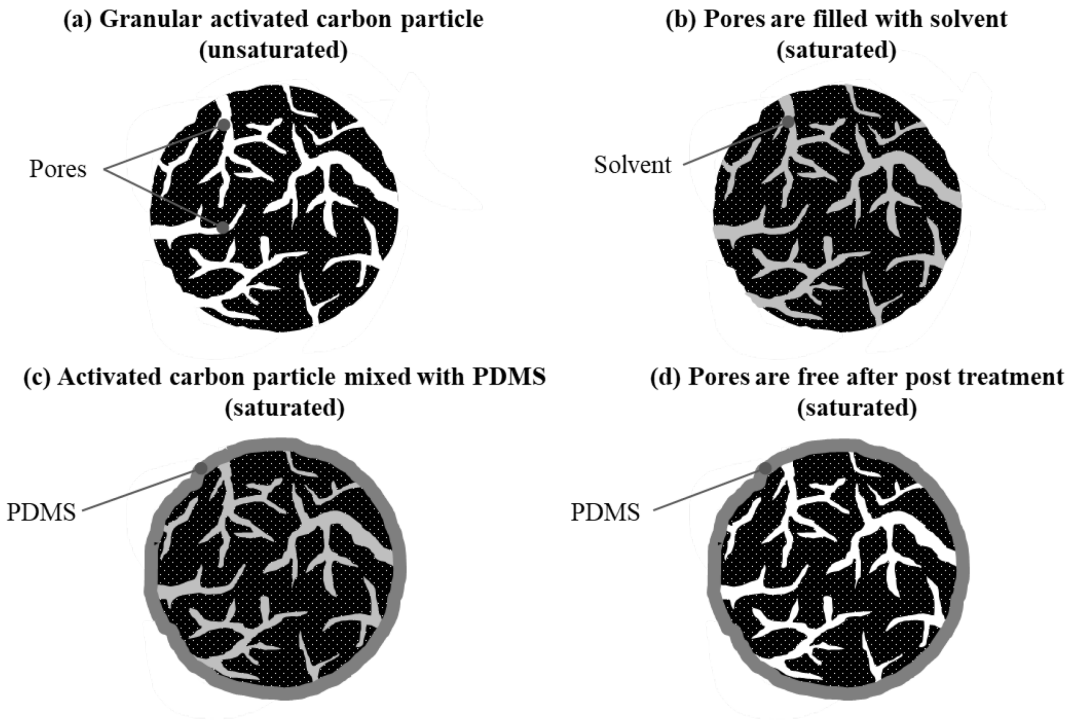

Figure 5.14 Solvent saturation technique of activated carbon particles.

5.2.1 EDX analysis to investigate pore blockage

There is no characterization technique that definitely assesses pore blockage. In this work, Energy-Dispersive X-ray Spectroscopy (EDX) was used to obtain qualitative evidence on pore blockage. The chemical formula of PDMS is $CH_3[Si(CH_3)_2O]_nSi(CH_3)_3$, thus, it was aimed to observe PDMS penetration by detecting presence of silicon (Si) with EDX in a sample. For EDX analysis, relatively large activated carbon particles with a mean diameter of d_{50} = 431 µm (particle size distribution of 100 – 630 µm) were used to be able to manually cut a single carbon particle into two halves during sample preparation. The main characteristics of these large particles were identical to the particles used for previous investigations (see Table 3.2). Prior to use, activated carbon particles were stored in a vacuum drying oven at 100 mbar and 150 °C for 12 h to avoid adsorption of any contaminants.

In total 4 samples at two different PDMS concentrations were prepared. Two of these samples were saturated with isooctane. Isooctane was selected as the saturation solvent to fill the pores of the particles since it was already an additive of PDMS solution. To saturate the particles, isooctane was added onto the dried activated carbon particles. They were stirred with a shaker in a fume hood until the pores of the particles were completely filled with isooctane and the rest of the solvent was evaporated. Then, 5 wt% PDMS solution was added to these samples and stirred with a shaker in a fume hood while the bottles were open. The samples that no saturation was applied were directly stirred with 5 wt% PDMS. The required amount of PDMS was calculated depending on a factor of *f*, which describes the ratio between the volume of pores filled with PDMS and the total volume of pores as following:

$$f = \frac{V_{PDMS\ filled\ pores}}{V_{total\ pores}} = \frac{m_{PDMS}}{\rho_{PDMS} V_{total\ pores}} \quad (5.4)$$

where ρ_{PDMS} is the density of PDMS. The density of PDMS was experimentally determined as 0.984 ± 0.001 g cm^{-3} at 20 °C by Helmholtz Zentrum Geesthacht [20].

The samples were prepared at two different conditions of *f*; either the pores of the particles were partially (half) blocked by PDMS, where f = 0.5, or totally blocked, where f = 1.0. The amount of materials and concentration of PDMS used to prepare samples for the point-scanning are listed in Table 5.4. From each sample bottle, a single carbon particle was taken and manually cut into two halves with a blade. One-half of the particle was mounted on a specimen stub to analyze cross-section area of the particle with EDX point-scanning (PS) after sputter coating with gold. EDX point-scanning was performed on several predetermined depths of a single activated carbon particle starting from the surface through the center of the particle and Si presence was investigated. This was done by keeping the electron beam stationary on a series of spots and generating a spectrum that provides localized elemental information (Figure 5.15).

Table 5.4 EDX point-scanning (PS) samples.

EDX analysis	Sample no	Pre-treatment	AC [g]	PDMS [wt%]	Isooctane [g]	f	PDMS/AC [g.g^{-1}]
Point-scanning	PS-1	unsaturated	1.0	5.0	-	0.5	1.0
	PS-2	saturated	1.0	5.0	3.5	0.5	1.0
	PS-3	unsaturated	1.0	5.0	-	1.0	2.0
	PS-4	saturated	1.0	5.0	3.5	1.0	2.0

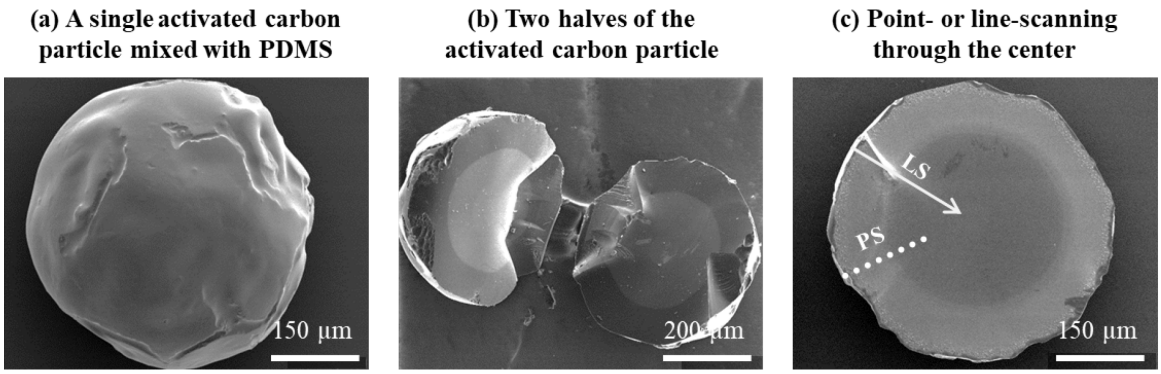

Figure 5.15 EDX point- and line-scanning analysis on a single activated carbon particle.

Figure 5.16 shows the number of counted X-rays over the energy of electron beam resulting peaks of detected individual elements in the unsaturated (PS-1) and saturated particle (PS-2) at 5 µm depth. EDX can detect many elements, but in this work the interesting elements were carbon (C) as the basic element in the particle being studied, Si as the indicator of polymer penetration, and gold (Au) as the result of sputter coating. The assumption made during the preparation of these two samples was that the half of the total volume of activated carbon pores was blocked, where f = 0.5. Si signals detected at 5 µm depths in the particles were too weak and the strength

difference between the signals was not significant for these two samples. Therefore, the influence of solvent saturation technique in these samples could not be observed with studied technique.

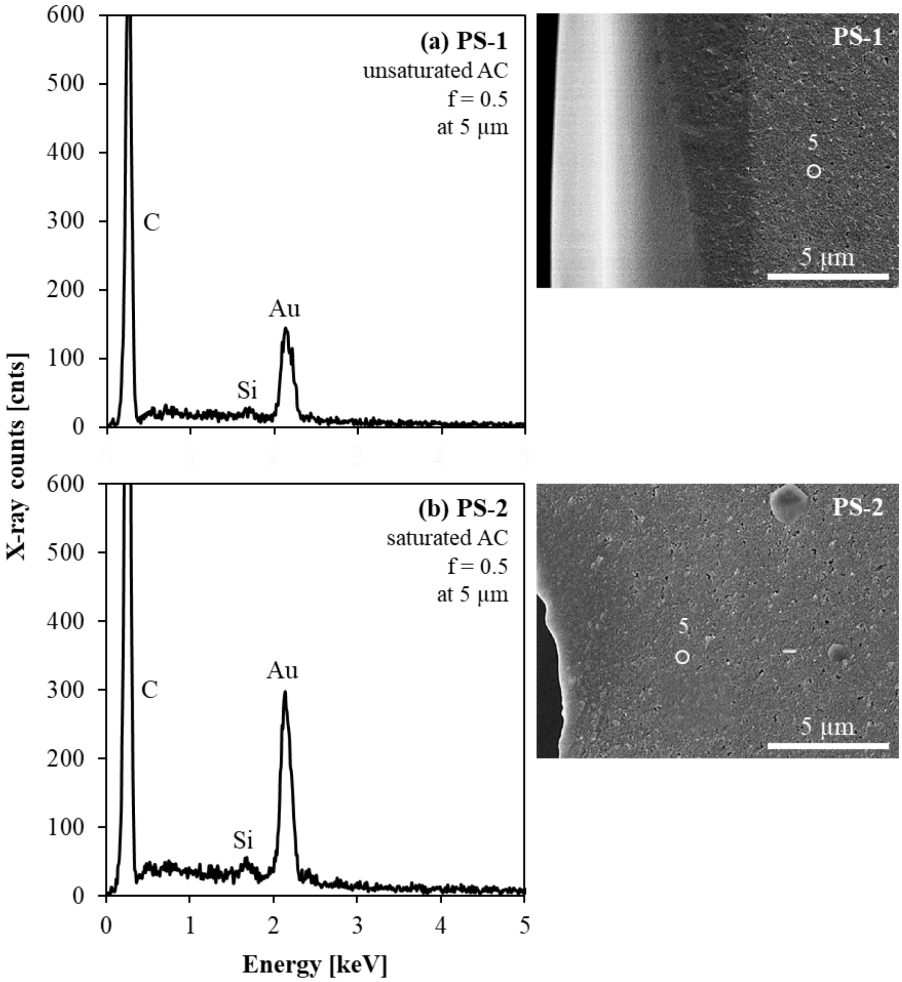

Figure 5.16 Cross-sectional SEM images (right) and EDX point-scanning (PS) spectrums (left) of (a) unsaturated AC PS-1, (b) saturated AC PS-2 at 5 µm depth (f = 0.5, *AC*: activated carbon).

Figure 5.17 shows the results of EDX point-scanning analysis of unsaturated (PS-3) and saturated particle (PS-4). These samples had higher amount of PDMS than that of PS-1 and PS-2, where the total pore volume of activated carbon was assumed to be completely blocked (f = 1.0). In the unsaturated sample, the scanning was performed at 5, 10, 15, 30, 50 and 70 µm. Si signal was detected at all depths. The strength of Si signal gradually decreased from 5 to 70 µm and no more Si was detected after 70 µm. In the saturated particle, scanning was performed in the same depths as unsaturated particle PS-3. However, Si signal was detected only up to 50 µm. Similar to PS-3, Si signal strength gradually decreased from the surface towards the center of the particle. More importantly, the number of detected X-ray was considerably fewer and the area of the Si peaks at all of the measured depths was smaller for the saturated particle than the unsaturated particle. This means that PDMS penetration in the saturated carbon particle was weaker than in the unsaturated particle. This result indicates that pore blockage with Si chains can be partially eliminated using solvent saturation method, which is an important advantage. It was also seen that the Si chains penetrate deeper when PDMS concentration was increased.

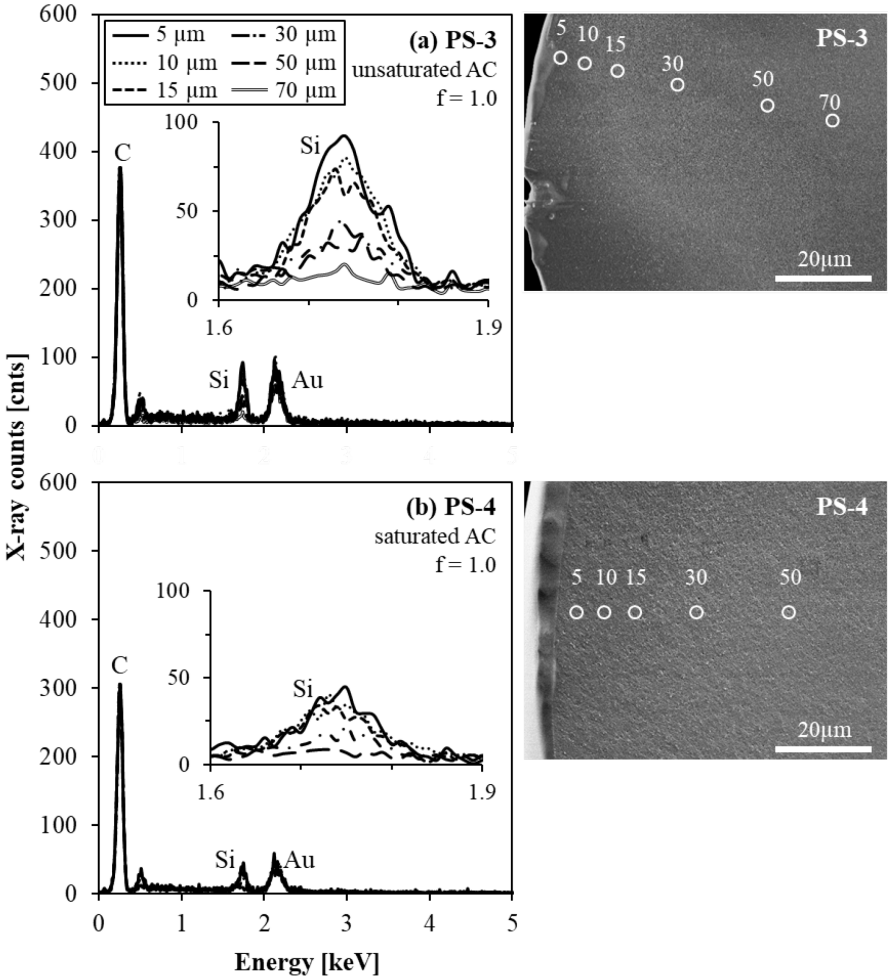

Figure 5.17 Cross-sectional SEM images (right) and EDX point-scanning (PS) spectrums (left) of (a) unsaturated AC PS-3, (b) saturated AC PS-4 at different depths up to 70 µm, (f = 1.0, *AC*: activated carbon).

With point-scanning analysis, only limited number of points on the cross-section of the particles were examined. To check reliability and reproducibility of the results, EDX line-scanning (LS) analysis was also performed, where the electron beam follows the line drawn on the sample image and generates a plot of the relative proportions of previously identified elements along the line. Since the line-scanning is conducted over more points along a line, the counting statistics are much better. Line-scanning analysis does not give direct elemental concentrations, but it is possible to determine the composition of individual components in a sample with the obtained data. The proportion of each element in the sample can be calculated by measuring the areas under the X-ray peaks. This provides semi-quantitative elemental composition of the interesting elements in a sample. EDX detects the identified elements and reports the data as atomic mass of detected individual elements as calculated by Equation 5.5:

$$\text{atomic percentage [\%]} = \frac{N_i}{N_t} \text{ x } 100 \qquad (5.5)$$

where N_i is the atomic mass of the individual element and N_t is the total atomic mass of elements.

Three different isooctane-saturated samples containing different amounts of 5 wt% PDMS were prepared for line-scanning analysis. All samples were prepared with the same amount of activated carbon particles and saturated with the same amount of isooctane. The required amounts of 5 wt% PDMS solution were calculated for 3 different factors of *f* (1.0, 0.5, and 0.2). Similar to point-scanning analysis, the line-scanning was applied to the cross-section area of one single carbon particle from the sample to detect Si penetration profile along axial direction. Oxygen (O), sulfur (S), and C signals were also studied. A total depth of 120 µm through the center of the particle was scanned with a speed of 20000 ms per each 5 µm (25 points in total). Measurements were carried out at a voltage of 20 kV. Line-scanning samples were investigated after sputter coating with gold. The amount of materials and the concentration of PDMS used to prepare samples for the line-scanning are listed in Table 5.5.

Table 5.5 EDX line-scanning (LS) samples.

EDX analysis	Sample no	Pre-treatment	AC	PDMS	Isooctane	f	PDMS/AC
			[g]	[wt%]	[g]		[$g.g^{-1}$]
Line-scanning	LS-1	saturated	1.0	5.0	5.0	1.0	2.0
	LS-2	saturated	1.0	5.0	5.0	0.5	1.0
	LS-3	saturated	1.0	5.0	5.0	0.2	0.5

Figure 5.18 shows the cross-sectional SEM images of line-scanning applied isooctane-saturated carbon particles and the atomic percentage of elements detected on the scanning line over the penetration depth. As expected, the highest percentage of atomic mass (between 95 and 98%) was occupied by carbon in all samples, because the sample of interest was a carbon particle. On the other hand, although the samples did not contain any sulfur source, lower than 1% atomic percentage of sulfur was detected in all samples. It stayed almost constant over the measured depth inside the particle. The reason why sulfur was detected in these samples could be an artifact depending on the settings of used scanning electron microscope, when the sputter coating was done with gold. The sulfur-Kα-X-ray line was adjacent to the gold-Mα-X-ray line. If the analysis window was too broad, gold-Mα-X-rays could be detected in the sulfur-Kα window. Oxygen was detected due to being an element in the polymer as Si. Atomic percentages of both oxygen and silicon decreased synchronically over the depth measured inside the particle.

To allow better interpretation of the results, atomic percentages of Si detected in 3 samples are plotted over the depth up to 80 µm in Figure 5.19. The highest atomic percentage of Si was detected in the first sample, LS-1, which was mixed with the highest amount of PDMS (PDMS/AC = 2.0 $g.g^{-1}$). The amount of detected Si in the second sample, LS-2 (PDMS/AC = 1.0 $g.g^{-1}$), was lower than that of LS-1, where less PDMS was added. Finally, the lowest Si penetration was achieved with the lowest PDMS addition in the third sample, LS-3 (PDMS/AC = 0.5 $g.g^{-1}$). These results reveal that the increasing the amount of PDMS added to cover the particles caused more penetration of polymer chains into the pores of carbon particles. After approximately 40 µm, no significant change in Si atomic percentage was detected and the values were extremely low and similar for all samples.

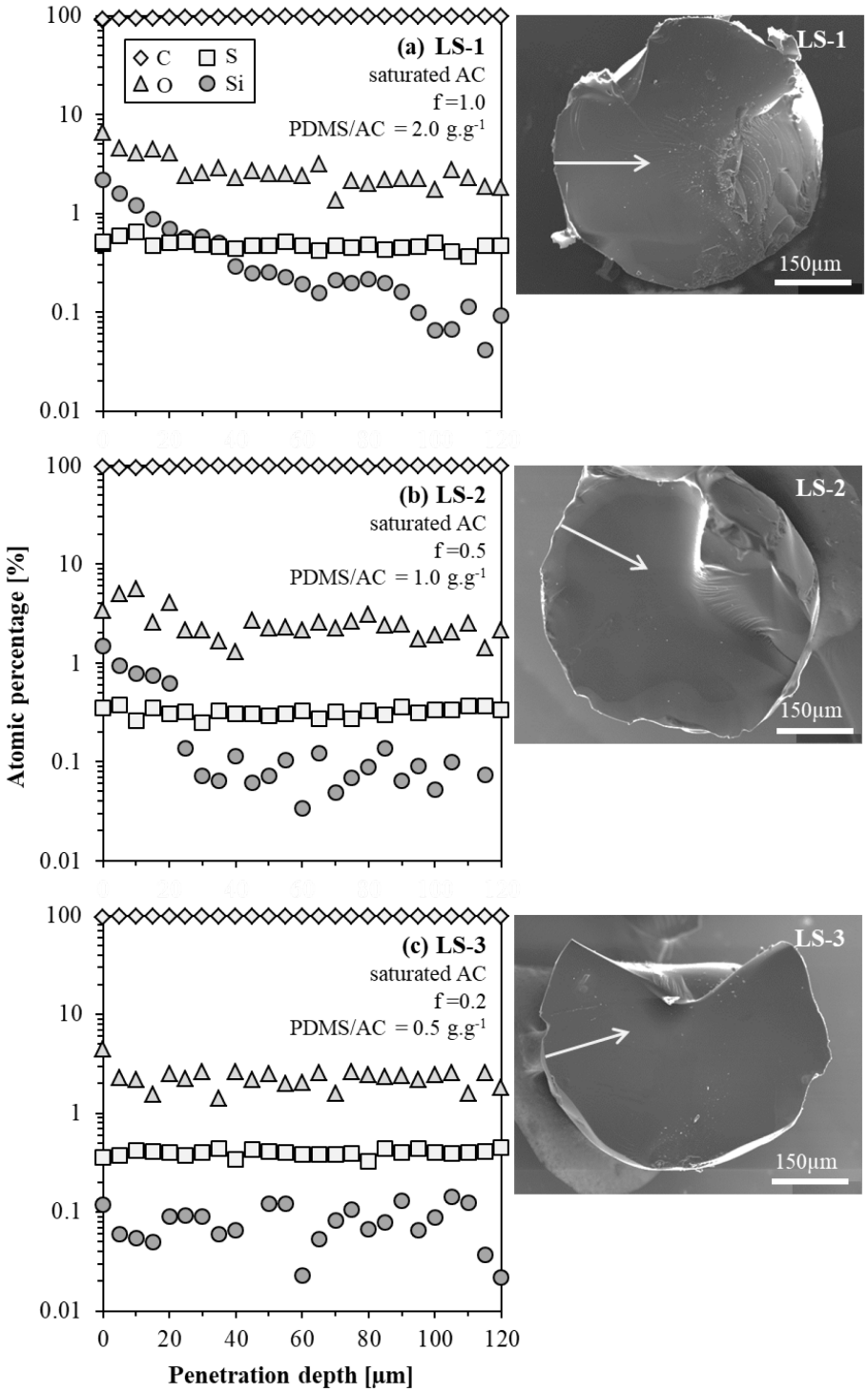

Figure 5.18 Cross-sectional SEM images (right) and atomic percentage of elements (left) in isooctane-saturated samples: (a) LS-1 (f = 1.0, PDMS/AC = 2.0 $g.g^{-1}$), (b) LS-2 (f = 0.5, PDMS/AC = 1.0 $g.g^{-1}$), and (c) (a) LS-3 (f = 0.2, PDMS/AC = 0.5 $g.g^{-1}$) (*AC*: activated carbon).

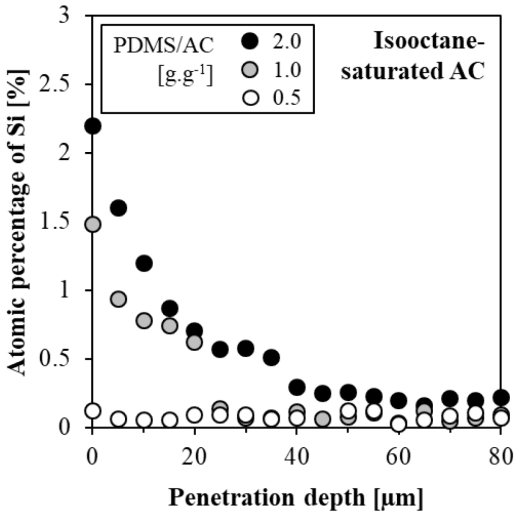

Figure 5.19 Comparison of Si atomic percentage in isooctane-saturated samples mixed with different amounts of PDMS.

Carbon particles used in the MMM production have generally smaller size (~3.5 µm) than the particles used here (d_{50} = 431 µm). Therefore, pore blockage should be further reduced, even under 1 µm penetration depth. Thus, different solvents were investigated following the same procedure in order to find the most suitable solvent to meet the 1 µm criterion.

Saturation of filler particles with other solvents

The solvent used for saturation is expected to desorb from the pores of the filler particles when particles are mixed with PDMS to free the pores for an efficient mass transport. Therefore, solvent-particle-polymer interactions are important. This relationship between solvent and the particle was quantified by Mahajan and Koros [91] as liquid-solid interaction strength parameter and toluene seemed to be the most suitable solvent in their study, where zeolite 4A was used as filler particles in PVAc. Another consideration is that the solvent for saturation should have lower boiling point than isooctane, so that the solvent can easily be evaporated and annealed during the post-treatment of the membranes. Ethanol, cyclohexane, n-heptane, and toluene were selected as the solvents having these characteristics. Si penetrations in saturated samples with these solvents were investigated and compared with that in isooctane-saturated sample. Boiling points of the selected solvents are listed in Table 5.6. Carbon particles were saturated with these solvents and then mixed with different amounts of 5 wt% PDMS solution. Sample preparation and EDX line-scanning were conducted as explained previously, unless otherwise stated. For each sample, a total length of 80 µm was scanned in every 5 µm.

Table 5.6 Boiling points of the solvents used for saturation.

Solvents	ethanol	cyclohexane	n-heptane	isooctane	toluene
Boiling point [°C]	78	81	98.4	99	111

Figure 5.20 plots atomic percentage of Si detected in saturated samples over the penetration depth. In samples saturated with ethanol, the amount of Si over the measurement depth was the lowest when compared to samples saturated with other solvents for all PDMS/AC ratios. The atomic percentage of Si decreased slightly with the decrease in PDMS/AC ratio. Toluene-saturated samples showed the same trend. However, the amounts of Si in the areas closer to the surface of the particles, especially in the first 10 µm depth, was higher than those in ethanol-saturated particles. Moreover, compared to isooctane, the atomic percentages of Si for all PDMS/AC ratios were lower in particles saturated either in toluene or ethanol. The atomic percentages of Si in the particles were slightly lower when n-heptane was used as saturation solvent than those when isooctane was used. For all PDMS/AC ratios, the highest amount of Si penetration was recorded when cyclohexane was used, barely reducing PDMS penetration. According to these results, ethanol and toluene seemed to be the two most suitable solvents for saturation of carbon particles for the mixed-matrix membranes targeted in the current work. However, saturation in either solvent did not completely eliminate PDMS penetration. A low degree of polymer penetration into the pores still occurred. Therefore, it is hard to claim that maximum 1 µm penetration depth criteria is achieved. To summarize, the results suggest that solvent saturation significantly reduces the pore blockage, rather than avoiding it completely.

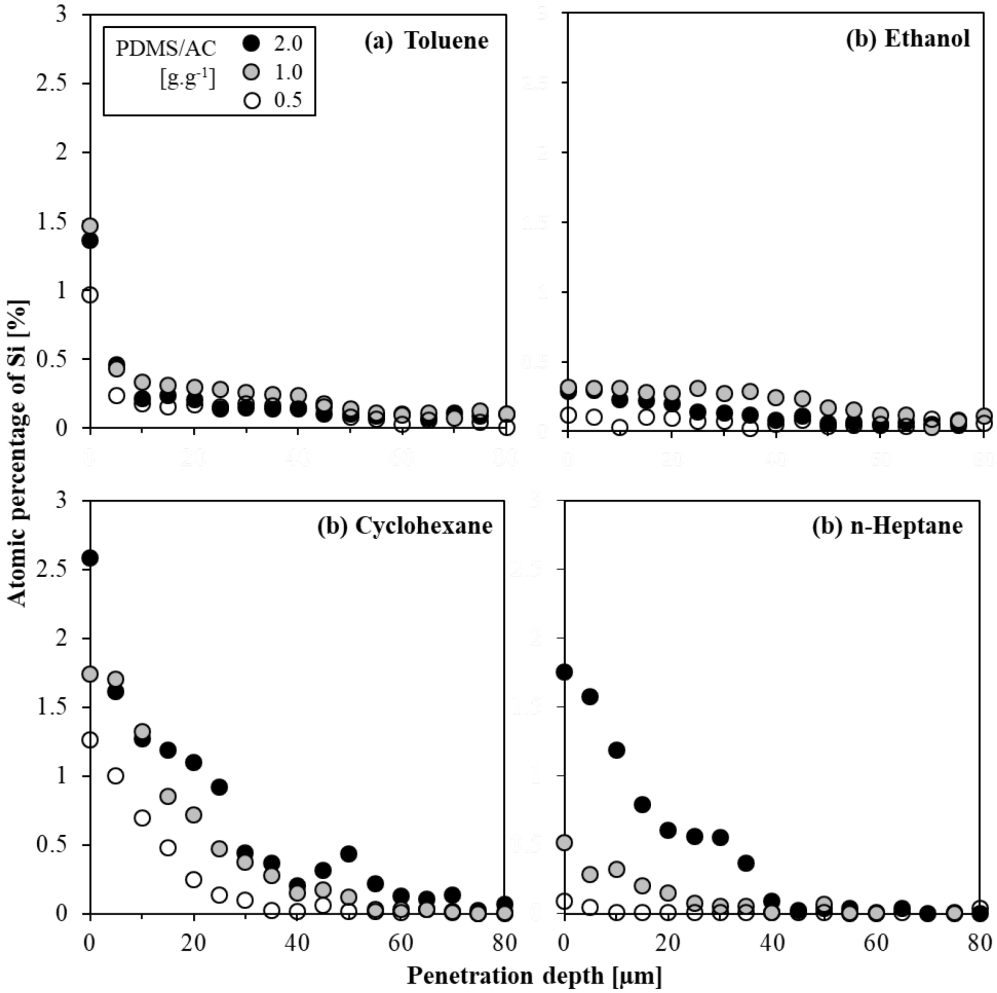

Figure 5.20 Comparison of Si atomic percentage in (a) toluene-, (b) ethanol-, (c) cyclohexane-, and (d) n-heptane-saturated samples mixed with different amounts of PDMS.

Limitations and drawbacks of EDX

When reaching conclusions with the results of an EDX-analysis, it is important to bear in mind some essential disadvantages of this technique. First of all, EDX-analysis did not give direct elemental concentrations of the samples, but allowed identification of particular elements and their relative proportions in atomic mass or weight percent.

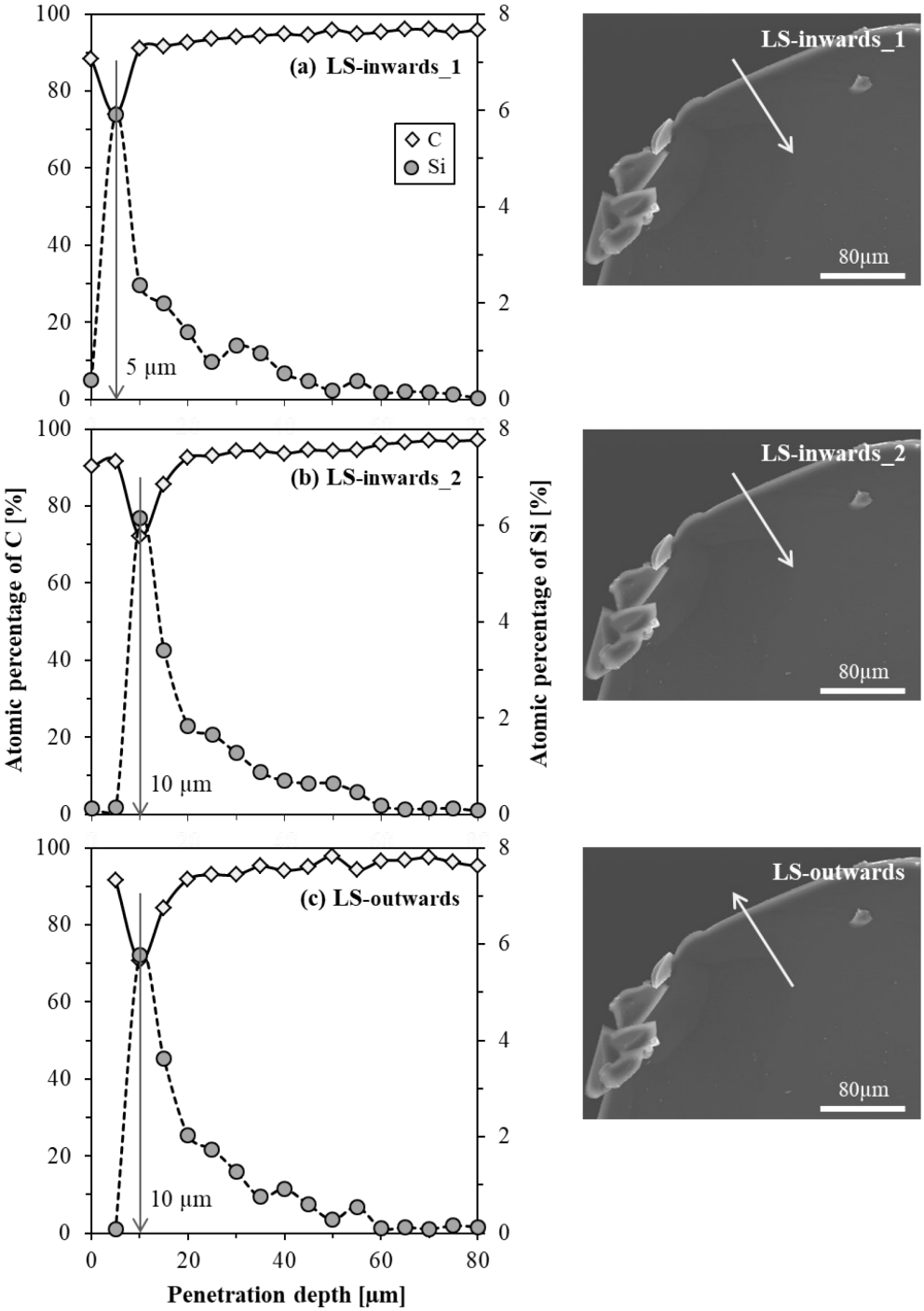

Figure 5.21 Starting point correction of EDX line-scanning results (n-heptane-saturated particle, PDMS/AC = 2 $g.g^{-1}$, background subtracted) SEM images (right) and atomic percentage of C and Si (left).

In this work, measurements were performed only with one single carbon particle from each sample. Although precision and accuracy of the technique has approached ± 2% and 95%, respectively, a sufficient number of carbon particles was not examined to get statistically meaningful results. The area of analysis was governed by the spreading and penetration of the electron beam. The analyzed area was a circle having a diameter of approximately 5 µm and the depth of ~ 1 µm and it was very surface-sensitive, limiting each measuring steps to a 5 µm distance. Sample preparation was another critical issue, where particles were cut with a blade. Due to this, PDMS was smeared on some locations near the edge of cross-section area, which might have affected the strength of the detected Si signals.

In the result analysis, to obtain more reliable relative concentrations, certain corrections were applied to the raw data. It was a necessity to perform background subtraction and correction of the starting point of the analyzed sample that was the largest uncertainty. In the area closer to the surface of the particle, a jump in Si concentration was detected due to a large PDMS layer coated on the surface of the particle. After the background subtraction, starting point of the particle was estimated by comparing the change in atomic percentage of C and Si. It was assumed that the point where particle started was, where Si concentration suddenly dropped and C concentration simultaneously increased. The data until that point was excluded from the diagrams. The reliability of the background subtraction and starting point correction was evaluated by repeating the line-scanning analysis 3 times, where first two measurements were performed inwards from the surface through the center of the particle and the last one was performed outwards from the center through the surface of the particle. An example of the measurements for the particle saturated in n-heptane is presented in Figure 5.21 and the corrected data is presented in Figure 5.22. In all measurements, 3 corrected results were in good agreement showing that the method was reliable. Therefore, values after background subtraction and starting point correction are presented in this work.

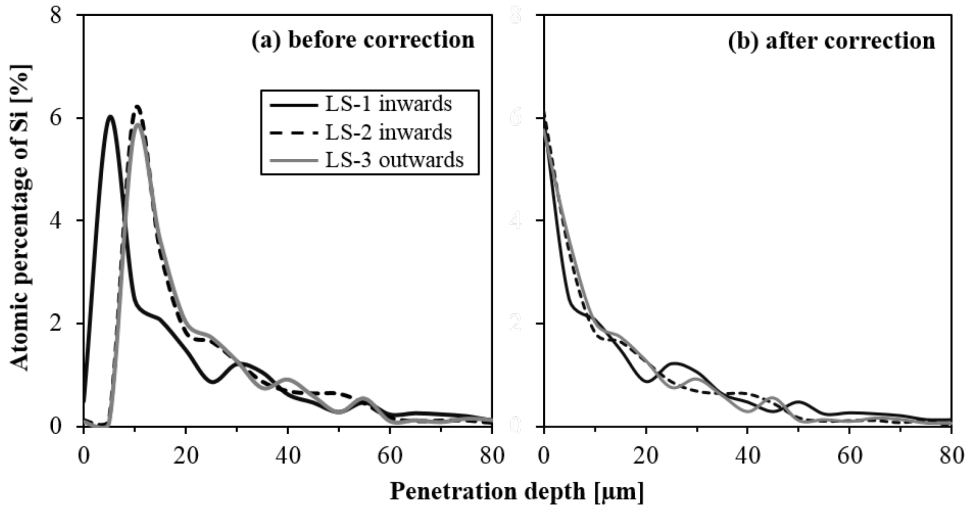

Figure 5.22 Atomic percentage of Si detected by EDX line-scanning: (a) before, (b) after the starting point correction (n-heptane-saturated particle, PDMS/AC = 2 $g.g^{-1}$, background subtracted).

5.2.2 Influence of solvent saturation on pure gas permeation

To understand how the saturation of activated carbon particles in different solvents can influence the final performance of the MMMs, gas permeation experiments were performed. Based on the EDX line-scanning results, cyclohexane and n-heptane, which had low performance to hinder the pore blockage, were decided to be excluded from the list of solvents for this set of experiments. Pure gas permeation performances of MMMs containing carbon particles that are saturated in toluene, ethanol, and isooctane (saturated MMMs) were evaluated. Additionally, pure gas permeation performances of unfilled PDMS and MMMs containing unsaturated carbon particles (unsaturated MMMs) were evaluated as reference materials.

MMMs were prepared with 20 wt% either saturated or unsaturated activated carbon loading (AC 100050, d_{50} = 3.5 µm). All MMMs were produced by following the most efficient mixing procedure (method-4) for activated carbon particles and PDMS as previously discussed in Section 5.1. The only difference was that in the last step of mixing procedure, a combination of magnetic stirring and high speed dispersing, was applied for 30 min, instead of 15 min. The membranes were cast at 300 µm initial thickness by motorized film applicator UA 3000. To obtain identical samples, the preparation protocols were strictly controlled and kept same for each sample.

Figure 5.23 compares the morphological structure of MMMs, in which activated carbon particles were either unsaturated or saturated with different solvents. SEM images indicated no undesired effect of different solvents used during the pre-treatment of activated carbon particles. The thickness of the separation layer of the membranes was measured from SEM images and the results are given in Table 5.7. This difference in thickness of the membranes occurred probably due to the manually adjusted initial casting thickness of the film applicator.

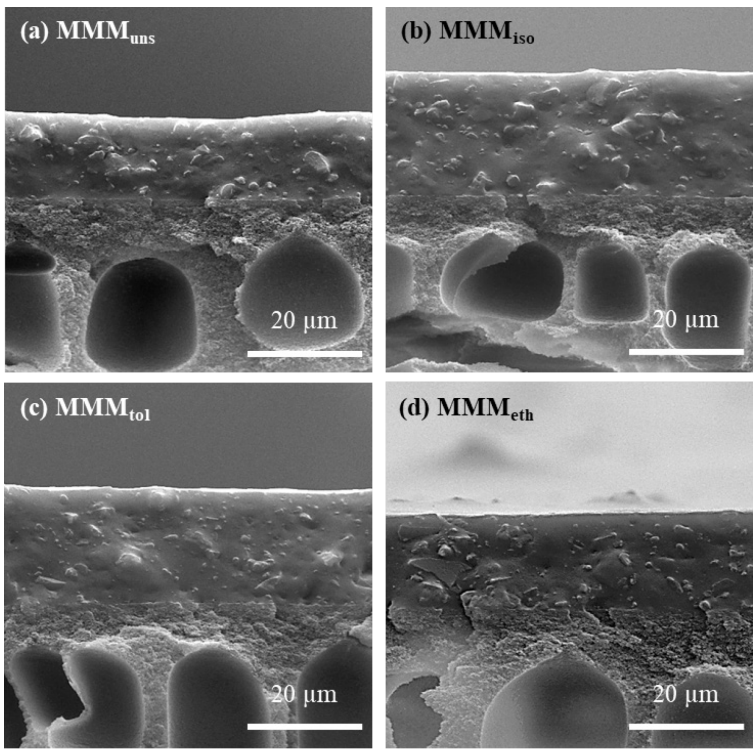

Figure 5.23 Cross-sectional SEM images of MMMs (a) unsaturated, (b) isooctane-saturated, (c) toluene-saturated, and (d) ethanol-saturated with 20 wt% AC loading.

Table 5.7 Average separation layer thickness of the membranes used for the investigation of the influence of solvent saturation.

Membrane	Thickness [µm]	SD [µm]	RSD [%]
PDMS	22.91	0.60	2.59
$MMM_{unsaturated}$	15.12	0.52	3.41
$MMM_{isooctane}$	22.68	0.62	2.73
$MMM_{toluene}$	21.24	0.63	2.96
$MMM_{ethanol}$	15.42	0.53	3.44

The feed pressure was varied from 0.75 to 2 bar for *n*-C_4H_{10}, and from 10 to 20 bar for CH_4 to obtain pure gas permeability data. Permeat pressure was varied from 0.2 to 0.5 bar for *n*-C_4H_{10}, and from 0.2 to 0.3 bar for CH_4. Measurements were performed at 20 °C. Figure 5.24 (a) and (b) present pure gas permeability of *n*-C_4H_{10} and CH_4 in unfilled PDMS and MMMs as function of mean fugacity, respectively. Experimental results were reported as explained in Section 4.3. The errors were calculated using the propagation of error method as discussed in Section 4.2. Pure gas *n*-C_4H_{10} and CH_4 permeability coefficients and *n*-C_4H_{10}/CH_4 permselectivity is given in Table 5.8.

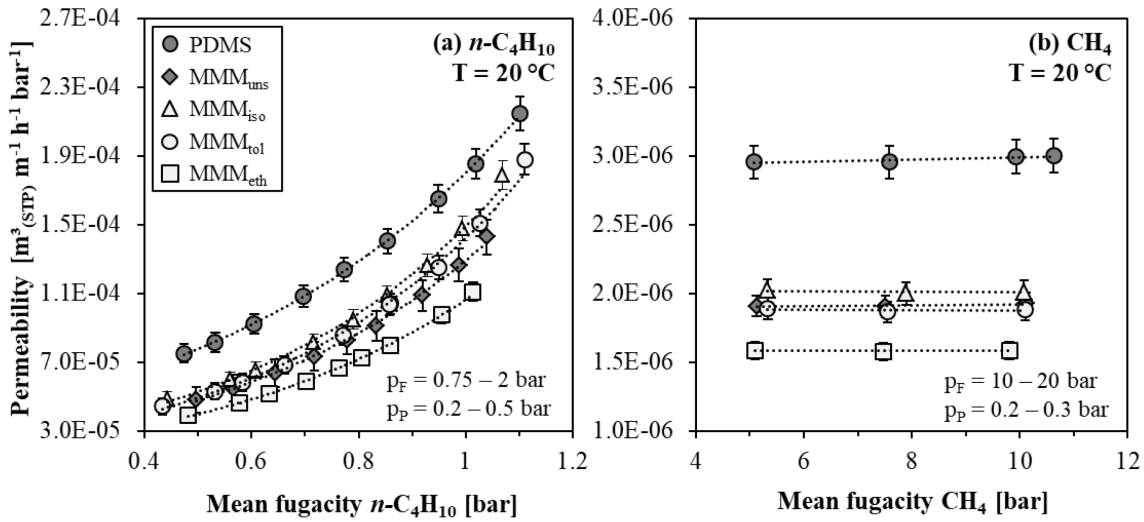

Figure 5.24 Pure gas permeability of (a) *n*-C_4H_{10} and (b) CH_4 in unfilled PDMS and unsaturated and isooctane/toluene/ethanol-saturated MMMs with 20 wt% AC loading (T = 20 °C). Dotted lines represent exponential and linear trend curves and the error bars were determined using the propagation of error method.

The first observation was that the PDMS membrane showed by far the highest *n*-C_4H_{10} and CH_4 permeability compared to the all types of MMMs. Embedding of particles into the polymer matrix reduced the permeability of both gases in all types of MMMs at different levels. It was seen that isooctane and toluene-saturated MMMs showed slightly higher *n*-C_4H_{10} permeability compared to

unsaturated MMMs. When ethanol-saturated particles were used, MMMs showed the lowest *n*-C_4H_{10} permeability, even lower than unsaturated MMMs. In case of CH_4, isooctane-saturated MMMs showed the highest permeability. When toluene-saturated particles were used, the permeability of MMMs has not changed significantly when compared to unsaturated MMMs. MMMs with ethanol-saturated particles showed the lowest permeability among all samples, similar to observations for *n*-C_4H_{10}. Moreover, for all types of MMMs, the slopes of the *n*-C_4H_{10} permeation over the investigated range of fugacity were higher than that in unfilled PDMS showing the desired influence of activated carbon particles. Isooctane or toluene saturation provided slightly higher slopes in permeation behavior of MMMs than those of unsaturated or ethanol-saturated MMMs. This makes isooctane and toluene feasible solvent candidates for saturation step.

Table 5.8 Pure gas *n*-C_4H_{10} and CH_4 permeability coefficients and *n*-C_4H_{10}/CH_4 permselectivity in unfilled PDMS and MMMs with 20 wt% AC loading (T = 20 °C).

Membrane	$P^0_{n-C4H10}$ [$m^3_{(STP)}$ m^{-1} h^{-1} bar^{-1}]	$m_{n-C4H10}$ [-]	$P = P^0_{CH4}$ [$m^3_{(STP)}$ m^{-1} h^{-1} bar^{-1}]	$\alpha^*_{n-C4H10/CH4}$ [-]
PDMS	3.34E-05 ± 2.71E-06	1.684	2.98E-06 ± 1.20E-07	11.2 ± 0.9
$MMM_{unsaturated}$	1.77E-05 ± 2.51E-06	1.986	1.91E-06 ± 7.76E-08	9.3 ± 1.3
$MMM_{isooctane}$	1.87E-05 ± 2.14E-06	2.077	2.01E-06 ± 8.21E-08	9.3 ± 1.1
$MMM_{toluene}$	1.70E-05 ± 2.32E-06	2.122	1.88E-06 ± 7.66E-08	9.1 ± 1.2
$MMM_{ethanol}$	1.53E-05 ± 1.55E-06	1.972	1.58E-06 ± 7.09E-08	9.4 ± 1.0

To better understand the effect of saturation, the reduction in *n*-C_4H_{10} and CH_4 permeability in MMM samples compared to unfilled PDMS is illustrated in Figure 5.25 (a) and (b). In all MMMs, the reduction of *n*-C_4H_{10} permeability was proportional to the fugacity. When unsaturated particles were embedded into PDMS, the permeability reduced from 38.3% to 24.9% at mean *n*-C_4H_{10} fugacities from 0.5 bar to 1.15 bar. Although the degree of reduction decreased as fugacity increased, it was still higher than 20 wt% filler loading at the maximum fugacity investigated, which means that the filler particles functioned as barriers, besides tortuosity. This led to the conclusion that pores of the particles were not completely free for the mass transport of *n*-C_4H_{10}. The MMMs prepared with toluene and isooctane-saturated particles showed lower reduction in permeability. Moreover, extend of reduction in these two membranes fell below the 20 wt% filler loading boundary after approximately 1 bar mean *n*-C_4H_{10} fugacity. This indicates that the blockage of the pores was hindered and the particles did not act as barriers anymore, enhancing the selected adsorption and selective surface diffusion. On the other hand, ethanol-saturated MMM showed the highest degree of reduction, even more than observed for unsaturated MMM.

Results showed that particles in the polymer matrix reduced the permeability of CH_4, being above 20% for all the tested MMMs. It was observed that the reduction of CH_4 permeability was similar when either toluene-saturated or unsaturated particles were employed. The degree of reduction was less than all when isooctane-saturated particles are used and maximum reduction of permeability was recorded for the MMM containing ethanol-saturated particles.

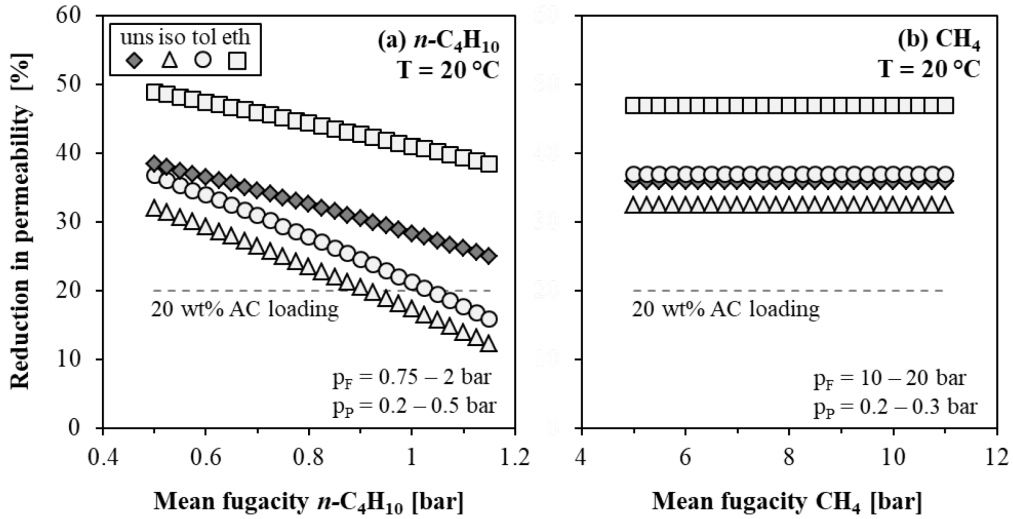

Figure 5.25 Reduction in pure gas permeability of (a) n-C_4H_{10} and (b) CH_4 in unsaturated and isooctane/toluene/ethanol-saturated MMMs with 20 wt% AC loading compared to unfilled PDMS (T = 20 °C).

5.2.3 Influence of solvent saturation on mixed gas selectivity

The separation performances of the unfilled PDMS and MMMs were obtained from the mixed gas experiments using binary mixtures of 9 vol% n-C_4H_{10} in CH_4 at 5, 6, and 7 bar feed pressure. The mixed gas experiments were performed at atmospheric permeate pressure (p_P = ca. 1 bar) at 20 °C. The mixed gas permeability of each component is presented in Figure 5.26 as a function of corresponding mean fugacity.

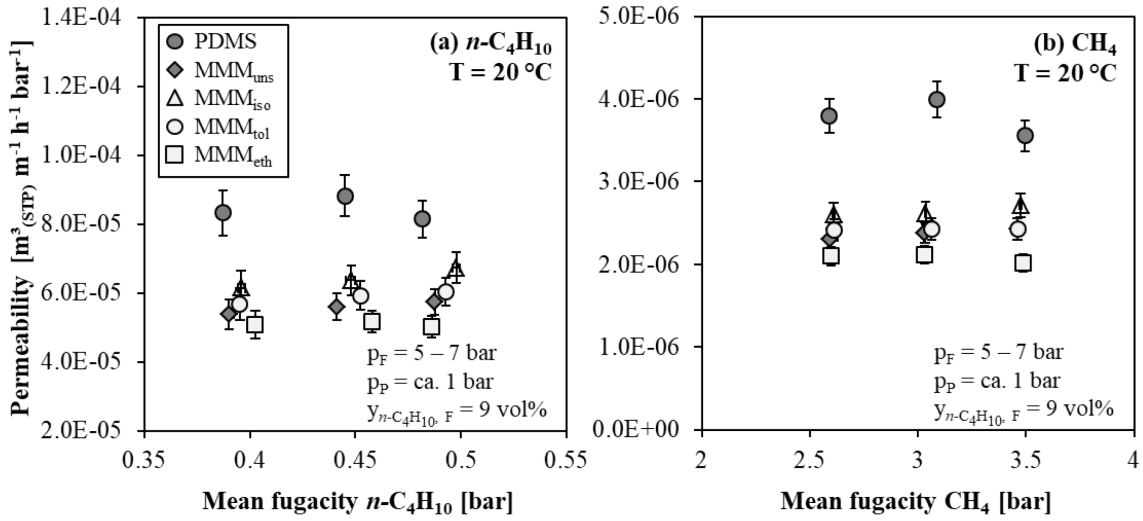

Figure 5.26 Mixed gas permeability of (a) n-C_4H_{10} and (b) CH_4 in unfilled PDMS and unsaturated and isooctane/toluene/ethanol-saturated MMMs with 20 wt% AC loading for binary mixtures of 9 vol% n-C_4H_{10} in CH_4 (T = 20 °C). The error bars are determined using propagation of error method.

Similar to pure gas data all MMMs, containing either saturated or unsaturated particles, showed lower *n*-C_4H_{10} and CH_4 permeability than unfilled PDMS membranes. The *n*-C_4H_{10} permeability indistinctly increased with the increase of mean *n*-C_4H_{10} fugacity for MMMs containing either isooctane or toluene saturated particles. A similar trend was observed for unfilled PDMS membranes except for the measurements at mean *n*-C_4H_{10} fugacity of 0.48 bar. CH_4 permeability was almost constant and independent of fugacity. For both type of gases, isooctane-saturated MMM showed the highest permeability. The difference between the permeability of toluene and isooctane-saturated MMMs was minor and both of them showed higher permeabilities than that of observed for unsaturated MMM. The lowest *n*-C_4H_{10} and CH_4 permeabilities were determined with ethanol-saturated MMMs and the values did not change with increasing the mean fugacities of the gases.

EDX-analysis results showed that, ethanol and toluene provided the best performance to hinder pore blockage among the investigated solvents. However, pure and mixed gas permeation results presented here were contrary to the expectations based on the results of EDX line-scanning analysis, ethanol-saturation showing the lowest permeability. It has to be considered here that the set of saturated MMMs investigated in this section was produced by following the most efficient mixing procedure (method-4) previously discussed in Section 5.1. However, the last mixing step of method-4, which is a combination of magnetic stirring and high speed dispersing, was applied for 30 min. It was previously observed that MMMs containing ethanol-saturated particles, which were mixed for 15 min (see MMMc in Figure 5.11 and Table 5.3), showed higher pure gas permeability values than MMMs when the particles were mixed for 30 min (MMMd) for both studied gases. Due to the lack of full data set of MMMs containing isooctane or toluene-saturated particles mixed for 15 min, a comparision of the permeability of these membranes could not be presented here. Based on the outcomes of Section 5.1, it is anticipated that higher pure and mixed gas permeability values than those of presented here can be achieved with MMMs when isooctane or toluene saturated-particles are mixed for 15 min.

Mixed gas selectivities of these membranes are presented in Figure 5.27. Unfilled PDMS showed the lowest selectivity of all samples. This means that MMMs showed superior gas separation performance compared to unfilled PDMS. Moreover, all MMMs containing saturated particles showed higher selectivities than that of MMM containing unsaturated particles. This indicates that the saturation of the activated carbon particles with either of these solvents hindered the pore blockage and enhanced the overall selectivity. Using either ethanol, isooctane or toluene-saturated particles gave MMMs slightly higher mixed gas selectivities at all pressures when compared to that of observed for MMMs containing unsaturated particles without a significant difference between their selectivity.

Based on these observations, solvent saturation protocol for the filler particles is strongly recommended, where it simultaneously decreases the risk of blockage of the filler pores by the polymer chains' penetration and enhances the overall separation performance. MMMs prepared with the activated carbon particles saturated with ethanol, isooctane or toluene showed improved mixed gas selectivities compared to MMMs containing unsaturated particles. Considering that, the hypothesis derived from the EDX-analysis that ethanol and toluene were the two most suitable solvents to prevent pore blockage can be hold true. Dispersing activated carbon particles in isooctane during the membrane preparation provided almost the same mixed gas selectivity as these membranes. Therefore, it is suggested to use either ethanol, toluene or isooctane for the saturation of activated carbon particles in MMM preparation.

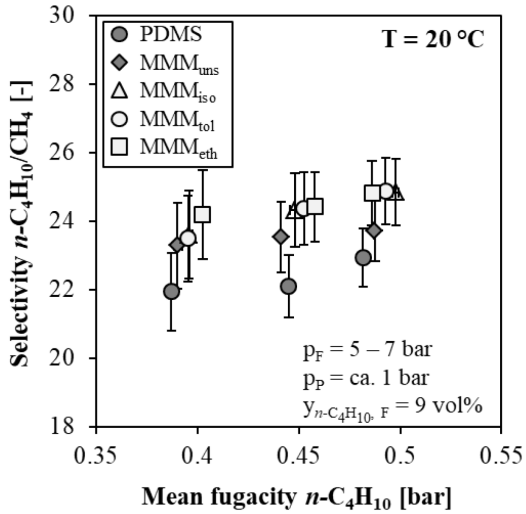

Figure 5.27 Mixed gas selectivity of unfilled PDMS and unsaturated and isooctane/toluene/ethanol-saturated MMMs with 20 wt% AC loading for binary mixtures of 9 vol% n-C_4H_{10} in CH_4 (T = 20 °C). The error bars were determined using propagation of error method.

It is worthwhile to note that the optimal solvent may depend on the properties of the polymer and the filler particles used to form MMM in another system. For example, contrary to the MMMs composed of toluene-primed zeolite 4A particles and PAVc investigated by Mahajan and Koros [91], an improvement in selectivity was observed in this work with the MMMs composed of toluene and isooctane-saturated activated carbon particles and PDMS. However, it could not be fully determined whether the activated carbon pores were completely free when they were embedded in the PDMS matrix

5.3 Post-treatment of membranes

Post-treatment conditions may influence the properties of a membrane as well as other preparation steps. Membranes formed under identical preparation steps could lead to different permeation performance attributed to the post-treatment conditions. The literature lacks the systematic investigation of the influence of the post-treatment conditions on the final performance of the MMMs.

Post-treatment of a membrane usually consists of two steps: evaporation at room temperature and further heat treatment in a vacuum oven [163]. Evaporation involves the drying of the polymer/particle suspension, which is cast on a support structure, in a fume hood at room temperature. This step allows most of the solvent to evaporate until the membrane is ready for the further annealing. Further heat treatment under partial vacuum at high temperature provides an environment to evaporate the rest of the solvent and to complete cross-linking in the membrane. During the post-treatment, the polymer matrix undergoes shrinkage due to the solvent removal. Shrinkage causes considerable stress that weakens the adhesion between the polymer and filler particles. If the selected polymer is a suitable and flexible one with a low glass transition temperature, such as PDMS, it shows desired affinity for the filler particles, where the stress is

low [91]. However, treating membranes at high temperatures would shrink them irreversibly, where membranes become useless.

To obtain information on how to prepare MMMs with excellent gas separation properties, evaporation in the fume hood, and further heat treatment conditions and duration in the vacuum oven were investigated in this section. Accordingly, pure and mixed gas permeation performances of the membranes treated at different post-treatment conditions were evaluated to determine the most suitable condition, at which membranes show enhanced performance.

5.3.1 Comparison of post-treatment conditions

A drying test that represents post-treatment steps of a membrane was developed as schematically depicted in Figure 5.28. Firstly, a solvent is added to the activated carbon particles in a petri dish, which represents the saturation of the filler particles. Then, saturated particles were stored in the fume hood to evaporate excess solvent at room temperature, where the evaporation step of the post-treatment was represented. Lastly, saturated particles were subjected to heat treatment in a vacuum drying oven at 110 mbar and 110 °C.

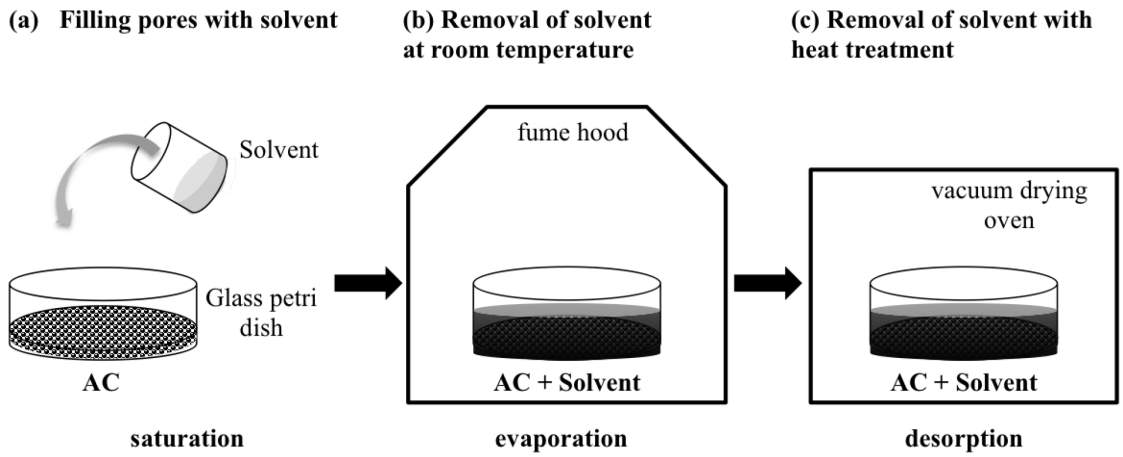

Figure 5.28 Test procedure representing post-treatment steps of a membrane.

Evaporation in the fume hood

To evaluate the evaporation process in the fume hood, five activated carbon samples, which were saturated with a solvent, were prepared in the petri dishes. For this investigation, isooctane, toluene or ethanol was used to saturate activated carbon particles (AC 100050, d_{50} = 3.5 µm). Approximately 2 g of solvent was used for saturation of 0.5 g activated carbon particles in one petri dish, which was enough to fill the pores of activated carbon particles completely. Samples were stored in the fume hood at room temperature and the weight of the samples was measured at predetermined time steps. The amount of remaining solvent was calculated by subtraction of the measured weight of the petri dish and known weight of the dried activated carbon from the total weight of the sample. The pore volume that was still filled by the remaining solvent during the evaporation in the fume hood was calculated as shown by Equation 5.6.

$$\text{Filled pore volume [\%]} = \frac{V_{\text{remaining solvent}}}{V_{\text{total pore of carbon}}} \text{ x } 100 = \frac{\left(\frac{M_{\text{remaining solvent}}}{\rho_{\text{solvent}}}\right)}{V_{\text{total pore of carbon}}} \text{ x } 100 \qquad (5.6)$$

The filled pore volume of the samples as a function of time is presented in Figure 5.29. The results are given as the average of samples that were saturated with one of the solvents. Evaporation experiments were repeated three times on different days and the observed precision between runs was lower than 5%.

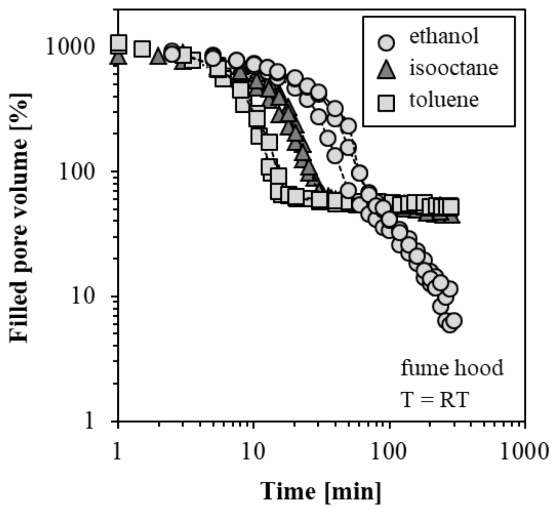

Figure 5.29 Filled pore volume of saturated-AC with different solvents during evaporation in the fume hood (*RT = room temperature*).

Results showed that isooctane and toluene evaporates faster than ethanol. A major amount of isooctane and toluene evaporated in 35 min. After that, the filled pore volume of the samples was not significantly changed by time. For all solvents, the longer the evaporation was, the less the pores were filled. For ethanol-saturated samples, filled pore volume was decreasing with increasing time. After 4 h of evaporation, the values were fluctuated. It has to be considered that results might be different in case of solvent removal from a membrane. It was anticipated that longer evaporation time would be necessary to obtain low filled pore volume of the filler particles when PDMS membranes or MMMs were subjected to drying in a fume hood. Therefore, one day evaporation in the fume hood at room temperature was selected to dry all types of membranes produced in this work as the first step of the post-treatment.

Heat treatment temperature

After evaporation at room temperature, membranes undergo heat treatment in a vacuum drying oven to remove residual solvent to completely free pores of activated carbon. Different heat treatment temperatures may affect the gas separation performance of the membranes. In the study of Duan et al. [163] permeabilities of MMMs prepared with different polymers and metal organic frameworks (MOFs) considerably improved when treatment temperature was increased from 150 to 200 °C. The main reason for that was the effective removal of the residual solvent during the

post-treatment at higher temperatures. However, mixed gas selectivity remained unchanged. In this work, mild heat treatment temperature was applied. Because the upper layer of support structure made of porous polyester (PE) could withstand the heating up to 150 °C [164]. In order to avoid any possible defects, annealing of the membranes were carried out in a vacuum oven at 110 °C and 110 mbar.

Heat treatment condition

Heat treatment efficiency can be enhanced by aeration or applying purge with an inert gas. In a vacuum drying oven, nitrogen is a standard medium that is applied to shorten drying time and to enhance the drying process. Nitrogen does not react with the stored material and it has a lower specific gravity than air, which purges out the heavier air when it is introduced into the vacuum drying oven.

The influence of heat treatment on filled pore volume of the samples was investigated for four different conditions. Samples were prepared in the same way as described above for evaporation samples. For this investigation, isooctane-saturated activated carbon samples were used, which were already dried in the fume hood at room temperature for one day. The first set of samples was allowed to dry further in the vacuum drying oven at 110 °C and 110 mbar. Although the drying process was interrupted twice to weight the samples in order to calculate the filled pore volume at determined time steps; this condition was called *continuous drying*. The second set of samples was allowed to dry under identical conditions as the first set of samples. Different from the first samples, the drying process was interrupted at every 2 h for 10 min aeration breaks, which was called *batch drying*. The third set of samples was allowed to dry under a partial vacuum with nitrogen circulation at 110° C and 110 mbar, which was called *continuous drying with N_2*. Here again, the system was interrupted twice to weight the samples. The fourth set of samples was allowed to dry under identical condition with nitrogen circulation, but the system was interrupted almost at every 4 h for 10 min aeration breaks, which was called *batch drying with N_2.*

After 28 h drying, 36% of the total pore volume of the samples, which were subjected to continuous drying, was still filled by isooctane, as can be seen in Figure 5.30. This value reduced to 23% under batch drying with 10 min aeration breaks at every 2 h. As expected, it was possible to have higher free pore volume after the heat treatment where nitrogen circulation was applied. After 28 h, 8.2% and 4.7% of the pores were still filled with isooctane under continuous drying with N_2 and batch drying with N_2, respectively. Batch drying in either way, with or without N_2 circulation, ensured less filled pore volume than continuous drying. Moreover, in all cases the change in filled pore volume percentage after 18 h was negligible. Although batch drying with N_2 provided the highest free pore volume, applying aeration breaks at every 4 h for 10 min was not a practical process. Therefore, it was decided to apply continuous heat treatment with N_2 to the membranes for 18 h without having additional aeration breaks.

The required time for the heat treatment in a vacuum oven for the samples that were saturated with other solvents were investigated under identical conditions. Toluene and ethanol-saturated activated carbon samples were prepared in glass petri dishes in the same way. These samples were initially subjected to drying at room temperature for one day in the fume hood. Then, samples were continuously dried in the vacuum oven at 110° C and 110 mbar with N_2 circulation. Figure 5.31 shows average filled pore volume percentage of toluene and ethanol-saturated samples compared to isooctane-saturated samples. Such in evaporation results, toluene-saturated samples dried faster than isooctane-saturated samples and the least filled pore volume percentage

was achieved with ethanol-saturated samples after 28 h drying. After 18 h, no change in filled pore volume percentage was observed for toluene and ethanol-saturated samples as well.

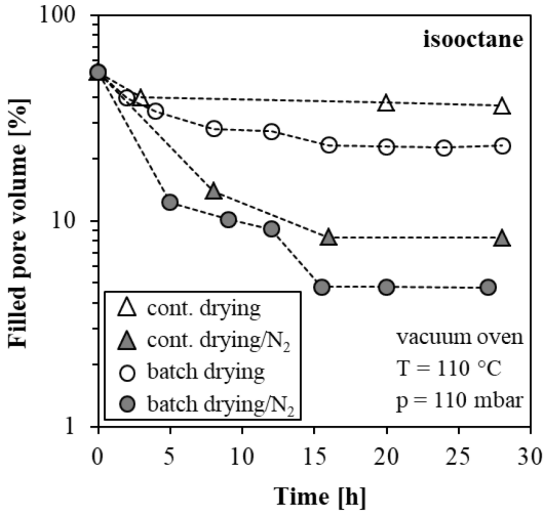

Figure 5.30 Filled pore volume of isooctane-saturated AC dried at different heat treatment conditions.

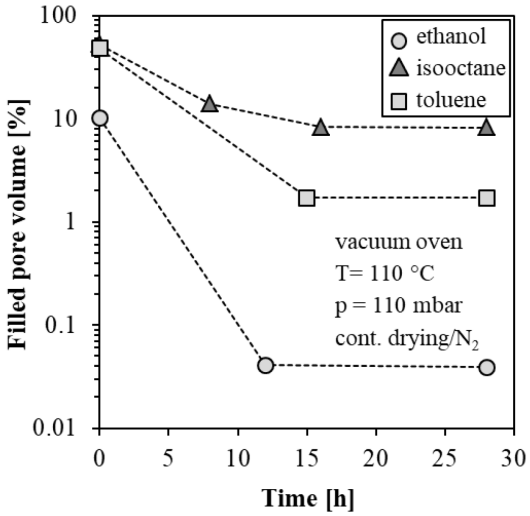

Figure 5.31 Filled pore volume of saturated-AC with different solvents continuously dried with N_2 circulation.

Based on these results, the conclusion is that membranes should undergo heat treatment in a vacuum oven at 110° C and 110 mbar for at least 18 h with N_2 circulation, independently of the type of solvent used for saturation during the pre-treatment. The duration of the heat treatment can be extended up to 24 h. Additionally, ethanol seems to desorb easier than isooctane and toluene from the pores of the activated carbon during evaporation in the fume hood and heat treatment in the vacuum oven.

5.3.2 Influence of heat treatment duration on pure gas permeation

To investigate the influence of the heat treatment duration on the pure gas permeation, MMMs prepared with 20 wt% ethanol-saturated activated carbon particles (AC 100050, d_{50} = 3.5 µm) in PDMS were used. MMMs were produced by following the most efficient mixing procedure for activated carbon particles and PDMS as previously discussed in Section 5.1. Both unfilled PDMS membranes and MMMs were cast at 300 µm initial thickness by motorized film applicator UA 3000.

The cast PDMS sheet was allowed to dry in the fume hood at room temperature for one day. Afterwards, before being heat-treated in the oven, one stamp was cut out from the sheet for investigations (*PDMS/no heat treatment*). The rest of the PDMS sheet was subjected to heat treatment in the vacuum oven at 110 °C and 110 mbar for 24 h with N_2 circulation. Then, another stamp from the sheet was taken out (*PDMS/24 h heat treatment*). In the same way, the rest of the PDMS sheet was allowed to further dry in the vacuum oven under identical conditions for 144 h in total and the last stamp was cut out from the sheet in order to investigate extreme heat treatment duration (*PDMS/144 h heat treatment*). The same procedure was followed for MMM samples and 3 stamps out of an MMM sheet were also made. Figure 5.32 shows the cross-sectional SEM images and Table 5.9 summarizes the average thickness of these stamps.

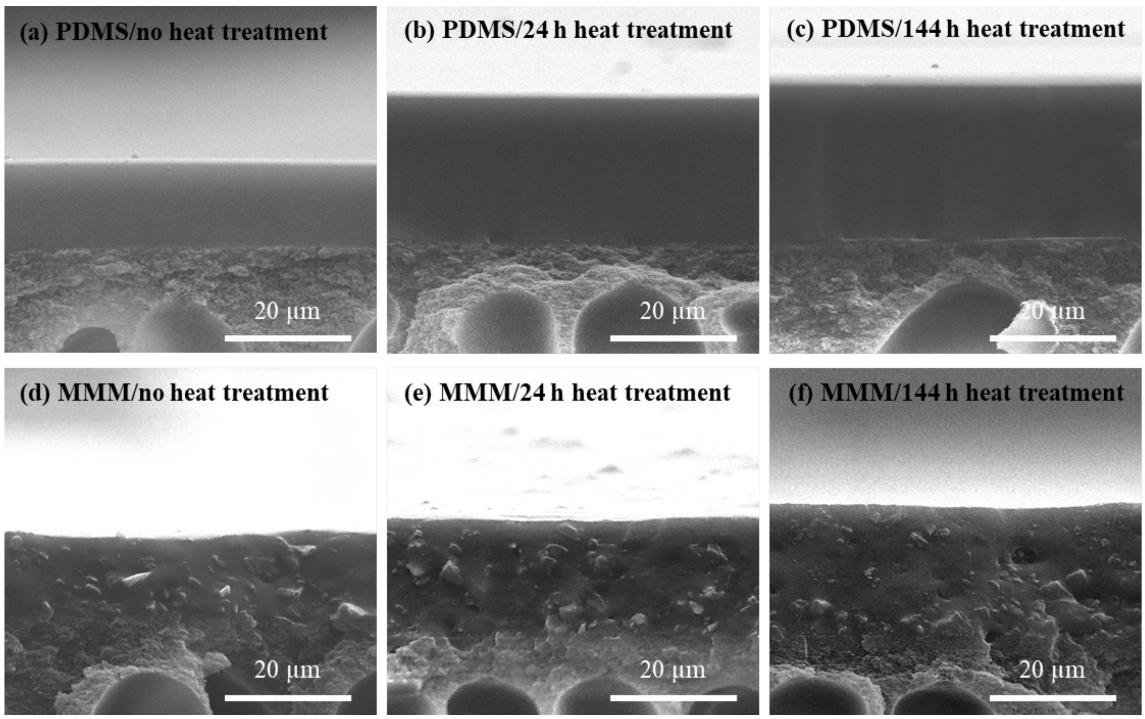

Figure 5.32 Cross-sectional SEM images of the membranes used for heat treatment investigation.

There were no interfacial defects in separation layer of the samples. However, thickness increased with the increase of heat treatment duration. This can be explained with a morphological change of PDMS regarding fractional free volume alterations that occurs during the heat treatment, which may also modifies gas transport mechanism.

Table 5.9 Average separation layer thickness of the membranes used for heat treatment investigation.

Membrane/heat treatment	Thickness [µm]	SD [µm]	RSD [%]
PDMS/no	14.13	0.78	5.49
PDMS/24 h	22.45	0.54	2.42
PDMS/144 h	25.02	1.78	7.11
MMM/no	14.98	1.29	8.62
MMM/24 h	19.66	0.55	2.80
MMM/144 h	21.70	1.39	6.43

The weight of the unfilled PDMS and MMM stamps were measured using an analytical balance with high precision. Both membranes showed weight loss during the heat treatment as illustrated in Figure 5.33. These results reveal that a sharp removal of the solvent from the pores occurred within the first 24 h and the amount of solvent continuously reduced up to 144 h.

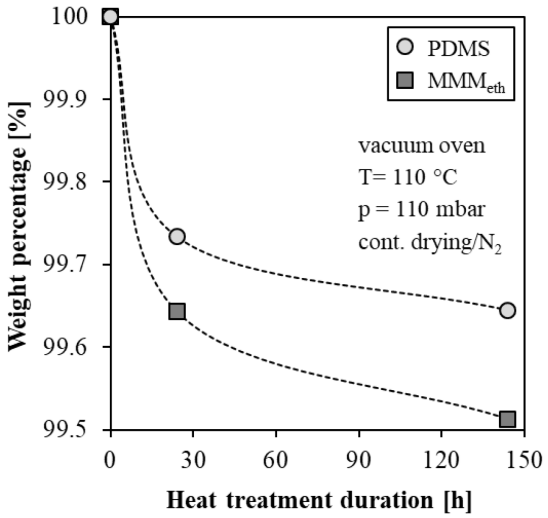

Figure 5.33 The change in weight of the membranes during the heat treatment.

The pure gas *n*-C_4H_{10} and CH_4 permeation behaviors in these membranes were determined at 15 °C and the results are presented in Figure 5.34 (a) and (b), respectively. The feed pressure was varied from 0.75 to 2 bar for *n*-C_4H_{10} and from 10 to 20 bar for CH_4. Permeat pressure was varied from 0.2 to 0.5 bar for *n*-C_4H_{10}, and from 0.2 to 0.3 bar for CH_4. Each pure gas measurement was repeated 3 times and experimental results were reported as explained in Section 4.3. The errors were calculated using the propagation of error method as discussed in Section 4.2. The determined pure gas *n*-C_4H_{10} and CH_4 permeability coefficients and *n*-C_4H_{10}/CH_4 permselectivity of the membranes are listed in Table 5.10.

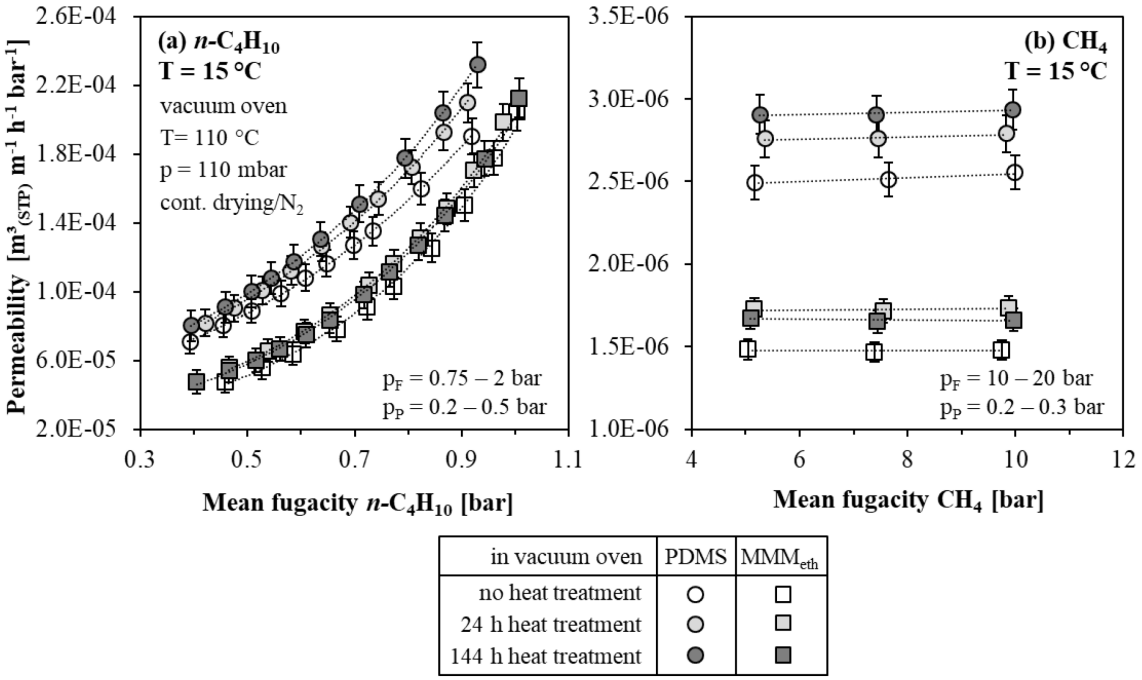

Figure 5.34 Influence of heat treatment duration on pure gas permeability of (a) *n*-C_4H_{10} and (b) CH_4 in unfilled PDMS and ethanol-saturated MMM with 20 wt% AC loading (T = 15 °C).

Table 5.10 Pure gas *n*-C_4H_{10} and CH_4 permeability coefficients and *n*-C_4H_{10}/CH_4 permselectivity of the membranes heat-treated for different durations (T = 15 °C).

Membrane/ heat treatment	$P^0_{n\text{-}C_4H_{10}}$ [$m^3_{(STP)}$ m^{-1} h^{-1} bar^{-1}]	$m_{n\text{-}C_4H_{10}}$ [-]	P_{CH_4} [$m^3_{(STP)}$ m^{-1} h^{-1} bar^{-1}]	$\alpha^*_{n\text{-}C_4H_{10}/CH_4}$ [-]
PDMS/no	3.44E-05 ± 3.43E-06	1.865	2.52E-06 ± 1.02E-07	13.7 ± 1.4
PDMS/24 h	3.64E-05 ± 3.81E-06	1.929	2.77E-06 ± 1.12E-07	13.2 ± 1.4
PDMS/144 h	3.65E-05 ± 4.47E-06	1.991	2.91E-06 ± 1.18E-07	12.5 ± 1.5
MMM/no	1.35E-05 ± 2.07E-06	2.667	1.48E-06 ± 6.02E-08	9.1 ± 1.4
MMM/24 h	1.73E-05 ± 2.13E-06	2.476	1.72E-06 ± 7.02E-08	10.0 ± 1.2
MMM/144 h	1.67E-05 ± 2.21E-06	2.492	1.66E-06 ± 6.79E-08	10.0 ± 1.3

For both membranes, *n*-C_4H_{10} and CH_4 permeabilities increased when they were treated at 110 °C and 110 mbar up to 24 h. Unfilled PDMS and MMM samples showed different gas permeation trends. For unfilled PDMS, treatment duration for 144 h slightly increased *n*-C_4H_{10} and CH_4 permeabilities due to the removal of residual solvent. For MMM, *n*-C_4H_{10} and CH_4 permeabilities were enhanced with 24 h treatment. This could be attributed to the re-opened activated carbon pores due to the removal of the residual solvent, which provides a continuous pathway for gas permeation. However, *n*-C_4H_{10} and CH_4 permeabilities remained almost unchanged in MMM when treatment duration was 144 h. The most likely reason for that could be slower desorption of the solvent from the pores of the activated carbon compared to unfilled PDMS due to the presence of activated carbon particles distributed in the polymer matrix in case of MMM. With these

measurements, it is confirmed that heat treatment duration effects both morphology and pure gas permeation behavior of the membranes.

5.3.3 Influence of heat treatment duration on mixed gas selectivity

The separation performance of the membranes was obtained from the mixed gas experiments using binary mixtures of 16 vol% *n*-C_4H_{10} in CH_4 at 5.5 bar feed pressure at 15 °C. Experiments were performed at atmospheric permeate pressure (p_P = ca. 1 bar). Each mixed gas measurement was repeated 3 times and experimental results were reported as explained in Section 4.3. The errors were calculated using the propagation of error method as discussed in Section 4.2. The average mixed gas permeabilities of *n*-C_4H_{10} and CH_4 are plotted over heat treatment duration in Figure 5.35 (a) and (b), respectively and mixed gas selectivity is given in Figure 5.36.

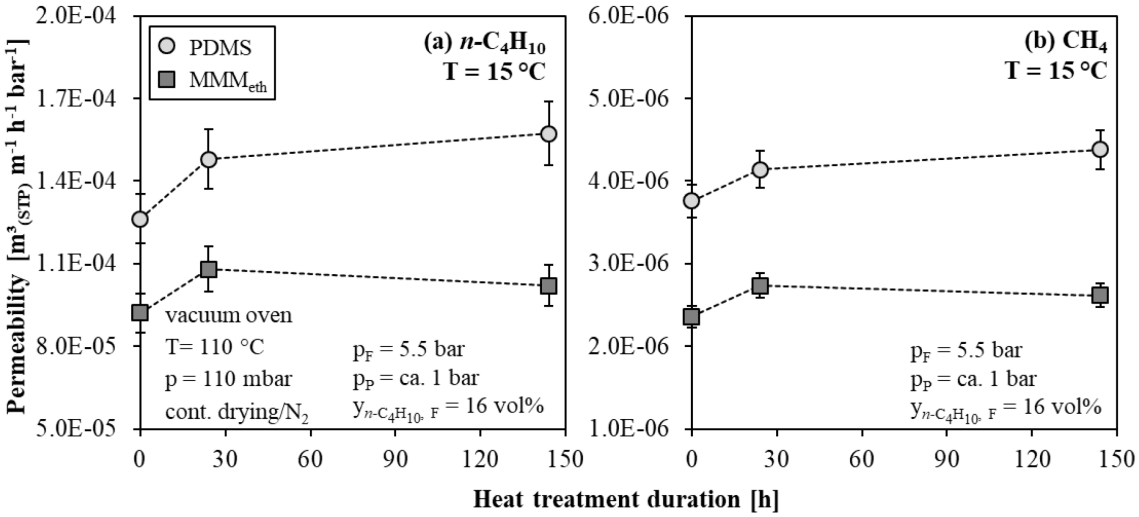

Figure 5.35 Influence of heat treatment duration on mixed gas permeability of (a) *n*-C_4H_{10} and (b) CH_4 in unfilled PDMS and ethanol-saturated MMM with 20 wt% AC loading (T = 15 °C).

Both *n*-C_4H_{10} and CH_4 permeabilities in PDMS obviously increased with heat treatment for 24 h. A slight increment was also observed when heat treatment was increased up to 144 h. Similar to pure gas permeation, more solvent desorbed from the polymer with longer heat treatment duration. Consequently, diffusivity of gases should be increased as well, while the solubility of them remain unchanged [163]. For MMM, 24 h heat treatment increased both *n*-C_4H_{10} and CH_4 permeabilities. The reason for that is combined effects of increased gas diffusivity due to the increased free volume in the polymer and increased free volume in the pores of the activated carbon particles. However, 144 h heat treatment did not change both *n*-C_4H_{10} and CH_4 permeabilities significantly.

To sum up, 24 h heat treatment in a vacuum drying oven at 110 °C and 110 mbar is required for both types of membranes to enhance their separation performances. However, heat treatment longer than 24 h does not improve separation performances of the membranes. These results also reveal that heat treatment duration clearly has an influence on separation performance of the membranes.

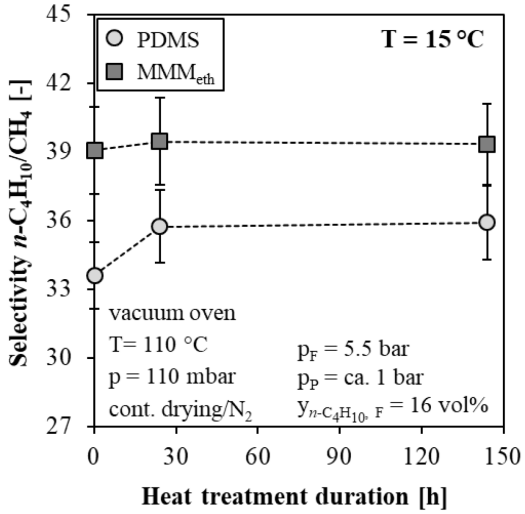

Figure 5.36 Influence of heat treatment duration on mixed gas selectivity for binary mixtures of 16 vol% n-C_4H_{10} in CH_4 in unfilled PDMS and ethanol-saturated MMM with 20 wt% AC loading (T = 15 °C).

5.4 Particle loading

A sufficient amount of filler particles in the polymer matrix is crucial to improve performance of an MMM by achieving percolation threshold. Furthermore, increasing the filler loading is usually constrained by agglomeration of the particles, which could lead to the defects such as voids. Defect formation potentially reduces the separation performance of the membrane as well as its mechanical strength. In the MMM literature, particle loadings lower than 20 wt% (or 20 vol%) are mostly considered as low loadings and particle loadings higher than 20 wt% are considered as high loadings [93].

In this section, the influence of activated carbon loading into PDMS matrix on membrane morphology and gas permeation was evaluated to identify the best loading. For preliminary tests, MMMs containing 20, 30, and 40 wt% ethanol-saturated activated carbon particles (AC 100050, d_{50} = 3.5 µm) were used. MMMs were produced by following the most efficient mixing procedure for activated carbon particles and PDMS as previously discussed in Section 5.1. To avoid any possible errors during preparation, all MMMs were produced using the same 9 wt% PDMS solution. The membranes were cast at 500 µm initial thickness by the motorized film applicator UA 3000 and subjected to identical post-treatment as previously discussed in Section 5.3. The morphology of the membranes was analyzed by SEM images as presented in Figure 5.37.

It was previously observed that MMMs with 20 wt% particle loading show good contact between polymer and filler particles. At such low loading, filler particles are usually better distributed compared to higher loadings and demonstrate good mechanical and film-forming properties. At higher particle loading (30 wt%), inhomogeneities in the cross-sectional area and roughness on the surface were observed. Moreover, membrane was defective due to the void and pinhole formation. Pushing the particle loading to a higher level (40 wt%) extremely increased these failures, where the integrity of the membrane was destroyed. In both MMMs with 30 and 40 wt% loading, the amount of particles in the PDMS matrix were too much to be sufficiently covered by the polymer, which was essential to form a defect-free MMM. At such high loadings, particles

strongly come together and form agglomerates, where percolation transition mostly occurs [42, 165]. Depending on these observations from SEM images, 20 wt% was selected to be the maximum particle loading to prepare MMMs for further investigations. In this way, a good contact between PDMS and activated carbon particles is ensured and probability of defect formation, such as cracks or pinholes, is significantly avoided.

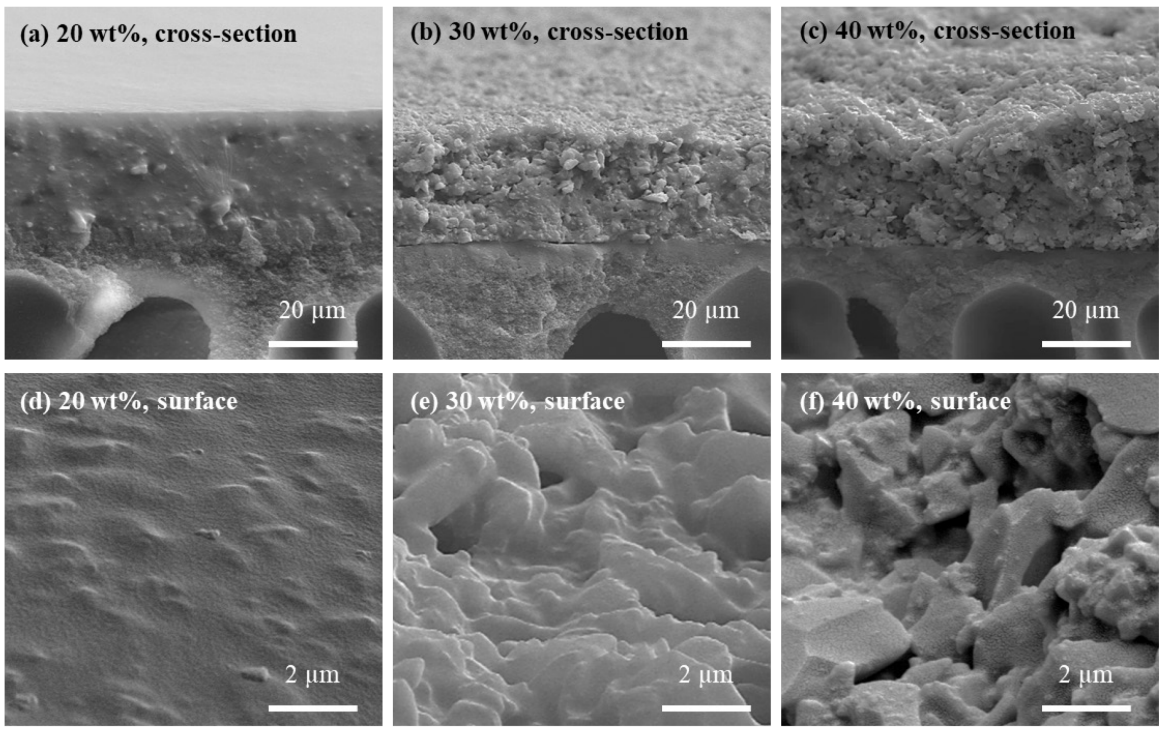

Figure 5.37 Cross-sectional and surface SEM images of MMMs with 20 – 40 wt% AC loading.

5.4.1 Influence of particle loading on pure gas permeation

To investigate the effect of particle loading on pure and mixed gas permeation behavior, MMMs were prepared containing 5, 10, 15, and 20 wt% ethanol-saturated particle loadings. MMMs were prepared under identical conditions as described above. SEM images presented in Figure 5.38 indicated that a good MMM formation was realized without defects when the particle loading was less than or equal to 20 wt%. The average thickness of the separation layer slightly increased with increasing particle loading as listed in Table 5.11.

Pure gas permeation measurements of *n*-C_4H_{10} and CH_4 were performed at 20 °C under vacuum on the permeate side of the membrane (p_P = 0.2 – 0.5 bar). The feed pressure was varied from 0.75 to 2 bar for *n*-C_4H_{10} and from 10 to 20 bar for CH_4. Each pure gas measurement was repeated 3 times and experimental results were reported as explained in Section 4.3. The errors were calculated using the propagation of error method discussed in Section 4.2.

Figure 5.39 (a) and (b) present pure gas permeabilities of *n*-C_4H_{10} and CH_4 in unfilled PDMS and MMMs with different activated carbon loadings. Determined pure gas *n*-C_4H_{10} and CH_4 permeability coefficients and *n*-C_4H_{10}/CH_4 permselectivity of the membranes are listed in Table 5.12. Permeation behaviour of *n*-C_4H_{10} in MMM with 5 wt% loading was almost the same as the permeation in unfilled PDMS up to 0.9 bar mean *n*-C_4H_{10} fugacity. A slight increase of *n*-C_4H_{10}

permeation in MMM with 5 wt% loading compared to unfilled PDMS was observed at mean *n*-C_4H_{10} fugacity higher than 0.9 bar. At 10 wt% particle loading, *n*-C_4H_{10} permeability slightly reduced. Increasing the particle loading up to 15 wt% and 20 wt% loadings gradually reduced *n*-C_4H_{10} permeability. The important outcome of this investigation was that the *m* value (or slope) of the exponential trend of *n*-C_4H_{10} permeation increased with increasing particle. For all particle loadings, the *m* values of MMMs were higher than that of unfilled PDMS. This indicates that mass transport through the activated carbon particles occurs even at low particle loadings. In case of CH_4, the same reduction trend in permeability of MMMs was observed with increasing the particle loading.

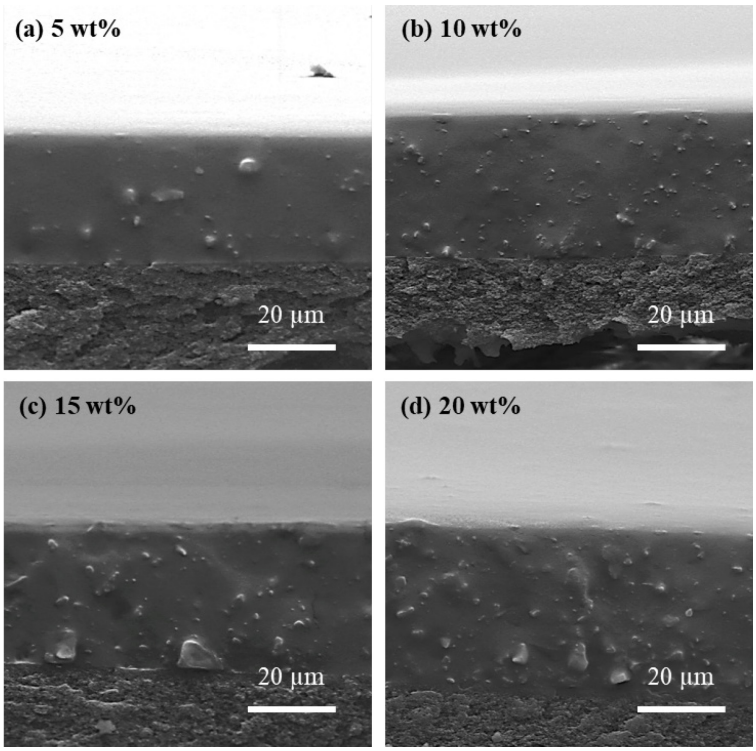

Figure 5.38 Cross-sectional SEM images of MMMs with 5 – 20 wt% AC loading.

Table 5.11 Average separation layer thickness of the membranes used for particle loading investigation.

Membrane	Loading [wt%]	Thickness [µm]	SD [µm]	RSD [%]
PDMS	0	24.88	0.86	3.46
MMM	5	25.67	2.05	7.99
	10	26.20	1.37	5.23
	15	27.30	1.77	6.48
	20	27.65	1.14	4.12

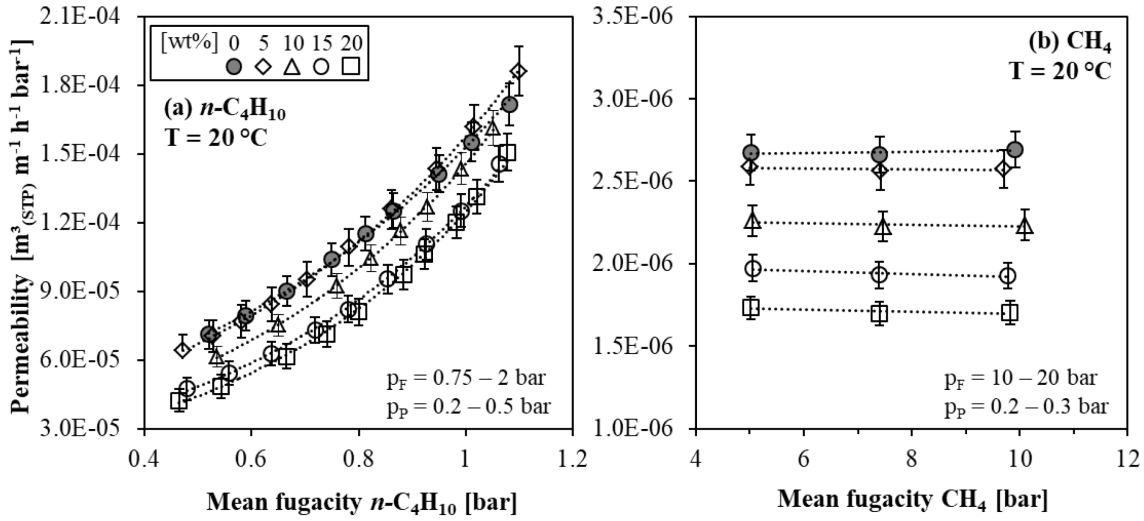

Figure 5.39 Influence of particle loading on pure gas permeability of (a) n-C_4H_{10} and (b) CH_4 in ethanol-saturated MMMs with 5 – 20 wt% AC loading (T = 20 °C). Dotted lines represent exponential and linear trend curves and the error bars were determined using the propagation of error method.

Table 5.12 Pure gas n-C_4H_{10} and CH_4 permeability coefficients and n-C_4H_{10}/CH_4 permselectivity of the membranes used for particle loading investigation (T = 20 °C).

Loading [wt%]	$P^0_{n\text{-}C_4H_{10}}$ [$m^3_{(STP)}$ m^{-1} h^{-1} bar^{-1}]	$m_{n\text{-}C_4H_{10}}$ [-]	P_{CH_4} [$m^3_{(STP)}$ m^{-1} h^{-1} bar^{-1}]	$\alpha^*_{n\text{-}C_4H_{10}/CH_4}$ [-]
0	3.15E-05 ± 3.09E-06	1.581	2.67E-06 ± 1.09E-07	11.8 ± 1.2
5	2.85E-05 ± 3.44E-06	1.711	2.57E-06 ± 1.14E-07	11.1 ± 0.6
10	2.22E-05 ± 2.24E-06	1.880	2.24E-06 ± 9.17E-08	9.9 ± 0.6
15	1.84E-05 ± 2.48E-06	1.932	1.94E-06 ± 7.79E-08	9.5 ± 0.5
20	1.56E-05 ± 2.24E-06	2.077	1.71E-06 ± 7.02E-08	9.1 ± 1.3

Using Equation 5.3, the reduction in n-C_4H_{10} and CH_4 permeabilities in MMMs with different particle loadings was calculated referring to the permeabilty in unfilled PDMS at several mean n-C_4H_{10} fugacities. Figure 5.40 (a) illustrates the reduction in n-C_4H_{10} permeability in MMM samples. In MMMs, except for the membrane with 5 wt% loading, the degree of reduction in n-C_4H_{10} permeability was almost twice as much as the percentage of activated carbon loading at low pressures. For example, at 0.5 bar mean n-C_4H_{10} fugacity the reductions in n-C_4H_{10} permeability at 10, 15 and 20 wt% loadings were 17.9, 30.2 and 36.3%, respectively. At the same pressure, this value was 3.4% for the MMM with 5 wt% loading. The degree of reduction in n-C_4H_{10} permeability reduced when the pressure, or mean n-C_4H_{10} fugacity, was increased. For example, at 1.15 bar mean n-C_4H_{10} fugacity, the reductions of n-C_4H_{10} permeability at 10, 15 and 20 wt% loadings were 0.3, 12.3 and 12.1%, respectively. At the same pressure, the MMM containing 5 wt% activated carbon achieved 5.1% higher n-C_4H_{10} permeability than that of PDMS. The reduction in CH_4 permeabilities in MMM samples are presented in Figure 5.40 (b).

The CH_4 permeability reductions in MMMs with 5, 10, 15 and 20 wt% loading were 3.8, 16.3, 27.4 and 36.0%, respectively. These values were almost equal to reduction of *n*-C_4H_{10} permeability at low mean *n*-C_4H_{10} fugacity (0.5 bar) with an insignificant difference.

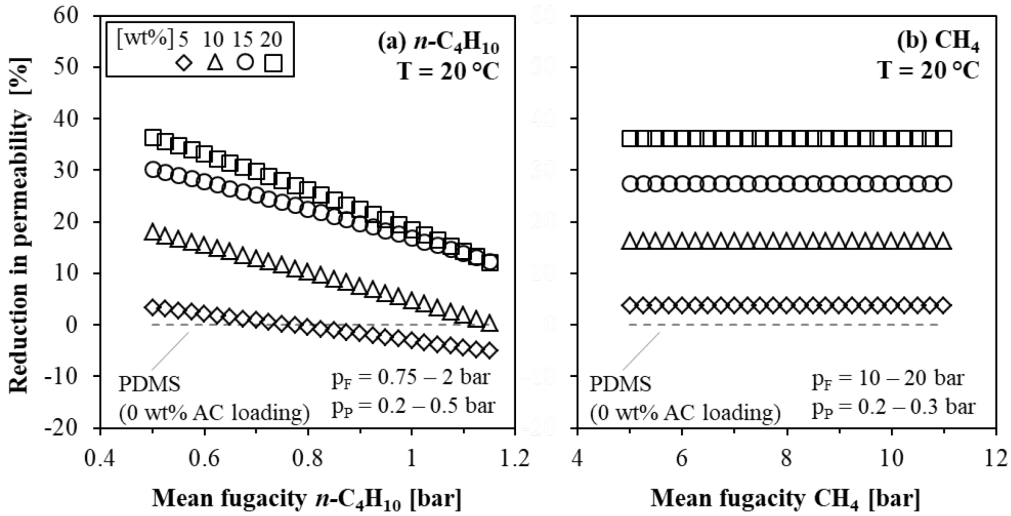

Figure 5.40 Reduction in pure gas permeability of (a) *n*-C_4H_{10} and (b) CH_4 in ethanol-saturated MMMs with 5 – 20 wt% AC loading compared to unfilled PDMS (T = 20 °C).

Permeability thickness dependence

For both gases, it was observed that there was a discrepancy between pure gas permeation data of MMMs with 20 wt% particle loading investigated previously in Section 5.1 and in this section. The pure gas *n*-C_4H_{10} and CH_4 permeability coefficients of the MMMs prepared and measured for this investigation (see data in Table 5.12, MMM with 20 wt% AC loading) were somewhat lower than those of the MMMs prepared and measured for the investigation in Section 5.1 (see data in Table 5.3, MMMc). The MMM samples used for both investigations were prepared under identical conditions. The only differences were the initial casting thickness and the production batch of the support structure. The MMM samples used for this investigation were cast at 500 µm initial thickness and the MMM samples used in Section 5.1 were cast at 300 µm initial thickness. Due to the different initial casting thickness, the final thickness of the dried membranes were also different. The average thicknesses of the MMM samples used for this investigation and used in Section 5.1 were 27.6 and 23.5 µm, respectively. Islam and Buschatz [166, 167] suggested that permeability of a membrane became thickness-dependent when the thickness was below a critical value due to non-equilibrium sorption desorption surface reactions at the interface of thin membranes. Pinnau and He [50] measured *n*-C_4H_{10}/CH_4 mixed gas selectivities in PDMS membranes with 150 µm thickness and compared their results with those published by Schultz and Peinemann [45], who used PDMS membranes with 10 µm thickness. Experiments were conducted under the same experimental conditions and selectivity of the thick PDMS membrane was two times more than that of the thin PDMS membrane. Researchers suggested that reported separation performances of the membranes could be significantly affected by the concentration polarization due to the thickness of the membrane [4]. The average thickness of the membranes used for the mentioned two investigations were very close to each other. Therefore, the influence of the thickness might be ignored. However, using different types of support structures might

influence the gas permeation behavior in the membranes as well. A systematic study would be interesting to determine the influence of support structures on the pure and mixed gas permeabilities of the MMMs.

5.4.2 Influence of particle loading on mixed gas selectivity

The mixed gas experiments were performed with binary gas mixtures of 9 vol% *n*-C_4H_{10} in CH_4 at 5 and 10 bar feed pressure and at atmospheric permeate pressure (p_P = ca. 1 bar) at 20 °C. Each mixed gas experiment was repeated 3 times and experimental results were reported as explained in Section 4.3. The errors were calculated using the propagation of error method discussed in Section 4.2.

The mixed gas permeabilities in both membranes are presented in Figure 5.41 as a function of activated carbon loading. At both feed pressures, the permeability of *n*-C_4H_{10} and CH_4 through the MMM samples reduced when activated carbon loading was increased. The same trend was reported by Mushardt et al. [42] for mixed gas permeation of *n*-C_4H_{10} and CH_4 in MMM samples composed of POMS and the same activated carbon used in work up to 40 wt% loading. Süer et al. [107] studied the effects of particle loading on permeabilities of several gases (CO_2, He, O_2, N_2, and Ar) in PES membranes using two types of zeolites. They reported a decrease up to a certain extent of loading (8 wt% for zeolite 13X and 25 wt% for zeolite 4A). At higher loadings, an increase of permeabilities was observed. In this work, no recovery in permeabilities was observed for both gases up to 20 wt% particle loading in PDMS matrix. The decrease in permeabilities of both gases up to 10 wt% loading was not significant. However, the influence of particles on permeability was especially noticeable when the activated carbon loading was 15 and 20 wt%. This indicates that the swelling of PDMS was reduced and a favorable environment for the gas molecules was created in the polymer matrix to be adsorbed on the activated carbon pores.

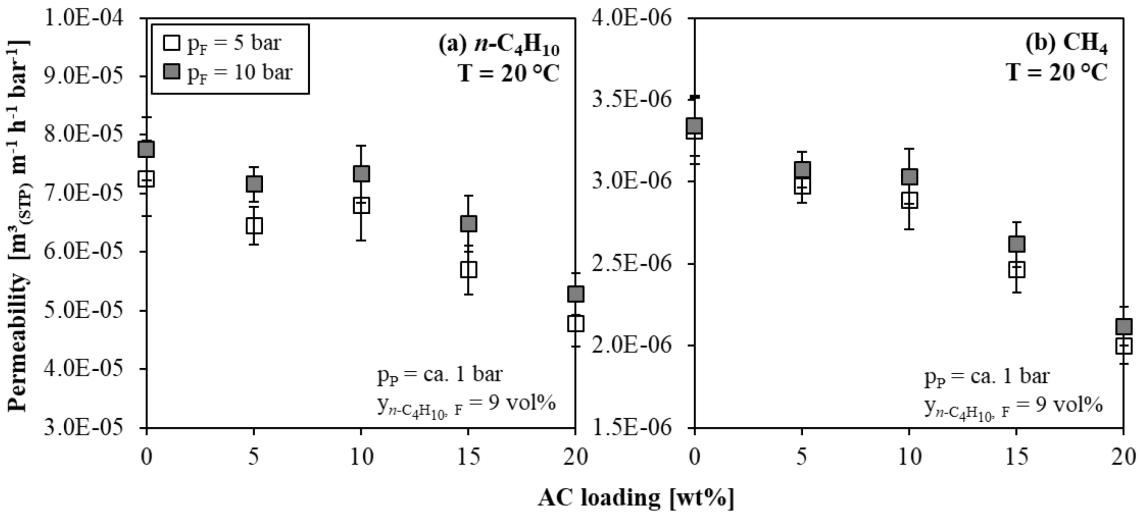

Figure 5.41 Influence of particle loading on mixed gas permeability of (a) *n*-C_4H_{10} and (b) CH_4 in unfilled PDMS and ethanol-saturated MMMs with 5 – 20 wt% AC loading for binary mixtures of 9 vol% *n*-C_4H_{10} in CH_4 (T = 20 °C). The error bars were determined using the propagation of error method.

The permeabilities of both gases slightly increased when the feed pressure was increased from 5 to 10 bar. Feed pressure is an important parameter that influences the permeability, which will be discussed in detail in Section 6.1. It is nevertheless of interest to briefly mention here that at higher partial pressures, the solubility of *n*-C_4H_{10} in the polymer is higher, consequently, the *n*-C_4H_{10} induced swelling of the PDMS. The more adsorption of *n*-C_4H_{10} occurs in the activated carbon pores as well [42, 50].

Figure 5.42 presents *n*-C_4H_{10}/CH_4 mixed gas selectivity of the membranes. The selectivity of both types of membranes increased with increasing feed pressure independently of the particle loading. Increasing feed pressure at a constant temperature and feed composition leads to enhanced sorption of *n*-C_4H_{10} in the polymer. Thus, swelling caused by dissolution of *n*-C_4H_{10} in the polymer matrix is more pronounced at higher pressures, which leads to increased chain mobility as well as selectivity [42, 50]. At feed pressure of 10 bar, an increase of selectivity was observed by increasing the amount of activated carbon up to 20 wt%. At 5 bar feed pressure, although the selectivity fluctuated with the gradual increase of activated carbon content, a linear trend of increasing in selectivity was observed over the investigated range of activated carbon loading from 0 to 20 wt%.

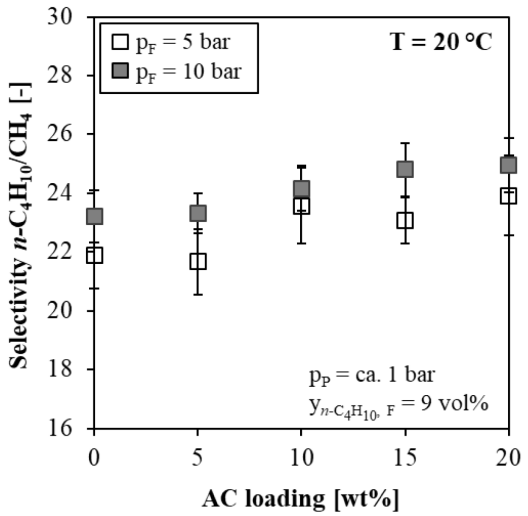

Figure 5.42 Influence of particle loading on mixed gas selectivity in unfilled PDMS and ethanol-saturated MMMs with 5 – 20 wt% AC loading for binary mixtures of 9 vol% *n*-C_4H_{10} in CH_4 (T = 20 °C). The error bars were determined using the propagation of error method.

The results showed that 20 wt% is the optimum activated carbon loading in PDMS matrix, where the MMMs sufficiently establish a percolative network necessary for the mass transport. By achieving percolation threshold, a preferential flow pathway through the filler particles is available. At lower loadings, activated carbon particles act as barriers rather than enhancers since the particle content is beneath the percolation threshold. At higher loadings, MMMs show failure in terms of physical appearance.

5.5 Gutter layer

In an MMM, the support structure is not responsible for mass transport. However, several studies showed that the support structure might significantly influence the permeation behavior and separation performance of a gas separation or pervaporation membrane depending on its pore structure [168-170]. Moreover, addition of a gutter layer between the active separation layer and the support structure to achieve high permeation and selectivity impacts gas permeation behavior and separation performance of the membranes in different ways [46, 171-173]. For instance, Kattula et al. [172] investigated the effect of a gutter layer on membrane performance using a 3D computational model. In their modeling approach, they reported that the gutter layer enhanced the permeation values of a penetrant through a polymeric gas separation membrane up to some extent, but reduced overall selectivity. Li et al. [173] produced lab-scale MMMs composed of poly(trimethylsilyl)propyne (PTMSP) and ZIF-7 nanoparticles on a PAN support structure with and without PTMSP gutter layer. They experimentally determined pure gas permeabilities of CO_2, N_2, and CH_4 and concluded that both permeability and selectivity increased when a gutter layer was applied, which was not in agreement with the model of Kattula et al. These researchers reported CO_2/N_2 and CO_2/CH_4 permselectivities and the mixed gas selectivities were not determined. On the other hand, Wijmans and Pingjiao [174] performed simulations using computational fluid dynamics (CFD) for composite membranes with a gutter layer and showed that the gutter layer could significantly improve the permeance of the membranes while modestly reduced the selectivity.

In this section, the impact of using a gutter layer on the morphology of the membranes and their pure and mixed gas permeation performances were investigated.

5.5.1 Influence of gutter layer on pure gas permeation

To investigate the impact of a gutter layer on gas permeation performance, unfilled PDMS membranes and MMMs were prepared using two different support structures: one structure with a gutter layer and the other structure without gutter layer. During the preparation of PDMS membranes, one-half of the PDMS solution was cast on a support structure without gutter layer while the other half was cast on a support structure with gutter layer. MMMs were prepared in the same way. For all membranes, the same 9 wt% PDMS solution was used to avoid any inevitable difference originating from the preparation of PDMS solution. MMMs contained 20 wt% ethanol-saturated activated carbon particles (AC 100050, d_{50} = 3.5 µm) and they were produced following the most efficient preparation procedure discussed in Section 5.1 and post-treated as described in Section 5.3. All membranes investigated in this section were cast at 300 µm initial thickness.

As mentioned previously in Section 3.1.4, the support structures (with and without gutter layer) used in this work were provided by Helmholtz-Zentrum Geesthacht. The support structure without gutter layer consists of an upper porous polyester (PE) layer and a carded web bottom layer of polyacrylonitrile (PAN). The support structure with gutter layer was produced by casting relatively low concentrated PDMS solution (0.5 wt%) on top of it with an ultrathin thickness (150 – 200 nm) as schematically depicted in Figure 3.6.

SEM images of the membranes presented in Figure 5.43 revealed that PDMS membranes had dense and smooth structure when they were cast on a support structure either with or without a

gutter layer. In MMMs, activated carbon particles were homogeneously distributed in polymer matrix without forming large agglomerates for both cases. The average separation layer thickness of the PDMS membrane with gutter layer was 4.0% thicker than that of the PDMS membrane without gutter layer as listed in Table 5.13 This difference is minor and corresponded to ± 3.5% measurement accuracy of the separation layer thickness, which was also used for propagation of error calculations to estimate the possible uncertainty of the collected data. However, the average separation layer of MMM with gutter layer was 12.3% thicker than that of MMM without gutter layer. This is a significant thickness difference considering identical preparation conditions. This indicates that it was possible to prevent polymer penetration into the pores of support structure by adding a thin gutter layer between active separation layer and the support structure. The presence of the filler particles embedded in polymer matrix improved the effectiveness of the gutter layer.

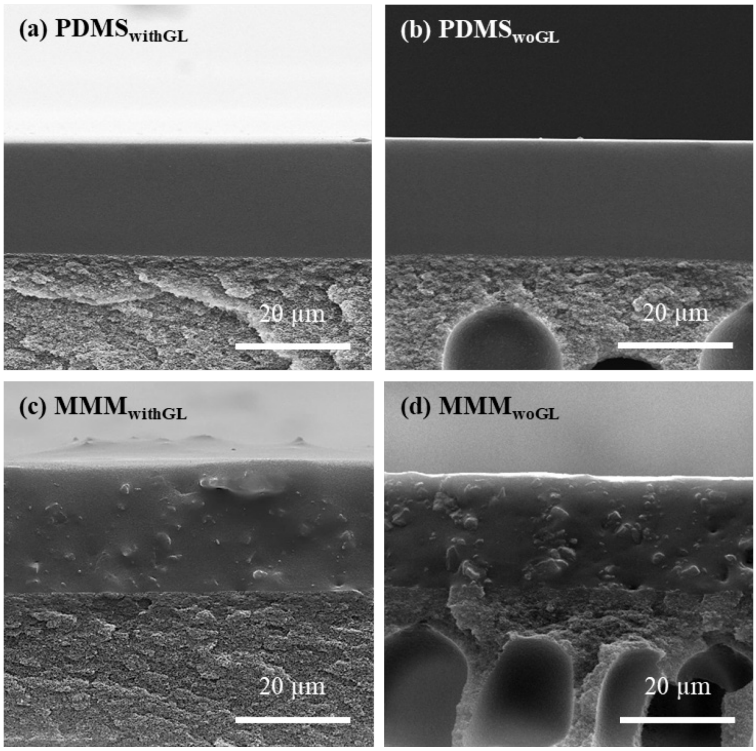

Figure 5.43 Cross-sectional SEM images of (a) PDMS with GL, (b) PDMS without GL, (c) MMM with GL, (d) MMM without GL. MMMs have 20 wt% ethanol-saturated AC (*GL*: gutter layer).

Pure gas permeability data was obtained between 0.75 and 2 bar feed pressure for *n*-C_4H_{10}, and between 10 and 20 bar feed pressure for CH_4. For both gases, measurements were performed under vacuum on the permeate side of the membrane (p_P = 0.2 – 0.5 bar) at 20 °C. Figure 5.44 (a) and (b) show pure gas permeability of *n*-C_4H_{10} and CH_4 in unfilled PDMS and MMMs as function of mean fugacity, respevtively. Each pure gas measurement was repeated 3 times and experimental results were reported as explained in Section 4.3. The errors were calculated using the propagation of error method discussed in Section 4.2. Table 5.14 lists determined permeability coefficients and *n*-C_4H_{10}/CH_4 permselectivities.

Table 5.13 Average separation layer thickness of the membranes used for gutter layer investigation.

Membrane	Thickness [µm]	SD [µm]	RSD [%]
$PDMS_{withGL}$	22.91	0.60	2.59
$PDMS_{woGL}$	21.99	0.68	2.86
MMM_{withGL}	22.06	0.75	3.40
MMM_{woGL}	19.34	0.56	2.92

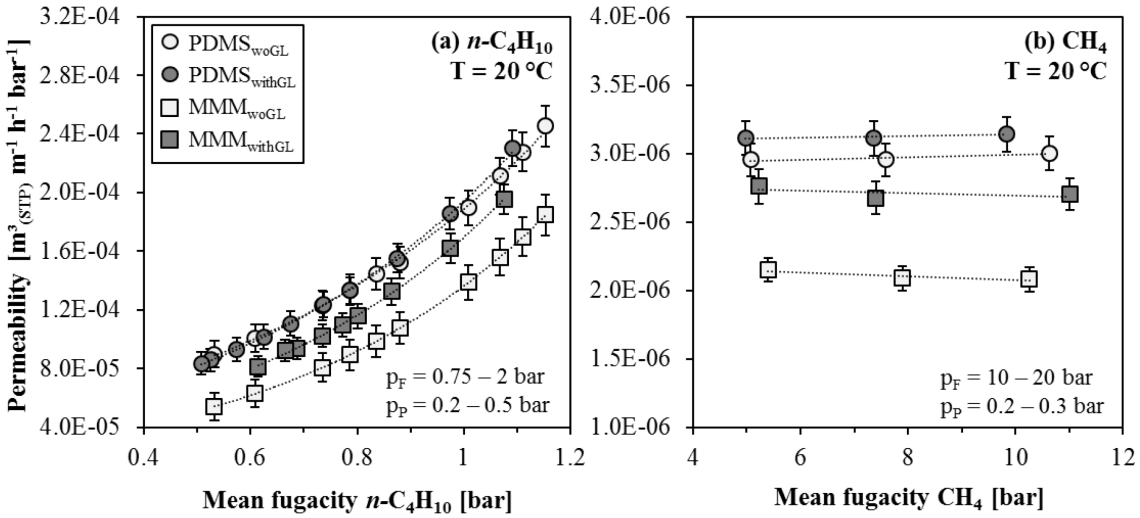

Figure 5.44 Pure gas permeability of (a) n-C_4H_{10} and (b) CH_4 in unfilled PDMS and ethanol-saturated MMMs with 20 wt% AC loading with and without gutter layer (T = 20 °C). Dotted lines represent exponential and linear trend curves and the error bars were determined using the propagation of error method (*GL*: Gutter layer).

Table 5.14 Pure gas n-C_4H_{10} and CH_4 permeability coefficients and n-C_4H_{10}/CH_4 permselectivity of the membranes used for gutter layer investigation (T = 20 °C, *GL*: Gutter layer).

Membrane	$P^0_{n\text{-}C_4H_{10}}$ [m³$_{(STP)}$ m^{-1} h^{-1} bar^{-1}]	$m_{n\text{-}C_4H_{10}}$ [-]	P_{CH_4} [m³$_{(STP)}$ m^{-1} h^{-1} bar^{-1}]	$\alpha^*_{n\text{-}C_4H_{10}/CH_4}$ [-]
$PDMS_{withGL}$	3.45E-05 ± 3.91E-06	1.729	3.12E-06 ± 1.26E-07	11.1 ± 1.3
$PDMS_{woGL}$	3.72E-05 ± 3.81E-06	1.613	3.01E-06 ± 1.26E-07	12.4 ± 1.3
MMM_{withGL}	2.57E-05 ± 2.49E-06	1.887	2.71E-06 ± 1.21E-07	9.5 ± 0.9
MMM_{woGL}	1.88E-05 ± 1.05E-06	1.980	2.10E-06 ± 8.75E-08	9.1 ± 1.3

When n-C_4H_{10} permeation in unfilled PDMS membranes is compared, almost the same permeability was obtained with PDMS membrane with and without gutter layer up to 0.9 bar

mean n-C_4H_{10} fugacity. After this point, the n-C_4H_{10} permeability of the PDMS membrane with gutter layer moderately increased. At 1.15 bar mean n-C_4H_{10} fugacity, n-C_4H_{10} permeability of PDMS membrane with gutter layer was 5.5% higher than that of PDMS membrane without gutter layer. Permeability of n-C_4H_{10} in MMM with gutter layer was considerably higher than that of MMM without gutter layer. The enhancement in n-C_4H_{10} permeability of the MMM with gutter layer was 23.3% and 18.5% at 0.5 bar and 1.15 bar mean n-C_4H_{10} fugacity, respectively. In case of CH_4, gutter layer increased the average CH_4 permeability in PDMS to some extent (3.5%). Similar to n-C_4H_{10}, permeability of CH_4 was significantly higher in MMM with gutter layer than that of MMM without gutter layer (22.5%).

Figure 5.45 (a) and (b) illustrate the reduction in n-C_4H_{10} and CH_4 permeability in MMM samples compared to unfilled PDMS membrane according to Equation 5.3. For n-C_4H_{10}, the degree of reduction in permeability was proportional to the fugacity. The reduction in n-C_4H_{10} permeability in MMM without gutter layer was 39.2% at 0.5 bar mean n-C_4H_{10} fugacity. It reduced to 22.9% at 1.15 bar mean n-C_4H_{10} fugacity. In MMM with gutter layer, the reduction of n-C_4H_{10} permeability was 19.4% and 10.6% at 0.5 bar and 1.15 bar mean n-C_4H_{10} fugacity, respectively. Comparing the reduction in CH_4 permeability, MMM without gutter layer showed 30% reduction and with gutter layer the reduction was 13.1%, which was less than 20 wt% particle loading. Apparently, casting membranes on a support structure with gutter layer improved the pure gas permeations of both gases. The enhancement of pure gas permeabilities of both gases with gutter layer in unfilled PDMS membranes was found to be less dominant compared to those in MMMs.

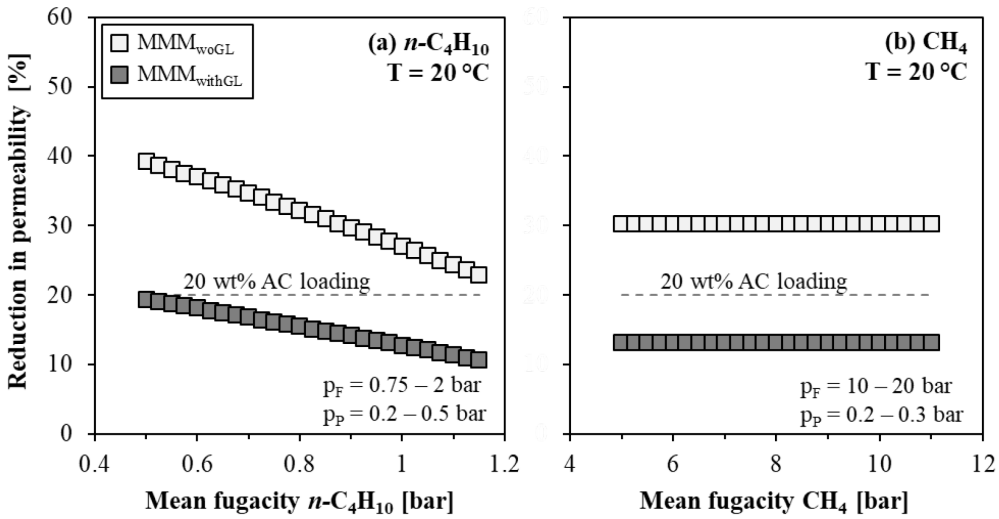

Figure 5.45 Reduction in pure gas permeability of (a) n-C_4H_{10} and (b) CH_4 in ethanol-saturated MMMs with 20 wt% AC loading with and without gutter layer compared to unfilled PDMS (T = 20 °C).

The resistance in a support structure is one of the parameters that determine the permeation and selectivity of a composite membrane [63]. The surface morphology of the support structure, depending on its porosity and pore size, geometrically restricts the diffusion of the penetrant in the active separation layer of the membrane [172]. Restriction of the support structure increases the diffusion length, as a result, permeability is reduced. Introducing a gutter layer between active separation layer and support structure provides prefential pathways for the penetrant and

diminishes the restriction of the support structure without adding significant transport resistance. Kattula et al. [172] computationally demonstrated diffusion pathways of a penetrant in a composite membrane with gutter layer. They suggested that the pathways of a penetrant were almost parallel to the permeation direction where the mass transfer resistance was high. The benefit of the gutter layer was that the diffusion pathways through the pores of the support structure are bending in the gutter layer, which minimizes the pore restriction. A plausible reason of the enhancement of pure gas permeability with gutter layer in this work might be the reduced pore restriction.

5.5.2 Influence of gutter layer on mixed gas selectivity

The mixed gas permeabilities of *n*-C_4H_{10} and CH_4 were determined at 20 °C using binary mixtures of 4 - 6 vol% *n*-C_4H_{10} in CH_4. Experiments were performed at feed pressures from 5 to 30 bar and atmospheric permeate pressure (p_P = ca. 1 bar). Each experiment was repeated 3 times and experimental results were reported as explained in Section 4.3. The errors were calculated using the propagation of error method discussed in Section 4.2.

The mixed gas permeabilities are presented in Figure 5.46 as function of corresponding mean fugacity of the components. No significant difference was observed between the *n*-C_4H_{10} permeability values in PDMS membranes with and without gutter layer. Likewise pure gas permeation, permeability of *n*-C_4H_{10} in MMM with gutter layer was significantly higher than that in MMM without gutter layer. Gutter layer did not significantly increase the CH_4 permeability in PDMS membranes. Similar to pure gas permeability, CH_4 permeation in MMM with gutter layer was considerably higher than that of MMM without gutter layer.

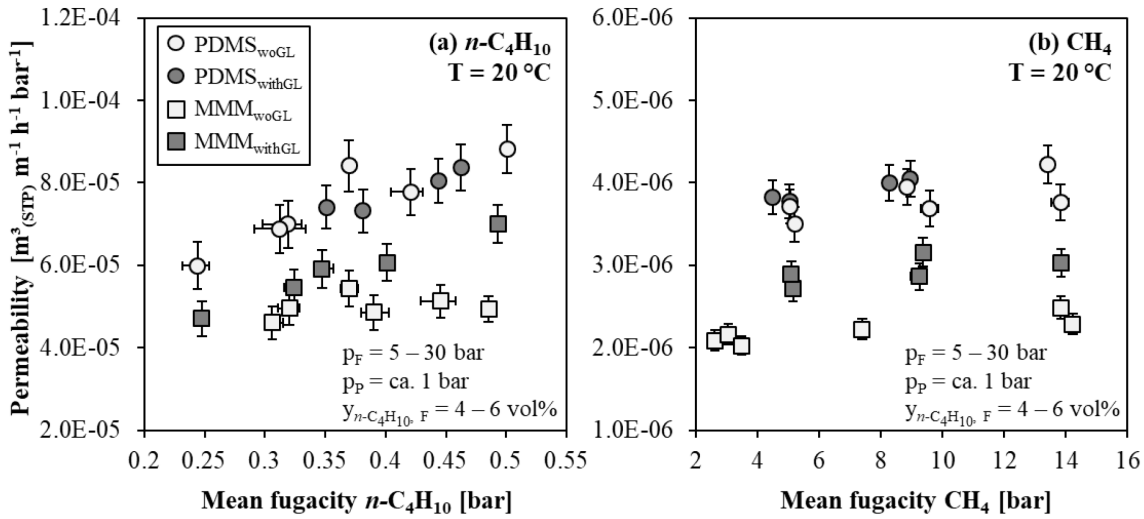

Figure 5.46 Mixed gas permeability of (a) *n*-C_4H_{10} and (b) CH_4 in unfilled PDMS and ethanol-saturated MMMs with 20 wt% AC loading with and without gutter layer for binary mixtures of 4 – 6 vol% *n*-C_4H_{10} in CH_4 (T = 20 °C). Error bars were determined using the propagation of error method.

Results in Figure 5.47 show a remarkable difference in mixed gas selectivities of PDMS membranes and MMMs with and without gutter layer. In general, mixed gas selectivities of both membranes without gutter layer were found to be higher than those of with gutter layer. Additionally, the enhancement of selectivity with MMMs was substantially greater in case of no gutter layer. This indicates that separation performance of a membrane is notably influenced by the mass transfer resistance in the support layer [80]. The gutter layer used in this work was a dense PDMS layer. Due to its high permeability, the gutter layer allows the penetrant to easily permeate into the surface pores without adding significant transport resistance, thus reducing the geometric restriction characteristic of membranes.

Introducing a gutter layer between separation layer and support structure increased the permeability up to some extent, however, the fact remained that the overall selectivity reduced. The gas transport through the membrane depends on the characteristics of the different layers of the composite membrane as well as the interaction of porous support layer and the gutter layer [175]. A reason for the lower selectivity of the membranes with gutter layer could be related to improper selection of gutter layer material. The simulations performed by Kattula et al. [172] suggested that more permeable and selective gutter layer materials and porous support with higher porosity should be preferred to achieve enhanced gas separation performances. The results in this work suggest that a gutter layer is necessary to form MMMs with high permeabilities. However, the gutter layer should have good compatibility with the selective layer and the support structure for the formation of defect-free MMMs with improved separation performance.

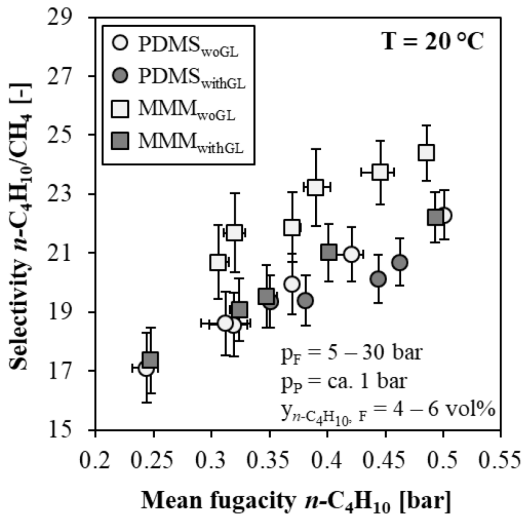

Figure 5.47 Mixed gas selectivity in PDMS and ethanol-saturated MMMs with 20 wt% AC loading with and without gutter layer for binary mixtures of 4 – 6 vol% n-C_4H_{10} in CH_4 (T = 20 °C). Error bars were determined using the propagation of error method.

5.6 Comparison of polymers: PDMS and POMS

Separation performance of an MMM is mainly based on the selected continuous phase, which is the polymer. Different polymeric materials can be used to form an MMM in order to find appropriate matching of dispersed inorganic phase and polymeric continuous phase. In the scope

of MMMfGS project, POMS, which is a solubility-selective rubbery polymer, was also selected as continuous polymer phase.

Unfilled POMS membranes and MMMs composed of 20 wt% ethanol-saturated activated carbon and POMS (MMM_{POMS}) were prepared by H. Mushardt [19]. In the study of Mushardt, she used the same activated carbon particles used in this work provided by Blücher GmbH (AC 100050, d_{50} = 3.5 µm) and the same support structure with gutter layer used in this work produced by HZG. Pure gas permeabilities and mixed gas selectivities of unfilled POMS membranes and MMM_{POMS} prepared by Mushardt were determined at the laboratories of TU Berlin. Obtained results were compared with the previously measured unfilled PDMS and MMMs composed of PDMS filled with 20 wt% ethanol-saturated activated carbon (MMM_{PDMS}). Thus, the influence of different polymer phases using the same filler particles in an MMM was investigated.

The morphologies of POMS and MMM_{POMS} were analyzed from SEM images as presented in Figure 5.48. Average thickness of separation layer of the investigated membranes is listed in Table 5.15. Both membranes were thinner than PDMS and MMM_{PDMS}. A homogeneous particle distribution in POMS matrix and a good contact between POMS and activated carbon were observed. Due to the thinner initial casting thickness, consequently, thinner active separation layer of the membranes, both POMS and MMM_{POMS} showed surface roughness and thickness irregularity compared to PDMS and MMM_{PDMS}.

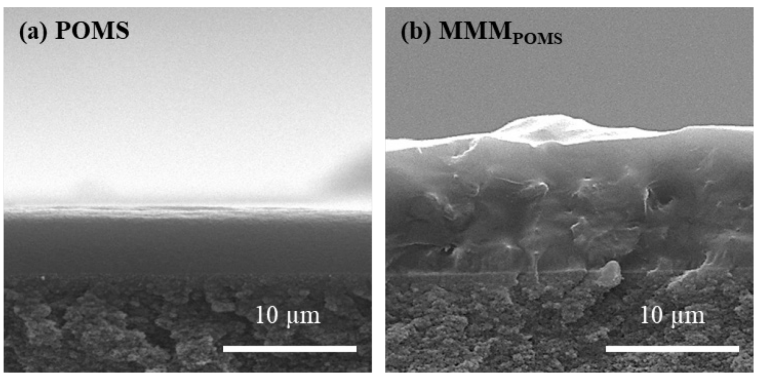

Figure 5.48 Cross-sectional SEM images of (a) unfilled POMS, (b) MMM composed of POMS and ethanol-saturated AC with 20 wt% particle loading.

Table 5.15 Average separation layer thickness of the unfilled POMS and MMM composed of POMS and ethanol-saturated AC with 20 wt% particle loading.

Membrane	Thickness [µm]	SD [µm]	RSD [%]
POMS	4.87	0.49	10.11
MMM_{POMS}	9.53	1.31	13.74

5.6.1 Pure gas permeation in POMS membranes

Pure gas permeation experiments were performed at 20 °C at feed pressures between 0.75 and 2 bar for *n*-C_4H_{10}, and between 10 and 20 bar for CH_4. Permeate pressure was between 0.2 - 0.5 bar for the measurements of both gases. Each pure gas measurement was repeated 3 times and experimental results were reported in Figure 5.49 as explained in Section 4.3. The errors were calculated using the propagation of error method discussed in Section 4.2.

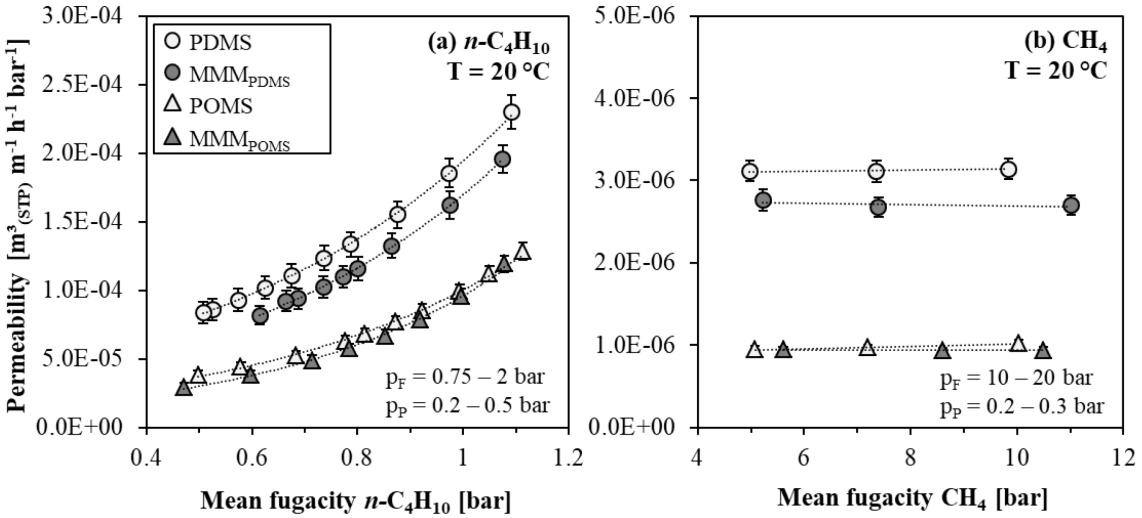

Figure 5.49 Pure gas permeability of (a) *n*-C_4H_{10} and (b) CH_4 in unfilled PDMS, POMS, and their MMMs with 20 wt% ethanol-saturated AC loading (T = 20 °C). Dotted lines represent exponential and linear trend curves and the error bars were determined using the propagation of error method.

Table 5.16 Pure gas *n*-C_4H_{10} and CH_4 permeability coefficients and *n*-C_4H_{10}/CH_4 permselectivity in unfilled PDMS, POMS, and their MMMs with 20 wt% ethanol-saturated AC loading (T = 20 °C).

Membrane	$P^0_{n\text{-}C_4H_{10}}$ [m³$_{(STP)}$ m^{-1} h^{-1} bar^{-1}]	$m_{n\text{-}C_4H_{10}}$ [-]	P_{CH_4} [m³$_{(STP)}$ m^{-1} h^{-1} bar^{-1}]	$\alpha^*_{n\text{-}C_4H_{10}/CH_4}$ [-]
PDMS	3.45E-05 ± 3.91E-06	1.729	3.12E-06 ± 1.26E-07	11.1 ± 1.3
MMM$_{PDMS}$	2.57E-05 ± 2.49E-06	1.887	2.71E-06 ± 1.21E-07	9.5 ± 0.9
POMS	1.37E-05 ± 1.12E-06	1.987	9.78E-07 ± 4.21E-08	14.0 ± 1.1
MMM$_{POMS}$	9.40E-06 ± 1.14E-06	2.324	9.37E-07 ± 3.83E-08	10.0 ± 1.2

POMS and MMM$_{POMS}$ showed the same *n*-C_4H_{10} and CH_4 permeation behavior as PDMS and MMM$_{PDMS}$, where *n*-C_4H_{10} permeability increased with increasing pressure and CH_4 permeability did not change when pressure was increased. However, the permeability values were lower than PDMS and MMM$_{PDMS}$ for both gases. The average *n*-C_4H_{10} permeability in PDMS was 2.2 times higher than that in POMS at 0.5 bar mean *n*-C_4H_{10} fugacity. When mean fugacity of *n*-C_4H_{10} increased to 1.15 bar, this difference slightly decreased and PDMS showed 1.9 times higher

n-C_4H_{10} permeability than POMS. The average CH_4 permeability in PDMS was approximately 3 times higher than that in POMS. This means that PDMS is more permeable for these gases than POMS. Determined pure gas *n*-C_4H_{10} and CH_4 permeability coefficients and *n*-C_4H_{10}/CH_4 permselectivity in unfilled POMS and MMM_{POMS} are listed in Table 5.16 in comparision with previously determined data for PDMS and MMM_{PDMS}.

Figure 5.50 (a) and (b) illustrate the calculated average reduction in *n*-C_4H_{10} and CH_4 permeability in both MMM_{POMS} and MMM_{PDMS} compared to unfilled POMS and PDMS according to Equation 5.3. In this was, the influence of particle loading in both polymer matrices was observed. Both MMMs show approximately 19% lower *n*-C_4H_{10} permeabilities than unfilled POMS and PDMS at 0.5 bar mean *n*-C_4H_{10} fugacity. The reduction in *n*-C_4H_{10} permeability reduced to 10.6% in MMM_{PDMS} at 1.15 bar mean *n*-C_4H_{10} fugacity. The reduction in *n*-C_4H_{10} permeability in MMM_{POMS} reached to – 0.8% at the same mean *n*-C_4H_{10} fugacity where the slope of the exponential trend of permeation was quite high (m = 2.324). This means that MMM_{POMS} showed 0.8% higher *n*-C_4H_{10} permeability than unfilled POMS. This result indicates that the combination of POMS and activated carbon showed promising permeation behaviour at relatively high *n*-C_4H_{10} mean fugacities or feed pressures and activated carbon particles in POMS matrix do not behave as impermeable barriers. When the CH_4 permeability was compared, the average reduction was 4.2% and 13.1% in MMM_{POMS} and MMM_{PDMS}, respectively. MMM_{POMS} showed better results for CH_4 permeability as well.

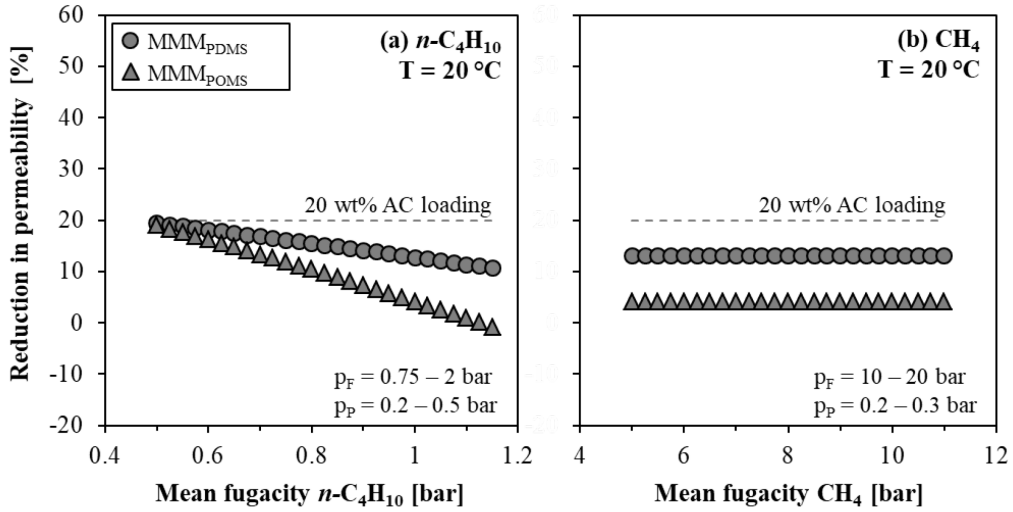

Figure 5.50 Reduction in pure gas permeability of (a) *n*-C_4H_{10} and (b) CH_4 in MMM_{POMS} and MMM_{PDMS} with 20 wt% ethanol-saturated AC loading compared to unfilled PDMS and POMS (T = 20 °C).

5.6.2 Mixed gas selectivity of POMS membranes

Mixed gas experiments were performed with binary mixtures of 4 - 6 vol% *n*-C_4H_{10} in CH_4 at 20 °C. The feed pressure was varied from 10 to 30 bar and permeate pressure was kept constant at atmospheric pressure (p_P = ca. 1 bar). Mixed gas selectivities of unfilled POMS and MMM_{POMS} were compared with the mixed gas selectitivies of unfilled PDMS and MMM_{PDMS}, which were determined under identical experimental conditions. Each mixed gas experimentwas repeated 3

times. Experimental results were reported in Figure 5.51 as explained in Section 4.3. The errors were calculated using the propagation of error method discussed in Section 4.2.

POMS is a derivative of PDMS where an octyl group substitutes one of the methyl groups. PDMS and POMS are two promising polymer materials used for the separation of higher hydrocarbons from methane in plenty of research papers [42, 45, 54] where POMS exhibits higher permselectivity and mixed gas selectivity than PDMS. Compared to the reference membrane PDMS used in this work, unfilled POMS showed notably higher selectivity over the investigated range of mean n-C_4H_{10} fugacity, which is in agreement with the previously reported literature. For instance, the average POMS selectivity was 12.0% higher than the average PDMS selectivity at 0.4 bar mean n-C_4H_{10} fugacity. MMM prepared with POMS and AC showed the highest selectivity. At 0.4 bar mean n-C_4H_{10} fugacity, MMM_{POMS} showed 6.3% higher selectivity than unfilled POMS. At the same experimental conditions, MMM_{PDMS} showed 3.9% higher selectivity than unfilled PDMS. These results reflected an enhancement in selectivity with incorporation of activated carbon particles in POMS matrix, while keeping the good contact between two phases. This makes POMS a more suitable for continuous phase than PDMS to form MMMs using the selected activated carbon particles as inorganic dispersed phase.

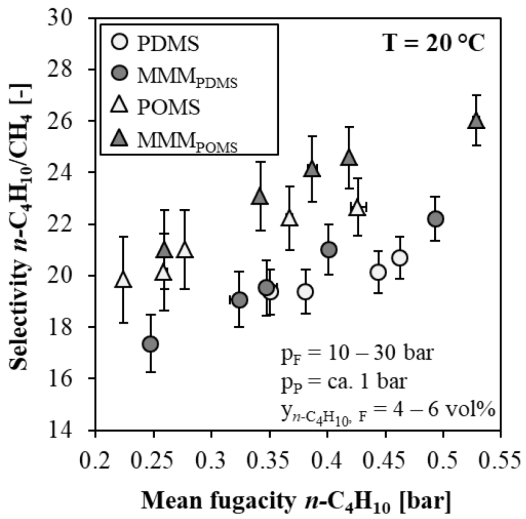

Figure 5.51 Mixed gas selectivity in unfilled PDMS and POMS, and their MMMs with 20 wt% ethanol-saturated AC loading for binary mixtures of 4 – 6 vol% n-C_4H_{10} in CH_4 (T = 20 °C). The error bars were determined using propagation of error method.

5.7 Comparison of inorganic fillers: activated carbon and zeolite Y

The purpose of the dispersed phase in an MMM is to improve gas separation property of the selected polymer. The proper material selection plays an essential role to create a complementary combination of polymer and inorganic filler and to determine the final separation performance of the membranes. Thus, both the continuous phase and the dispersed phase are important for successful MMM formation. This section investigates the ability of MMMs composed of PDMS and zeolite Y particles for n-C_4H_{10} and CH_4 pure gas permeation and mixed gas separation. Determined performances of the MMMs filled with zeolite Y (MMM_{Zeo}) were compared with the

performances of MMMs filled with activated carbon (MMM_{AC}). The material characteristics of the zeolite Y particles used in this work is given in Table 3.4 in Section 3.1.3.

MMM_{Zeo} samples were produced with the same method used for MMM_{AC} preparation and subjected to identical post-treatment as MMM_{AC}. MMM_{Zeo} samples were produced using 9 wt% PDMS solution with 20 wt% ethanol-saturated particle loading. Both MMM_{Zeo} and unfilled PDMS membranes were cast at 300 µm initial thickness by motorized film applicator UA 3000 on a support structure without gutter layer. The morphology of the MMM_{Zeo} was analyzed from SEM images as presented in Figure 5.52 and compared with the morphology of MMM_{AC}. SEM observation confirmed that the zeolite Y particles were completely covered by the PDMS and well dispersed within the PDMS matrix. Additionally, no surface or cross-sectional cracks and no voids at the PDMS/zeolite Y interface were observed. However, a high roughness on the surface of the MMM_{Zeo} was observed probably due to the formed zeolite agglomerates. The average thickness of the separation layer obtained from several SEM images of the membranes is given in Table 5.17. No significant difference was observed between the final thicknesses of the MMMs with two different fillers.

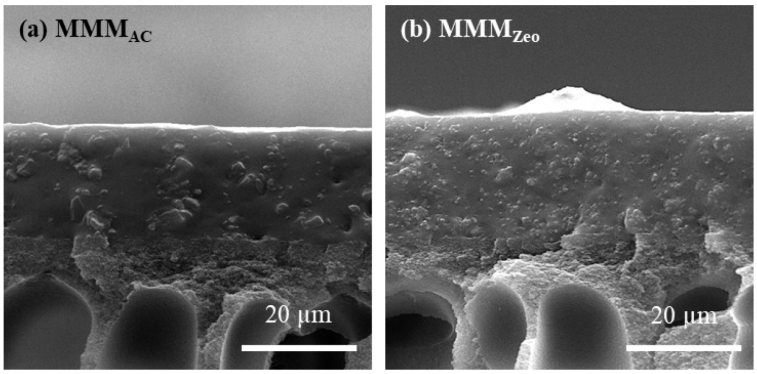

Figure 5.52 Cross-sectional SEM images of MMMs with 20 wt% ethanol-saturated (a) AC, (b) zeolite Y particles.

Table 5.17 Average separation layer thickness of the MMMs with 20 wt% ethanol-saturated AC and zeolite Y particles.

Membrane	Thickness [µm]	SD [µm]	RSD [%]
MMM_{AC}	19.34	0.56	2.92
MMM_{Zeo}	20.17	0.60	3.00

5.7.1 Pure gas permeation in the membranes with zeolite Y

Pure gas *n*-C_4H_{10} permeability in MMM_{Zeo} was determined at the feed pressures between 0.70 and 1.2 bar. Higher feed pressures could not be applied due to the operating range of the permeate flow meter available at the gas permeation setup while performing experiments with MMM_{Zeo}. For all membranes, the feed pressure was varied from 10 to 20 bar to obtain pure gas CH_4

permeability. Pure gas measurements were performed at permeate pressures between 0.2 and 0.5 bar at 20 °C. Each pure gas measurement was repeated 3 times and experimental results were reported as explained in Section 4.3. The errors were calculated using the propagation of error method discussed in Section 4.2.

Figure 5.53 (a) and (b) present pure gas permeabilities of *n*-C_4H_{10} and CH_4 in unfilled PDMS, MMM_{AC}, and MMM_{Zeo}. Determined pure gas *n*-C_4H_{10} and CH_4 permeability coefficients and *n*-C_4H_{10}/CH_4 permselectivity of these membranes are listed in Table 5.18. MMM_{Zeo} showed the same *n*-C_4H_{10} and CH_4 permeation behavior as MMM_{AC}. Permeability of *n*-C_4H_{10} through the MMM_{Zeo} increased with increasing mean fugacity of *n*-C_4H_{10} due to the plasticization of the polymer. On the contrary, the permeability of CH_4 stayed constant. Both pure gas permeabilities in MMM_{Zeo} were lower than those in unfilled PDMS. MMM_{Zeo} exhibited slightly higher *n*-C_4H_{10} permeability than MMM_{AC}, but the same CH_4 permeability. Similar to MMM_{AC}, the main reasons of the reduction in permeability in MMM_{Zeo} are the longer diffusion path due to the tortuosity by embedding of particles into PDMS and the reduction in the gas solubility caused by the substitution of the polymer with the particles acting as non-sorbing barriers.

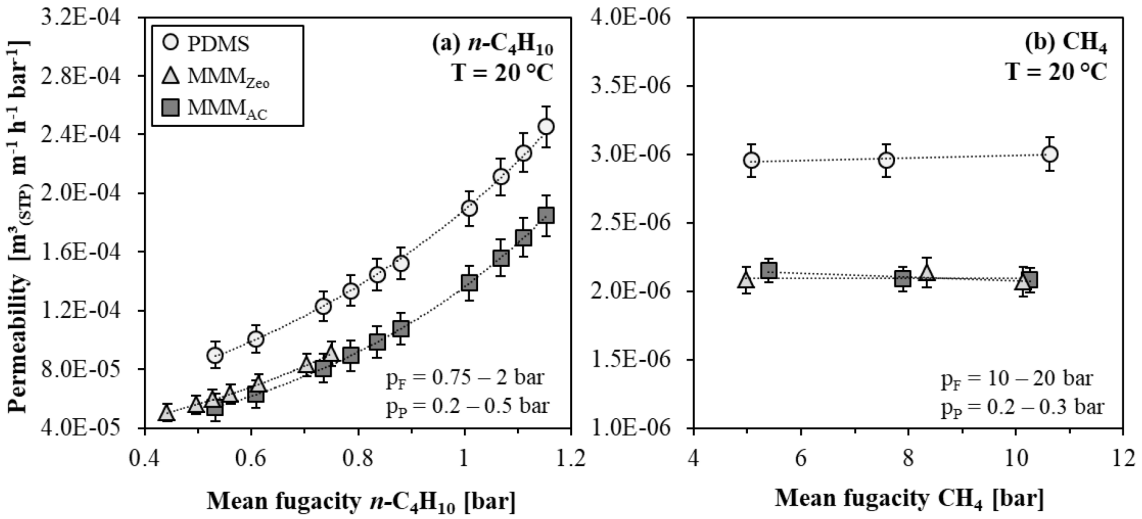

Figure 5.53 Pure gas permeability of (a) *n*-C_4H_{10} and (b) CH_4 in unfilled PDMS and MMMs with 20 wt% ethanol-saturated particle loading (T = 20 °C). Dotted lines represent exponential and linear trend curves and the error bars were determined using the propagation of error method.

Table 5.18 Pure gas *n*-C_4H_{10} and CH_4 permeability coefficients and *n*-C_4H_{10}/CH_4 permselectivity in unfilled PDMS and MMMs with 20 wt% ethanol-saturated AC and zeolite Y loading (T = 20 °C).

Membrane	$P^0_{n\text{-}C_4H_{10}}$ [$m^3_{(STP)}$ m^{-1} h^{-1} bar^{-1}]	$m_{n\text{-}C_4H_{10}}$ [-]	P_{CH_4} [$m^3_{(STP)}$ m^{-1} h^{-1} bar^{-1}]	$\alpha^*_{n\text{-}C_4H_{10}/CH_4}$ [-]
PDMS	3.72E-05 ± 3.81E-06	1.613	3.01E-06 ± 1.26E-07	12.4 ± 1.3
MMM_{AC}	1.88E-05 ± 1.05E-06	1.980	2.10E-06 ± 8.75E-08	9.0 ± 0.5
MMM_{Zeo}	2.18E-05 ± 1.22E-06	1.901	2.10E-06 ± 1.04E-07	12.4 ± 1.6

Figure 5.54 (a) and (b) illustrate the calculated reduction in n-C_4H_{10} and CH_4 permeability in both MMMs compared to unfilled PDMS according to Equation 5.3. From 0.5 to 1.15 bar mean n-C_4H_{10} fugacity, permeability of n-C_4H_{10} reduced from 39.2 to 22.9% in MMM_{AC} and from 32.5 to 18.7% in MMM_{Zeo}. The n-C_4H_{10} permeability reduction in MMM_{AC} was higher than that in MMM_{Zeo}, which makes MMM_{Zeo} a good candidate to form MMM as well as the MMM_{AC}. No difference in reduction of CH_4 permeability between MMMs with different filler particles was observed since they showed the same CH_4 permeability.

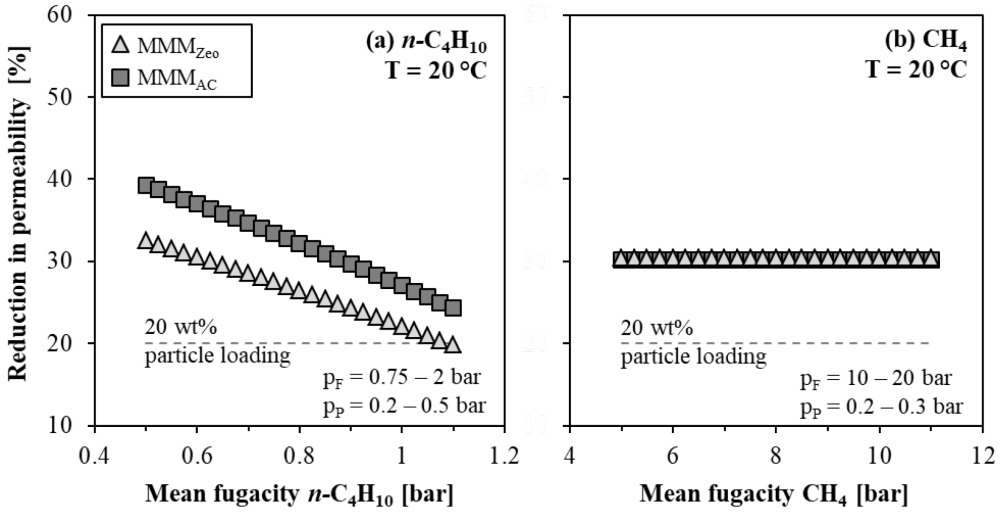

Figure 5.54 Reduction in pure gas permeability of (a) n-C_4H_{10} and (b) CH_4 in MMMs with 20 wt% ethanol-saturated particle loading compared to unfilled PDMS (T = 20 °C).

5.7.2 Mixed gas selectivity of the membranes with zeolite Y

Separation performance of the MMM_{Zeo} samples was evaluated with mixed gas experiments using binary mixtures of 4 vol% n-C_4H_{10} in CH_4. Experiments were performed at constant temperature of 20 °C, constant permeate pressure of atmospheric pressure (p_P = ca. 1 bar), and feed pressures between 10 to 30 bar. Determined mixed gas selectivity of MMM_{Zeo} samples was compared with the selectivity of unfilled PDMS and MMM_{AC}. Each mixed gas experiment was repeated 3 times. Experimental results were reported as explained in Section 4.3. The errors were calculated using the propagation of error method discussed in Section 4.2.

Figure 5.55 shows the mixed gas selectivity of the membranes as function of mean n-C_4H_{10} fugacity. Incorporation of zeolite Y particles in PDMS exhibited almost the same selectivity as unfilled PDMS membranes. Zeolites are the most commonly used inorganic filler material used in MMMs, however, no enhancement of n-C_4H_{10}/CH_4 selectivity was achieved in this work within the investigated range of operating parameters. This was probably due to their size-selective nature, which was not suitable for solution-diffusion mechanism. PDMS/zeolite Y did not appear to be a promising material combination to improve gas separation properties of the MMMs for n-C_4H_{10}/CH_4 separations. It has to be noted here that a different solvent saturation, for instance isooctane or toluene, particle loading, or another polymer as continuous phase may lead different outcomes.

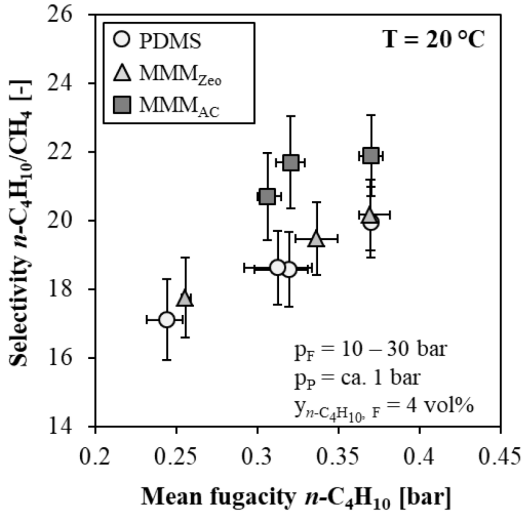

Figure 5.55 Mixed gas selectivity in unfilled PDMS and MMMs with 20 wt% ethanol-saturated particle loading for binary mixtures of 4 vol% n-C_4H_{10} in CH_4 (T = 20 °C). Error bars are determined using the propagation of error method.

6 Results and Discussion Part II: Influence of Operating Parameters

The performance of an MMM is determined by membrane properties including selection of appropriate dispersed phase and filler particles, filler content, and morphological parameters such as filler type and shape. Besides, the overall separation performance of a membrane strongly depends on process-related parameters i.e., feed pressure, permeate pressure, temperature and feed composition. An excellent membrane can show poor performance under inappropriate operating conditions. To optimize membrane separation systems, the membrane performance should be evaluated under various operating conditions.

Section 6 aims to systematically screen the pure and mixed gas *n*-C_4H_{10} and CH_4 permeation through the MMMs composed of PDMS and activated carbon under different operating conditions to find the right combination of the operating parameters, which would improve separation performance. Performance of the MMMs was compared to the performance of the unfilled PDMS membranes as the reference polymer under identical conditions. This investigation also provides reasonable experimental data for validation of models, which include influence of such operating conditions.

MMM samples investigated in this section contain 20 wt% ethanol-saturated activated carbon particles (AC 100050, d_{50} = 3.5 µm) with respect to mass of PDMS. Unless otherwise specified, all MMMs were produced by following the most efficient mixing procedure as previously discussed in Section 5.1. Both MMMs and PDMS membranes were cast onto a support structure without gutter layer at 300 µm initial thickness by motorized film applicator UA 3000. They underwent the same post-treatment that was drying at room temperature for one day in a fume hood and further annealing at 110 °C and 110 mbar for at least 18 h in a vacuum oven.

6.1 Influence of feed pressure

The performance of a membrane is reported by taking into account the driving forces for permeation. In membrane gas separation, feed pressure has a significant influence on driving force.

6.1.1 Comparison of pure and mixed gas permeation at different feed pressures

Several pure and mixed gas experiments were reported in Section 5, which were performed at different feed pressures. Pure gas permeability data is required to understand fundamentals of transport of the individual gases through a mambrane, however, it is not sufficient to evaluate separation performance of the membrane. Mixed gas permeability data is important to investigate

coupling or competitive effects of *n*-C_4H_{10} and CH_4 in the feed mixture [42, 51] and necessary to evaluate actual separation performance of the membranes.

Figure 6.1 (a) and (b) compare pure gas permeability of *n*-C_4H_{10} and CH_4 in unfilled PDMS membranes and MMMs with 20 wt% ethanol-saturated AC loading and mixed gas permeability of both gases in the same membranes for binary mixtures of 4 vol% *n*-C_4H_{10} in CH_4 at 20 °C. For pure gas experiments, the feed pressure was varied from 0.75 to 2 bar and from 10 to 20 bar to obtain *n*-C_4H_{10} and CH_4 permeability, respectively. Vacuum was applied on the permeate side (p_P = 0.2 – 0.5 bar). The mixed gas experiments of unfilled PDMS were performed at 10, 20 and 30 bar feed pressures. The mixed gas experiments of MMMs were performed at 15 and 30 bar feed pressures. For mixed gas experiments, no vacuum was applied on the permeate side (p_P = ca. 1 bar). Experiments were repeated at least 3 times and the results were reported as explained in Section 4.3. The errors were calculated using the propagation of error method discussed in Section 4.2. Results are given as a function of mean fugacity, which was calculated as the average between feed and permeate fugacities.

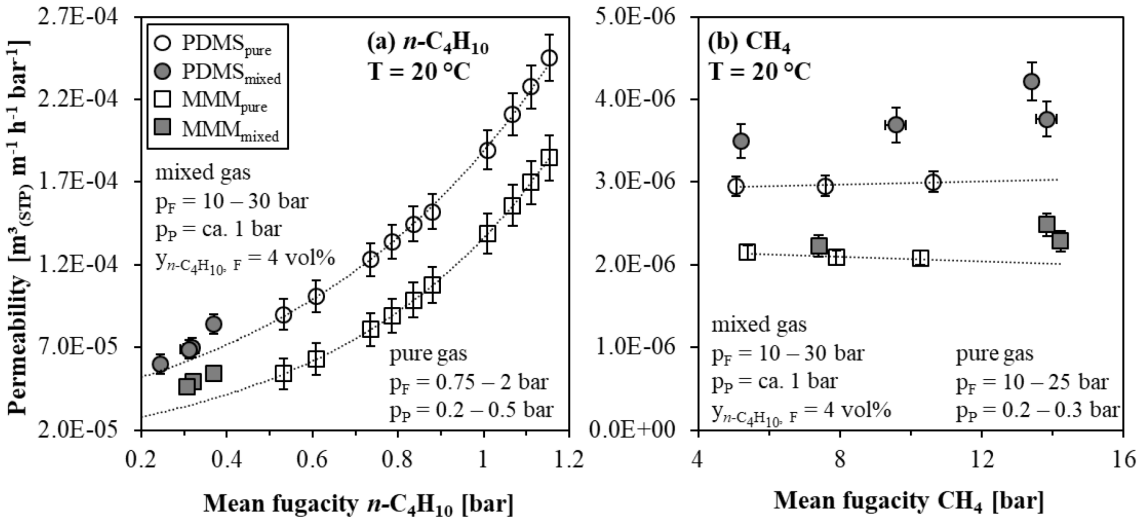

Figure 6.1 Influence of feed pressure on pure and mixed gas permeability (for binary mixtures of 4 vol% *n*-C_4H_{10} in CH_4) of (a) *n*-C_4H_{10} and (b) CH_4 in unfilled PDMS and MMMs with 20 wt% ethanol-saturated AC loading (T = 20 °C). Dotted lines represent exponential and linear trend curves and the error bars were determined using the propagation of error method.

To briefly remember the permeation behaviour of investigated gases in polymer membranes: CH_4 exhibits minor or no change in permeability with increasing feed pressure whereas *n*-C_4H_{10} exhibits increasing permeability, which is in aggrement with the findings of other researchers [51, 118, 176]. The pressure dependency of permeability is attributed to interactions between plasticization, hydrostatic pressure, and penetrant solubility [74, 118]. Plasticization refers to the increase of penetrant diffusivity resulting from increased free volume in the polymer due to the high concentration of the penetrant in the polymer [74, 177]. Typically, higher hydrocarbons act as plasticizing component in a rubbery polymer. Besides, high penetrant pressure can create a competing effect by slightly compressing the polymer matrix and reducing the available free volume for penetrant diffusion. Penetrant solubility in rubbery polymers usually increases with pressure. As a result of these factors, strongly soluble penetrant *n*-C_4H_{10} plasticizes the PDMS

matrix with its high concentration in the polymer, which leads to increased permeability of the component due to solution-controlled permeation in PDMS. Since the low-sorbing penetrant CH_4 does not plasticize the PDMS, its permeability is independent of feed pressure. In an MMM, the increase in *n*-C_4H_{10} permeability with increasing mean fugacity of *n*-C_4H_{10} can be explained with solution of *n*-C_4H_{10} in PDMS and adsorption on AC. Adsorbtion of *n*-C_4H_{10} strongly depends on fugacity or feed pressure at a constant temperature. In this work, no feed pressure or mean fugacity dependency was observed for CH_4 in both unfilled PDMS membranes and MMMs. This is a typical permeation behaviour of non-condensable gases in polymer, where the permeation is diffusion-controlled.

Figure 6.1 (a) shows that *n*-C_4H_{10} mixed gas permeability increased with increasing feed pressure or mean fugacity for both PDMS membranes and MMMs. The permeation of *n*-C_4H_{10} through the polymer affects the structure of the polymer chains. A reason of increase in permeability of PDMS is the *n*-C_4H_{10}-induced swelling caused by increased *n*-C_4H_{10} sorption at higher partial pressures in the feed. Due to its lower partial pressure in the mixture, the mean fugacity of *n*-C_4H_{10} in mixed gas experiments was lower than the mean fugacity of *n*-C_4H_{10} in pure gas experiments. However, the swelling of PDMS by higher hydrocarbon vapors can be significant even at low feed pressures. For instance, De Angelis et al. [178] experimentally determined 30 vol% swelling of PDMS membrane with propane permeation through the membrane at 7 atm (~7.093 bar).

Moreover, swelling of the PDMS leads to an increase in polymer chain mobility, which results in a significant increase in *n*-C_4H_{10} diffusion coefficient as the larger penetrant component compared to the increase in CH_4 diffusion coefficient as the smaller penetrant component [50]. In case of MMMs, the increase of permeability is caused by combined effect of high dissolution of *n*-C_4H_{10} and enhanced adsorption of *n*-C_4H_{10} on AC. Additionally, the presence of dispersed filler particles in the polymer matrix reduces the polymer chain mobility and lowers the swelling. As the exponential trend of *n*-C_4H_{10} pure gas permeation was extrapolated to the lower *n*-C_4H_{10} mean fugacity, it was seen that MMMs showed slightly higher *n*-C_4H_{10} mixed gas permeability than the pure gas permeability while PDMS membranes showed almost the same *n*-C_4H_{10} permeability in both pure and mixed gas measurements.

In PDMS membranes, mixed gas CH_4 permeability was noticeably higher than the pure gas CH_4 permeability, because of the plasticization with *n*-C_4H_{10}. Khanbabaei et al. [118]. experimentally investigated pure and mixed gas permeation of CH_4 and *n*-C_4H_{10} in MMMs composed of PDMS and fumed silica particles and they observed the same behavior. CH_4 is the component of the mixture, which does not swell the polymer itself; however, the swelling of *n*-C_4H_{10} creates an environment that is more favorable for CH_4 to be dissolved in polymer. Furthermore, additional pathways occur in polymer matrix, which facilitate CH_4 diffusion. In MMMs, mixed gas CH_4 permeability was slightly higher than pure gas CH_4 permeability. This can be explained by the lower swelling of the polymer. Due to the presence of activated carbon particles, some of *n*-C_4H_{10} is absorbed by the activated carbon and less amount of *n*-C_4H_{10} is dissolved in the polymer matrix [54]. The presence of *n*-C_4H_{10} increased CH_4 permeability while the presence of CH_4 did not significantly change *n*-C_4H_{10} permeability. Additionally, due to the higher swelling of *n*-C_4H_{10} at higher feed pressures and the favorable environment for CH_4 solution, CH_4 permeability slightly became dependent of feed pressure in mixed gas measurements.

6.1.2 Mixed gas selectivity at different feed pressures

Mixed gas selectivity of binary mixtures of 4 vol% *n*-C_4H_{10} in CH_4 in unfilled PDMS and MMMs are presented in Figure 6.2 (a) and (b), respectively, as a function of feed pressure and mean fugacity of *n*-C_4H_{10}. Mixed gas experiments at each feed pressure were repeated at least 3 times. These experimental results were previously presented in Figure 5.13 (unfilled PDMS and MMMc). To clearly observe the influence of feed pressure and mean *n*-C_4H_{10} fugacity, experimental results are not reported here as average selectivity as explained in Section 4.3. In contrary, selectivity of each individual mixed gas measurement is plotted separetely to compare the scattering of the measured data in both cases. The individual error in each experiment was calculated by the propagation of error method as discussed in Section 4.2.

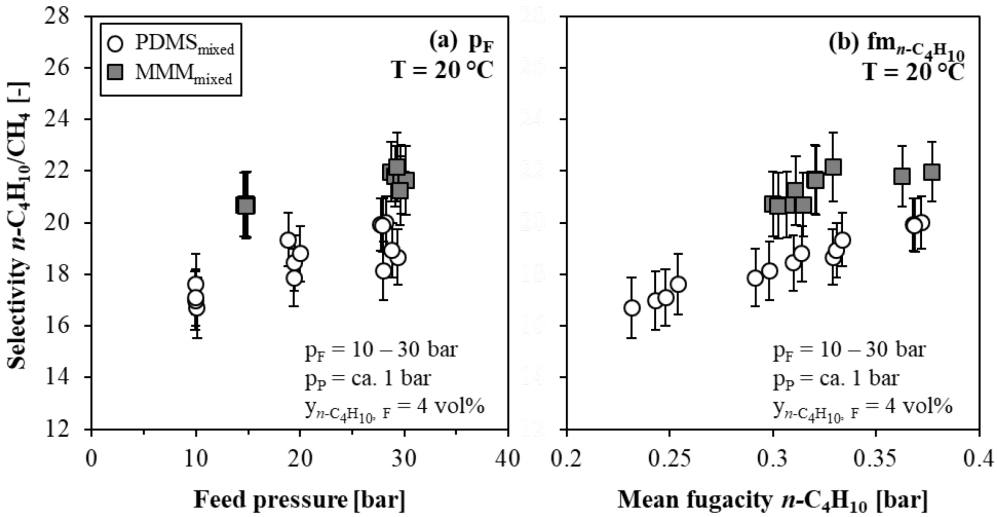

Figure 6.2 Mixed gas selectivity in unfilled PDMS and MMMs with 20 wt% ethanol-saturated AC loading for binary mixtures of 4 vol% *n*-C_4H_{10} in CH_4 (T = 20 °C) (a) as a function of feed pressure, (b) as a function of mean fugacity of *n*-C_4H_{10}. Error bars were determined using the propagation of error method.

Figure 6.2 (a) shows that incresing feed pressure increased the selectivity of both membranes. The changes in the free volume of the polymer due to the plasticization and the molecular motion of the polymer is resulted in an improvement of selectivity with increasing feed pressure. The measured selectivity of MMMs was higher than that of PDMS over the investigated range of pressure. As mentioned before, the presence of activated carbon particles reduces the swelling of the PDMS layer and a selective surface flow through the pores of activated carbon particles occurs with a preferential surface diffusion of *n*-C_4H_{10} over CH_4. A selective surface flow in the adsorbed phase is crucial for the mass transfer mechanism inside the dispersed phase of a sorption-selective MMM whereas CH_4 diffusion is effectively hindered by the formation of a condensed layer.

Figure 6.2 (b) shows the same experimental data as a function of mean *n*-C_4H_{10} fugacity. As discussed before, the binary mixtures of *n*-C_4H_{10}/CH_4 were prepared with a tolerance of ± 8 vol% in terms of *n*-C_4H_{10} concentration. Although this tolerance is accurate enough, the difference of the *n*-C_4H_{10} concentrations in the feed mixture in small quantities led to significant difference of

n-C_4H_{10} feed fugacities. Plotting the mixed gas selectivity data as a function of mean *n*-C_4H_{10} fugacity reveals the importance of the *n*-C_4H_{10} partial pressure, correspondingly, *n*-C_4H_{10} concentration in the feed mixture. Therefore, in a subsequent section of this work, the influence of the feed composition will be discussed in great depth as another process-related variable.

6.2 Influence of permeate pressure

Permeability is a strong function of penetrant concentration in a polymer for condensable gases. Both pressures significantly affect the concentration in the polymer; therefore, the permeability depends on both feed and permeate pressures [179].

6.2.1 Pure gas permeation at different permeate pressures

Due to the limitations of the experimental gas permeation setup, no mixed gas experiments were conducted under vacuum on the permeate side of the membranes. Therefore, the influence of permeate pressure only on pure gas permeability could be investigated in this section by installing a vacuum pump on the permeate side of the membrane test cell. The permeate pressure was varied between 0.2 and 0.5 bar. The feed pressure was varied from 0.75 to 2 bar for *n*-C_4H_{10} and from 10 to 25 bar for CH_4 pure gas measurements. Experiments were performed at 20 °C.

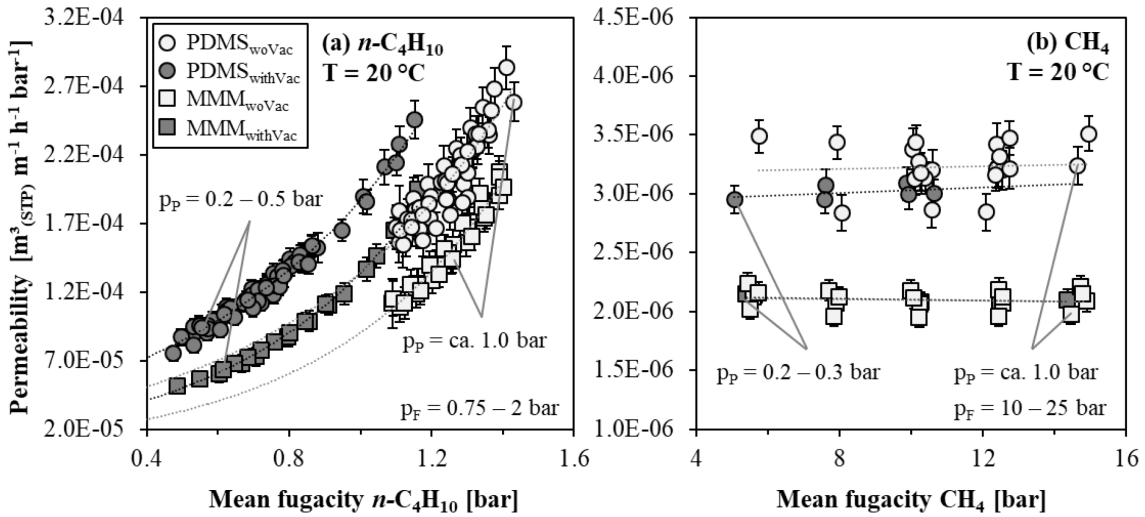

Figure 6.3 Influence of permeate pressure on pure gas permeability of (a) *n*-C_4H_{10} and (b) CH_4 in unfilled PDMS and MMMs with 20 wt% ethanol-saturated AC loading (T = 20 °C). Dotted lines represent exponential and linear trend curves and the error bars were determined using the propagation of error method.

The pure gas *n*-C_4H_{10} permeability as a function of mean *n*-C_4H_{10} fugacity is presented in Figure 6.3 (a). For both unfilled PDMS membranes and MMMs, permeability increased when permeate pressure decreased. For instance, at 0.8 bar mean *n*-C_4H_{10} fugacity, unfilled PDMS membranes showed 34.9 ± 6.9% higher *n*-C_4H_{10} permeability when the permeate pressure was lowered from 1

to 0.25 bar. In MMMs, *n*-C_4H_{10} permeability increased by 55.7 ± 6.0% when the permeate pressure was lowered from 1 to 0.25 bar at the same mean fugacity of *n*-C_4H_{10}. This means that decreasing the permeate pressure at a fixed feed pressure increases the driving force for permeation, hence, gas flux through the membrane. For unfilled PDMS, the average CH_4 permeability without vacuum on the permeate side was slightly higher than that of with vacuum as illustrated in Figure 6.3 (b). However, almost no change in CH_4 permeability was observed for MMMs by changing the permeate pressure. Experimental results are listed in Table 6.1.

Table 6.1 – Pure gas *n*-C_4H_{10} and CH_4 permeability coefficients and *n*-C_4H_{10}/CH_4 permselectivity in unfilled PDMS and MMMs with 20 wt% ethanol-saturated AC loading (T = 20 °C) with and without applying vacuum on permeate side.

Membrane	$P^0_{n\text{-}C_4H_{10}}$ [$m^3_{(STP)}$ m^{-1} h^{-1} bar^{-1}]	$m_{n\text{-}C_4H_{10}}$ [-]	P_{CH_4} [$m^3_{(STP)}$ m^{-1} h^{-1} bar^{-1}]	$\alpha^*_{n\text{-}C_4H_{10}/CH_4}$ [-]
$PDMS_{withVac}$	3.72E-05 ± 3.81E-06	1.613	3.01E-06 ± 1.26E-07	12.4 ± 1.3
$PDMS_{woVac}$	3.02E-05 ± 1.54E-06	1.499	3.23E-06 ± 3.37E-07	9.3 ± 0.5
$MMM_{withVac}$	1.88E-05 ± 1.05E-06	1.980	2.10E-06 ± 8.75E-08	9.0 ± 0.5
MMM_{woVac}	1.15E-05 ± 1.95E-07	2.039	2.10E-06 ± 1.45E-07	5.5 ± 0.1

The data presented in Figure 6.3 are not displayed as average permeabilty but as a collection of individual measurements of each stamp and repetitions of them with the individual error calculated by propagation of error method. It was observed from these scatter plots that the permeation data of unfilled PDMS membranes and MMMs without vacuum on permeat side were widely distributed for both gases. On the other hand, the permeation data obtained with vacuum on permeate side showed narrower distribution, which provides higher measurement precision as well.

When pure gas permeabilities of components are compared with and without applying vacuum on permeate side at a fixed feed pressure, the data can be an indicator for mixed gas separation performances of the membranes. Figure 6.4 (a) and (b) compare *n*-C_4H_{10} and CH_4 pure gas permeability in unfilled PDMS and MMMs at 20 °C as a function of permeate pressure at a constant feed pressures of 1.25 and 20 bar for *n*-C_4H_{10} and CH_4, respectively. No variation in CH_4 permeability was observed for both membranes. For unfilled PDMS membranes and MMMs, the average CH_4 permeability stayed constant at 3.12E-06 and 2.08E-06 $m^3_{(STP)}$ m^{-1} h^{-1} bar^{-1}, respectively. On the other hand, *n*-C_4H_{10} permeability increased as permeate pressure increased. For instance, permeability of *n*-C_4H_{10} increased from 1.32E-04 to 1.66E-04 $m^3_{(STP)}$ m^{-1} h^{-1} bar^{-1} in unfilled PDMS membranes as the permeate pressure increased from 0.35 to 1.06 bar. For MMMs, permeability increased from 8.89E-05 to 1.23E-04 $m^3_{(STP)}$ m^{-1} h^{-1} bar^{-1} as the permeate pressure increased from 0.32 to 1.07 bar. These trends were in agreement with findings of other researchers. Raharjo [180] reported the same trends for *n*-C_4H_{10} and CH_4 mixed gas permeability for the binary gas mixtures of 6 vol% *n*-C_4H_{10} in CH_4 at 11.2 atm feed pressure and 0 °C in PDMS. Musthard et al. [54] investigated separation performance of MMMs composed of POMS and the 20 wt% ethanol-saturated AC for binary gas mixtures of 5 vol% *n*-C_4H_{10} in CH_4 at 30 bar

feed pressure and 20 °C. In both studies, better n-C_4H_{10}/CH_4 selectivities were achieved at high permeate pressures compared to the selectivities obtained at low permeate pressures.

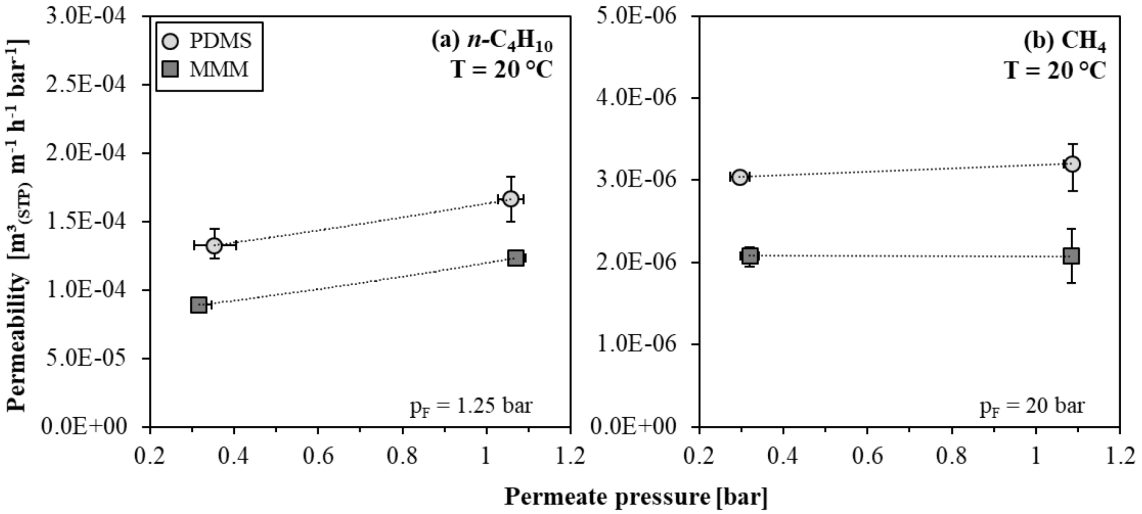

Figure 6.4 Influence of permeate pressure on pure gas permeability of (a) n-C_4H_{10} and (b) CH_4 in unfilled PDMS and MMM with 20 wt% ethanol-saturated AC loading at fixed feed pressures (T = 20 °C). Dotted lines represent exponential and linear trend curves and the error bars were determined using the propagation of error method.

Observations reveal that both permeability and selectivity are significantly sensitive to permeate pressure, particularly for condensable vapor n-C_4H_{10}. These results suggest that operating MMMs composed of PDMS and AC at high permeate pressures is energy and cost effective without vacuum pumps on the permeate side of the membranes. However, mixed gas selectivity of the membranes should also be evaluated at different permeate pressures in order to determine the suitable permeate pressure at which a membrane should be operated.

6.3 Influence of temperature

The permeation process involves solution, diffusion and adsorption. Since these processes are temperature dependent, it is necessary to investigate influence of the temperature on performance of the membranes.

The influence of temperature was determined with pure and mixed gas experiments. The MMMs, which were used to investigate pure gas n-C_4H_{10} permeation and n-C_4H_{10}/CH_4 mixed gas selectivity in this section, were produced by following the most efficient mixing procedure for PDMS and AC as discussed in the Section 5.1. Only for pure gas CH_4 permeation measurements at different temperatures, a set of MMM samples was used, which was prepared with longer mixing time. The mixing condition for PDMS/AC suspension for these MMMs was a combination of magnetic stirring at 400 min^{-1} and high speed disperser at 10000 min^{-1} for 30 min, instead of 15 min.

6.3.1 Pure gas permeation at different temperatures

Pure gas experiments were performed under vacuum condition on the permeate side of the membrane. Permeate pressure was adjusted between 0.2 and 0.5 bar. The feed pressure was varied from 0.75 to 2 bar and from 10 to 25 bar to obtain n-C_4H_{10} and CH_4 permeability data, respectively. Experiments were performed at 10, 20, 30, and 40 °C. The pure gas permeability of n-C_4H_{10} and CH_4 in unfilled PDMS and MMM over mean n-C_4H_{10} fugacity is presented in Figure 6.5. Permeability of n-C_4H_{10} increased as temperature decreased for both types of membranes. Unlike n-C_4H_{10}, lowering the temperature caused the CH_4 permeability to decrease. Since the permeation in PDMS and MMM is solubility-controlled, these trends are strongly related to temperature dependency of solution.

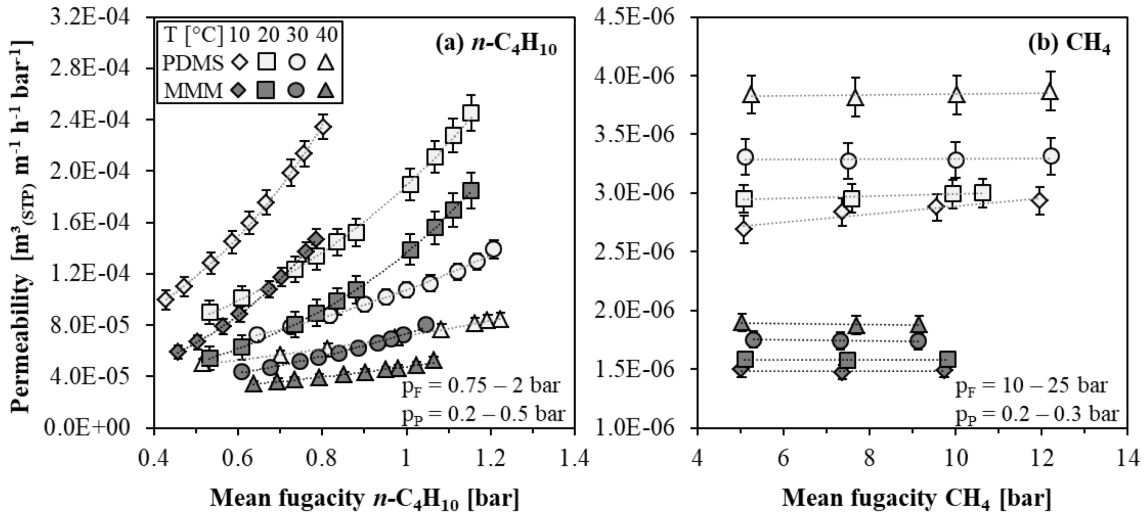

Figure 6.5 Influence of temperature on pure gas permeability of (a) n-C_4H_{10} and (b) CH_4 in unfilled PDMS and MMMs with 20 wt% ethanol-saturated AC loading. Dotted lines represent exponential and linear trend curves and the error bars were determined using the propagation of error method.

Reconsidering Equations 2.30, 2.31 and 2.32, temperature dependency of solubility, permeability, and diffusion coefficient is given as follows:

$$P_i = P_0 \exp\left(-\frac{E_p}{RT}\right) \tag{2.30}$$

$$S_i = S_0 \exp\left(-\frac{\Delta H_S}{RT}\right) \tag{2.31}$$

$$D_i = D_0 \exp\left(-\frac{E_d}{RT}\right) \tag{2.32}$$

where, activation energy of diffusion E_d can be calculated by Equation 2.33 using E_p and ΔH_s values as follows:

$$E_p = E_d + \Delta H_S \tag{2.33}$$

The infinite dilution values of activation energy of permeation E_p were reported previously by several authors for n-C_4H_{10} and CH_4 [50, 51], which are in good agreement with each other within the experimental error. For instance, Raharjo et al. [51] reported infinite dilution values of E_p as -7.2 ± 2 and 6.8 ± 0.6 kJ mol^{-1} for n-C_4H_{10} and CH_4, respectively. From the thermodynamic point of view, the negative value of E_p for n-C_4H_{10} indicates that permeability increases as temperature decreases. Vice versa, the positive value of E_p for CH_4 for indicates that permeability increases as temperature increases. Raharjo et al. [51] also reported the heat of sorption ΔH_S values as –23 ± 0.5 and -5.8 ± 0.3 kJ mol^{-1} for n-C_4H_{10} and CH_4, respectively. The negative ΔH_S values indicate exothermic sorption process, where solubility decreases as temperature increases. Additionally, Raharjo et al. [51] reported infinite dilution values of E_d as 17 ± 3 and 12.6 ± 0.7 kJ mol^{-1} for n-C_4H_{10} and CH_4, respectively. Similarly, the positive value of E_d increases diffusion coefficient with temperature increases. Since the fractional free volume (FFV) of PDMS increases with increasing temperature, diffusion coefficients of both gases increase as well [2].

Infinite dilution permeability coefficients of n-C_4H_{10}, average permeability coefficients of CH_4, and n-C_4H_{10}/CH_4 permselectivity in unfilled PDMS and MMM are presented Table 6.2. The change in infinite dilution permeability coefficients of n-C_4H_{10} in PDMS from 10 to 40 °C was in the range of 3.72E-05 and 3.33E-05 $m^3_{(STP)}$ m^{-1} h^{-1} bar^{-1}, which indicates 10.5% decrease in permeability. For MMM, the infinite dilution permeability coefficients of n-C_4H_{10} increased from 1.64E-05 to 1.87E-05 $m^3_{(STP)}$ m^{-1} h^{-1} bar^{-1} in the same temperature range, which indicates 13.8% increase in permeability. Extremly high slope of fitted exponential trend to the experimental data at 10 °C ($m_{n\text{-}C4H10}$ = 2.789) underestimated the infinite dilution permeability value of n-C_4H_{10} by extrapolation. Apart from the results at 10 °C, no significant change in infinite dilution permeability coefficients of n-C_4H_{10} in MMM from 20 to 40 °C was observed.

Table 6.2 – Pure gas n-C_4H_{10} and CH_4 permeability coefficients and n-C_4H_{10}/CH_4 permselectivity in unfilled PDMS and MMMs with 20 wt% ethanol-saturated AC loading at 10 - 40 °C.

Membrane	T [°C]	$P^0_{n\text{-}C_4H_{10}}$ [$m^3_{(STP)}$ m^{-1} h^{-1} bar^{-1}]	$m_{n\text{-}C_4H_{10}}$ [-]	P_{CH_4} [$m^3_{(STP)}$ m^{-1} h^{-1} bar^{-1}]	$\alpha^*_{n\text{-}C_4H_{10}/CH_4}$ [-]
PDMS	10	3.72E-05 ± 3.78E-06	2.308	2.84E-06 ± 1.16E-07	13.1 ± 1.3
	20	3.72E-05 ± 3.81E-06	1.613	3.01E-06 ± 1.26E-07	12.4 ± 1.3
	30	3.49E-05 ± 2.60E-06	1.126	3.29E-06 ± 1.44E-07	10.6 ± 0.8
	40	3.33E-05 ± 1.81E-06	0.765	3.66E-06 ± 2.18E-07	9.1 ± 0.5
MMM	10	1.64E-05 ± 2.66E-06	2.789	1.49E-06 ± 6.07E-08	11.1 ± 1.8
	20	1.88E-05 ± 1.05E-06	1.980	1.60E-06 ± 6.45E-08	10.9 ± 1.5
	30	1.87E-05 ± 1.57E-06	1.369	1.74E-06 ± 7.10E-08	10.7 ± 0.9
	40	1.87E-05 ± 1.14E-06	0.938	1.88E-06 ± 7.57E-08	9.9 ± 0.6

However, it has to be considered that both n-C_4H_{10} solubility in PDMS and adsorption on activated carbon are dependent on feed and permeate pressures as well. To understand better the influence of temperature on pure gas permeability, permeability values of n-C_4H_{10} were compared

at higher feed pressure or mean fugacity of n-C_4H_{10}. Exemplary, Figure 6.6 compares the pure gas infinite dilution permeability coefficients of n-C_4H_{10} (at mean n-C_4H_{10} fugacity = 0 bar) with n-C_4H_{10} permeabilities at mean n-C_4H_{10} fugacity of 0.7 bar in unfilled PDMS membranes and MMMs at different temperatures. The influence of temperature on pure gas permeability of n-C_4H_{10} was seen clearly at higher values of mean n-C_4H_{10} fugacity. In PDMS, n-C_4H_{10} permeability increased from 5.70E-05 to 1.87E-04 $m^3_{(STP)}$ m^{-1} h^{-1} bar^{-1} when temperature was lowered from 40 to 10 °C at a constant mean n-C_4H_{10} fugacity of 0.7 bar. In MMMs, n-C_4H_{10} permeability increased from 3.60E-05 at 40 °C to 1.16E-04 $m^3_{(STP)}$ m^{-1} h^{-1} bar^{-1} at 10 °C at the same mean n-C_4H_{10} fugacity. This equals to 69.7% and 10.5% increase of n-C_4H_{10} permeability in PDMS membranes and MMMs, respectively. At lower temperatures, n-C_4H_{10} shows higher solubility in PDMS. Higher dissolution of n-C_4H_{10} in PDMS causes loosing of the polymer chains by swelling and creates a favorable environment for diffusion. In addition, the difference in n-C_4H_{10} permeability between PDMS membranes and MMMs decreased as temperature increased. This may be due to the slower diffusion in MMMs with the presence of activated carbon particles in PDMS layer. The permeability of CH_4 in PDMS membranes increased from 2.84E-06 to 3.66E-06 $m^3_{(STP)}$ m^{-1} h^{-1} bar^{-1} and from 1.49E-06 to 1.88E-06 $m^3_{(STP)}$ m^{-1} h^{-1} bar^{-1} in MMMs by lowering the temperature from 40 to 10 °C. This equals 28.8 and 26.8% increase in PDMS and MMM, respectively.

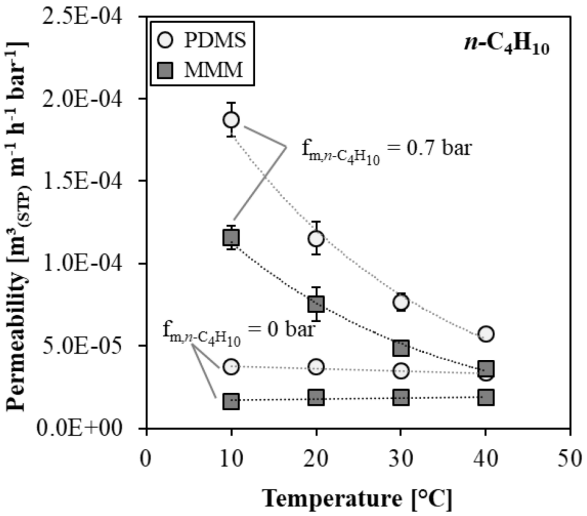

Figure 6.6 Influence of temperature on pure gas infinite dilution permeability coefficient of n-C_4H_{10} (at mean n-C_4H_{10} fugacity = 0 bar) and permeability of n-C_4H_{10} at 0.7 bar mean n-C_4H_{10} fugacity in unfilled PDMS and MMM with 20 wt% ethanol-saturated AC loading.

Figure 6.7 (a) and (b) illustrate the reduction in n-C_4H_{10} and CH_4 permeability in MMM samples compared to unfilled PDMS according to Equation 5.3. No enhancement of CH_4 permeation in MMMs was observed at different temperatures, which means that the increase of CH_4 permeation by increasing temperature in MMMs and PDMS were proportional. On ther other hand, the reduction of n-C_4H_{10} permeability was decreasing as the temperature decreases, except for low n-C_4H_{10} mean fugacity at 10 °C. Certainly, permeability is strongly influenced by n-C_4H_{10} solubility in PDMS and adsorption on activated carbon pores, especially at higher pressures and lower temperatures, which was evidenced by data in Figure 6.7.

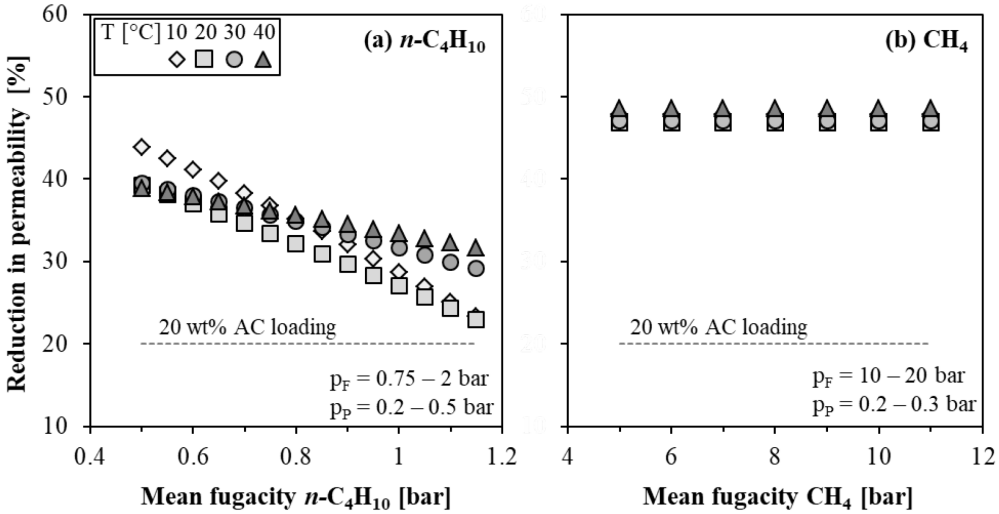

Figure 6.7 Reduction in pure gas permeability of (a) n-C_4H_{10} and (b) CH_4 in MMMs with 20 wt% ethanol-saturated AC loading compared to unfilled PDMS at different temperatures.

The determined pure gas permeation data in this work was compared with the data reported by Raharjo et al. [51]. In Figure 6.8 (a) pure gas permeability data of n-C_4H_{10} in PDMS at different temperatures is plotted in Barrer as a function of feed fugacity of n-C_4H_{10} in atm on a semi-logarithmic plot. Similarly, in Figure 6.8 (b) pure gas permeability data of CH_4 in PDMS are plotted as a function of feed fugacity of CH_4 in atm.

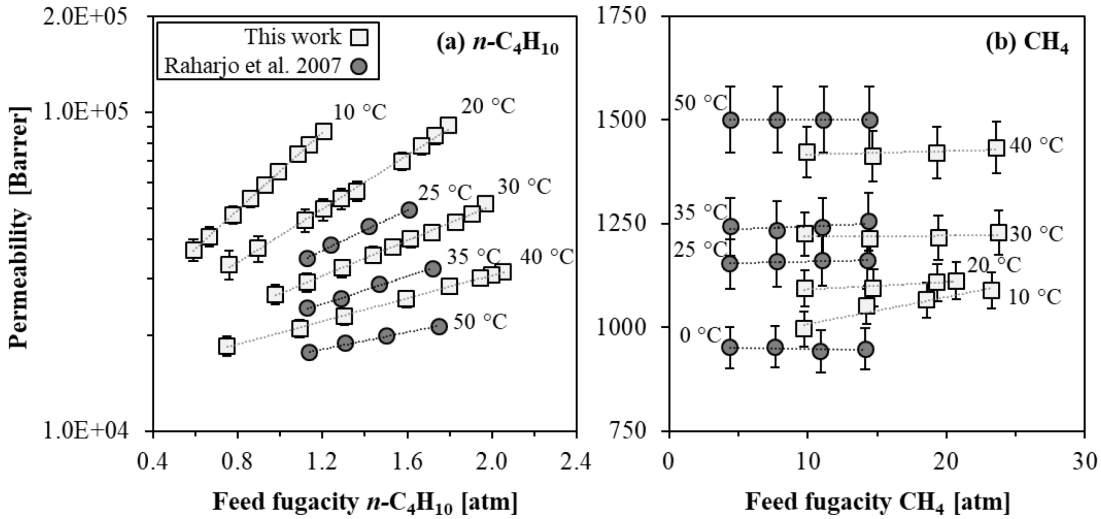

Figure 6.8 Comparision of pure gas permeability data of (a) n-C_4H_{10} and (b) CH_4 in PDMS with literature as a function of feed fugacity at different temperatures. Dotted lines represent exponential and linear trend curves and the error bars were determined using the propagation of error method.

In measurements of Raharjo et al, the permeate side of the membrane was swept with helium resulting in an assumed partial pressure of the measured component in permeate side close to

0 bar. In this work, the permeate pressure ranged between 0.2 and 0.5 bar and 0.2 and 0.3 bar for measurements of n-C_4H_{10} and CH_4, respectively. As discussed in previous section, permeate pressure significantly influences the permeability, particularly for highly condensable gas n-C_4H_{10}. Considering relatively low permeate pressures applied in this work with respect to the numerous studies in the literature, to compare the data of this work obtained under vacuum on permeate side with the data determined by helium sweep on permeate side is acceptable. Apparently, pure gas data for both gases obtained in this work are in excellent agreement with the previously reported permeability values in the literature considering the inevitable errors in measurements and differences in measured polymer samples. Moreover, this agreement represents the high accuracy of the measurements conducted in this work.

6.3.2 Mixed gas permeation at different temperatures

Pure gas experiments showed that the permeation of n-C_4H_{10} is governed by its solubility and the solubility increases with a decrease in temperature. Therefore, mixed gas selectivities of unfilled PDMS membranes and MMMs were determined at 10 °C, which was the lowest possible temperature to perform experiments with the designed gas permeation setup. Results were compared with the measurements performed at 20 °C. Experiments were performed with binary mixtures of 6.5 and 9 vol% of n-C_4H_{10} in CH_4. Experiments with unfilled PDMS membranes were performed at 10 and 20 bar feed pressure at 10°C, and at 5, 6, 7, and 10 bar feed pressure at 20 °C. Experiments with MMMs were performed at 5 and 6 bar feed pressure at 10 °C, and at 5, 6, and 7 bar feed pressure at 20 °C.

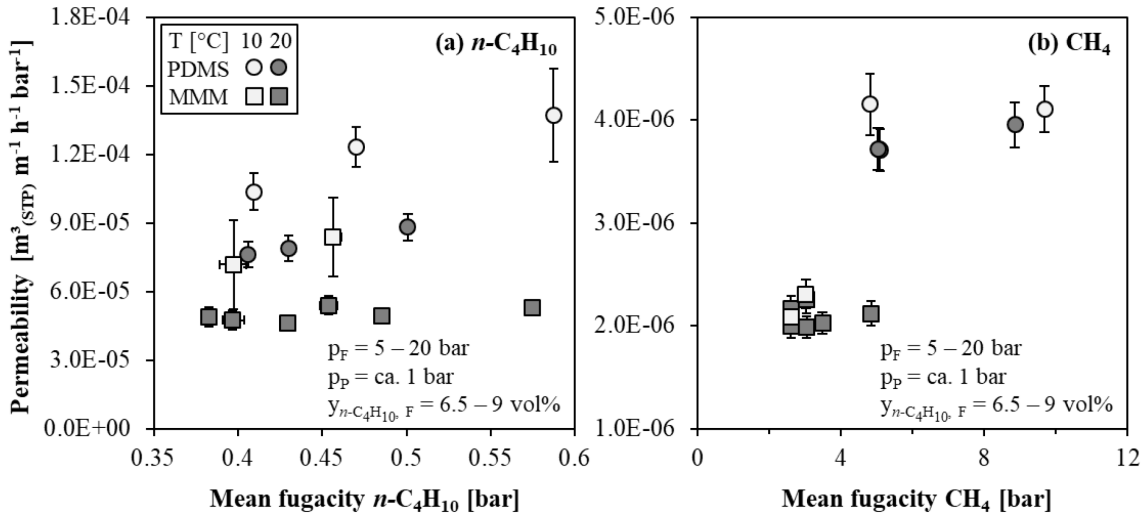

Figure 6.9 Influence of temperature on mixed gas permeability of (a) n-C_4H_{10} and (b) CH_4 in unfilled PDMS and MMMs with 20 wt% ethanol-saturated AC loading for binary mixtures of 6.5 and 9 vol% n-C_4H_{10} in CH_4. The error bars were determined using propagation of error method.

Figure 6.9 (a) shows mixed gas permeability of n-C_4H_{10} in both membranes as a function of mean n-C_4H_{10} fugacity. The mixed gas permeability of n-C_4H_{10} in MMMs slightly increased at 20 °C when mean n-C_4H_{10} fugacity was increased. For example, average permeability of n-C_4H_{10}

increased from 4.90E-05 to 5.35E-05 $m^3_{(STP)}$ m^{-1} h^{-1} bar^{-1} when mean fugacity of *n*-C_4H_{10} increased from 0.4 to 0.57 bar, which is equal to 9.3% increase. At 10 °C, *n*-C_4H_{10} permeability in MMMs was 7.18E-05 and 8.24E-05 $m^3_{(STP)}$ m^{-1} h^{-1} bar^{-1} at 0.4 and 0.45 bar mean *n*-C_4H_{10} fugacity, respectively. This is equal to 14.8% increase in *n*-C_4H_{10} permeability. When the temperature was lowered from 20 to 10 °C, *n*-C_4H_{10} permeability increased 46.6% at 0.4 bar mean *n*-C_4H_{10} fugacity and 63.9% at 0.45 bar mean *n*-C_4H_{10} fugacity. This means the enhancement in *n*-C_4H_{10} permeability in MMMs by lowering the temperature becomes more significant at higher mean *n*-C_4H_{10} fugacity values. For PDMS membranes at 20 °C, permeability of *n*-C_4H_{10} increased from 7.52E-05 to 9.69E-05 $m^3_{(STP)}$ m^{-1} h^{-1} bar^{-1} when mean fugacity of *n*-C_4H_{10} was increased from 0.4 to 0.57 bar, which is equal to 28.9% increase in *n*-C_4H_{10} permeability. This means that the influence of increasing pressure is more pronounced in PDMS membranes than that in MMMs. At 10 °C, permeability of *n*-C_4H_{10} increased from 1.05E-04 to 1.36E-04 $m^3_{(STP)}$ m^{-1} h^{-1} bar^{-1} from 0.4 to 0.57 bar mean fugacity of *n*-C_4H_{10} in PDMS, which was almost equal to the increase at 20 °C (28.7%). This behaviour is due to the higher solubility of *n*-C_4H_{10} in PDMS, consequently, higher degree of swelling, and more adsorption of *n*-C_4H_{10} on activated carbon pores. These trends are in good aggreement with pure gas permeation data.

Figure 6.9 (b) shows mixed gas permeability of CH_4 in both membranes as a function of mean CH_4 fugacity. For MMMs, no significant difference of CH_4 permeability was observed between 10 and 20 °C. For unfilled PDMS membranes, CH_4 permeability slightly increased as temperature decreased. The average CH_4 permeabilities at 20 and 10 °C were 3.79E-06 and 3.99E-06 $m^3_{(STP)}$ m^{-1} h^{-1} bar^{-1} in PDMS, and 2.11E-06 and 2.19E-06 $m^3_{(STP)}$ m^{-1} h^{-1} bar^{-1} in MMM. CH_4 mixed gas permeability in MMMs stayed almost the same. Because, the enhanced diffusivity of CH_4 at higher temperature was suppressed in the presence of *n*-C_4H_{10}.

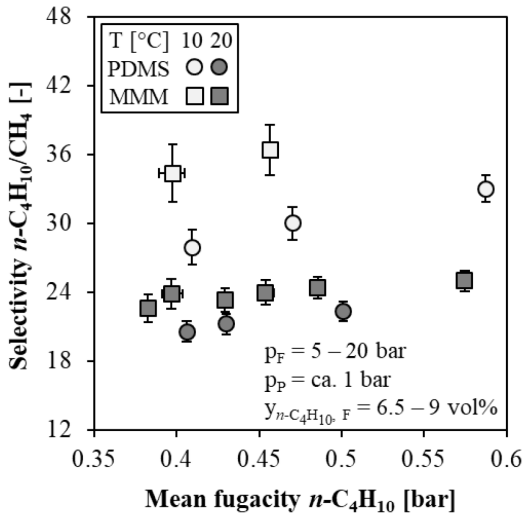

Figure 6.10 Influence of temperature on mixed gas selectivity in unfilled PDMS and MMMs with 20 wt% ethanol-saturated AC loading for binary mixtures of 6.5 and 9 vol% *n*-C_4H_{10} in CH_4. The error bars were determined using propagation of error method.

Mixed gas selectivities are presented in Figure 6.10 as a function of mean *n*-C_4H_{10} fugacity. Apparently, lowering the temperature from 20 to 10°C led to improved selectivity for both membranes. For instance, MMMs showed 52.1% higher selectivity at 10 °C compared to 20 °C at

0.45 bar mean n-C_4H_{10} fugacity. Similarly, selectivity of unfilled PDMS membranes increased 36.2% at the same conditions when temperature was decreased from 20 to 10 °C. Moreover, the enhancement in selectivity with MMMs compared to unfilled PDMS membranes was more pronounced at 10 °C than that at 20 °C in the investigated range of mean n-C_4H_{10} fugacity. At 0.45 bar mean n-C_4H_{10} fugacity at 20 °C, MMMs showed 11.2% enhancement in n-C_4H_{10}/CH_4 mixed gas selectivity compared to unfilled PDMS membranes. At 10 °C, MMMs achieved 24.2% enhancement at the same conditions.

According to these results, it can be concluded that permeation is strongly controlled by solubility and it is especially pronounced at lower temperatures. Additionally, adsorption capacities of n-C_4H_{10} and CH_4 on AC (see Figure 3.5) increase with decreasing temperature. Due to the combined effect of solution and adsorption mixed gas selectivity of MMMs increases with decreasing temperature. To benefit from this behavior, it is advantageous to operate a gas separation system at the lowest possible temperature. Moreover, as mean n-C_4H_{10} fugacity increases selectivity keeps increasing within the range of investigated operating parameters. Therefore, it is interesting to investigate influence of higher n-C_4H_{10} concentrations in the feed mixture on selectivity of both membranes.

6.4 Influence of feed composition

Penetrant concentration in a membrane shows fluctuations depending on the feed and permeate compositions that cause several challenges for industrial separation systems. Low concentration of the desired component to be separated in the feed creates less driving force for the separation whereas high concentration may cause extreme swelling or changes in polymer structure [54]. In this section, therefore, the influence of the n-C_4H_{10} concentration in the feed mixture, as the more soluble and adsorbable component, on the membrane selectivity was investigated to determine favorable conditions for operation.

6.4.1 Mixed gas selectivity at different feed compositions

Mixed gas experiments were performed with binary mixtures of 4 – 19 vol% n-C_4H_{10} in CH_4 at several feed pressures from 5 to 30 bar depending on the total pressure of the prepared feed mixture. Experiments were performed at atmospheric permeate pressure. As the lowest possible temperature, experiments were conducted at 10 °C and the results were compared with the data obtained at 20 °C. Desired volumetric (or molar) concentration of the n-C_4H_{10} in the feed composition was the limiting factor for the total pressure of the binary mixture. For example, it was possible to perform mixed gas experiments with binary mixture of 4 vol% n-C_4H_{10} in CH_4 at 10, 20, and 30 bar feed pressure using the same feed mixture. Although the maximum initial total pressure of the feed mixture was approximately 48 bar, pressure drop until the steady-state during the startup procedure enabled to perform mixed gas experiments at highest feed pressure of 30 bar. Similarly, mixed gas experiments with binary mixture of 6.5 vol% n-C_4H_{10} in CH_4 were performed only at 10 and 20 bar feed pressure using the same feed mixture due to the maximum initial total pressure of the feed mixture, which was almost 30 bar. Due to the same reason, mixed gas experiments with higher than 6.5 vol% n-C_4H_{10} in CH_4 were performed only at feed pressures of 5, 6, 7 and 10 bar. Resulting mean n-C_4H_{10} fugacities as a function of feed pressure of the

mixed gas experiments using several feed mixtures with different *n*-C_4H_{10} concentrations are depicted in Figure 6.11 for both temperatures.

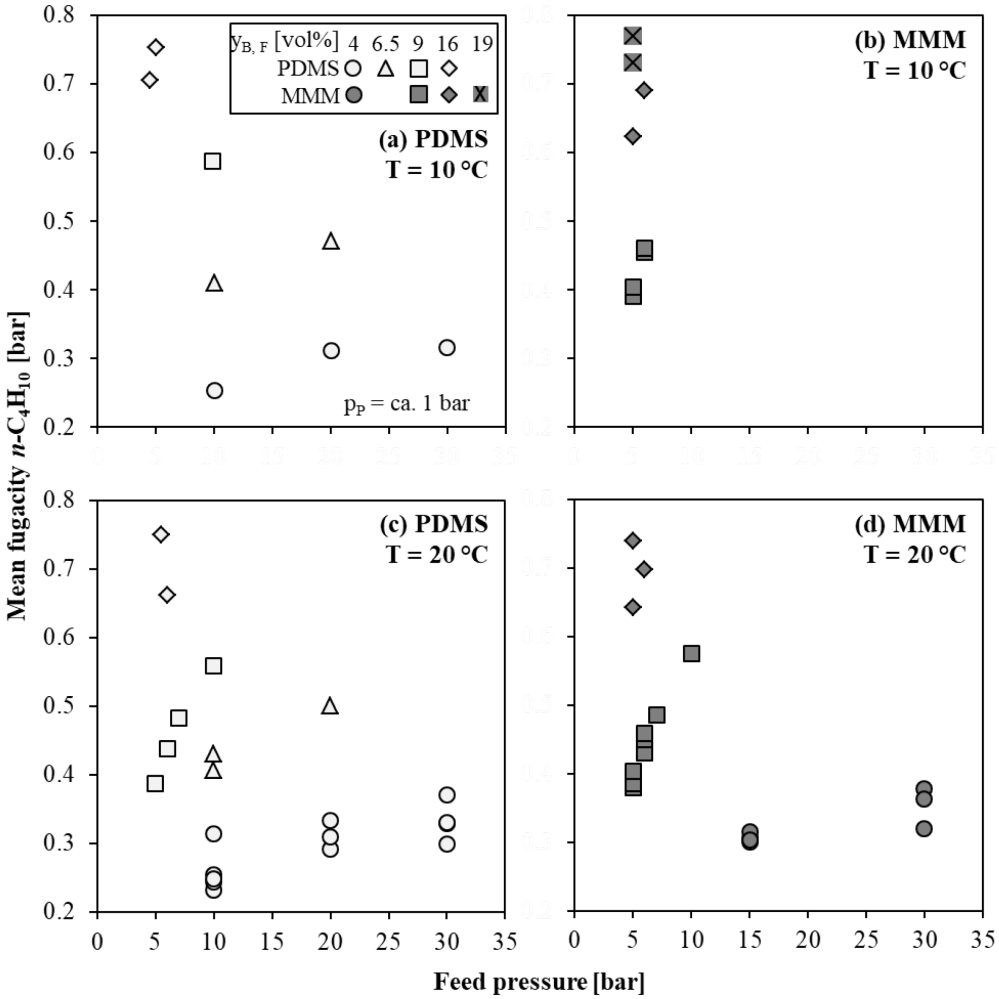

Figure 6.11 Experimental conditions of mixed gas analysis with (a) unfilled PDMS at 10 °C, (b) MMMs at 10 °C, (c) unfilled PDMS at 20 °C, (d) MMMs at 20 °C.

Mixed gas permeabilities of *n*-C_4H_{10} and CH_4 at 10 and 20 °C in unfilled PDMS membranes and MMMs as a function of mean *n*-C_4H_{10} fugacity are presented in Figure 6.12. At both temperatures, the permeability of *n*-C_4H_{10} showed an increase in both membranes with the increase of *n*-C_4H_{10} concentration in the feed mixture. As expected, *n*-C_4H_{10} permeability values at 10 °C in unfilled PDMS and MMM were higher than those at 20 °C. This is associated with solubility and adsorption characteristics of *n*-C_4H_{10} in PDMS and on activated carbon. More *n*-C_4H_{10} dissolves and adsorbs at higher *n*-C_4H_{10} concentrations and at lower temperatures. For instance, at 20 °C in PDMS, the average mixed gas permeability of *n*-C_4H_{10} increased from 7.74E-05 to 1.11E-04 $m^3_{(STP)}$ m^{-1} h^{-1} bar^{-1} when mean *n*-C_4H_{10} fugacity increased from 0.4 to 0.7 bar. By lowering the temperature to 10 °C, the mixed gas permeability of *n*-C_4H_{10} increased from 1.07E-04 to 1.84E-04 $m^3_{(STP)}$ m^{-1} h^{-1} bar^{-1} in PDMS membranes from 0.4 to 0.7 bar mean *n*-C_4H_{10} fugacity. At both temperatures, permeability behaviors in PDMS membranes were exponential and the slope of the trend at 10 °C (1.80) was greater than that at 20 °C (1.20). In

MMMs, the mixed gas permeability of n-C_4H_{10} increased exponentially from 5.07E-05 to 7.36E-05 $m^3_{(STP)}$ m^{-1} h^{-1} bar^{-1} at 20 °C and from 7.40E-05 to 1.28E-04 $m^3_{(STP)}$ m^{-1} h^{-1} bar^{-1} at 10 °C, when the mean n-C_4H_{10} fugacity increased from 0.4 to 0.7 bar. Likewise, the slope of exponential trend at 10 °C (1.82) was greater than that at 20 °C (1.24) for MMMs. As discussed before, the n-C_4H_{10} permeability in MMMs was lower than that in PDMS membranes at both temperatures. However, the difference of mixed gas n-C_4H_{10} permeabilities between PDMS membranes and MMMs became less significant at 10 °C compared to that at 20 °C. For instance, at 0.7 bar mean n-C_4H_{10} fugacity, n-C_4H_{10} permeability of MMMs was 33.6 and 30.9% lower than those of PDMS membranes at 20 and 10 °C, respectively.

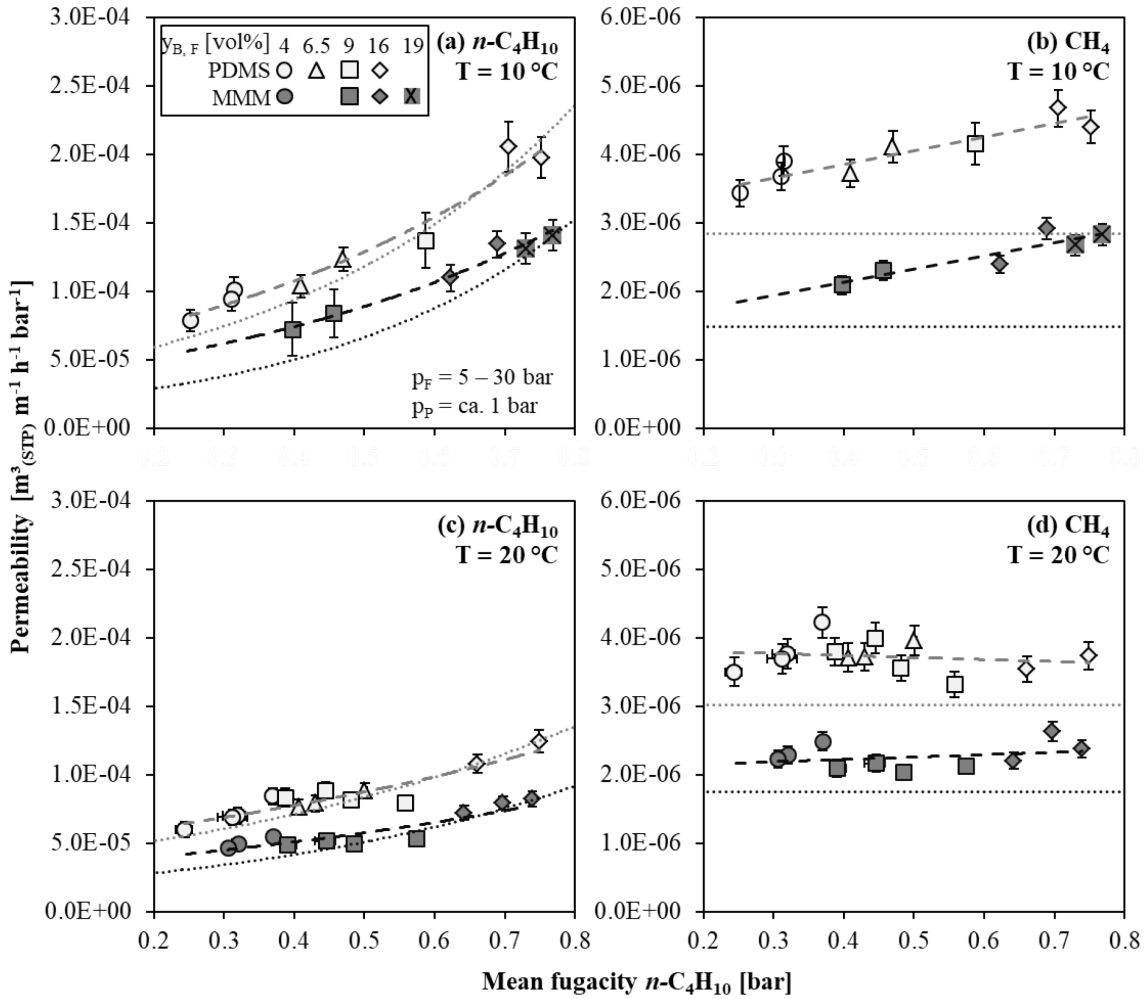

Figure 6.12 Influence of feed composition on mixed gas permeability of (a) n-C_4H_{10} at 10 °C, b) CH_4 at 10 °C, (c) n-C_4H_{10} at 20 °C, and (d) CH_4 at 20 °C in unfilled PDMS and MMMs with 20 wt% ethanol-saturated AC loading for binary mixtures of 4 – 19 vol% n-C_4H_{10} in CH_4. Dashed lines represent mixed gas permeability exponential trend curves of for n-C_4H_{10} and linear trend curves for CH_4. Dotted lines represent pure gas permeability exponential trend curves of for n-C_4H_{10} and linear trend curves for CH_4. The error bars were determined using propagation of error method.

When the pure gas n-C_4H_{10} permeability data at 20 °C was extrapolated to the lower mean n-C_4H_{10} fugacity, it coincided well with the mixed gas permeability data for both membranes when the mean n-C_4H_{10} fugacity was higher than 0.6 bar. This corresponds to the feed n-C_4H_{10} concentrations greater than 9 vol%. This means that n-C_4H_{10} permeability was not influenced by the presence of CH_4 when the feed n-C_4H_{10} concentration was greater than 9 vol%. However, at lower mean n-C_4H_{10} fugacities, in other words when the feed n-C_4H_{10} concentration was lower than 9 vol%, n-C_4H_{10} mixed gas permeability was slightly higher than pure gas permeability. This means that the amount of CH_4 was high enough to influence n-C_4H_{10} permeability. At 10 °C, the pure and mixed gas permeability coincided when the mean n-C_4H_{10} fugacity was 0.7 bar where the feed n-C_4H_{10} concentrations were greater than or equal to 16 vol%. The difference between pure and mixed gas n-C_4H_{10} permeability at lower mean n-C_4H_{10} fugacities was more pronounced.

At both temperatures, the presence of n-C_4H_{10} increased CH_4 permeability. Due to the plasticization of the PDMS by n-C_4H_{10}, diffusion of CH_4 increases. At 20 °C, increasing mean n-C_4H_{10} fugacity did not change CH_4 mixed gas permeability in both membranes. The average CH_4 mixed gas permeability stayed constant at 3.73E-06 and 2.26E-06 $m^3_{(STP)}$ m^{-1} h^{-1} bar^{-1} for PDMS membranes and MMMs, respectively. PDMS membranes showed 23.9% higher CH_4 permeability in mixed gas experiments compared to pure gas experiments. The increase of CH_4 permeability in mixed gas experiments for MMMs was only 7.6%. This means that CH_4 permeability increased in both membranes in the presence of n-C_4H_{10}. The influence of n-C_4H_{10} presence in PDMS membranes was more pronounced than in MMMs.

Mixed gas permeation behavior of CH_4 changed at 10 °C. Increasing mean n-C_4H_{10} fugacity increased CH_4 permeability in both membranes. CH_4 permeability increased from 3.86E-06 to 4.45E-06 $m^3_{(STP)}$ m^{-1} h^{-1} bar^{-1} and from 2.12E-06 to 2.70E-06 $m^3_{(STP)}$ m^{-1} h^{-1} bar^{-1} in PDMS membranes and MMMs, respectively, when the mean n-C_4H_{10} fugacity increased from 0.4 to 0.7 bar. Moreover, mixed gas CH_4 permeabilities were 35.6 and 200% higher than pure gas CH_4 permeabilities in PDMS membranes at 0.4 and 0.7 bar mean n-C_4H_{10} fugacity, respectively. In MMMs, mixed gas CH_4 permeabilities were 43 and 81.6% higher than pure gas CH_4 permeabilities at 0.4 and 0.7 bar mean n-C_4H_{10} fugacity, respectively. The increase in CH_4 permeability is related to n-C_4H_{10} concentration in the membrane. As n-C_4H_{10} fugacity increases, conditions are in favor for higher n-C_4H_{10} sorption. Such high concentrations of n-C_4H_{10} create an environment in which CH_4 becomes more soluble. Since n-C_4H_{10} is more soluble at lower temperatures, the concentration of n-C_4H_{10} in the membrane is higher at lower temperature that makes plasticization more important. This explains the significant increase of CH_4 mixed gas permeability at 10 °C.

The influence of feed composition on mixed gas selectivity is given in Figure 6.13 as function of mean n-C_4H_{10} fugacity and feed pressure. When the selectivity plots as function of mean n-C_4H_{10} fugacity are considered, selectivity of both membranes increased as n-C_4H_{10} concentration was increased in the feed mixture at both tempreatures. At 20 °C, MMMs showed slightly higher selectivity than PDMS membranes. At 10 °C, both membranes showed higher selectivities than those at 20 °C. Furthermore, the improvement of selectivity with MMM was more significant. When the same data was plotted as function of feed pressure, it was clearly demonstrated that the influence of feed composition, in terms of n-C_4H_{10} concentration in the feed mixture, on selectivity is stronger than the influence of feed pressure. For instance, PDMS membranes showed 22.8 selectivity with the binary mixture of 4 vol% n-C_4H_{10} in CH_4 at 10 bar feed pressure. Increasing feed pressure from 10 to 30 bar increased the selectivity of PDMS membranes to 25.9 with the same feed mixture, which is equal to 13.5% enhancement of selectivity. PDMS

membranes showed selectivity value of 33.0 at 10 bar feed pressure with increasing *n*-C_4H_{10} concentration from 4 to 9 vol% in the feed mixture, which is equal to 44.6% enhancement in selectivity. The same behavior was observed for MMMs. At 10 °C and 5 bar feed pressure, the selectivity of MMMs increased from 34.3 to 49.9 when the *n*-C_4H_{10} concentration was increased from 9 to 19 vol% in the feed mixture, which is equal to 45.3% enhancement in selectivity. Using the same binary mixture of 9 vol% *n*-C_4H_{10} in CH_4, the selectivity of MMMs increased from 34.3 to 36.4 when the feed pressure was increased from 5 to 6 bar, which is equal to only 5.9% enhancement in selectivity. The influence of feed pressure was more significant at lower temperature.

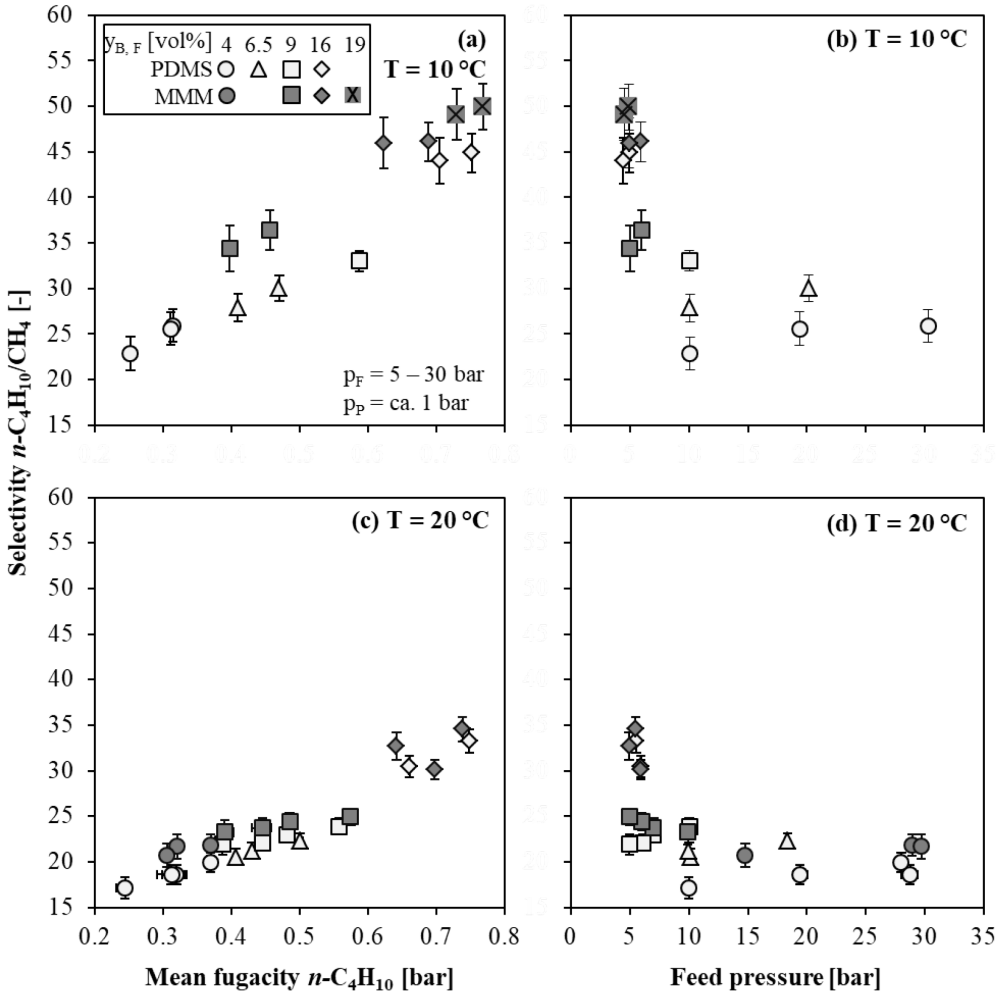

Figure 6.13 Influence of feed composition on mixed gas selectivity of unfilled PDMS and MMMs with 20 wt% ethanol-saturated AC loading for binary mixtures of 4 – 19 vol% *n*-C_4H_{10} in CH_4 (a) as a function of mean *n*-C_4H_{10} fugacity at 10 °C, (b) as a function of feed pressure at 10 °C, (c) as a function of mean *n*-C_4H_{10} fugacity at 20 °C, and (d) as a function of feed pressure at 20 °C. The error bars were determined using propagation of error method.

Figure 6.14 presents the enhancement of mixed gas selectivity with MMMs compared to unfilled PDMS membranes at 10 and 20 °C as a function of mean *n*-C_4H_{10} fugacity. The enhancement is given as percentage, which was calculated as the ratio of difference between average selectivity of

MMMs and PDMS membranes to the selectivity of PDMS membranes at constant mean *n*-C_4H_{10} fugacity and temperature. At the mean *n*-C_4H_{10} fugacity of 0.3 bar at 20 °C, the enhancement of selectivity with MMMs was equal to 13.0%. The difference between MMMs and unfilled PDMS selectivities slightly but not significantly decreased up to 0.5 bar mean *n*-C_4H_{10} fugacity, which corresponds to a range of *n*-C_4H_{10} concentration in the feed composition between 6.5 and 9 vol% depending on the applied feed pressure. In this range of *n*-C_4H_{10} concentration in the feed mixture, the benefit of activated carbon particles in the PDMS was clearly seen with the improved selectivity of MMMs compared to unfilled PDMS. At mean *n*-C_4H_{10} fugacities greater than 0.5 bar, the improvement of selectivity significantly decreased and reached at a value of 1.45% at the 0.75 bar mean *n*-C_4H_{10} fugacity.

The enhancement of selectivity with MMMs was more significant at 10 °C. The selectivity of MMMs initially increased from 14.8 to 30% with increasing the mean *n*-C_4H_{10} fugacity from 0.3 to 0.6 bar. At mean fugacities of *n*-C_4H_{10} higher than 0.6 bar, which approximately corresponds to *n*-C_4H_{10} concentrations in the feed mixture higher than 9 vol%, the selectivity enhancement started to decrease. This trend can be explained by a blocking effect and a competitive sorption effect [180]. At sufficiently high *n*-C_4H_{10} concentrations, polymer becomes saturated and plasticization becomes more significant. At lower temperatures, the concentration of *n*-C_4H_{10} in the polymer is even higher. This means that the high amount of dissolved *n*-C_4H_{10} in the polymer causes significant swelling, where additional pathways for the CH_4 diffusion are created. Additionally, in such excessive swelling cases, CH_4 solution in polymer considerably reduces due to the competition sorption effect. As a result, selectivity reduces.

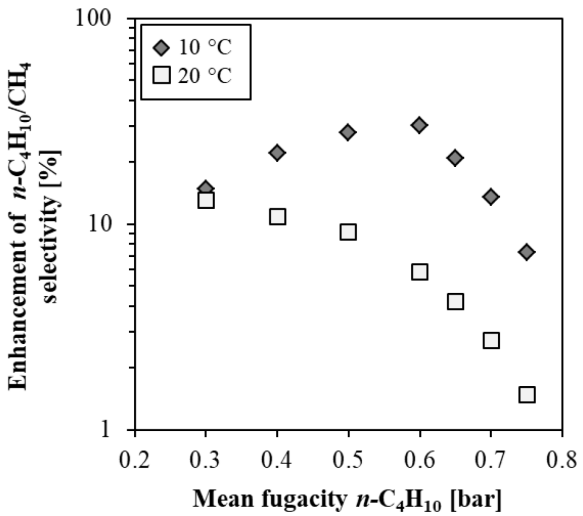

Figure 6.14 The enhancement of mixed gas selectivity with MMMs with 20 wt% ethanol-saturated AC loading for binary mixtures of 4 – 19 vol% *n*-C_4H_{10} in CH_4 at 10 and 20 °C.

These results proved that the MMMs prepared in this work containing 20 wt% ethanol-saturated activated carbon particles in PDMS show effective recovery of higher hydrocarbon *n*-C_4H_{10} from the binary mixtures of *n*-C_4H_{10}/CH_4. Moreover, MMMs are highly beneficial for the separations of binary mixtures of *n*-C_4H_{10}/CH_4 containing less than or equal to 9 vol% *n*-C_4H_{10} at low operating temperatures, such as 10 °C. Considering feed and permeate pressures applied in this work, 9 vol% *n*-C_4H_{10} concentration corresponds approximately 0.6 bar mean *n*-C_4H_{10} fugacity at

10 °C. It should be noted that the beneficial mean n-C_4H_{10} fugacity to operate MMMs can be slightly different in other separation systems depending on the applied feed and permeate pressures and the temperature.

.

7 Summary

7.1 Conclusions

This work focused on two main aims: (i) to develop a reliable procedure for preparation of reproducible and defect-free MMMs with improved separation performance, and (ii) to screen the performance of the produced MMMs under various operating conditions. Binary mixtures of *n*-C_4H_{10}/CH_4 were selected as model vapor/gas mixture. PDMS was selected as continuous rubbery polymer phase of the MMMs. Since PDMS has a very flexible chain, it has almost no sieving ability. However, PDMS is more permeable to larger, more condensable organic vapors than to smaller and less condensable permanent gases, which makes it a good candidate for the removal of *n*-C_4H_{10} from CH_4. AC particles were selected as inorganic dispersed phase of the MMMs due to their unique pore structure having molecular sieving ability, surface chemistry and mechanical strength. AC particles used in this work show high sorption selectivity for *n*-C_4H_{10}, which makes them appropriate inorganic fillers for the investigations of *n*-C_4H_{10}/CH_4 separation.

MMMs were prepared as thin film composite membranes on laboratory scale and morphologically characterized via the cross-sectional and the surface area SEM analysis. Performance of the membranes was evaluated by pure gas permeation and mixed gas selectivity measurements under varying operating conditions.

In gas permeation calculations, it was observed that extremely small variations in measurements of individual physical quantities produced huge differences in overall outcomes. Therefore, great emphasis was particularly put on error analysis to provide highly accurate experimental data with well-estimated error. Propagation of error method was used to evaluate individual uncertainties and combination of uncertainties in pure and mixed gas permeability and selectivity measurements, to confirm the validity and reliability of the results. In addition to this, the impact of those uncertainties on the calculated permeability and selectivity was analyzed, which was crucial to find out the main contributing factor.

Based on the outcomes, the concluding remarks can be listed as follows:

(i) The preparation procedure of MMMs strongly effects the permeability of the studied gases. A preparation strategy, including fundamental steps from priming the filler particles to the post-treatment of the membranes, to from reproducible and defect-free MMMs was successfully developed.

- The order of the preparation steps and the variation in the mixing time of the casting suspension mainly effects the PDMS/AC interactions and the morphology of the membranes.
- The most efficient method (method-4 as described in Section 5.1) to prepare PDMS/AC suspension, which provides uniformly distributed particles within the PDMS layer, consists of the following steps: (1) AC particles are dispersed in a solvent and ultrasonication is applied for 5 min., (2) one-third of the 12 wt% PDMS solution is added to the saturated particles, if isooctane or toluene is used for saturation (in case of ethanol

saturation: half of the 9 wt% PDMS solution is added), and mixed by a magnetic stirrer at 400 min^{-1} for 15 min, (3) the remaining PDMS solution is added to the mixture and mixed with a combination of a HSD at 10000 min^{-1} and a magnetic stirrer at 400 min^{-1} for 15 min.

- Dispersing AC particles in a solvent (saturation of AC particles) prior to mixing with PDMS solution significantly decreases the extend of polymer penetration into the pores of filler particles (pore blockage) and enhances the selectivity. Toluene, isooctane, and ethanol were found to be the most suitable solvents for the saturation step, since most significant decrease in pore blockage was observed when these solvents were employed.
- The cross-sectional and surface area SEM images of MMM stamps indicated that the loading of AC less than or equal to 20 wt% resulted in a well-dispersed particles in the PDMS matrix. The morphology between AC and PDMS was good, and the produced membranes were defect-free. In addition to this, gas permeation results showed that 20 wt% is the optimum AC loading, where MMMs sufficiently establish a percolative network necessary for the mass transport.
- Post-treatment conditions, as well as the other membrane preparation steps, significantly influence the properties of the membranes. For example, it was observed that drying the membranes at room temperature for one day in a fume hood and further annealing at 110°C and 110 mbar for at least 18 h in a vacuum oven provided enhanced permeability and selectivity.
- Introducing a gutter layer between active separation layer and support structure increased the permeability up to some extent, however, reduced the overall selectivity.
- POMS was less permeable for pure *n*-C_4H_{10} and CH_4 than the reference membrane PDMS used in this work. However, MMMs based on POMS and AC exhibited higher permselectivity and mixed gas selectivity than MMMs made of PDMS and AC. This makes POMS a more suitable polymer matrix than PDMS.
- MMMs based on zeolite Y particles and PDMS showed slightly increased pure gas permeability. However, no improvement in selectivity compared to MMMs based on AC and PDMS was observed. These results revealed that PDMS and zeolite Y is not a promising material combination to improve gas separation properties of the MMMs for *n*-C_4H_{10}/CH_4 separations.

(ii) Selection of an appropriate dispersed phase and filler particles, filler content, and morphological properties determine the performance of an MMM. Additionally, process-related parameters i.e., feed pressure, permeate pressure, temperature and feed composition, strongly influence the overall separation performance of the membranes. At specific operating conditions, as given below, MMMs showed enhanced separation performances.

- Selectivity of the MMMs improved by incresing the feed pressure up to 30 bar.
- The permeability and the selectivity were sensitive to permeate pressure as well. Increasing permeate pressure at constant feed pressure and temperature enhanced pure gas permeability.
- Mixed gas selectivity of MMMs increased with decreasing temperature. Temperatures studied in this work ranged from 10 to 40 °C and 10 °C was found to be the most beneficial temperature to operate MMMs. Therefore, it may be advantageous to operate gas separation systems at the lowest possible temperature.
- Increasing *n*-C_4H_{10} concentration in the feed mixture, correspondingly mean fugacity of *n*-C_4H_{10}, increased the selectivity of the membranes. MMMs are highly beneficial for the

separation of binary mixtures of n-C_4H_{10}/CH_4 containing less than or equal to 9 vol% n-C_4H_{10} (which corresponds approximately 0.6 bar mean fugacity of n-C_4H_{10} at 10 °C) at low operating temperatures, such as 10 °C.
- From the varied operating parameters, the feed composition was found to have the strongest influence on the selectivity of the membranes at a constant temperature.

(iii) The calculated values of selectivity was considerably sensitive to the measurement accuracy. Small uncertainties in the feed and permeate gas compositions led to large errors in calculated gas selectivity. The reliability of the calculated permeability and selectivity values was analyzed by propagation of error method.

- The total uncertainty of the permeability and selectivity measurements was 4 – 9%, the errors in the measurements of n-C_4H_{10} concentration being the main contributing factor.
- Technical and operational optimizations were performed to improve measurement accuracy of the gas chromatography and to reduce the experimental error.
- Calibration procedure of the gas chromatography was intensively studied, as it was crucial to perform accurate measurements and to produce reliable results.
- The precision of the gas chromatography measurements for n-C_4H_{10} concentration was evaluated as ±0.08%, estimated as RSDOM of the measurements, with 95% confidence.

To briefly summarize, AC inclusion can deliver attractive MMMs, if a proper polymer is selected. Embedding AC particles into the PDMS matrix lowers pure gas permeability but enhances the overall selectivity. This makes MMMs composed of PDMS and AC good candidates for n-C_4H_{10}/CH_4 separations, which are the gases concerned in this study. MMM production strategies including many variables during preparation significantly effect membrane performance. The developed strategy in this work, which is design of MMMs based on PDMS and AC, can be directly used for other material combinations as well, modified, or further investigated. The material selection to form a MMM depends on the application requirements. Combination of an improper polymer matrix and fillers or ineffective defect elimination may lead to low performances of MMMs. Moreover, operating conditions, such as feed composition and temperature, have significant impact on permeability and selectivity. If optimum operating conditions are found, a significant enhancement of selectivity is achievable. The MMMs produced in this work show great potential to compete with conventional membrane technology. At specific operating conditions, MMMs can be good team-workers at industrial scale separations.

7.2 Future Outlook

Possibilities to improve separation performance of the MMMs, related to preparation procedure and operating conditions, are briefly introduced below.

Pre-treatment of filler particles

Based on the EDX-analysis results, ethanol showed the best performance to hinder pore blockage among the investigated solvents. However, the difference in mixed gas selectivity of the MMMs containing ethanol, isooctane or toluene-saturated particles was not significant, as presented in

Figure 5.27 in Section 5.2. The difference was observed only in gas permeability. Although the full data set concerning the MMMs that are prepared with toluene and isooctane-saturated AC particles are not obtained, the preliminary experiments reveal that the permeability results, when these solvents were used, were better than the results obtained with ethanol. These preliminary findings suggest that toluene or isooctane may be as well promising solvents to obtain superior control over gas permeability and selectivity of the targeted MMMs for *n*-C_4H_{10}/CH_4 separation. Therefore, future studies with these two solvents should focus on designing a detailed study that will generate enough data points for a clearer conclusion. Recommendations to focus would be to investigate the influence of membrane preparation steps on the performance of the MMMs containing either isooctane or toluene-saturated AC particles. Additionally, the performance of those MMMs under varying operating conditions should be evaluated to begin with higher concentration of condensable hydrocarbon component in the feed mixture (for instance, between 4 and 9 vol% *n*-C_4H_{10} in CH_4). Furthermore, higher feed pressures than 30 bar and low temperatures such as 10 °C may reveal superior performance of MMMs that are prepared with isooctane or toluene-saturated particles.

Cross-linking degree of PDMS

The structure of PDMS can be described as a cross-linked network of polymer chains. The arrangement of these polymer chains determine the mechanical properties of PDMS [181]. As described previously in Section 3.2.1, all PDMS membranes used in this work were prepared at the same cross-linker/pre-polymer ($R_{H/V}$ = 0.02062) and catalyst/pre-polymer ($R_{Pt/V}$ = 0.02234) ratios. The swelling degree and the permeation characteristics of the PDMS are expected to change by modification of the polymer at other cross-linker/pre-polymer ratios [143]. For instance, modifications of cross-linking step in the PDMS network may restrict the swelling by tightening the space between polymer chains and reducing the diffusion of the penetrants. Consequently, permeation may reduce [182]. This may influence the penetration of PDMS into the pores of support layer as well. On the other hand, excess of cross-linker in the polymer matrix may be the reason of the presence of unreacted Si-H groups with the Si-V ends of PDMS. Unreacted cross-linker can generate cross-linker agglomerates or branching, which causes a heterogeneous polymer matrix and decreases polymer swelling, as observed by Stafie et al. [143].

Several researchers studied the cross-linking mechanism of PDMS for nanofiltration membranes [47, 183-186]. Concerning gas permeation, Hillock and Koros [187] investigated plasticization of propanediol monoester; cross-linkable (PDMC) polymer for CO_2/CH_4 separations. A significant difference in CO_2 pure gas permeability and CO_2/CH_4 selectivity between cross-linked and un-cross-linked polymer was observed. Their results showed that plasticization could be controlled by reducing polymer chain mobility. However, no systematic study has been performed concerning the influence of cross-linking degree on gas permeation properties of unfilled PDMS membranes and MMMs composed of PDMS and activated carbon, which is very attractive for further studies in this field.

In this work, preliminary experiments were performed to investigate the influence of cross-linking degree of PDMS on the performance of the membranes using *n*-C_4H_{10} and CH_4. PDMS solutions, using three different cross-linker/pre-polymer ($R_{H/V}$) ratios, were prepared. Either unfilled PDMS membranes or MMMs containing 20 wt% ethanol-saturated AC particles were prepared with these PDMS solutions. Pure gas *n*-C_4H_{10} permeability and mixed gas *n*-C_4H_{10}/CH_4 selectivity of these membranes are presented in Figure 7.1 (a) and (b), respectively. The pure *n*-C_4H_{10}

permeability behaviour in both PDMS membranes and MMMs was only slightly changed when cross-linker/pre-polymer ratio was changed. However, the influence of cross-linking degree of PDMS on mixed gas selectivity was significant.

These results suggest that manipulating polymer chains by changing the cross-linker/pre-polymer ratio affects the mechanical properties of PDMS, consequently the gas separation performance of the generated membranes. These preliminary results reported here may provide a guideline for the future work to achieve a desired cross-linker/pre-polymer ratio, which may lead a significant improvement on the selectivity of the membranes. However, further experiments should be conducted such that sufficient amount of data must be provided to gain a deeper insight for clear conclusions.

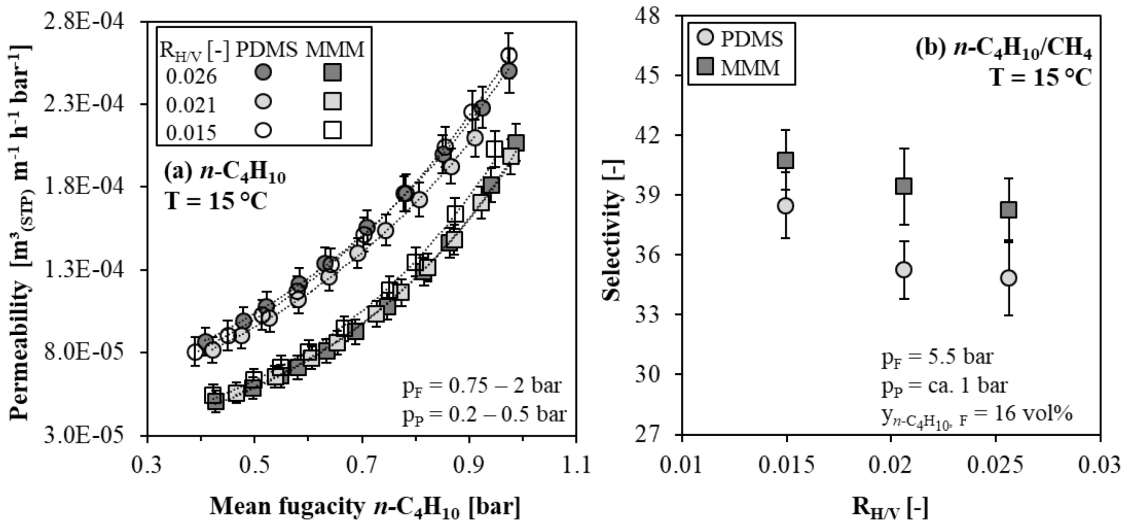

Figure 7.1 Influence of PDMS cross-linking degree on (a) pure gas *n*-C_4H_{10} permeability (b) mixed gas selectivity for binary mixtures of 16 vol% *n*-C_4H_{10} in CH_4 in unfilled PDMS and MMMs with 20 wt% ethanol-saturated AC loading. Dotted lines in (a) represent exponential trend curves. The error bars are determined using the propagation of error method.

Operating parameters

Natural gas is typically treated at relatively high pressures, i.e. between 30 to 60 bar [28]. Therefore, it would be interesting to investigate separation performance of the produced MMMs at feed pressures higher than 30 bar. Additionally, the range of the investigated operating parameters in this work could be expanded. For instance, the influence of permeate pressure was investigated only at two different permeate pressures. To get a broader understanding, the number of the experimental points could be increased.

List of References

1. Ravanchi, M. T., Kaghazchi, T., and Kargari, A., Application of membrane separation processes in petrochemical industry: A Review, Desalination. 235:1-3 (2009) 199-244.

2. Favre, E., Polymeric membranes for gas separation, in Comprehensive Membrane Science and Engineering, (eds E. Drioli and L. Giorno), 2010, Elsevier: Italy. p. 155-212.

3. Brunetti, A., Bernardo, P., Drioli, E., and Barbiert, G., Membrane Engineering: Progress and Potentialities in Gas Separations, in Membrane Gas Separation, (eds Y. Yampolskii and B.D. Freeman), 2010, John Wiley & Sons, Ltd.: West Sussex, United Kingdom. p. 281-312.

4. Baker, R. W., Membrane Technology and Applications, 3rd ed. 2012, California: John Wiley & Sons, Ltd. p. 588.

5. Bernardo, P., Drioli, E., and Golemme, G., Membrane gas separation: a review/state of the art, Industrial & Engineering Chemistry Research. 48:10 (2009) 4638-4663.

6. GMT Membrantechnik GmbH. Last update: Apr. 16th 2019. Available from: http://www.gmtmem.com.

7. Mahler AGS GmbH. Last update: Apr. 16th 2019. Available from: http://www.mahler-ags.com/company.htm.

8. BORSIG GmbH. Last update: Apr. 16th 2019. Available from: http://mt.borsig.de/en/home.html.

9. Novamem Ltd. Last update: Apr. 16th 2019. Available from: http://novamem.com/.

10. Sterling SIHI GmbH. Last update: Apr. 16th 2019. Available from: http://www.sterlingsihi.com/cms/home/products-services/engineered-systems/membrane-systems.html.

11. Baker, R. W., Future directions of membrane gas separation technology, Industrial & Engineering Chemistry Research. 41:6 (2002) 1393-1411.

12. Robeson, L. M., Correlation of separation factor versus permeability for polymeric membranes, Journal of Membrane Science. 62:2 (1991) 165-185.

13. Chung, T. S., Jiang, L. Y., Li, Y., and Kulprathipanja, S., Mixed matrix membranes (MMMs) comprising organic polymers with dispersed inorganic fillers for gas separation, Progress in Polymer Science. 32:4 (2007) 483-507.

14. Vu, D. Q., Koros, W. J., and Miller, S. J., Mixed matrix membranes using carbon molecular sieves - I. Preparation and experimental results, Journal of Membrane Science. 211:2 (2003) 311-334.

15. Aroon, M. A., Ismail, A. F., Matsuura, T., and Montazer-Rahmati, M. M., Performance studies of mixed matrix membranes for gas separation: A review, Separation and Purification Technology. 75:3 (2010) 229-242.

16. Davey, C., Leak, D., and Patterson, D., Hybrid and mixed matrix membranes for separations from fermentations, Membranes. 6:1 (2016) 17.

17. Dechnik, J., Gascon, J., Doonan, C. J., Janiak, C., and Sumby, C. J., Mixed-matrix membranes, Angewandte Chemie International Edition. 56:32 (2017) 9292-9310.

18. Bakhtiari, O., Mosleh, S., Khosravi, T., and Mohammadi, T., Preparation, characterization and gas permeation of polyimide mixed matrix membranes, Journal of Membrane Science 1:1 (2011) 1-8.

19. Mushardt, H., receivable PhD thesis, in Universität Hamburg, Germany.

20. Kramer, V., Löslichkeitsselektive Mixed Matrix Membranen zur Gaspermeation - Experimentelle Untersuchung und Entwicklung eines Stofftransportmodells, PhD thesis in Chair of Chemical & Process Engineering, Technische Universität Berlin, Berlin Germany. 2017 p. 198.

21. Linde AG Engineering Division: Air separeation. Last update: Apr. 16th 2019. Available from: https://www.linde-engineering.com/en/process_plants/cryogenic_plants/index.html.

22. Yampolskii, Y. and Freeman, B., Membrane gas separation. 2010: John Wiley and Sons Ltd. p. 370.

23. Wen, X., Process for gas separation by solvent or absorbent, 2018. U.S. Patent, US 2019/0001256 A1.

24. Galizia, M., Chi, W. S., Smith, Z. P., Merkel, T. C., Baker, R. W., and Freeman, B. D., 50th Anniversary Perspective: Polymers and Mixed Matrix Membranes for Gas and Vapor Separation: A Review and Prospective Opportunities, Macromolecules. 50:20 (2017) 7809-7843.

25. Stookey, D. J., Gas-separation Membrane Applications, in Membrane Technology, (eds S.P. Nunes and K.V. Peinemann), 2006, WILEY-VCH Verlag GmbH & Co. KGaA: Weinheim, Germany. p. 119-150.

26. Baker, R. W., Membrane Gas-separation: Applications, in Membrane Operations. Innovative Separations and Transformations, (eds E. Drioli and L. Giorno), 2009, WILEY-VCH Verlag GmbH & Co. KGaA: Weinheim, Germany. p. 167-194.

27. Chong, K., Lai, S.-O., Thiam, H. S., Teoh, H. C., and Heng, S., Recent progress of oxygen/nitrogen separation using membrane technology. Vol. 11. 2016. p. 1016-1030.

28. Baker, R. W. and Lokhandwala, K., Natural gas processing with membranes: An overview, Industrial & Engineering Chemistry Research. 47:7 (2008) 2109-2121.

29. Ladewig, B. and Al-Shaeli, M. N. Z., Fundamentals of Membrane Bioreactors: Materials, Systems and Membrane Fouling. 2017, Singapore: Springer Nature Singapore Pte Ltd. p. 150.

30. Lobo, A., Cambiella, Á., Benito, J. M., Pazos, C., and Coca, J., Ultrafiltration of oil-in-water emulsions with ceramic membranes: Influence of pH and crossflow velocity, Journal of Membrane Science. 278:1 (2006) 328-334.

31. Misrar, W., Loutou, M., Saadi, L., Mansori, M., Waqif, M., and Favotto, C., Cordierite containing ceramic membranes from smectetic clay using natural organic wastes as pore-forming agents, Journal of Asian Ceramic Societies. 5:2 (2017) 199-208.

32. Achiou, B., Elomari, H., Bouazizi, A., Karim, A., Ouammou, M., Albizane, A., Bennazha, J., Alami Younssi, S., and El Amrani, I. E., Manufacturing of tubular ceramic microfiltration membrane based on natural pozzolan for pretreatment of seawater desalination, Desalination. 419:(2017) 181-187.

33. Al-Mufachi, N. A., Rees, N. V., and Steinberger-Wilkens, R., Hydrogen selective membranes: A review of palladium-based dense metal membranes, Renewable and Sustainable Energy Reviews. 47:(2015) 540-551.

34. Suzuki, A., Yukawa, H., Nambu, T., Matsumoto, Y., and Murata, Y., Consistent description of hydrogen permeability through metal membrane based on hydrogen chemical potential, International Journal of Hydrogen Energy. 39:15 (2014) 7919-7924.

35. Leelachaikul, P., Castro-Dominguez, B., Takagaki, A., Sugawara, T., Kikuchi, R., and Oyama, S. T., Perfluorooctanol-based liquid membranes for H2/O2 separation, Separation and Purification Technology. 122 (2014) 431-439.

36. Yamaguchi, T., Takagaki, A., Sugawara, T., Kikuchi, R., and Oyama, S. T., Supported fluorocarbon liquid membranes for hydrogen/oxygen separation, Journal of Membrane Science. 520 (2016) 272-280.

37. Verweij, H., Inorganic membranes, Current Opinion in Chemical Engineering. 1:2 (2012) 156-162.

38. Chen, X. Y., Vinh-Thang, H., Ramirez, A. A., Rodrigue, D., and Kaliaguine, S., Membrane gas separation technologies for biogas upgrading, Royal Society of Chemistry Advances. 5:31 (2015) 24399-24448.

39. Jones, R. G., Kahovec, J., Stepto, R., Wilks, E. S., Hess, M., Kitayama, T., and Metanomski, W. V., Compendium of Polymer Terminology and Nomenclature IUPAC Recommendations 2008. 2009, Cambridge, UK: The Royal Society of Chemistry Publishing. p. 443.

40. Freeman, B. D. and Pinnau, I., Polymeric materials for gas separations, in Polymer Membranes for Gas and Vapor Separation, (eds B.D. Freeman and I. Pinnau), 1999, American Chemical Society. p. 1-27.

41. Arruebo, M., Coronas, J., Menéndez, M., and SantamaríA, J., Separation of hydrocarbons from natural gas using silicalite membranes, Separation and Purification Technology. 25:1–3 (2001) 275-286.

42. Mushardt, H., Kramer, V., Hülagü, D., Brinkmann, T., and Kraume, M., Development of Solubility Selective Mixed Matrix Membranes for Gas Separation, Chemie Ingenieur Technik. 86:1-2 (2014) 83-91.

43. Yave, W., Shishatskiy, S., Abetz, V., Matson, S., Litvinova, E., Khotimskiy, V., and Peinemann, K. V., A Novel Poly(4-methyl-2-pentyne)/TiO2 Hybrid Nanocomposite Membrane for Natural Gas Conditioning: Butane/Methane Separation, Macromolecular Chemistry and Physics. 208:22 (2007) 2412-2418.

44. Ohlrogge, K., Peinemann, K. V., Wind, J., and Behling, R. D., The separation of hydrocarbon vapors with membranes, Separation Science and Technology. 25:13-15 (1990) 1375-1386.

45. Schultz, J. and Peinemann, K. V., Membranes for separation of higher hydrocarbons from methane, Journal of Membrane Science. 110:1 (1996) 37-45.

46. Naik, P. V., Bernstein, R., and Vankelecom, I. F. J., Influence of support layer and PDMS coating conditions on composite membrane performance for ethanol/water separation by pervaporation, Journal of Applied Polymer Science. 133:28 (2016) 1-12.

47. Ben Soltane, H., Roizard, D., and Favre, E., Effect of pressure on the swelling and fluxes of dense PDMS membranes in nanofiltration: an experimental study, Journal of Membrane Science. 435:0 (2013) 110-119.

48. Rezakazemi, M., Shahidi, K., and Mohammadi, T., Sorption properties of hydrogen-selective PDMS/zeolite 4A mixed matrix membrane, International Journal of Hydrogen Energy. 37:22 (2012) 17275-17284.

49. Rezakazemi, M., Shahidi, K., and Mohammadi, T., Hydrogen separation and purification using crosslinkable PDMS/zeolite A nanoparticles mixed matrix membranes, International Journal of Hydrogen Energy. 37:19 (2012) 14576-14589.

50. Pinnau, I. and He, Z., Pure- and mixed-gas permeation properties of polydimethylsiloxane for hydrocarbon/methane and hydrocarbon/hydrogen separation, Journal of Membrane Science. 244:1-2 (2004) 227-233.

51. Raharjo, R. D., Freeman, B. D., Paul, D. R., Sarti, G. C., and Sanders, E. S., Pure and mixed gas CH_4 and *n*-C_4H_{10} permeability and diffusivity in poly(dimethylsiloxane), Journal of Membrane Science. 306:1-2 (2007) 75-92.

52. Raharjo, R. D., Freeman, B. D., and Sanders, E. S., Pure and mixed gas CH4 and n-C4H10 sorption and dilation in poly(dimethylsiloxane), Journal of Membrane Science. 292:1-2 (2007) 45-61.

53. Clarizia, G., Algieri, C., and Drioli, E., Filler-polymer combination: a route to modify gas transport properties of a polymeric membrane, Polymer. 45:16 (2004) 5671-5681.

54. Mushardt, H., Müller, M., Shishatskiy, S., Wind, J., and Brinkmann, T., Detailed investigation of separation performance of a MMM for removal of higher hydrocarbons under varying operating conditions, Membranes. 6:1 (2016) 16.

55. Nunes, S. P., Schultz, J., and Peinemann, K.-V., Silicone membranes with silica nanoparticles, Journal of Materials Science Letters. 15:13 (1996) 1139-1141.

56. Mohamad, M. B., Fong, Y. Y., and Shariff, A., Gas separation of carbon dioxide from methane using polysulfone membrane incorporated with zeolite-T, Procedia Engineering. 148:(2016) 621-629.

57. Shahid, S. and Nijmeijer, K., Matrimid®/polysulfone blend mixed matrix membranes containing ZIF-8 nanoparticles for high pressure stability in natural gas separation, Separation and Purification Technology. 189 (2017) 90-100.

58. Zulhairun, A. K., Subramaniam, M. N., Samavati, A., Ramli, M. K. N., Krishparao, M., Goh, P. S., and Ismail, A. F., High-flux polysulfone mixed matrix hollow fiber membrane incorporating mesoporous titania nanotubes for gas separation, Separation and Purification Technology. 180 (2017) 13-22.

59. Moghadassi, A. R., Rajabi, Z., Hosseini, S. M., and Mohammadi, M., Fabrication and modification of cellulose acetate based mixed matrix membrane: Gas separation and physical properties, Journal of Industrial and Engineering Chemistry. 20:3 (2014) 1050-1060.

60. Moghadassi, A. R., Rajabi, Z., Hosseini, S. M., and Mohammadi, M., Fabrication and modification of cellulose acetate based mixed matrix membrane: Gas separation and physical properties, Journal of Industrial and Engineering Chemistry. 20:3 (2017) 1050-1060.

61. Ma, C., Zhang, C., Labreche, Y., Fu, S., Liu, L., and Koros, W. J., Thin-skinned intrinsically defect-free asymmetric mono-esterified hollow fiber precursors for crosslinkable polyimide gas separation membranes, Journal of Membrane Science. 493 (2015) 252-262.

62. Qiu, W., Xu, L., Chen, C.-C., Paul, D. R., and Koros, W. J., Gas separation performance of 6FDA-based polyimides with different chemical structures, Polymer. 54:22 (2013) 6226-6235.

63. Ohlrogge, K., Wind, J., and Brinkmann, T., Membranes for recovery of volatile organic compounds, in Comprehensive Membrane Science and Engineering, (eds E. Drioli and L. Giorno), 2010, Elsevier: Italy. p. 213-242.

64. Nunes, S. P. and Peinemann, K. V., Membrane Technology in the Chemical Industry. Membrane Gas Separation. 2006, Weinheim: WILEY-VCH Verlag GmbH & Co. KGaA. p. 337.

65. Wijmans , J. G. and Baker, R. W., The solution-diffusion model: A unified approach to membrane permeation, in Materials Science of Membranes for Gas and Vapor Separation, (eds Y. Yampolskii, I. Pinnau, and B. Freeman), 2006, John Wiley & Sons Ltd.: Chichester. p. 159-188.

66. Melin, T. and Rautenbach, R., Membranverfahren, 3rd ed. 2007: Springer. p. 571.

67. Brinkmann, T., Modellierung und Simulation der Membranverfahren Gaspermeation, Dampfpermeation und Pervaporation, in Membranen: Grundlagen,Verfahren und industrielle Anwendungen, (eds K. Ohlrogge and K. Ebert), 2006, WILEY-VCH Verlag GmbH & Co. KGaA: Weinheim, Germany. p. 273-333.

68. Wijmans, J. G., Process performance = membrane properties + operating conditions, Journal of Membrane Science. 220:1-2 (2003) 1-3.

69. Baker, R. W., Wijmans, J. G., and Huang, Y., Permeability, permeance and selectivity: a preferred way of reporting pervaporation performance data, Journal of Membrane Science. 348:1-2 (2010) 346-352.

70. Vinh-Thang, H. and Kaliaguine, S., Predictive models for mixed-matrix membrane performance: A review, Chemical Reviews. 113:7 (2013) 4980-5028.

71. Diestel, L., Wang, N., Schulz, A., Steinbach, F., and Caro, J., Matrimid-based mixed matrix membranes: Interpretation and correlation of experimental findings for zeolitic imidazolate frameworks as fillers in H2/CO2 separation, Industrial & Engineering Chemistry Research. 54:3 (2015) 1103-1112.

72. Ghosal, K. and Freeman, B. D., Gas separation using polymer membranes: an overview, Polymers for Advanced Technologies. 5:11 (1994) 673-697.

73. Fang, S. M., Stern, S. A., and Frisch, H. L., Free volume model of permeation of gas and liquid-mixtures through polymeric membranes, Chemical Engineering Science. 30:8 (1975) 773-780.

74. Merkel, T. C., Bondar, V. I., Nagai, K., Freeman, B. D., and Pinnau, I., Gas sorption, diffusion, and permeation in poly(dimethylsiloxane), Journal of Polymer Science Part B-Polymer Physics. 38:3 (2000) 415-434.

75. Alpers, A., Hochdruckpermeation mit selektiven Polymermembranen für die Separation gasförmiger Gemische, PhD thesis in Universität Hannover. (1997) p. 168.

76. Stern, S. A., Fang, S. M., and Frisch, H. L., Effect of pressure on gas permeability coefficients. A new application of “free volume” theory, Journal of Polymer Science Part A-2: Polymer Physics. 10:2 (1972) 201-219.

77. Stern, S. A., Fang, S. M., and Jobbins, R. M., Permeation of gases at high pressures, Journal of Macromolecular Science, Part B. 5:1 (1971) 41-69.

78. Dixon-Garrett, S. V., Nagai, K., and Freeman, B. D., Ethylbenzene solubility, diffusivity, and permeability in poly(dimethylsiloxane), Journal of Polymer Science Part B: Polymer Physics. 38:11 (2000) 1461-1473.

79. Lei, G. Y. and Eirich, F. R., Permeability of gases through filled and filled rubber membranes, PhD thesis in Aerospace Engineering and Applied Mechanics and Chemistry Polytechnic Institute of Brooklyn, Brooklyn. (1970) p. 159.

80. Rautenbach, R. and Helmus, F. P., Some considerations on mass-transfer resistances in solution diffusion-type membrane processes, Journal of Membrane Science. 87:1-2 (1994) 171-181.

81. Robeson, L. M., The upper bound revisited, Journal of Membrane Science. 320:1-2 (2008) 390-400.

82. Robeson, L. M., Freeman, B. D., Paul, D. R., and Rowe, B. W., An empirical correlation of gas permeability and permselectivity in polymers and its theoretical basis, Journal of Membrane Science. 341:1-2 (2009) 178-185.

83. Moghadassi, A. R., Rajabi, Z., Hosseini, S. M., and Mohammadi, M., Preparation and characterization of (PVC-blend-SBR) mixed matrix gas separation membrane filled with zeolite, Arabian Journal for Science and Engineering. 39:2 (2013) 605-614.

84. Bastani, D., Esmaeili, N., and Asadollahi, M., Polymeric mixed matrix membranes containing zeolites as a filler for gas separation applications: A review, Journal of Industrial and Engineering Chemistry. 19:2 (2013) 375-393.

85. Garcia, M. G., Marchese, J., and Ochoa, N. A., High activated carbon loading mixed matrix membranes for gas separations, Journal of Materials Science. 47:7 (2012) 3064-3075.

86. Noble, R. D., Perspectives on mixed matrix membranes, Journal of Membrane Science. 378:1-2 (2011) 393-397.

87. Chung, T.-S., Chan, S. S., Wang, R., Lu, Z., and He, C., Characterization of permeability and sorption in Matrimid/C60 mixed matrix membranes, Journal of Membrane Science. 211:1 (2003) 91-99.

88. Husain, S. and Koros, W. J., Mixed matrix hollow fiber membranes made with modified HSSZ-13 zeolite in polyetherimide polymer matrix for gas separation, Journal of Membrane Science. 288:1-2 (2007) 195-207.

89. Hussain, M. and Koenig, A., Mixed-Matrix Membrane for Gas Separation: Polydimethylsiloxane Filled with Zeolite, Chemical Engineering & Technology. 35:3 (2012) 561-569.

90. Mahajan, R., Burns, R., Schaeffer, M., and Koros, W. J., Challenges in forming successful mixed matrix membranes with rigid polymeric materials, Journal of Applied Polymer Science. 86:4 (2001) 881-890.

91. Mahajan, R. and Koros, W. J., Factors controlling successful formation of mixed-matrix gas separation materials, Industrial & Engineering Chemistry Research. 39:8 (2000) 2692-2696.

92. Zimmerman, C. M., Singh, A., and Koros, W. J., Tailoring mixed matrix composite membranes for gas separations, Journal of Membrane Science. 137:1-2 (1997) 145-154.

93. Dong, G., Li, H., and Chen, V., Challenges and opportunities for mixed-matrix membranes for gas separation, Journal of Materials Chemistry A. 1:15 (2013) 4610-4630.

94. Li, Y., Chung, T.-S., Cao, C., and Kulprathipanja, S., The effects of polymer chain rigidification, zeolite pore size and pore blockage on polyethersulfone (PES)-zeolite A mixed matrix membranes, Journal of Membrane Science. 260:1-2 (2005) 45-55.

95. Li, Y., Guan, H.-M., Chung, T.-S., and Kulprathipanja, S., Effects of novel silane modification of zeolite surface on polymer chain rigidification and partial pore blockage in polyethersulfone (PES)–zeolite A mixed matrix membranes, Journal of Membrane Science. 275:1–2 (2006) 17-28.

96. Lee, J. Y., Wang, Y. N., Tang, C. Y. Y., and Huo, F. W., Mesoporous silica gel-based mixed matrix membranes for improving mass transfer in forward osmosis: Effect of pore size of filler, Scientific Reports. 5:1 (2015) 16808.

97. Bhatia, S. K., Liu, F., and Arvind, G., Effect of pore blockage on adsorption isotherms and dynamics: Anomalous adsorption of iodine on activated carbon, Langmuir. 16:8 (2000) 4001-4008.

98. Duval, J. M., Kemperman, A. J. B., Folkers, B., Mulder, M. H. V., Desgrandchamps, G., and Smolders, C. A., Preparation of zeolite filled glassy polymer membranes, Journal of Applied Polymer Science. 54:4 (1994) 409-418.

99. Lin, H. Q., Van Wagner, E., Freeman, B. D., Toy, L. G., and Gupta, R. P., Plasticization-enhanced hydrogen purification using polymeric membranes, Science. 311:5761 (2006) 639-642.

100. Gonzo, E. E., Parentis, M. L., and Gottifredi, J. C., Estimating models for predicting effective permeability of mixed matrix membranes, Journal of Membrane Science. 277:1-2 (2006) 46-54.

101. Pal, R., Permeation models for mixed matrix membranes, Journal of Colloid and Interface Science. 317:1 (2008) 191-198.

102. Maxwell, J. C., A treatise on electricity and magnetism. Vol. 2. 1873, London: Oxford University Press.

103. Bruggeman, D. a. G., Berechnung verschiedener physikalischer Konstanten von heterogenen Substanzen. I. Dielektrizitätskonstanten und Leitfähigkeiten der Mischkörper aus isotropen Substanzen, Annalen der Physik. 416:7 (1935) 636-664.

104. Lewis, T. and Nielson, L., Dynamic mechanical properties of particulate-filled composite, Journal of Applied Polymer Science. 14:6 (1970) 1449-1471.

105. Pal, R., New Models for Thermal Conductivity of Particulate Composites, Journal of Reinforced Plastics and Composites. 26:7 (2007) 643-651.

106. Kulprathipanja, S., Funk, E. W., Kulkarni, S. S., and Chang, Y. A., Separation of a monosaccharide with mixed matrix membranes, 1988. U.S. Patent, US 4735193 A.

107. Süer, M. G., Bac, N., and Yilmaz, L., Gas permeation characteristics of polymer-zeolite mixed matrix membranes, Journal of Membrane Science. 91:1-2 (1994) 77-86.

108. Tantekin-Ersolmaz, Ş. B., Atalay-Oral, Ç., Tatlıer, M., Erdem-Şenatalar, A., Schoeman, B., and Sterte, J., Effect of zeolite particle size on the performance of polymer–zeolite mixed matrix membranes, Journal of Membrane Science. 175:2 (2000) 285-288.

109. Jiang, L. Y., Chung, T. S., and Kulprathipanja, S., Fabrication of mixed matrix hollow fibers with intimate polymer–zeolite interface for gas separation, AIChE Journal. 52:8 (2006) 2898-2908.

110. Mahajan, R. and Koros, W. J., Mixed matrix membrane materials with glassy polymers. Part 1, Polymer Engineering and Science. 42:7 (2002) 1420-1431.

111. Mahajan, R. and Koros, W. J., Mixed matrix membrane materials with glassy polymers. Part 2, Polymer Engineering and Science. 42:7 (2002) 1432-1441.

112. Jia, M.-D., Pleinemann, K.-V., and Behling, R.-D., Preparation and characterization of thin-film zeolite-PDMS composite membranes, Journal of Membrane Science. 73:2-3 (1992) 119-128.

113. Vankelecom, I. F. J., Scheppers, E., Heus, R., and Uytterhoeven, J. B., Parameters Influencing Zeolite Incorporation in Pdms Membranes, Journal of Physical Chemistry. 98:47 (1994) 12390-12396.

114. Duval, J. M., Folkers, B., Mulder, M. H. V., Desgrandchamps, G., and Smolders, C. A., Adsorbent filled membranes for gas separation. Part 1. Improvement of the gas separation properties of polymeric membranes by incorporation of microporous adsorbents, Journal of Membrane Science. 80:1-3 (1993) 189-198.

115. Kusworo, T. D., Ismail, A. F., Mustafa, A., and Budiyono, Application of activated carbon mixed matrix membrane for oxygen purification, International Journal of Science and Engineering. 1:1 (2010) 21-24.

116. Marchese, J., Anson, M., Ochoa, N. A., Pradanos, P., Palacio, L., and Hernandez, A., Morphology and structure of ABS membranes filled with two different activated carbons, Chemical Engineering Science. 61:16 (2006) 5448-5454.

117. Anson, M., Marchese, J., Garis, E., Ochoa, N., and Pagliero, C., ABS copolymer-activated carbon mixed matrix membranes for CO2/CH4 separation, Journal of Membrane Science. 243:1-2 (2004) 19-28.

118. Khanbabaei, G., Vasheghani-Farahani, E., and Rahmatpour, A., Pure and mixed gas CH4 and n-C4H10 permeation in PDMS-fumed silica nanocomposite membranes, Chemical Engineering Journal. 191 (2012) 369-377.

119. Alpers, A., Keil, B., Lüdtke, O., and Ohlrogge, K., Organic vapor separation: Process design with regards to high-flux membranes and the dependence on real gas behavior at high pressure applications, Industrial & Engineering Chemistry Research. 38:10 (1999) 3754-3760.

120. Prausnitz, J. M., Lichtenthaler, R. N., and De Azevedo, E. G., Molecular thermodynamics of fluid-phase equilibria, 3rd ed. (1999), New Jersey: Prentice Hall PTR. p. 860.

121. Lüdecke, C. and Lüdecke, D., Thermodynamik: Physikalisch-chemische Grundlagen der thermischen Verfahrenstechnik, ed. Springer-Verlag. (2000), Berlin Heidelberg. p. 827.

122. Kaul, B. K. and Prausnitz, J. M., 2nd virial-coefficients of gas-mixtures containing simple fluids and heavy hydrocarbons, Industrial & Engineering Chemistry Fundamentals. 16:3 (1977) 335-340.

123. Ghannam, M. T. and Esmail, M. N., Rheological properties of poly(dimethylsiloxane), Industrial & Engineering Chemistry Research. 37:4 (1998) 1335-1340.

124. Cai, Z., Qiu, W., Shao, G., and Wang, W. P., A new fabrication method for all-PDMS waveguides, Sensors and Actuators A: Physical. 204 (2013) 44-47.

125. Duel, L. and Owen, M. J., ESCA studies of silicone release coatings, The Journal of Adhesion. 16:1 (1983) 49-59.

126. Khanbabaei, G., Vasheghani-Farahani, E., and Rahmatpour, A., Permeability, solubility, and diffusivity of methane and butane in diphenylsiloxane-dimethylsiloxane copolymer membranes, Journal of Macromolecular Science Part B-Physics. 50:12 (2011) 2376-2392.

127. Kamiya, Y., Naito, Y., Terada, K., Mizoguchi, K., and Tsuboi, A., Volumetric properties and interaction parameters of dissolved gases in poly(dimethylsiloxane) and polyethylene, Macromolecules. 33:8 (2000) 3111-3119.

128. Anand, M., Langsam, M., Rao, M. B., and Sircar, S., Multicomponent gas separation by selective surface flow (SSF) and poly-trimethylsilylpropyne (PTMSP) membranes, Journal of Membrane Science. 123:1 (1997) 17-25.

129. Böhringer, B., Gonzalez, O., Eckle, I., Mueller, M., Giebelhausen, J., Schrage, C., and Fichtner, S., Polymer-based Spherical Activated Carbons-From Adsorptive Properties to Filter Performance, Chemie Ingenieur Technik. 83:1-2 (2011) 53-60.

130. Do, D. D., Adsorption Analysis: Equilibria and Kinetics. 1998, London: Imperial College Press. p. 892.

131. Zhu, W. D., Groen, J. C., Kapteijn, F., and Moulijn, J. A., Adsorption of butane isomers and SF6 on Kureha activated carbon: 1. Equilibrium, Langmuir. 20:13 (2004) 5277-5284.

132. Wang, X., French, J., Kandadai, S., and Chua, H. T., Adsorption measurements of methane on activated carbon in the temperature range (281 to 343) K and pressures to 1.2 MPa, Journal of Chemical & Engineering Data. 55:8 (2010) 2700-2706.

133. Chatterjee, A. and Mizukami, F., Location and role of exchangeable cations in zeolite catalysis: a first principle study, Chemical Physics Letters. 385:1 (2004) 20-24.

134. Ackley, M. W., Rege, S. U., and Saxena, H., Application of natural zeolites in the purification and separation of gases, Microporous and Mesoporous Materials. 61:1 (2003) 25-42.

135. Sircar, S. and Myers, A., Gas Separation by Zeolites, in Handbook of Zeolite Science and Technology, (eds S.M. Auerbach, K.A. Carrado, and P.K. Dutta), (2003), Marcel Dekker AG: U.S.A. p. 53.

136. Zeolyst International: Zeolite Y. Last update: Mar. 13th 2019. Available from: https://www.zeolyst.com/our-products/standard-zeolite-powders/zeolite-y.html.

137. Ravenelle, R. M., Heterogeneous catalysts in aqueous phase reforming environments: an investigation of material stability, PhD thesis in School of Chemical and Biomolecular Engineering, Georgia Institute of Technology, Atlanta, USA. (2011) p. 181.

138. Mao, Z. and Sinnott, S. B., Separation of organic molecular mixtures in carbon nanotubes and bundles: Molecular dynamics simulations, The Journal of Physical Chemistry B. 105:29 (2001) 6916-6924.

139. Air Liquide: N-Butane N25. Last update: Mar. 13th 2019. Available from: https://produkte.airliquide.de/gasekatalog/pdb/n-butann25.pdf.

140. Air Liquide: Methane N25. Last update: Mar. 13th 2019. Available from: https://produkte.airliquide.de/gasekatalog/pdb/methann25.pdf.

141. Strathmann, H., Giorno, L., and Drioli, E., Basic Aspects in Polymeric Membrane Preparation, in Comprehensive Membrane Science and Engineering, (eds E. Drioli and L. Giorno), (2010), Elsevier: Italy. p. 91-112.

142. Esteves, A. C. C., Brokken-Zijp, J., Laven, J., Huinink, H. P., Reuvers, N. J. W., Van, M. P., and De With, G., Influence of cross-linker concentration on the cross-linking of PDMS and the network structures formed, Polymer. 50:16 (2009) 3955-3966.

143. Stafie, N., Stamatialis, D. F., and Wessling, M., Effect of PDMS cross-linking degree on the permeation performance of PAN/PDMS composite nanofiltration membranes, Separation and Purification Technology. 45:3 (2005) 220-231.

144. Blenke, H., Bohner, K., and Schuster, S., Beitrag zur optimalen Gestaltung chemischer Reaktoren, Chemie Ingenieur Technik. 37:3 (1965) 289-294.

145. Grob, R. L. and Barry, E. F., Modern practice of gas chromatography. 2004: John Wiley & Sons, Inc.

146. Saffaj, T., Ihssane, B., Jhilal, F., Bouchafra, H., Laslami, S., and Sosse, S. A., An overall uncertainty approach for the validation of analytical separation methods, Analyst. 138:16 (2013) 4677-4691.

147. Stepan, R., Hajslova, J., Kocourek, V., and Ticha, J., Uncertainties of gas chromatographic measurement of troublesome pesticide residues in apples employing conventional and mass spectrometric detectors, Analytica Chimica Acta. 520:1-2 (2004) 245-255.

148. Bevington, P. R. and Robinson, D. K., Data Reduction and Error Anlaysis for the Physical Sciences, 3rd ed. (2003), New York: McGraw-Hill Companies, Inc. . p. 337.

149. Taylor, J. R., An introduction to error analysis: The study of uncertainties in physical measurements, 2nd ed. (1982), California: University Science Books. p. 349.

150. Myung, I. J., Tutorial on maximum likelihood estimation, Journal of Mathematical Psychology. 47:1 (2003) 90-100.

151. Ismail, A. F. and David, L. I. B., A review on the latest development of carbon membranes for gas separation, Journal of Membrane Science. 193:1 (2001) 1-18.

152. Ahmad, J. and Hagg, M. B., Preparation and characterization of polyvinyl acetate/zeolite 4A mixed matrix membrane for gas separation, Journal of Membrane Science. 427 (2013) 73-84.

153. Cong, H. L., Radosz, M., Towler, B. F., and Shen, Y. Q., Polymer-inorganic nanocomposite membranes for gas separation, Separation and Purification Technology. 55:3 (2007) 281-291.

154. Sadrzadeh, M., Saljoughi, E., Shahidi, K., and Mohammadi, T., Preparation and characterization of a composite PDMS membrane on CA support, Polymers for Advanced Technologies. 21:8 (2010) 568-577.

155. Zhang, Y. Z., Li, H., Lin, J., Li, R., and Liang, X. P., Preparation and characterization of zirconium oxide particles filled acrylonitrile-methyl acrylate-sodium sulfonate acrylate copolymer hybrid membranes, Desalination. 192:1-3 (2006) 198-206.

156. Kim, S., Pechar, T. W., and Marand, E., Poly(imide siloxane) and carbon nanotube mixed matrix membranes for gas separation, Desalination. 192:1-3 (2006) 330-339.

157. Ciobanu, G., Carja, G., and Ciobanu, O., Structure of mixed matrix membranes made with SAPO-5 zeolite in polyurethane matrix, Microporous and Mesoporous Materials. 115:1-2 (2008) 61-66.

158. Kim, S., Chen, L., Johnson, J. K., and Marand, E., Polysulfone and functionalized carbon nanotube mixed matrix membranes for gas separation: Theory and experiment, Journal of Membrane Science. 294:1-2 (2007) 147-158.

159. Xiao, Y., Yu Wang, K., Chung, T.-S., and Tan, J., Evolution of nano-particle distribution during the fabrication of mixed matrix TiO2-polyimide hollow fiber membranes, Chemical Engineering Science. 61:18 (2006) 6228-6233.

160. Ismail, A. F. and Kusworo, T. D., Fabrication and characterization of polyimide/polyethersulfone-fumed silica mixed matrix membrane for gas separation, Reaktor. 11:1 (2007) 30-37.

161. Barrer, R. M., Barrie, J. A., and Raman, N. K., Solution and diffusion in silicone rubber II—The influence of fillers, Polymer. 3 (1962) 605-614.

162. Vu, D. Q., Koros, W. J., and Miller, S. J., Mixed matrix membranes using carbon molecular sieves - II. Modeling permeation behavior, Journal of Membrane Science. 211:2 (2003) 335-348.

163. Duan, C., Jie, X., Liu, D., Cao, Y., and Yuan, Q., Post-treatment effect on gas separation property of mixed matrix membranes containing metal organic frameworks, Journal of Membrane Science. 466 (2014) 92-102.

164. Shishatskiy, S., Nistor, C., Popa, M., Nunes, S. P., and Peinemann, K. V., Polyimide asymmetric membranes for hydrogen separation: Influence of formation conditions on gas transport properties, Advanced Engineering Materials. 8:5 (2006) 390-397.

165. Eremin, Y. S. and Grekhov, A. M., Calculation of percolating clusters characteristics in mixed matrix membrane with CNT, Physics Procedia. 72 (2015) 37-41.

166. Islam, M. A. and Buschatz, H., Assessment of thickness-dependent gas permeability of polymer membranes, Indian Journal of Chemical Technology. 12:1 (2005) 88-92.

167. Islam, M. A., Buschatz, H., and Paul, D., Non-equilibrium surface reactions—a factor in determining steady state diffusion flux, Journal of Membrane Science. 204:1–2 (2002) 379-384.

168. Huang, L. W. and Mccutcheon, J. R., Impact of support layer pore size on performance of thin film composite membranes for forward osmosis, Journal of Membrane Science. 483 (2015) 25-33.

169. Tan, S., Li, L., Zhang, Z., and Wang, Z., The influence of support layer structure on mass transfer in pervaporation of composite PDMS-PSF membranes, Chemical Engineering Journal. 157:2-3 (2010) 304-310.

170. Offeman, R. D. and Ludvik, C. N., Thin film composite membranes and their use method of preparation and use, (2013). U.S. Patent, US 8617395 B2.

171. Kouketsu, T., Duan, S., Kai, T., Kazama, S., and Yamada, K., PAMAM dendrimer composite membrane for CO2 separation: Formation of a chitosan gutter layer, Journal of Membrane Science. 287:1 (2007) 51-59.

172. Kattula, M., Ponnuru, K., Zhu, L., Jia, W., Lin, H. Q., and Furlani, E. P., Designing ultrathin film composite membranes: the impact of a gutter layer, Scientific Reports. 5 (2015) 15016.

173. Li, T., Pan, Y., Peinemann, K.-V., and Lai, Z., Carbon dioxide selective mixed matrix composite membrane containing ZIF-7 nano-fillers, Journal of Membrane Science. 425–426 (2013) 235-242.

174. Wijmans, J. G. and Hao, P., Influence of the porous support on diffusion in composite membranes, Journal of Membrane Science. 494 (2015) 78-85.

175. Lillepärg, J., Breitenkamp, S., Shishatskiy, S., Pohlmann, J., Wind, J., Scholles, C., and Brinkmann, T., Characteristics of gas permeation behaviour in multilayer thin film composite membranes for CO_2 separation, Membranes. 9:2 (2019) 22.

176. Ghadimi, A., Norouzbahari, S., Sadrzadeh, M., and Mohammadi, T., Improvement in gas separation properties of a polymeric membrane through the incorporation of inorganic nano-particles, Polymers for Advanced Technologies. 23:7 (2012) 1101-1111.

177. Jordan, S. M. and Koros, W. J., Permeability of Pure and Mixed Gases in Silicone-Rubber at Elevated Pressures, Journal of Polymer Science Part B-Polymer Physics. 28:6 (1990) 795-809.

178. De Angelis, M. G., Merkel, T. C., Bondar, V. I., Freeman, B. D., Doghieri, F., and Sarti, G. C., Hydrocarbon and fluorocarbon solubility and dilation in poly(dimethylsiloxane): Comparison of experimental data with predictions of the Sanchez-Lacombe equation of state, Journal of Polymer Science Part B-Polymer Physics. 37:21 (1999) 3011-3026.

179. Prabhakar, R. S., Raharjo, R., Toy, L. G., Lin, H. Q., and Freeman, B. D., Self-consistent model of concentration and temperature dependence of permeability in rubbery polymers, Industrial & Engineering Chemistry Research. 44:5 (2005) 1547-1556.

180. Raharjo, R. D., Mixed gas sorption and transport study in solubility selective polymers, PhD thesis in Faculty of the Graduate School of The University of Texas at Austin, The University of Texas at Austin, Austin. (2007) p. 234.

181. Liu, M., Sun, J. R., Sun, Y., Bock, C., and Chen, Q. F., Thickness-dependent mechanical properties of polydimethylsiloxane membranes, Journal of Micromechanics and Microengineering. 19:3 (2009)

182. Cao, C., Chung, T. S., Liu, Y., Wang, R., and Pramoda, K. P., Chemical cross-linking modification of 6FDA-2,6-DAT hollow fiber membranes for natural gas separation, Journal of Membrane Science. 216:1-2 (2003) 257-268.

183. Gao, Z. M., Nahrup, J. S., Mark, J. E., and Sakr, A., Poly(dimethylsiloxane) coatings for controlled drug release. II. Mechanism of the crosslinking reaction in emulsion, Journal of Applied Polymer Science. 91:4 (2004) 2186-2194.

184. Hillock, A. M. W., Crosslinkable Polymide Mixed Matrix Membranes for natural Gas Purification, PhD Thesis in Georgia Institute of Technology. (2005) p. 220.

185. Mani, S., Cassagnau, P., Bousmina, M., and Chaumont, P., Cross-linking control of PDMS rubber at high temperatures using TEMPO nitroxide, Macromolecules. 42:21 (2009) 8460-8467.

186. Simpson, T. R. E., Tabatabaian, Z., Jeynes, C., Parbhoo, B., and Keddie, J. L., Influence of interfaces on the rates of crosslinking in poly(dimethyl siloxane) coatings, Journal of Polymer Science Part a-Polymer Chemistry. 42:6 (2004) 1421-1431.

187. Hillock, A. M. W. and Koros, W. J., Cross-Linkable Polyimide Membrane for Natural Gas Purification and Carbon Dioxide Plasticization Reduction, Macromolecules. 40:3 (2007) 583-587.